U. S. Department of Energy
1000 Independence Avenue, S.W.
Washington, D.C. 20585

Fiscal Year 2022: First Quarter

Progress Reports:
Advanced Battery Materials Research (BMR) Program
&
Battery500 Consortium

Released April 2022
for the period of October – December 2021

Approved by

Tien Q. Duong
Manager, Advanced Battery Materials Research Program & Battery500 Consortium
Batteries & Electrification R&D
Office of Energy Efficiency and Renewable Energy – Vehicle Technologies Office
U.S. Department of Energy

ACKNOWLEDGMENTS

This report has been edited by the following team members:

- **T. A. Zachry,** Energy & Environmental Resources Group
- **Patricia H. Smith,** Naval Surface Warfare Center – Carderock

TABLE OF CONTENTS

Battery500 Consortium Program

TABLE OF FIGURES

TABLE OF TABLES

A MESSAGE FROM THE MANAGER: ADVANCED BATTERY MATERIALS RESEARCH AND BATTERY500 CONSORTIUM

This quarter, the Vehicle Technologies Office (VTO) introduces 21 new efforts to develop next-generation batteries that can outperform present lithium-ion batteries. A list of the new projects is provided in the Table below. Projects conducted by the national laboratories and academia that focus on accelerating solid-state electrolyte technology will be managed by Dr. Simon Thompson. Ms. Haiyan Croft will assist in managing university/industry efforts to develop lithium-sulfur and lithium-air batteries. The progress of these new projects will be reported within this and future BMR quarterly reports.

Institution	Title	Principal Investigator
Argonne National Laboratory	Multifunctional Gradient Coatings for Scalable, High-Energy-Density Sulfide-Based Solid-State Batteries	Justin Connell
Argonne National Laboratory	Development of All-Solid-State Battery Using Anti-Perovskite Electrolytes	Zonghai Chen
Argonne National Laboratory	Electrolytes for High-Energy, All-Solid-State, Lithium-Metal Batteries	Guiliang Xu
Argonne National Laboratory	Synthesis of Composite Electrolytes with Integrated Interface Design	Sanja Tepavcevic
Brookhaven National Laboratory	Inorganic-Polymer-Composite Electrolyte with Architecture Design for Lithium-Metal Solid-State Batteries	Enyuan Hu
Lawrence Livermore National Laboratory	Three-Dimensional Printing of All-Solid-State Lithium Batteries	Jianchao Ye
Lawrence Livermore National Laboratory	Integrated Multiscale Model for Design of Robust, Three-Dimensional, Solid-State Lithium Batteries	Brandon Wood
National Renewable Energy Laboratory	Low-Pressure All-Solid-State Cells	Anthony Burrell
Oak Ridge National Laboratory	Precision Control of the Lithium Surface for Solid-State Batteries	Andrew Westover
Oak Ridge National Laboratory	Substituted Argyrodite Solid Electrolytes and High-Capacity Conversion Cathodes for All-Solid-State Batteries	Jagjit Nanda
Oak Ridge National Laboratory	Lithium Halide-Based Superionic Solid Electrolytes and High-Voltage Cathode Interface	Jagjit Nanda
Oak Ridge National Laboratory	Polymer Electrolytes for Stable, Low-Impedance, Solid-State Battery Interfaces	X. Chelsea Chen
Pacific Northwest National Laboratory	Stable Solid-State Electrolyte and Interface for High-Energy All-Solid-State Lithium-Sulfur Battery	Dongping Lu
Pennsylvania State University	Development of Li-S Battery Cells with High Energy Density and Long Cycling Life	Donghai Wang
Stanford University	Thioborate Solid-State Electrolytes for Practical All-Solid-State Batteries	Yi Cui
University of California, Berkeley	Polyester-Based Block Copolymer Electrolytes for Lithium-Metal Batteries	Nitash Balsara
University of California, Berkeley	Ion Conductive High Li^+ Transference Number Polymer Composites for Solid-State Batteries	Bryan McCloskey
University of California, Berkeley	Solid-State Batteries with Long Cycle Life and High Energy Density through Materials Design and Integration	Gerbrand Ceder
University of California, San Diego	Strategies to Enable Lean Electrolytes for High Loading and Stable Lithium-Sulfur Batteries	Y. Shirley Meng
University of Illinois, Chicago	Development of a High-Rate Lithium-Air Battery Using a Gaseous CO_2 Reactant	Amin Salehi-Khojin
University of Pittsburg	New Engineering Concepts to High-Energy-Density Lithium-Sulfur Batteries	Prashant Kumta

A few notable achievements from BMR investigators during October 1, 2021, through December 31, 2021, are summarized below:

- The team led by Jeff Sakamoto at the University of Michigan investigated the tradeoffs between lithium thickness (or capacity) and current density during lithium stripping when using thin Li-metal anodes between 5-20 µm with 17-µm thick $Li_7La_3Zr_2O_{12}$ (LLZO) electrolytes. They demonstrated that higher current densities and thinner lithium films increase the instability in lithium stripping. These results have significant general implications for using thin Li-metal anodes with oxide-based solid electrolytes.

- Deyang Qu and the team at the University of Wisconsin, Milwaukee, successfully made thin halide-based solid-electrolyte separators less than 50-µm thick, leveraging small amounts of polytetrafluoroethylene (PTFE) binders, and successfully laminated them to 80-µm thick cathodes. The electrolyte was flexible and achieved an ionic conductivity of ~ 1 mS/cm.

- The University of Illinois, Chicago, (Amin Salehi-Khojin group) explored a Li-air battery based on a carbon dioxide reactant. They discovered a novel transition metal dichalcogenide alloy structure that serves as a cathode catalyst and a bi-functional redox mediator that works in synergy with ionic-liquid-based electrolyte that promotes high-rate battery operation. The battery is capable of operating under 0.3 mA/cm^2 and high capacities of 0.3 mAh/cm^2 (corresponding to 3000 mAh/g) up to 100 cycles.

- The Argonne National Laboratory team (Chris Johnson and Khalil Amine) combined *in situ* synchrotron-based X-ray diffraction and X-ray absorption spectroscopy to reveal the capacity fade of O3 sodium layered oxide $NaNi_{0.4}Mn_{0.4}Co_{0.2}O_2$ cathode at both low (2.0-3.8 V) and high (2.0-4.4 V) voltage. Their results show that charging voltage limit does not play a dominant role in triggering capacity fade of O3 sodium layered cathodes with native lattice strain.

- Marca Doeff's team at Lawrence Berkeley National Laboratory improved an ion-exchange process for making a lepidocrocite-structured $Mg_{0.37}Ti_{1.815}O_4$ phase. The replacement of interlayer monovalent cations with divalent magnesium increases the number of available sites for sodium insertion during electrochemical sodiation. This electrode was found to cycle better than the sodiated version.

- The Brookhaven National Laboratory team (Xiao-Qing Yang and Enyuan Hu) carried out structure evolution studies of $NaMnFeCoNiO_2$, using synchrotron-based X-ray diffraction, and high-angle annular dark field – scanning transmission electron microscopy. They found that after the first-charge process, the atomic structure of $NaMnFeCoNiO_2$ is partially transformed from O3-type to P3-type, resulting in a mixture of O3 and P3 structure in this high-energy-density cathode material after the first cycle.

The Battery500 Consortium, led by Pacific Northwest National Laboratory, was awarded a Phase II co-operative agreement. This effort is one of the largest battery research programs in the world and includes members from Brookhaven National Laboratory, Idaho National Laboratory, SLAC National Accelerator Laboratory, Binghamton University (State University of New York), Stanford University, University of California at San Diego, and the University of Washington. Scientists from Texas A&M University, the Pennsylvania State University, University of Maryland, and General Motors will also be supporting the effort. The aim of the program remains the same as Phase I—demonstration of a cell that delivers triple the specific energy (500 watt-hours per kilogram, compared to the 170-200 watt-hours) of today's electric vehicle batteries and the ability to achieve 1,000 cycles. To accomplish this aggressive goal, the program is divided into three key areas (Materials and Interfaces, Electrode Architecture, and Cell Fabrication, Testing, and Diagnosis) and a cross-cutting effort to ensure a rapid cell-level integration of any new advances in materials and components.

A few notable achievements from the Battery500 Team this quarter include:

- Arumugam Manthiram's Team from the University of Texas, Austin, designed, synthesized, and studied a novel, cobalt- and manganese-free, high-nickel cathode, ($LiNi_{0.93}Al_{0.05}Ti_{0.01}Mg_{0.01}O_2$). The material displayed the highest capacity retention, with 82% after 800 cycles, compared to 60% for $LiNi_{0.90}Mn_{0.05}Co_{0.05}O_2$ and 52% for $LiNi_{0.94}Co_{0.06}O_2$. The team also demonstrated that a simple manganese salt additive can significantly improve Li-metal plating morphology.

- The Xiao-Qing Yang and Enyuan Hu team at Brookhaven National Laboratory utilized an X-ray pair distribution function technique combined with molecular dynamics simulations to probe the Li-solvation structures in liquid electrolytes. It was found that in high concentration electrolyte, the solvation structure promotes the anion reduction for solid electrolyte interphase (SEI) formation, while the low concentration electrolyte promotes solvent reduction, showing that better lithium metal protection is obtained using a high concentration electrolyte.

- Perla Balbuena's team at Texas A&M University applied a new *ab initio* simulation approach to evaluate barriers for lithium cation transport and deposition with simultaneous SEI formation on the lithium anode. They showed in high concentration electrolyte that a significant increase in the energy barriers for cation diffusion and the ion complexes trapped in the high concentration electrolyte can slow down their surface deposition, enabling a thick and compact SEI to be built through anion decomposition, whereas the barriers are significantly lower in localized high concentration electrolytes while keeping an anion-dominated SEI.

On a final note, the VTO will hold its Annual Merit and Peer Evaluation meeting from June 21 to 23, 2022. This hybrid event will accommodate both in-person and virtual attendance. The in-person meeting will be at the Washington Hilton hotel in Washington, D. C. Additional information may be found online (www.energy.gov/eere/vehicles/annual-merit-review-agenda). I hope to see you there.

On behalf of the VTO team,

Tien Q. Duong

Tien Q. Duong
Manager, Advanced Battery Materials Research Program & Battery500 Consortium
Batteries & Electrification R&D
Energy Efficiency and Renewable Energy
U.S. Department of Energy

TASK 1 – Solid-State Electrolytes

Team Lead: Andrew Westover, Oak Ridge National Laboratory

Summary and Highlights

The U. S. Department of Energy (DOE) has made a clear goal of realizing next-generation batteries with an energy density greater than 500 Wh/kg, that can cycle for more than 300 cycles, and that can demonstrate high-rate capabilities. To achieve this step-change in battery performance, a significant change in the battery chemistry and cell design is needed. This task focuses on developing solid-state electrolytes (SSEs) that enable Li-metal anodes and high-energy cathodes to achieve just such a step change. This task includes 12 projects centered in DOE national laboratories and 13 in companies and universities. These projects span the gamut of different materials for SSEs, interfacial design strategies to enable Li-metal anodes, and high-energy cathodes. Together, they can significantly impact the successful realization of the DOE battery performance targets.

In summary, the projects focus on research and development of a range of solid electrolytes (SEs), including:

- sulfur ceramics and glasses (1.1 – 1.9),
- oxide ceramics (1.10 – 1.13),
- halides and anti-perovskites (1.13 – 1.15),
- polymers (1.16 – 1.18),
- composites (1.19 – 1.22),
- multiple electrolytes / full cells (1.23 – 1.24), and
- Li-metal – SSE interface (1.25).

These projects encompass common research themes essential to achieving high-energy solid-state batteries (SSBs), including:

- engineering high ionic conductivity > 1 mS/cm,
- developing electrolytes that are stable with various high-energy cathodes, including layered oxide cathodes, high-voltage spinels, and conversion cathodes such as sulfur and FeF_3,
- developing electrolytes or interfaces that are stable with lithium metal,
- developing thin SEs 20-100 µm thick, and
- understanding the mechanics of SSBs.

Highlights

- The team led by J. Sakamoto at the University of Michigan (UM) investigated the tradeoffs between lithium thickness (or capacity) and current density during lithium stripping when using thin Li-metal anodes between 5-20 µm with 17-µm thick $Li_7La_3Zr_2O_{12}$ (LLZO) electrolytes. They demonstrated that higher current densities and thinner lithium films increase the instability in lithium stripping. These results have significant general implications for using thin Li-metal anodes with oxide-based SEs.
- D. Qu and the team at the University of Wisconsin, Milwaukee (UWM) successfully made thin halide-based SE separators less than 50-µm thick, leveraging small amounts of polytetrafluoroethylene (PTFE) binders, and successfully laminated them to 80-µm thick cathodes. The electrolyte was flexible and achieved an ionic conductivity of ~ 1 mS/cm.

- N. Balsara and the Lawrence Berkeley National Laboratory (LBNL) team successfully synthesized novel polyester-based polymer electrolytes (PEs) as one of the key building blocks for a new type of block co-polymer electrolyte.

Task 1.1 – Multifunctional Gradient Coatings for Scalable, High-Energy-Density Sulfide-Based Solid-State Batteries
(Justin Connell, Argonne National Laboratory)

Project Objective. This task seeks to develop scalable approaches to synthesize gradient-coated sulfide SSE particles to improve their air/moisture tolerance and provide chemical compatibility with Li-metal anodes and high-voltage oxide cathodes. The compositional gradient is targeted to provide the additional advantage of lower interfacial impedance due to mitigation of detrimental, spontaneously formed space charge layers and/or elemental interdiffusion at the sulfide SSE-oxide cathode interface.

Impact. Development of coated SSE materials that provide stable, low-impedance interfaces with both anode and cathode will enable high-energy-density, all-solid-state full cells with improved cyclability at high rates relative to benchmarked, uncoated materials. Coating the SSE directly will also remove the need for separate anode and cathode coatings, significantly reducing the cost and complexity associated with materials processing while maintaining compatibility with roll-to-roll manufacturing.

Approach. The team will leverage a surface science-based, integrated experimental-theoretical approach to synthesize gradient-coated SSE powders, characterize the structure, composition, and intrinsic stability of coated SSEs in contact with reactive electrodes, and directly correlate this understanding with their electrochemical performance. Gradient coatings will be developed using atomic layer deposition (ALD) and/or physical mixing methodologies viable at the kg/ton scale, ensuring technical and commercial relevance of the final, optimized coating process. Well characterized, model surfaces will be used to understand the electronic structure and chemical stability of the gradient coatings as a function of gradient composition and thickness to understand the effect of space-charge layers and chemical reactions on interface resistance. They will accelerate development and optimization of the gradient coatings for improved performance in full cells by establishing a tight feedback loop between materials synthesis and experimental/computational characterization of interfacial (electro)chemistry.

Out-Year Goals. The out-year goals are to demonstrate high-energy-density, low-impedance full cells assembled from fully optimized, gradient-coated SSE powders, high-energy-density cathodes, and Li-metal anodes. The team will also significantly improve the ability to manipulate the formation of space-charge layers at sulfide SSE-oxide cathode interfaces based on mechanistic understanding of the extent to which they can be mitigated to reduce overall cell impedance.

Collaborations. This project funds work within multiple divisions and directorates at Argonne National Laboratory (ANL) and includes in-kind contributions from Solid Power.

Milestones

1. Baseline Li||Li symmetric cell testing and characterization of uncoated argyrodite SSEs. (Q2, FY 2022; In progress)
2. Chemical stability characterization of gradient coatings for argyrodite SSEs. (Q3, FY 2022).
3. Computational assessment of electronic structure of candidate gradient coating chemistries. (Q4, FY 2022)
4. Identification of multiple gradient coating chemistries that deliver > 50% reduction in weight gain during humidified air exposure. (Q1, FY 2023)

Progress Report

Progress for this new project will be reported next quarter.

Patents/Publications/Presentations

The project has no patents, publications, or presentations to report this quarter.

Task 1.2 – Electrolytes for High-Energy, All-Solid-State, Lithium-Metal Batteries (Guiliang Xu, Argonne National Laboratory)

Project Objective. The project objective is to develop ultra-thin (< 30 µm) sulfide SSEs with high room-temperature ionic conductivity (> 0.01 S/cm) and high chemical/mechanical/electrochemical stability, and further integrate them with lithium metal and high-loading selenium-doped sulfur (Se-S) cathodes through rational interface engineering to develop all-solid-state Li-S batteries (ASSLSBs) with high energy density and long cycle life.

Impact. The project is related to development and mass production of high-performance sulfide SSEs for high-energy all-solid-state Li-S pouch cells. The success of the proposed project in meeting or exceeding DOE targets can promote the practical implementation of Li-S battery in electric vehicles (EVs), electric aviation, and grid energy storage, and hence significantly reduce oil dependence and emissions of carbon dioxide. It can also mitigate the domestic supply challenge on the critical raw battery materials (for example, nickel and cobalt).

Approach. The thickness and chemical/interfacial stability of sulfide SSEs are the critical challenges for energy density, cycle life, and mass production of all-solid-state Li-S pouch cells. The team will combine innovative material design, electrode architecture fabrication, and advanced diagnostics tools to address these challenges. Specifically, the approaches include: (1) improving air stability and ionic conductivity of sulfides through synthetic control and cation/anion doping, (2) fabrication of flexible thick SeS cathode supported thin sulfide electrolytes to ensure intimate contact and increase the energy density, (3) stabilizing Li-metal/sulfide electrolytes interface via interlayer and additives design to increase the critical current density (CCD) of lithium stripping/platting, (4) advanced Li-S pouch cell design, and (5) multiscale advanced diagnostic such as *in situ* X-ray diffraction (XRD), X-ray absorption spectroscopy (XAS), X-ray imaging, and focused ion beam – scanning electron microscopy (FIB-SEM) to understand and overcome the degradation pathways.

Out-Year Goals. The out-year goals are to scale up the optimal sulfide SSEs to develop Ah-level all-solid-state Li-S pouch cells that can reach a cell energy density of > 500 Wh/kg with 80% capacity retention for > 300 cycles at a current density of > 1 mA/cm^2.

Collaborations. The team is closely collaborating with top scientists at University of Chicago (X. Huang) and at Advanced Photon Source (C. Sun, W. Xu, D. Zhang, and J. Deng) and Center for Nanoscale Materials (Y. Liu and M. Chan) of ANL for *in situ* diagnostics on the synthesis and aging mechanism of the proposed sulfide SSEs.

Milestones

1. Set up a dedicated lab for synthesis, processing, and characterization of sulfide SSEs. (Q1, FY 2022; In progress)
2. Revealing the formation and degradation mechanism of sulfide SSE. (Q2, FY 2022; In progress)
3. Composition tuning of sulfide SSE. (Q3, FY 2022; In progress)
4. Development of doped sulfide SSE with high room-temperature ionic conductivity (> 1 mS/cm) and air stability. (Q4, FY 2022; In progress)

Progress Report

Progress for this new project will be reported next quarter.

Patents/Publications/Presentations

The project has no patents, publications, or presentations to report this quarter.

Task 1.3 – Thioborate Solid-State Electrolytes for Practical All-Solid-State Batteries
(Yi Cui, Stanford University)

Project Objective. This project aims to develop novel lithium thioborates (lithium-boron-sulfur, LBS) as a new class of SSEs to realize high-performance all-solid-state batteries (ASSBs), with a particular focus on addressing the technical challenges in electrolyte synthesis, cell integration, failure diagnostics, and scale-up. The approach will be technologically transformative to the current solutions for ASSB development. For the final deliverables, ASSBs with the ability to reach an energy density of 500 Wh/kg and maintain 80% capacity for at least 300 cycles will be demonstrated.

Impact. The project approaches provide new directions toward developing high-conductivity and electrochemically stable sulfur-based electrolytes for ASSBs. Such high-performance electrolytes can enable the practical realization of ASSBs with a high energy density and improved safety.

Approach. The long-term project has a multi-step approach toward integration of LBS with high-voltage cathodes, with steps 1-3 as the focus for this year:

1. Fabricate undoped LBS powders using an all-solid-state synthesis method to achieve high ionic conductivity, low electronic conductivity, and a wide operational voltage window.
2. Integrate LBS SSEs into symmetric Li/LBS/Li cells and into full batteries using high-voltage cathodes including lithium Ni-Mn-Co (NMC) oxide.
3. Study atomic, particle, and cell-scale Li-metal-SSE interface development and dendrite growth mechanisms in SSEs using advanced characterization tools. Use knowledge to better develop SSEs and modify interfaces for stable cycling in full cells.
4. Fabricate doped LBS powders and develop particle/surface modifications to increase ionic conductivity as well as stability in full batteries and in air for glovebox-free synthesis.
5. Use density functional theory (DFT) to guide development of new doped LBS materials and to explore interactions at solid-solid interfaces.

Out-Year Goals. In the following year, the team will develop solid-state reaction methods to synthesize undoped LBS powders and construct Li/LBS/Li symmetric cells to test the electrochemical performance of synthesized LBS. Meanwhile, the team will utilize advanced characterization tools [for example, cryogenic electron microscopy (cryo-EM), X-ray computed tomography (CT), etc.] to resolve the nanostructure of Li/LBS interphase and investigate the electrochemical stability between LBS and lithium metal.

Collaborations. The Y. Cui group is collaborating with W. Chueh's group (advanced characterization) and E. Reed's group (crystal structure computation) at Stanford as well as with Y. Liu (advanced characterization) at SLAC National Accelerator Laboratory (SLAC).

Milestones

1. Develop solid-state reaction methods to synthesize undoped LBS powders with high ionic conductivity. (Q1, FY 2022; In progress)
2. Construct Li/LBS/Li symmetric cells for electrochemical characterizations. (Q2, FY 2022; In progress)
3. Study the evolution of Li/LBS interphase. (Q3, FY 2022)
4. Resolve the nanostructure of Li/LBS interphase using advanced characterizations (for example, cryo-EM, X-ray CT, etc.). Achieve ionic conductivity of LBS SSE of 1.0×10^{-3} S cm^{-1}. (Q4, FY 2022)

Progress Report

In collaboration with the E. Reed group at Stanford, the team discovered that the theoretical ionic conductivity of LBS SSEs can reach 74 mS cm^{-1}. Motivated by these calculations and by the possibility of discovering a new class of SSEs made from earth-abundant elements, they are working to develop LBS SSEs with high ionic conductivity and high stability for application in full batteries. First, they worked to synthesize high-purity $Li_{10}B_{10}S_{20}$ SSE (Figure 1). Currently, they are working to synthesize high-purity $Li_5B_7S_{13}$ SSE. By altering the ratio of starting materials, high-temperature sintering procedure, and total length of sintering, they have been able to synthesize a mixed-phase $Li_5B_7S_{13}$/$Li_{10}B_{10}S_{20}$ SSE. Another important task of this project is to increase the yield of the reaction to grams scale. Using a new reactor setup, they have increased the quantity that can be produced in one reaction to > 10 grams.

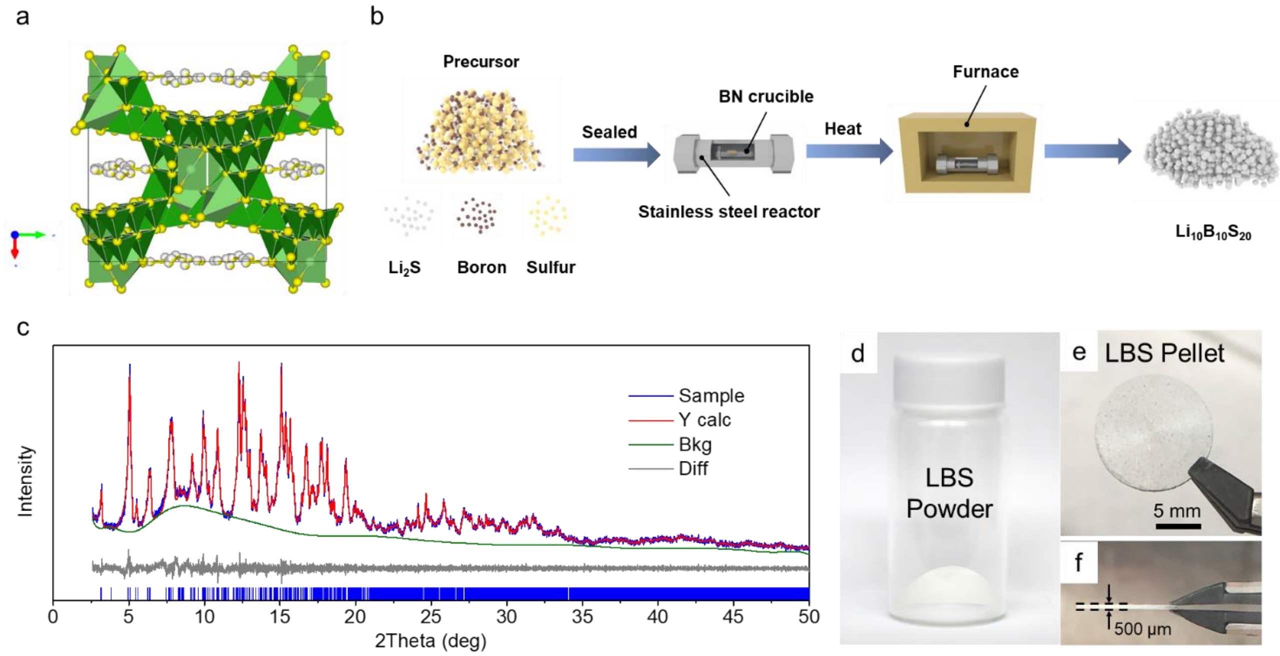

Figure 1. (a) The crystal structure of $Li_{10}B_{10}S_{20}$. (b) Schematic illustration of the synthesis of the $Li_{10}B_{10}S_{20}$ powder. (c) X-ray diffraction (XRD) data fitting of $Li_{10}B_{10}S_{20}$. Experimental data are shown in blue line; the red line denotes the calculated pattern; the difference profile is shown in grey; and calculated positions of the XRD peaks are shown as vertical ticks. (d) Photo image of $Li_{10}B_{10}S_{20}$ powder. (e-f) Photo image of $Li_{10}B_{10}S_{20}$ pellet from (e) top view and (f) side view.

Patents/Publications/Presentations

The project has no patents, publications, or presentations to report this quarter.

Task 1.4 – Substituted Argyrodite Solid Electrolytes and High-Capacity Conversion Cathodes for All-Solid-State Batteries
(Jagjit Nanda, Oak Ridge National Laboratory)

Project Objective. The project aims at synthesis and fabrication of Li-ion conducting argyrodite SEs with nominal composition Li_6PS_5X, where X = chlorine and/or bromine. The team will combine electrochemical impedance spectroscopy (EIS) with complementary *in situ* spectroscopy and microscopy to identify buried interfacial side-reaction products and quantify the voltage losses associated with these side reactions. Specifically, they plan to investigate the interfacial reaction between various Li_6PS_5X SE and Li-ion cathodes belonging to different structural families [transition metal (TM)-based sulfides and fluorides (for example, FeS_2 and FeF_2) and high-voltage layered oxides (for example, $LiNi_{0.8}Mn_{0.1}Co_{0.1}O_2$, NMC-811). New dopants such as niobium and partial substitution of sulfur with oxygen will be explored to improve stability of argyrodite SEs against lithium metal and high-voltage cathodes.

Impact. The proposed work addresses key technical barriers to achieve Li-metal SSBs with energy densities of > 450 Wh/kg and 1,000 Wh/L, which are critical for next-generation EVs. Integrating new sulfide SEs prepared through scalable, low-cost solvent-mediated routes with high capacity, earth abundant conversion cathodes (for example, sulfur, FeF_3, and FeS_2) will lower SSB cost to $80/kWh and eliminate use of critical materials such as cobalt and nickel.

Approach. Scalable solution-based processing routes will be developed to produce freestanding sulfide/binder solid-state separators with thicknesses < 50 µm and area specific resistance (ASR) < 50 $\Omega\,cm^2$. These ultra-thin separators will be integrated with Li-metal anodes and high areal capacity conversion cathodes (for example, sulfur, FeS_2, and FeF_3) to demonstrate lab-scale prototype SSBs. As a cross-cut activity, various *in situ* and *ex situ* passivation methods will be combined with enabling characterization techniques to facilitate Li^+ transport across electrode/SE interfaces.

Out-Year Goals. Optimize SSB performance by: (1) varying cathode composition, particle size, and porosity, (2) applying halide-rich and carbon layers at electrode/electrolyte interfaces, and (3) evaluating how stack pressure (0.1-10 MPa) and temperature (25-75°C) impact performance. Targets: room-temperature cycling with areal capacities > 5 mAh/cm^2, current densities > 2 mA/cm^2, stack pressures < 1 MPa, and < 20% capacity fade over 300 cycles.

Collaborations. D. Hallinan and his group are funded collaborators to develop the binder system for sulfide SEs and evaluate compatibility with cathode and Li-metal. P. Jena from Virginia Commonwealth University will be an unfunded collaborator on DFT modeling of bulk Li-ion transport and *ab initio* molecular dynamics (AIMD) at SE interfaces.

Milestones

1. Produce Li_6PS_5X (X = Cl, Br, and/or I) SEs using solvent-mediated routes with ionic conductivity $\geq 1 \times 10^{-3}$ S/cm^{-1} at room temperature. (Q1, FY 2022)
2. Optimize synthesis and annealing conditions to obtain phase-pure SE Li_6PS_5X powders. Evaluate structure using XRD, Raman, and neutron scattering. (Q2, FY 2022)
3. Compare the structure and Li^+ conductivity of Li_6PS_5X prepared through solvent-mediated versus mechano-chemical and solid-state routes. (Q3, FY 2022)
4. Integrate SSB using Li_6PS_5X SE with a working cathode and thin Li-metal anode for testing and capacity optimization. (Q4, FY 2022)

Progress Report

Progress for this new project will be reported next quarter.

Patents/Publications/Presentations

The project has no patents, publications, or presentations to report this quarter.

Task 1.5 – Stable Solid-State Electrolyte and Interface for High-Energy, All-Solid-State, Lithium-Sulfur Battery
(Dongping Lu, Pacific Northwest National Laboratory)

Project Objective. The project objective is to address material and interfacial barriers of sulfide-based solid-state electrolyte (S-SSE) for deep cycling of Li-metal anode in all-solid-state lithium batteries (ASSLBs). All proposed work will be focused on development of highly conductive sulfide Li^+ conductors with extremely low Li/SSE interfacial resistance and ultra-thin multifunctional interlayer to enable deep and stable lithium cycling. The SEs and interlayer assembly achieved in the project will be tested at practical conditions and validated in realistic Li-S pouch cells.

Impact. ASSLBs have the potential to achieve higher energy and power densities, extending the range of EVs and reducing charging time simultaneously. The success of the project would advance the research and deployment of superionic SEs and protective Li-compatible interlayers to support the DOE Vehicle Technologies Office (VTO) target of developing next-generation ASSLBs for EVs, accelerating market acceptance of long-range EVs required by the EV Everywhere Grand Challenge.

Approach. The project proposes the following approach: (1) to develop Li-compatible superionic sulfide-based SSEs and effective coating approaches, (2) to stabilize Li/SSE interface by employing a multifunctional interlayer, (3) to enable robust Li^+/e^- mixed conduction network for a high-loading sulfur cathode, (4) to develop dry processing for SSE film, cathode, and interlayer fabrication, and (5) to advance the mechanism study of the sulfur cathode, lithium anode, and interfaces by multiscale characterization and multiscale modeling.

Out-Year Goals. This project has the following out-year goals:

- Development of Li-metal-compatible S-SSEs with Li/SSE interfacial resistance $< 5\ \Omega cm^2$ and room-temperature Li^+ conductivity > 5 mS/cm.
- Operation of lithium anode at CCD > 1 mA/cm^2, and lithium cycling for at least 400 cycles.
- Ultra-thin multifunctional interlayer to enable deep lithium cycling > 4 mAh/cm^2 to couple high areal-capacity cathode.
- Dry processing of an SSE/interlayer assembly with an overall ionic conductivity > 1 mS/cm.
- Validation of the S-SSE, high-areal capacity cathode, and bilayer assembly in a realistic Li-S pouch cell.

Collaborations. This project engages in collaboration with the following: D. Y. Qu (UWM), C. M. Wang (Pacific Northwest National Laboratory, PNNL), H. Du (Ampcera Inc.), J. Bao (PNNL), and Z. Liu (Thermo Fisher Scientific).

Milestones

1. Synthesis of lithium halides doped S-SSE to realize low Li/SSE areal interfacial resistance (AIR $< 5\ \Omega cm^2$) and high room-temperature Li^+ conductivity ($\sigma \sim 6$ mS/cm). (Q1, FY 2022; In progress)
2. Development of surface treatment approach to improve moisture stability of S-SSE. (Q2, FY 2022)
3. Optimization, characterization, and simulation of Li/SSE interface and its dynamics. (Q3, FY 2022)
4. Optimization of external pressure to improve CCD (> 1 mA/cm^2) and Li/SSE/Li cycle life (> 400 cycles). (Q4, FY 2022)

Progress Report

Progress for this new project will be reported next quarter.

Patents/Publications/Presentations

The project has no patents, publications, or presentations to report this quarter.

Task 1.6 – Development of Thin, Robust, Lithium-Impenetrable, High-Conductivity, Electrochemically Stable, Scalable, and Low-Cost Glassy Solid Electrolytes for Solid-State Lithium Batteries (Steve Martin, Iowa State University of Science and Technology)

Project Objective. The project objective is to develop new Li^+-conducting mixed oxy-sulfide nitride (MOSN) glassy solid electrolytes (GSEs) that are impermeable to lithium dendrites, have high conductivities, are scalable through low-cost glass manufacturing, are chemically and electrochemically stable, and will enable low-cost, high-energy-density solid-state lithium batteries (SSLBs). The SSLBs constructed from these new GSEs will meet and exceed all program objectives: usable specific energy @ C/3 $\geq$ 350 Wh/kg, calendar life of 15 years, cycle life (C/3 deep discharge with < 20% energy fade) of 1000, and cost $\leq$ \$100/kWh.

Project Impact. This project will enable the team to demonstrate the following: (1) thin MOSN GSE films yield superior performance in a much safer, lower-cost, and Li-dendrite impenetrable form, and (2) high rate and long cycle life can be achieved in SSLBs using thin-film MOSN GSEs. The new GSEs in SSLBs are anticipated to increase energy density (anode basis) from ~ 300 mAh/g to ~ 4,000 mAh/g, enabling replacement of internal combustion engines in both light-duty and heavy-duty vehicles. Each 20% reduction in the ~ 1.6 billion liters of gasoline used per day in the United States would reduce CO_2 emissions by ~ 4 billion kg or 2×10^{12} l of CO_2 per day. The team will also increase scientific and engineering knowledge of thin-film GSEs in SSLBs.

Approach. The MOSN mixed glass former (MGF) glasses used for the GSEs in this project were developed in previous work to have the necessary thermal stability and high ionic conductivity for successful use as a drawn-film electrolyte. In this project, the glass chemistry will be tuned for even more desirable properties, by investigating structure-property relationships and testing variations in glass chemistry.

Out-Year Goals. Work will progress toward developing a glass capable of being drawn to 100-µm thickness, while having high conductivity and electrochemical stability and good cycling ability.

Collaborations. There are no active collaborations this quarter.

Milestones

1. Accomplish: Large MOSN MGF GSE preforms (10 cm x 0.5 cm x 30 cm) demonstrate < 1 vol% crystallization at 90°C above the glass transition temperature. (Q1, FY 2022; Completed)
2. Accomplish: Optimize draw conditions for MOSN GSE to achieve 5 m × 5 cm × < 50 µm thin films. (Q2, FY 2022; In progress)
3. Accomplish: Fabricate MOSN MGF Li|GSE|Li cells in intermediate area format, ~ 2 cm^2. (Q3, FY 2022; In progress)
4. *Go/No-Go Decision*: Fabricate MOSN MGF GSE cells in large format ~ 5 cm^2. Cells achieve targeted performance metrics. Analysis indicates technical approach capable of achieving performance targets. (Q4, FY 2022; In progress)

Progress Report

Task 1. Development of Optimized High Li^+ Conductivity MOSN MGF GSEs

Initiate Development of Preforms of MOSN MGF GSEs that do not Crystallize

This quarter, efforts continued to further develop and optimize compositions of the team's MOSN MGF GSEs. Previous efforts on the ISU-9 series continued, with minor setbacks. Between different batches of the ISU-9, z = 1.0 glass, a difference in working range was found of more than 70°C. From Raman spectroscopy done on each batch, it appears that the batch with the lower working range had free sulfur, leading to a lower crystallization temperature; work has been done to improve the purity and quality of the raw materials prior to melting. The team is testing different lithium silicates as dopants in this system.

Table 1. Chemical composition and naming scheme of various mixed oxy-sulfide nitride glasses.

Sample ID	Compositional Formula
ISU-5	$0.60Li_2S + 0.40SiS_2 + 0.1LiPO_3$
ISU-6	$0.58Li_2S + 0.315SiS_2 + 0.105LiPO_3$
ISU-7(x)	$0.58Li_2S + 0.315\ SiS_2 + 0.105\ [(1\text{-}x)\ Li_{0.67}PO_{2.87} + xLiPO_{2.83}N_{0.314}]$
ISU-8(x, y)	$yLi_2S + 0.75(1\text{-}y)SiS_2 + 0.25(1\text{-}y)LiP_{1\text{-}x}Al_xO_{3\text{-}x}$
GSE-1	$yLi_2S + (1\text{-}y)[(1\text{-}x)SiS_2 + xLiPO_3]$
ISU-9(z)	$0.58Li_2S + 0.315SiS_2 + 0.105[(1\text{-}z)LiPO_3 + zLi_2SiO_3]$

Efforts have been made to further understand the atomic level structures of one of the team's more promising MOSN GSEs, ISU-7. In particular, the various previously mentioned analytical spectroscopy techniques have been useful in identifying many of the chemical bonds in these glasses and other important structural information; however, they have been unable to detect nitrogen in the glass. As a result, the team has shifted to using techniques that are more sensitive to the elemental composition of these materials. Thus, X-ray photoelectron spectroscopy (XPS) was used to identify the elemental makeup in these MOSN MGF GSEs. The XPS spectra were collected for the ISU-7 series of glasses (Table 1) for $x = 0$, 0.1, and 0.2, and are given in Figure 2a. It can be noted in Figure 2 that not only can a nitrogen signal be easily detected for these glasses, the team can also determine from the chemical shift of the nitrogen 1s peak that nitrogen is present in two structural bonding configurations. One arrangement is tri-coordinated nitrogen (often referred to as NT), and the other is di-coordinated nitrogen (often referred to as ND). An example of these two types of nitrogen species is shown in Figure 2b. The presence of nitrogen is within expectations, and it is assuring that these GSEs do indeed contain nitrogen. However, it is significant to note that when carefully analyzing the XPS data, the presence of nitrogen can be seen in $x = 0$ where there is no LiPON incorporated into the sample. Nominally, of course, this sample should not contain any nitrogen. Given that is does, the team conducted experiments to determine the origin of the adventitious nitrogen in the nominally and supposedly nitrogen-free x = 0 GSE.

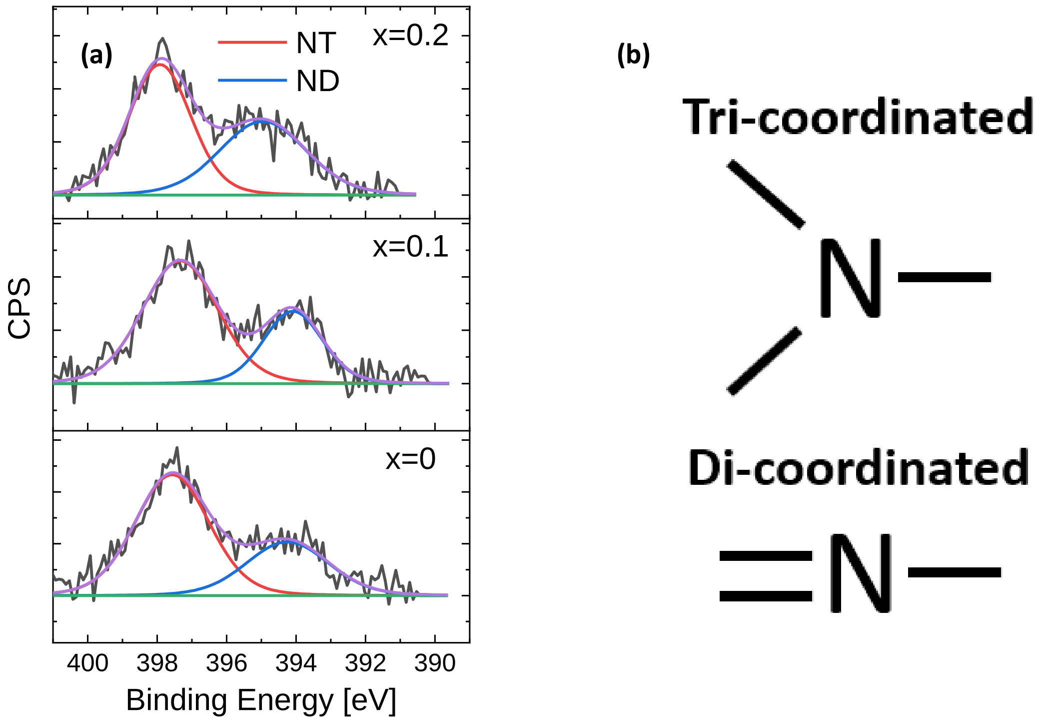

Figure 2. (a) X-ray photoelectron spectra of ISU-7 {$0.58Li_2S + 0.32SiS_2 + 0.1[(1\text{-}x)Li_{0.67}PO_{2.87} + xLiPO_{2.83}N_{0.314}]$} $x = 0$, 0.1, 0.2 with tri-coordinated (NT) and di-coordinated (ND) nitrogen modes present. (b) Examples of NT and ND nitrogen in the glassy solid electrolytes.

XPS was performed on the raw material $Li_{0.67}PO_{2.87}$ and, as seen in Figure 3a, both NT and ND are present. This material is synthesized outside of the glovebox using lithium carbonate and ammonium phosphate dibasic, $(NH_4)_2HPO_4$. The byproducts of this reaction are water, oxygen, and ammonia, and it appears that the ammonia byproduct reincorporates itself into the $Li_{0.67}PO_{2.87}$, similar to how the team's lab uses ammonolysis to synthesize LiPON. To test this hypothesis, $Li_{0.67}PO_{2.87}$ was then synthesized inside of the glovebox using pure and nitrogen-free Li_2O and P_2O_5. XPS was performed to determine if nitrogen was present in this glass. As expected, Figure 3b shows no substantial nitrogen signal in this material; thus, it was found that the synthesis of $Li_{0.67}PO_{2.87}$ outside the glovebox using nitrogen-bearing starting material, $(NH_4)_2HPO_4$, leads to incorporation of nitrogen into the starting material, which in turn leads to the presence of nitrogen in these GSEs.

The team then remade the ISU-7 series of GSEs using the $Li_{0.67}PO_{2.87}$ that was synthesized inside the glovebox without nitrogen precursors. After remaking ISU-7 with the new nitrogen-free $Li_{0.67}PO_{2.87}$, XPS was conducted on this new series of ISU-7 ($x = 0$, 0.1, 0.2) GSEs; the spectra are given in Figure 3. As can be seen and as expected, there is no nitrogen present in the $x = 0$ spectra and for $x = 0.1$ and 0.2, NT and ND are present. This is promising information, as this can provide insight into the impact that nitrogen incorporation has on GSE properties. Future studies will aim to use XPS to characterize the GSE structure to compare the difference between the starting material made inside the glovebox versus the material made outside the glovebox.

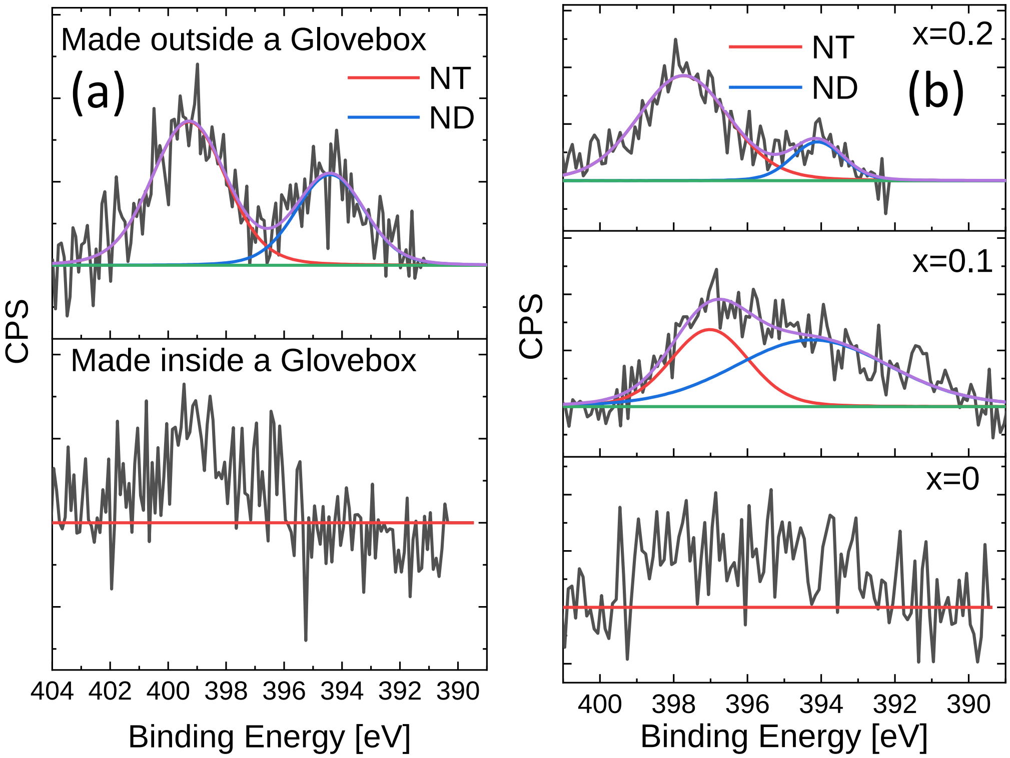

Figure 3. (a) X-ray photoelectron spectra (XPS) of $Li_{0.67}PO_{2.87}$ made outside the glovebox and inside the glovebox. (b) XPS spectra of ISU-7 (x = 0, 0.1, 0.2) with the new $Li_{0.67}PO_{2.87}$. Tri-coordinated nitrogen (NT) and di-coordinated nitrogen (ND) signal can only be seen in x = 0.1, 0.2, while x = 0 remains clear of any nitrogen signal.

Work has also been done to further explore the GSE-1 series. In the previous report, Fourier transformation infrared (FTIR) spectroscopy data were gathered for GSE-1, $y = 0.58$, $x = 0$ to 1. To further expand the study of these GSEs, the team also examined $y = 0.56$ and $y = 0.60$ glasses. Figure 4a-c shows the FTIR spectra of the $x = 0$, 0.2, 0.5, 0.8, one from each GSE-1, respectively, with $y = 0.60$, 0.58, and 0.56. It can be seen that each spectrum is rather similar. However, in comparison to the synthesis of these materials, it was found that for $y = 0.56$ and $y = 0.6$ GSEs, they readily crystallized at lower x-values around $x = 0.6$. This means that these GSEs will rather crystallize when more $LiPO_3$ is added to them, while $y = 0.58$ will not crystallize until $x = 0.7$. This information can assist in understanding the tunability of these GSEs. Future work will be conducted to incorporate nitrogen and determine the impact it can have on these materials.

To further characterize the crystallization and viscosity behavior of the project's glasses, differential scanning calorimetry (DSC) experiments were performed and analyzed to determine the crystallization temperature and the viscosity behavior through the Mauro–Yue–Ellison–Gupta–Allan model (MYEGA) model. As such, the team can now predict the viscosity behavior of other glasses at varying temperatures, including the ISU-9, $z = 1.0$ glass. Several samples of each series were run, and linear regression was utilized to determine the fragility index, m, along with an appropriate 95% confidence interval of the viscosity, with previously reported glass systems being retested to confirm results. These new viscosity curves are plotted in Figure 5.

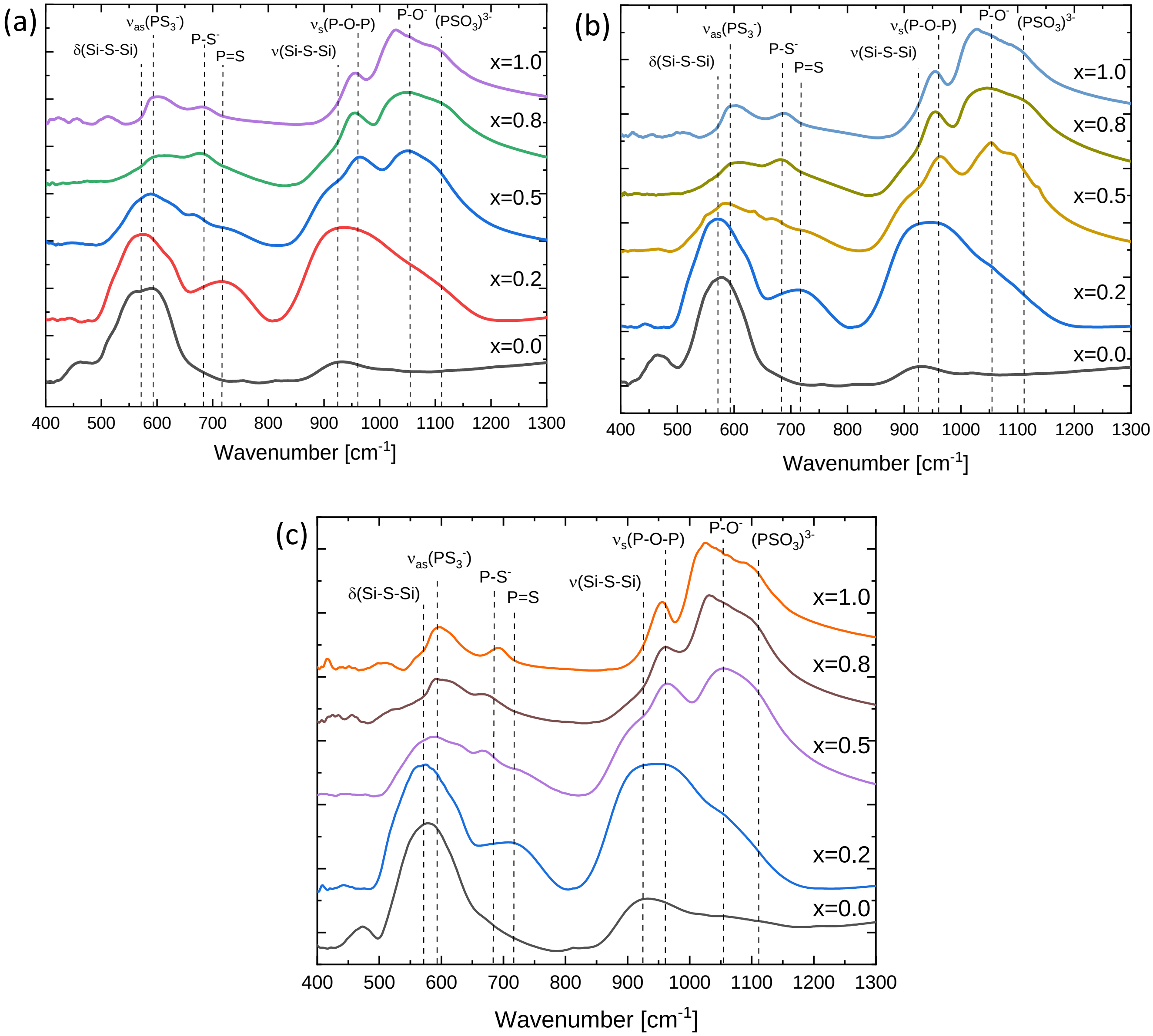

Figure 4. Fourier Transformation Infrared (FTIR) spectra of yLi$_2$S + (1-y)[xSiS$_2$ + (1-x)LiPO$_3$] series ranging from 0.0 ≤ x ≤ 1.0 with modes identified to respective bonds. For (a) y = 0.6, (b) y = 0.58, and (c) y = 0.56, these spectra appear similar; however, there are reductions in intensity in select modes suggesting that there is a change in chemistry.

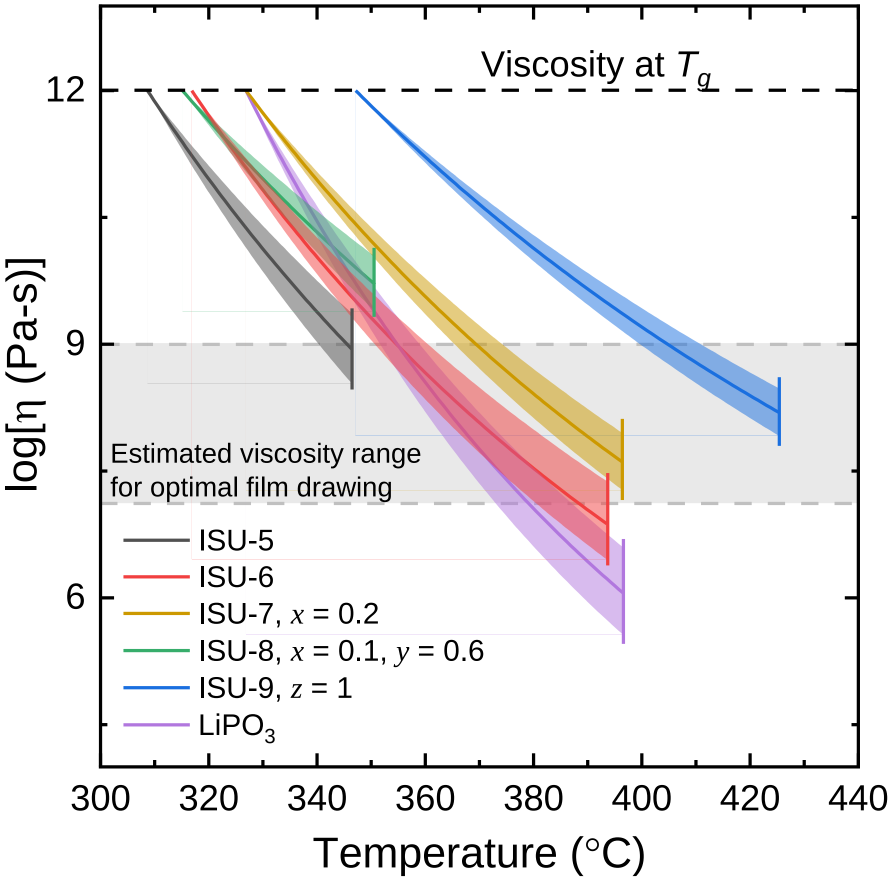

Figure 5. Plot showing the viscosity curves of various studied glass from the MYEGA model and their crystallization at 1°C/min heating rate. Shaded regions indicate a 95% confidence interval for the fragility parameter.

Task 2. Develop Micro-Sheet Glass Ribbon Processing Facility for GSEs

Continue to Develop and Optimize the GSE Micro-Sheet Glass Ribbon Processing Facility

Optimization efforts continued for the Micro-Sheet Glass Ribbon Processing Facility to improve ribbon drawing capabilities. Lithium metaphosphate ($LiPO_3$) film was produced in large quantities for testing cathode application techniques. While working with the $LiPO_3$, several tests were conducted. The drawing process was stopped, allowing the furnace to cool to room temperature, then restarted, with no breakage or loss of material. Several collection techniques for the finished film were tested, using a hot wire knife for clean collection of the $LiPO_3$ film, or for continuous removal of the edge material. Once the edge material was removed, the thin, flexible ribbon was rolled around a tube. Unfortunately, this was unsuccessful, with the $LiPO_3$ film breaking multiple times.

Additional work on improving surface quality of drawn thin film was conducted as part of a concurrent sodium GSE project. The thin glass ribbon produced by the drawing process is sensitive to moisture, and a pristine surface is necessary for optimal interfacial behavior when fabricating cells. Once pieces of film are collected, they are transferred to a separate glovebox, leading to some surface contamination. To prevent this, a new transfer container was designed that allows for a better seal and flushing of inert gas from nitrogen to argon. The equipment and procedures developed for these sodium GSE films will also be applied to lithium GSE films.

Task 3. Develop Processing Conditions Micro-Sheet Ribbons of MOSN MGF GSEs

Complete Optimization of Draw Conditions for Optimized MOS MGF GSEs < 50 μm

Work has started to produce ISU-6 glass in numerous small, high-quality batches, which can then be combined to form a large ~ 200 g preform. Previous large preforms made by melting and casting all of the ~ 200 g of glass from raw materials in a single melt and have experienced crystallization during the drawing process. These attempts were produced and melted as one large batch, which resulted in lower quality glass; any inhomogeneity in the preform may have caused heterogenous crystallization. Small-batch processing has been found to result in higher quality glass, for example, by preventing low-temperature heterogenous crystallization and allowing for drawing. Several batches have been completed with the intent to fully draw high-quality MOS GSE thin films next quarter. Prior to the small batches being combined and remelted into one homogenous melt, DSC experiments will be run to confirm homogeneity of the glass batches and ensure that each batch is on chemistry and high quality. Analysis of the glass transition and crystallization temperatures of each batch compared to expected values from previously studied small batches will enable this. Further testing through Raman spectroscopy may also be conducted to ensure that the short-range order structures of each batch are as expected and that no major impurities are present. Through the team's viscosity and crystallization studies of small batches of the various GSE compositions, current analysis indicates that a high-quality preform of ISU-6 will be able to be drawn into a thin film.

Task 4. Fabricate and Test ASSLB GSEs in Large Area Planar Formats

Complete Testing of Optimized MOSN MGF GSE in Intermediate Cell Format ASSLBs

Complete Testing of Optimized MOSN MGF GSE in Large-Cell Format ASSLBs

Cyclic voltammetry (CV) of the ISU-9, z = 1.0 composition was conducted in small-cell format to determine the electrochemical stability window of the GSE. The voltammogram is shown in Figure 6. Similar to previously reported data, the ISU-9 composition shows good stability in the range from 0-5 V versus Li/Li$^+$. Minor peaks are present from 0.8-2.2 V, which appear to be from residual sulfur from the SiS$_2$. These peaks appear smaller in this graph than for previously reported glass series, indicating that the ISU-9 series may be slightly more stable than previously reported compositions.

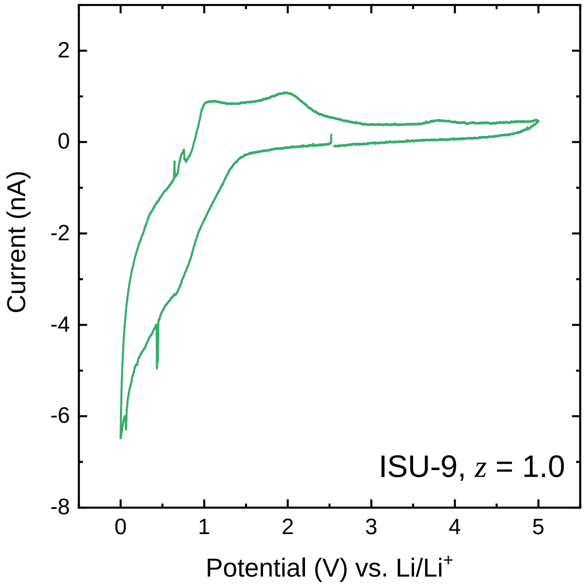

Figure 6. Cyclic voltammogram for the ISU-9, z = 1.0 composition showing overall stable behavior with minor oxidative peaks around 0.8-2.2 V.

To assess performance of the GSEs in a variety of full-cell formats, coin cells were assembled using indium foil as the anode, bulk ISU-6 as the GSE, and $LiFePO_4$-coated aluminum foil as the cathode material. A solvate ionic liquid (IL) consisting of a triglyme solvent and lithium trifluoromethanesulfonimide (LiTFSI) salt was placed at the cathode-GSE interface to reduce interfacial resistance. These cells were tested using CV and galvanostatic cycling. As seen in Figure 7a, CV of the full cells show two clear peaks correlating to the oxidation and reduction reactions of the In-Li system. There is a relatively large overpotential present in this cell that may be attributed to polarization in the relatively thick glass disk (~ 1 mm). It is believed that this polarization will decrease when utilizing a thin-film MOS GSE of significantly, that is, orders of magnitude, smaller overall impedance. No other undesired redox reactions were observed in the voltammogram. Galvanostatic cycling of the full cells revealed stable cycling up to 55 cycles at a charge rate of C / 20, shown in Figure 7b. Cycling also shows relatively high-capacity retention with small capacity changes between cycles believed to be from moderate temperature changes in the lab. Testing in a more temperature-controlled location would lead to more consistent results, and work is being done to better control the environment where cells are tested.

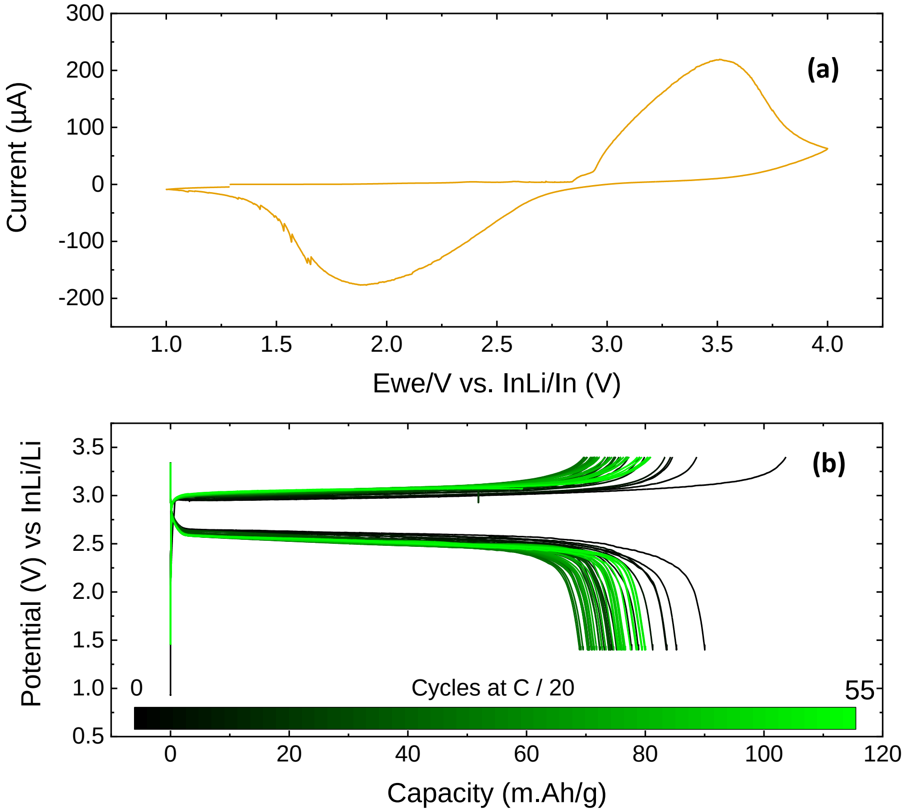

Figure 7. (a) Cyclic voltammogram showing stable redox behavior of an In | ISU-6 | $LiFePO_4$ full cell with a small amount of ionic liquid (IL) on the cathode. (b) Cycling behavior of an In | ISU-6 | $LiFePO_4$ full cell with a small amount of IL on the cathode showing stable cycling with low capacity fade.

Patents/Publications/Presentations

Presentations

- Glass & Optical Materials Division (GOMD) Annual Meeting (December 2021): "Structure and Electrochemical Properties of $0.6\ Li_2S + 0.3\ SiS_2 + LiP_{1-x}Al_xO_{3-x}$ Glassy Solid-State Electrolytes"; J. Wheaton, S. Leland, S. Kmiec, and S. Martin.
- GOMD Annual Meeting (December 2021): "The Incorporation of LiPON in the Mixed Oxy-Sulfide-Nitride Solid Electrolyte: $0.58\ Li_2S + 0.315\ SiS_2 + 0.105\ [(1\text{-}y)\ Li_{0.67}PO_{2.83} + y\ LiPO_{2.53}N_{0.31}]$"; V. Torres, P. Philipp, S. Kmiec, and S. Martin.

Task 1.7 – All-Solid-State Batteries Enabled by Multifunctional Electrolyte Materials
(Pu Zhang, Solid Power Inc.)

Project Objective. The project objective is to develop Li-metal SSBs enabled by multifunctional SSEs for EV application. The ultimate goal is scalable production of large-format ASSBs able to deliver ≥ 350 Wh/kg specific energy, ≥ 1000 cycle life, and ≤ $100/kWh cost.

Project Impact. The project is enabling scalable production of large-format ASSBs required by the vehicle market and is building domestic battery manufacturers as leaders in the global vehicle ASSB production. The proposed technology will address key limitations of state-of-the-art lithium batteries to meet DOE EV battery targets and accelerate their adoption as large-format EV batteries for sustainable transportation technology.

Approach. The project will develop a high-performance Li-metal solid-state cell enabled by a multifunctional SSE. The new SSE will (1) have high conductivity (up to 10 mS/cm), (2) be stable against lithium metal and high-voltage cathode (0-4.5 V), (3) promote uniform lithium plating (enabling > 2C charge rate), and (4) be compatible with large-scale manufacturing processes. The specific cell chemistry to be demonstrated will be the SSE with Li-metal anode and high-nickel-content Li-metal oxide cathode. The solid-state cell will be assembled by scalable roll-to-roll processes developed by Solid Power.

Out-Year Goals. In Year 1, multifunctional SSE will be developed with lithium ionic conductivity of $\geq 3 \times 10^{-3}$ S/cm. CCD of ≥ 6 mA/cm^2 will be achieved in a symmetric lithium cell. The SSE design concept will be proven by demonstrating cycle life of ≥ 200 in a full cell. In Year 2, SSE material will be optimized with lithium ionic conductivity of $\geq 5 \times 10^{-3}$ S/cm. Scalable cell assembly processes will be developed. Cycle life of ≥ 500 will be demonstrated in a full cell. In Year 3, large-format solid-state cells (> 2Ah) will be assembled/tested to meet the final goal: ≥ 350 Wh/kg, ≥ 1000 cycles, and ≤ $100/kWh cost.

Collaborations. The proposed team consists of Solid Power and a subcontractor, University of California, San Diego (UCSD). Solid Power (PI: P. Zhang) will develop the multifunctional SSE and other cell components, assemble cells, and conduct cell tests. UCSD (Principal Investigator, or PI: Y. S. Meng) will carry out material characterization by using advanced techniques such as XPS, cryogenic – scanning transmission electron microscopy (cryo-STEM) imaging, cryo-STEM energy dispersive X-ray spectroscopy (EDS), electron energy loss spectroscopy (EELS), and cryogenic – focused ion beam (cryo-FIB) milling. The UCSD team seeks to quantify the kinetics and evolution of each contributing factor and its impact on battery performance.

Milestones

1. Charge rate ≥ 2C. (Q1, FY 2022; Completed)
2. SSE film ≥ 10 m and ≤ 40 µm. (Q2, FY 2022; Completed)
3. Pouch cell ≥ 2 Ah. (Q3, FY 2022; In progress)
4. Cycle life ≥ 1000. (Q4, FY 2022; In progress)

Progress Report

Charge Rate ≥ 2C. A lab-scale pouch cell was assembled by using a multifunctional SSE separator, an NMC-622 composite cathode (at 3 mAh/cm^2), and a Li-metal foil anode. Rate capability of the cell was evaluated by charging and discharging symmetrically from C/10 to 2C at 70°C. As shown in Figure 8, the cell retained 78% capacity at 2C, when compared to C/10. This result indicates that a solid-state Li-metal cell is capable of fast charging at an elevated temperature. The future development focus will be demonstrating the fast charge capacity at lower temperatures.

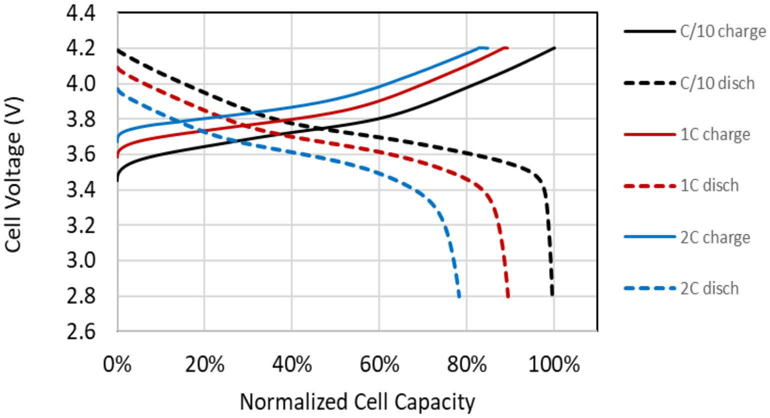

Figure 8. Rate capacity of an NMC/Li-metal solid-state pouch cell with multifunctional solid-state electrolyte at 70°C.

SSE Film Fabrication. The SSE separator coating process has been developed at pilot scale. A separator slurry was prepared by mixing the SSE powder, a binder, and a solvent by using a planetary mixer. The slurry was then cast on a carrier film on a slot-die coater. The separator length and thickness target (≥ 10 m and ≤ 40 µm) was met this quarter. Figure 9 shows a separator film of 30 µm as coated.

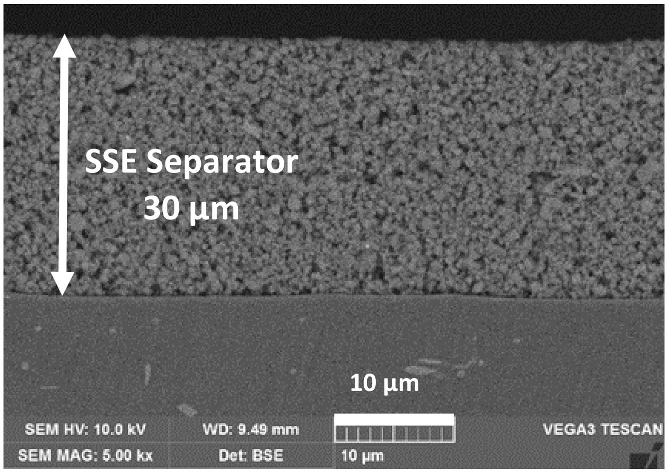

Figure 9. A slurry-cast solid-state electrolyte separator film ≤30 µm.

Patents/Publications/Presentations

The project has no patents, publications, or presentations to report this quarter.

Task 1.8 – Developing Materials for High-Energy-Density Solid-State Lithium-Sulfur Batteries (Donghai Wang, Pennsylvania State University)

Project Objective. The project objectives are to develop materials involving advanced S-C composite materials, solid additives, and sulfide-based SSEs, and to acquire knowledge for Li-S ASSBs. Li-S ASSBs with large areal sulfur loading (≥ 5 mg cm^{-2}) and high sulfur content (≥ 50 wt% in cathode), pairing with lithium or lithium alloy anode, will deliver a high initial specific capacity of over 1200 mAh g^{-1} at high charge/discharge rate (> 0.3 C) for 500 cycles with over 80% capacity retention.

Project Impact. This project aims to develop new materials to enable Li-S ASSBs with high energy density, excellent cycling stability, and good rate performance, and thus to build knowledge for fabrication of prototype Li-S ASSBs. Specifically, the developed new materials will greatly increase the specific capacity of sulfur and sulfur utilization at high areal sulfur loading, alleviate the interfacial problem between S-C composite and SSE within sulfur cathode, boost Li-ion conductivity, and improve moisture stability of glass and glass-ceramic sulfide-based SSE. Meeting the technical targets will potentially promote development of high-energy-density Li-S ASSBs and their practical application in EVs and plug-in hybrid EVs (PHEVs) and will also reduce petroleum consumption in the transportation sector by helping battery-powered vehicles become more accepted by consumers as a reliable source of transportation.

Approach. The project goal will be accomplished through developing new materials, together with in-depth characterization of sulfur cathode. Specifically, approaches to realize the project objectives include the following: (1) development of new carbon material with unique structure, high surface area, and large pore volume; (2) development of new S-C and S-C-M_xS_y materials (M = Li, Co, Ti, Mo, etc.) to facilitate electron/ion transport; (3) development of novel additives to tune interfacial behavior among components in the cathode; (4) development and optimization of new SSE through cation and anion doping with superior properties such as high ionic conductivity, good moisture, and stability; and (5) diagnostics, characterization, and cell tests on the developed new material or advanced sulfur cathode.

Out-Year Goals. The out-year goals are as follows: (1) develop and optimize sulfur cathode materials and synthesize new SEs (ionic conductivity above 5 mS cm^{-1} at room temperature), and (2) conduct characterization and performance tests on both material and electrode levels. The final demonstration will be all-solid-state sulfur cathodes with over 1200 mAh g^{-1} discharge capacity at 0.3 C discharge rate and 50 wt% sulfur content for 500 cycles at room temperature.

Collaborations. There are no active collaborations.

Milestones

1. Demonstrate sulfur cathode with high areal sulfur loading (≥ 5 mg cm^{-2}) and 50 wt% sulfur content over 1000 mAh g^{-1} discharge capacity at 0.1 C rate at 25°C for 10 cycles. (Q1, FY 2022; In progress)
2. Demonstrate new SE with ionic conductivity > 3 mS cm^{-1} at 25°C. (Q2, FY 2022; In progress)
3. Demonstrate sulfur cathode with high areal sulfur loading (≥ 5 mg cm^{-2}) and above 50 wt% sulfur content over 1000 mAh g^{-1} discharge capacity at 0.3 C rate at 25°C for 50 cycles. (Q3, FY 2022; In progress)
4. Demonstrate sulfur cathode with high sulfur content (> 50 wt%) and over 1200 mAh g^{-1} at 0.3 C rate for 500 cycles (< 20% capacity decay) at room temperature, and new SEs with ionic conductivity > 5 mS cm^{-1} at 25°C. (Q4, FY 2022; In progress)

Progress Report

New Sulfur Cathode for ASSLSBs. The team's previous findings revealed that a highly efficient ionic and electronic pathway within cathode composites plays an important role in improving the electrochemical performance of sulfur cathodes. Thus, they focus on developing novel advanced sulfur cathode materials with good component uniformity and efficient ionic and electronic pathways for ASSLSBs. Moreover, combined with the optimization of cathode compositions, cathode additives, and preparation processes, the new advanced sulfur cathode materials enabled superior sulfur utilization at room temperature. The cycling performance of the developed advanced sulfur cathode is illustrated in Figure 10. The sulfur cathode was first electrochemically activated at 0.05 A g^{-1} (based on the weight of the whole sulfur cathode) for three cycles and then subsequently cycled at 0.1 A g^{-1} (= 0.12 C). During the first few cycles, the discharge specific capacity can reach up to 1200 mAh g^{-1}. After increasing the current rate to 0.12 C, the cell can still achieve above 1000 mAh g^{-1} discharge capacity at room temperature. The sulfur cathode with moderate sulfur loading of 2.055 mg cm^{-2} and high sulfur content of 50 wt% shows superior cycling stability for over 250 cycles. Even after 250 cycles, the discharge specific capacity remains high at 987.8 mAh g^{-1}. Testing of the sulfur cathode with high areal sulfur loading ≥ 5 mg cm^{-2} is ongoing and will be reported on next quarter. Based on the excellent performance of sulfur cathode at moderate sulfur loading, the team expects the high discharge specific capacity could be maintained at higher areal sulfur loading, and the Q1 milestone could be fulfilled next quarter.

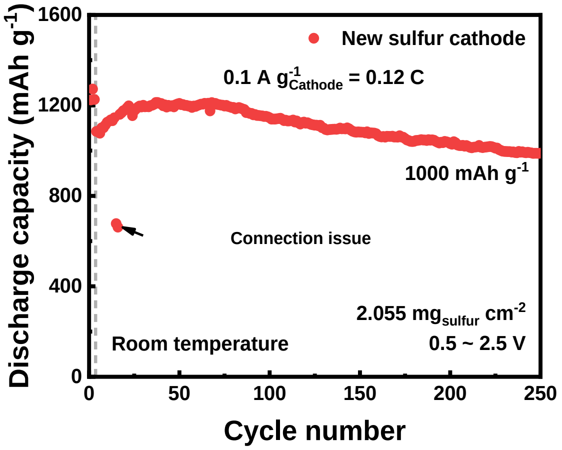

Figure 10. Long-term cycling performance of the new sulfur cathode composite under 0.1 A g^{-1} (= 0.12 C) between 0.5 V to 2.5 V at room temperature. The discharge capacity is based on the weight of sulfur.

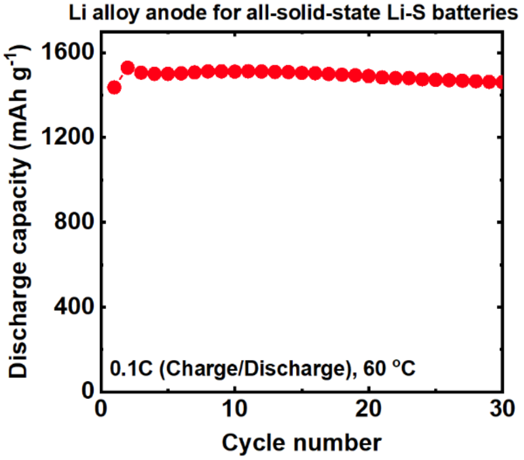

Figure 11. Long-term cycling performance of newly synthesized Li-alloy anode for all-solid-state Li-S batteries under 0.1 C rate at 60°C. Specific capacity is based on the weight of sulfur.

Li-Alloy Anodes for ASSLSBs. This quarter, the team also developed lithium alloy anodes for ASSLSBs. The lithium alloy is prepared by the high-energy ball-milling method with optimization of the composition, synthesis condition, and milling time. The discharge specific capacities of the sulfur cathode versus Li-alloy anode are illustrated in Figure 11. Under 0.1 C and between 1.1-2.8 V at 60°C, the initial discharge specific capacity can reach up to 1436.25 mAh g^{-1} (sulfur loading is ~ 2.19 mg cm^{-2}). After the 5th, 10th, and 20th cycles, discharge specific capacities are close to 1490 mAh g^{-1}. Even after the 30th cycle, the cell can still maintain 1460 mAh g^{-1} discharge specific capacity. It shows that Li-alloy anode has potential to be used in ASSLSBs and can have stable, long-term cycling performance.

Patents/Publications/Presentations

The project has no patents, publications, or presentations to report this quarter.

Task 1.9 – Hot Pressing of Reinforced Lithium-NMC All-Solid-State Batteries with Sulfide Glass Electrolyte

(Thomas Yersak, General Motors, LLC)

Project Objective. The project objective is to research, develop, and test Li-NMC ASSBs capable of achieving program performance metrics by implementing sulfide glass SSEs and hot-press processing in a dry-room environment. The performance of ASSBs with sulfide SSEs is limited because they are essentially green tapes with up to 20% porosity. In composite cathodes, the porosity limits energy density and power, while porosity in the separator acts as a conduit for Li-metal deposits if cycling conditions (C-rate, operating temperature, and pressure) are not strictly controlled. The project goal is to demonstrate that the hot-pressing method and appropriately formulated sulfide glass SSEs can eliminate porosity to enable Li-NMC ASSBs with energy density of > 350 Wh/kg.

Project Impact. The hot-press processing method and appropriately formulated sulfide glass SSEs may enable Li-NMC ASSBs with improved energy density > 350 Wh/kg. The General Motors (GM) processing technology depends on heating a sulfide glass SSE above its glass transition temperature, T_g, at which point it can consolidate via viscoplastic flow. In the composite cathode, hot-pressing provides liquid-like contact between the NMC cathode and SSE to increase energy density and power by enabling thick composite cathodes with high active material loading. Furthermore, cathode-supported sulfide glass separators can be made dense and thin by hot-pressing. A dense separator enables the use of Li-metal anodes because lithium deposits may be more effectively blocked, preventing cell shorting.

Approach. The sulfide SSE used in the composite cathode, otherwise known as the catholyte, will dictate the processing specifications for ASSB hot-pressing. Thermal stability can be achieved by NMC passivation and proper catholyte formulation. This project will systematically evaluate different NMC coatings, catholyte formulations, and hot-press processing specifications (temperature, time, and pressure). The performance of hot-pressed ASSBs will be compared to green baseline ASSBs and hot-pressed control ASSBs consisting of the β-Li_3PS_4 and Li_6PS_5Cl model SSEs. Electron microscopy will be employed to understand interfacial phenomena and track composite cathode microstructure before and after hot-pressing.

Out-Year Goals. In the second year of this project, a sulfide glass SSE will be formulated specifically for use as the separator. The separator glass SSE formulation will be designed to achieve full densification under the hot-press processing specifications determined for the catholyte. Separator glass formulation design will also consider cathodic stability, moisture stability, and ionic conductivity. Once a system of separator glass SSE and catholyte has been determined, the third year of the project will demonstrate hot-pressed full cells at the coin-cell and single-layer pouch-cell levels, meeting program target performance metrics.

Collaborations. GM will lead this project with no subrecipients.

Milestones

1. Report ionic conductivity of separators with multifunctional reinforcement. Decide whether to carry forward multifunctional reinforcement for the remainder of the project. (Q1, FY 2022; Completed)
2. Demonstrate that H2S generation of target separator glasses and catholytes can be cut by 50% in a -40°C dewpoint dry-room environment. Report functional characteristics of SSEs after exposure. (Q2, FY 2022; In progress)
3. Based on results collected during Budget Period 2, the best performing separator glasses will be carried forward for the remainder of the project. (Q3 FY 2022; In progress)
4. Retrofit glovebox: implement a simulated dry-room environment inside an inert glovebox by designing and installing custom equipment. (Q4, FY 2022)

Progress Report

This quarter, the team studied electrochemical performance of hot-pressed cathode composites with NCM cathode active material (CAM) and sulfide SSE catholytes. They reported that a cathode composite of NCM-622 and $75Li_2S\cdot25P_2S_5$ (glassy Li_3PS_4) retained adequate cyclability after hot-pressing at 200°C.[1] Hot-pressing of a cathode/separator stack consolidates SSE to improve energy density of the cathode composite and to block lithium deposits from shorting the separator. The second budget period, therefore, focuses on study of SSE materials for cathode-supported separators. This report will cover progress last quarter and this quarter. As previously communicated, the project was on hold until October 14, 2021, pending DOE Foreign National approval of critical contract resources. Three topics will be covered: namely, the process rheology of ternary glasses, the implementation of a 3-electrode test cell, and the evaluation of a multifunctional reinforcement.

The process rheology of glass electrolytes was assessed to improve consolidation of cathode-supported separators during hot pressing. This work supports the overall goal for Budget Period 2. The team studied the binary $70Li_2S\cdot30P_2S_5$ and the ternary $70Li_2S\cdot(30\text{-}x)P_2S_5\cdot xA$ glass compositions, where *A* represents a third glass component. They assessed process rheology by measuring porosity and sample diameter before and after hot pressing. A picture of samples after processing (Figure 12a) shows that the ternary glass composition decreases the load required to achieve adequate consolidation. In fact, the ternary sample's diameter increased by 79% under a 1 metric ton load (74 MPa nominal pressure), whereas the binary sample's diameter increased by only 12.6% under a higher 5 metric ton load (370 MPa nominal pressure). The team's previous work showed that NCM is susceptible to microcracking when consolidated at a 370 MPa pressure.[1] Decreasing the process load is critical to preserve mechanical integrity of high-Ni content polycrystalline NCM particles within the cathode support. Current work investigates lowering the process temperature and residence time to limit degradation of the NCM/catholyte interface within the cathode support.

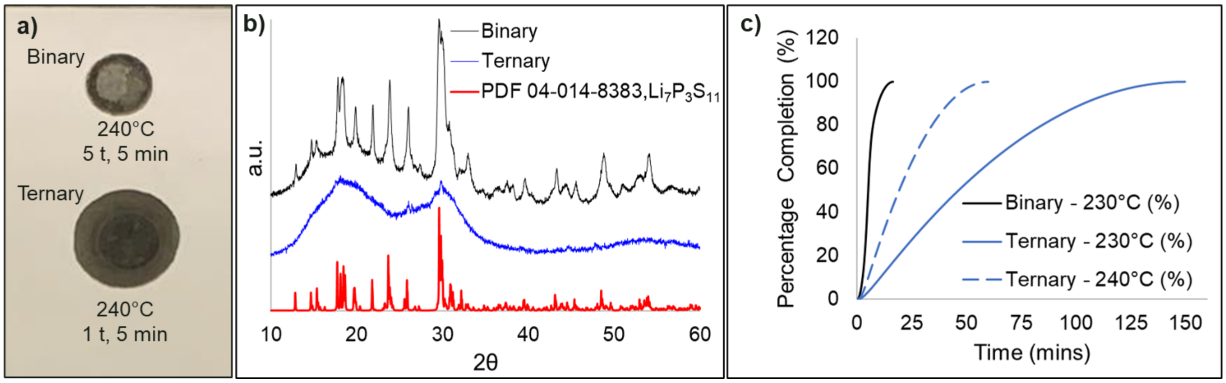

Figure 12. (a) Picture of reinforced solid-state electrolyte (SSE) pellets after hot pressing at 240°C for 5 minutes. (b) X-ray diffraction profiles of hot-pressed SSE pellets. The binary sample devitrifies to $Li_7P_3S_{11}$, while the ternary sample remains a glass. (c) Fractional extent of devitrification for binary and ternary samples as determined by integration of a differential scanning calorimetry exothermic feature.

To understand the ternary phase's improved process rheology, the team investigated the glasses with both XRD and DSC. Figure 12b presents the diffraction patterns of both binary and ternary glasses after hot pressing at 240°C for 10 minutes, and the patterns are indexed to the reflections of $Li_7P_3S_{11}$ (pdf #04-014-8383). The binary glass devitrified during hot pressing, while the ternary glass remained largely amorphous. It is well known that the viscosity of glasses increases substantially on devitrification as crystallites grow and physically interact. The team therefore attributes the superior processability of the ternary glass to its more sluggish crystallization kinetics. To confirm this suspicion, they conducted DSC experiments on the binary and ternary glasses. The binary glass had a crystallization onset of 272.79°C when dynamically heated at 10°C/minute, while the ternary glass had a higher crystallization onset of 294.25°C under the same conditions. Additionally, they also measured the time required to complete full crystallization (Figure 12c). It took the ternary glass over 2 hours to fully devitrify at 230°C, while the binary glass fully crystallized in less than 10 minutes at 230°C.

A 3-electrode test cell was implemented to meet the Q4 FY 2021 milestone and support failure analysis of SSE separators. A picture of the 3-electrode test cell is provided in Figure 13a, and a schematic of the 3-electrode test cell's cross section is provided in Figure 13b. It consists of a two-piece polyethylenimine (PEI) sleeve, 8-mm-diameter stainless-steel current collectors, and a reference electrode. The reference electrode is a ring of 30-µm-thick lithium foil supported by 10-µm-thick copper foil (Figure 13b, inset). The inside of the lithium ring is embedded within the SSE sample prior to testing. In the initial test, the working electrode was indium metal, the counter electrode was lithium metal, and the reference electrode was lithium metal. As shown in Figure 13c, once the indium working electrode is alloyed with lithium on application of a negative current, the reference electrode measures the correct voltage of 0.6 V. This 3-electrode cell is appropriate for all-solid-state test cells; however, its utility for semi-solid test cells remains to be evaluated. Further work is needed to provide a seal between the two pieces of the PEI sleeve to prevent leakage of a secondary electrolyte phase.

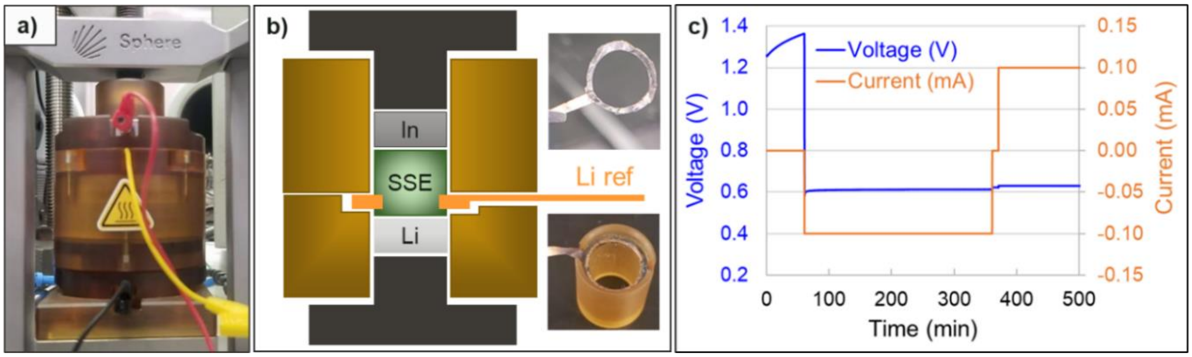

Figure 13. (a) Picture of a 3-electrode test cell used in this study. (b) Schematic of the 3-electrode test cell. The reference electrode is an annular Cu-foil disc with Li-metal coating held in place with a two-part sleeve. (c) Voltage and current versus time for a 3-electrode cell with a Li-metal counter electrode, an indium working electrode, and a lithium reference electrode.

Multifunctional reinforcement was evaluated to replace insulating aramid fibers to meet this quarter's milestone and reduce resistance of reinforced SSE separators. Al-doped LLZO fibers were obtained from a commercial vendor, and a scanning electron microscopy (SEM) image of the fibers is provided in Figure 14a. XRD analysis (Figure 14b) showed that the fibers were not pure cubic phase LLZO. A baseline separator of Li_3PS_4 + 3 wt% Kevlar fiber had an ionic conductivity of 0.187 mS/cm at room temperature. Li_3PS_4 separators with 3 wt% and 10 wt% LLZO fiber reinforcement had lower conductivities of 0.103 mS/cm and 0.08 mS/cm, respectively. LLZO fiber reinforcement is thus not considered for future work.

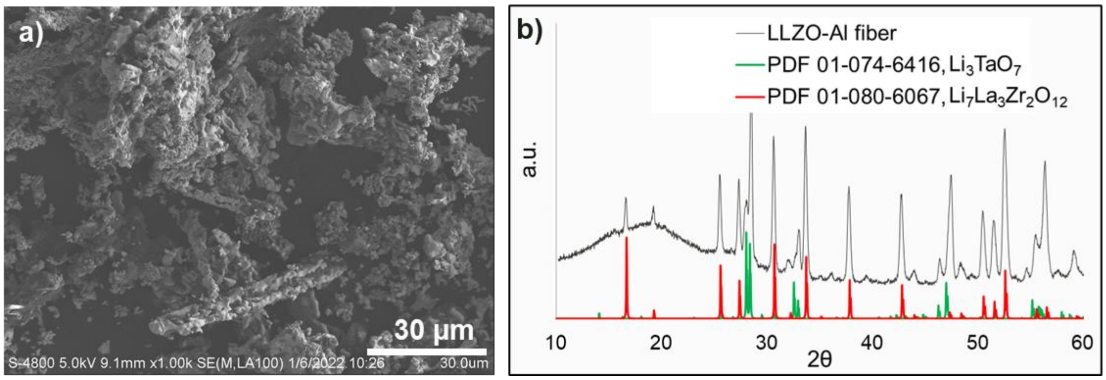

Figure 14. (a) Scanning electron microscopy image of LLZO fibers obtained from a commercial vendor. (b) X-ray diffraction profile of the LLZO fibers indicate a significant Li_3TaO_7 impurity.

Reference

[1] Yersak, T. A., et al. "Consolidation of Composite Cathodes with NCM and Sulfide Solid-State Electrolytes by Hot Pressing for All-Solid-State Li-Metal Batteries." *Journal of Solid State Electrochemistry* 26, No. 5 (2022): 1–10. doi: 10.1007/s10008-021-05104-8.

Patents/Publications/Presentations

Publication

- Yersak, T. A., et al. "Consolidation of Composite Cathodes with NCM and Sulfide Solid-State Electrolytes by Hot Pressing for All-Solid-State Li-Metal Batteries." *Journal of Solid State Electrochemistry* 26, No. 5 (2022): 1–10. doi: 10.1007/s10008-021-05104-8.

Task 1.10 – Three-Dimensional Printing of All-Solid-State Lithium Batteries (Jianchao Ye, Lawrence Livermore National Laboratory)

Project Objectives. The project has two primary objectives: (1) down select three-dimensional (3D) printing and post-processing approaches for SSE/cathode integration, and (2) understand battery failure mechanisms via *ex situ* and *in situ* characterization.

Impact. The adoption of thin separator layer, thick cathode structure, and metallic lithium anode will lead to EV batteries with > 350 Wh/kg energy density for increased mileage per charge. The higher ionic conductivity with suppression of lithium dendrite growth will allow high CCD for fast charging applications. The improved electrode/electrolyte contact will increase battery cycle life for long-term service.

Approach. The technical approaches include advanced manufacturing based on 3D printing and related techniques, *ex situ* / *in situ* characterizations, and battery testing. Direct ink writing (DIW) 3D-printing techniques will be employed to fabricate thin-film SSEs (< 100 μm), gradient SSEs, and 3D interfaces for battery performance evaluation. Three approaches including sintering-free, hybrid, and co-sintering will be investigated. The knowledge obtained from these approaches is transferable and complementary to each technique.

Out-Year Goals. The long-term vision of the team is to 3D-print all components of the ASSLBs to facilitate the scale-up of ASSLB manufacturing. In this project, the team will tackle the issues emerging from integrating SE with electrodes. The project goal is to demonstrate a successful 3D-printing approach to integrate SSE into electrodes and show reasonable capacity retention (that is, > 80%) after 300 cycles at current density ≥ 1 mA/cm^2.

Collaborations. The team will work closely with a computational partner (Task 3.11 led by B. Wood) to better understand battery failure mechanisms and design new battery architectures and chemistries for performance improvement.

Milestones

1. Determine the polymer / $Li_{6.75}La_3Zr_{1.75}Ta_{0.25}O_{12}$ (LLZTO) interfacial chemistry effects on the total ionic conductivity and Li$^+$ transference number. (Q2, FY 2022; In progress)
2. Improve conductivity and strength of composite polymer electrolytes (CPEs). (Q3, FY 2022; On schedule)
3. Obtain porous co-sintered LLZTO-SSE/NMC/C electrolyte/cathode bilayer structure. (Q4, FY 2022; On schedule)

Progress Report

Progress for this new project will be reported next quarter.

Patents/Publications/Presentations

The project has no patents, publications, or presentations to report this quarter.

Task 1.11 – Physical and Mechano-Electrochemical Phenomena of Thin-Film Lithium-Ceramic Electrolyte Constructs
(Jeff Sakamoto, University of Michigan)

Project Objective. While a small number of SEs exhibit high ionic conductivity (~ 1 mS cm at 298 K), few are stable against lithium metal. The garnet-type SE, based on the nominal formula $Li_7La_3Zr_2O_{12}$ (LLZO), is unique in that it is a fast ion conductor and—as demonstrated in the team's recent project (DE-EE-00006821)—is stable against lithium. Moreover, the team's former project successfully demonstrated a decrease in Li-LLZO interface resistance from 12,000 Ω cm^2 to 2 Ω cm^2 and stable cycling at 1 mA cm^2 for 100 cycles (± 15 µm of lithium per cycle). Although the past project demonstrated that LLZO is a viable SE for enabling batteries using metallic lithium, the studies used thick pellets (1 mm) and thick anodes (~ 500 µm). The goal of this project is to acquire a deep fundamental understanding of the physical and mechano-electrochemical phenomena that control the performance of cells consisting of thin LLZO (~ 10 µm), thin lithium anodes (~ 20 µm), and thin solid-state composite cathodes.

Project Impact. If successful, the project will gain knowledge to guide closely related commercialization efforts to scale the production of LLZO-based SSBs.

Approach. The team believes that to achieve a step increase in technology readiness level (TRL), the same performance characteristics previously shown should be demonstrated in technologically relevant cells, for example, thin LLZO and thin lithium.

Out-Year Goals. Out-year goals involve the following: custom thin-film composite (TFC) development, preliminary cycling studies, Vis cell development, lithium cycling, and polymer gel electrolyte (PGE) screening.

Collaborations. This project collaborates with N. Dasgupta and D. Siegel of UM, Mechanical Engineering.

Milestones

1. In thin lithium and thin LLZO TFC, determine the maximum $CCD^{plating}$ and $CCD^{stripping}$ versus depth of discharge (DOD) at fixed lithium thickness (17 µm). (Q1, FY 2022; Completed)
2. Long-term cycling tests to demonstrate $\geq$ 80% energy retention over 1000 cycles. (Q2, FY 2022; In progress)
3. In thin lithium and thin LLZO TFC, determine the max $CCD^{plating}$ and $CCD^{stripping}$ versus lithium thickness, DOD, stack press, and temperature. (Q3, FY 2022; In progress)
4. Optimize ALD coating technology to suppress reactions between the PGE and LLZO. (Q4, FY 2022; In progress)

Progress Report

Stripping Behavior of Thin Lithium

This study aims to understand the stripping behavior of thin lithium when paired with SE. It was shown that accessible capacity of lithium is affected by the thickness of lithium (10-30 µm) and current density (Figure 15). At fixed thickness (10 µm), lithium stripping is essentially uniform at the lower current densities. However, at ~ 0.4 mA/cm^2 a significant increase in polarization occurs, resulting in approximately half of the lithium accessible capacity (Figure 15a). At fixed lithium current density (0.4 mA/cm^2), the lithium accessible capacity increases with increases with lithium thickness (Figure 15b). The underlying mechanisms that control the accessible capacity of lithium as a function of thickness and current density likely involve the transport of lithium in lithium (self-diffusion), creep of lithium, and de-wetting or pore formation at the Li-SE interface. Results of this study will inform future efforts to improve discharge performance of SSLBs.

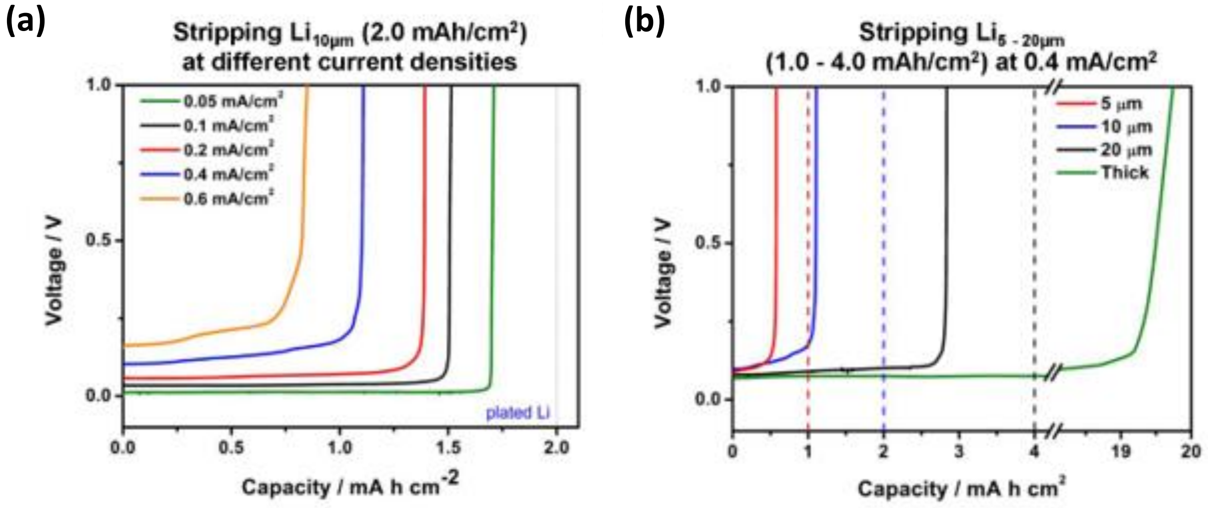

Figure 15. Characterization of the stripping behavior of thin lithium on solid electrolyte as a function of current densities and thicknesses. (a) Voltage responses of stripping thin lithium with fixed thickness (10 µm, 2.0 mAh/cm^2) at different current densities (0.05-0.6 mA/cm^2). (b) Voltage responses of stripping thin lithium with different thicknesses (5-20 µm, 1.0-4.0 mAh/cm^2) at fixed current density (0.4 mA/cm^2).

Patents/Publications/Presentations

Publications

- Haslam, C. G.,* J. B. Wolfenstine, and J. Sakamoto.* "The Effect of Aspect Ratio on the Mechanical Behavior of Li Metal in Solid-State Cells." *Journal of Power Sources* 520 (2022): 230831.
- Carmona, E. A., M. J. Wang,* Y. Song, J. Sakamoto,* and P. Albertus. "The Effect of Mechanical State on the Equilibrium Potential of Alkali Metal/Ceramic Single-Ion Conductor Systems." *Advanced Energy Materials* 11, No. 29 (2021): 2101355.
- Allen, J. L., B. A. Crear, R. Choudhury,* M. J. Wang,* D. T. Tran, L. Ma, P. M. Piccoli, J. Sakamoto,* and J. Wolfenstine. "Fast Li-Ion Conduction in Spinel-Structured Solids." *Molecules* 26, No. 9 (2021): 2625.
- Chang, W., R. May, M. Wang,* G. Thorsteinsson, J. Sakamoto,* L. Marbella, and D. Steingart. "Evolving Contact Mechanics and Microstructure Formation Dynamics of the Lithium Metal-$Li_7La_3Zr_2O_{12}$ Interface." *Nature Communications* 12, No. 1 (2021): 1–12.

Note: * indicates Sakamoto group

Presentations

- Michigan State Senate Committee on Energy Technology (December 7, 2021): Testimony on the Importance of Vehicle Electrification; J. Sakamoto with D. Gallimore, A. Stefanopoulou, and G. Less.
- International World Conference on Solid Electrolytes for Advanced Applications, Virtual (October 25–27, 2021): Conference Chair, J. Sakamoto and D. Siegel. The co-chairs were D. Siegel (University of Texas, or UT, Austin), C. Chan (Arizona State University), and V. Thangadurai (University of Calgary). There were approximately 30 invited speakers and 150 attendees. J. Sakamoto served as the primary organizer, a session chair, and a speaker. The virtual conference consisted of three live parallel sessions in the United States, Asia, and Europe (https://sites.google.com/umich.edu/3rdgarnetconference/).
- "Solid-State of Affairs" Industry Expert Roundtable (hosted by Bloomberg and Solid Power Inc.), Virtual (October 8, 2021): Panelist on Solid-State Batteries; J. Sakamoto (https://www.bloomberg.com/press-releases/2021-09-22/solid-power-to-host-and-stream-solid-state-of-affairs-industry-expert-roundtable-on-october-8-2021).
- *Popular Mechanics* (December 13, 2021): "Solid-State Batteries are Here and They're Going to Change How We Live"; J. Sakamoto and N. P. Dasgupta, featured SSB researchers.

Task 1.12 – Low Impedance Cathode/Electrolyte Interfaces for High-Energy-Density Solid-State Batteries
(Eric Wachsman and Yifei Mo, University of Maryland)

Project Objective. The project objective is to research, develop, and test Li-metal-based batteries that implement solid Li-ion conductors (LICs) equipped with NMC cathodes integrated into the Li-metal / Li-La-Zr (LLZ) tri-layer architecture. Specifically, the team will achieve the following: (1) identify and demonstrate interfacial layers to achieve low-impedance and stable NMC/LLZ interfaces; (2) develop novel processing techniques to fabricate NMC/LLZ composite cathodes with low interfacial resistance; and (3) enable high-performance ASSBs with an energy density of 450 Wh/kg and 1400 Wh/L and negligible degradation for 500 cycles.

Project Impact. Instability or high resistance at the interface of high-energy cathode materials with Li-garnet SEs limits the high-energy-density ASSLBs. This project will lead to a fundamental understanding of solid-electrolyte/solid-cathode interfaces and a unique and transformative LLZ framework to enable high-energy-density, safe Li-metal batteries approaching ~ 400 Wh/kg.

Approach. In this new project, the team will build on their demonstrated expertise with garnet electrolytes and ASSB cells to accomplish the following: (1) engineer interfaces to overcome high NMC/LLZ interfacial impedance and interfacial degradation; (2) develop processing and fabrication techniques to achieve high-loading NMC/LLZ composite cathodes with low resistance and high cyclability; and (3) integrate the NMC/LLZ cathodes into all-solid-state Li-metal/LLZ cells to achieve high-energy-density batteries.

Out-Year Goals. The project will solve the current challenges of integrating garnet SE with a cathode to achieve a high-performance ASSB using a high-energy-density Li-metal anode. The resultant high energy density and stability using both high-energy-density Li-metal anodes and NMC cathodes will open new applications in portable electronics, EVs, and beyond.

Collaborations. This project funds work at University of Maryland (UMD). The PI, E. Wachsman, will have management responsibility and will lead experimental efforts including garnet synthesis, interface processing, cell fabrication, and testing. The Co-PI, Y. Mo, will lead computational efforts on understanding stability between garnet and cathode and on identifying promising coating materials. In addition, E. Wachsman is actively collaborating with several universities and national laboratories through the U.S.–German cooperation on SSB interfaces.

Milestones

1. Thermochemical stability between LLZ and interface-coated NMC experimentally determined. (Q3, FY 2022; In progress)
2. Experimental results compared with computational results, and model refined for side reactions and process optimization. (Q4, FY 2022; In progress)
3. Ten-times reduction in interfacial impedance between coated LLZ/NMC and uncoated LLZ/NMC interfaces demonstrated by co-sintering. (Q4, FY 2022; In progress)
4. Tri-layer cell with composite NMC-LLZ cathode layer fabricated and measured. (Q1, FY 2023; In progress)
5. *Go/No-Go Decision*: Demonstrate final cell with achieved performance. (Q2, FY 2023; In progress)

COVID-19 Impact. Progress on experimental results was impacted by COVID-19, which closed labs for several months resulting in a 6-month, no-cost extension reflected in the milestone dates above.

Progress Report

The team studied the thermochemical stability between $Li_{6.75}La_3Zr_{1.75}Ta_{0.25}O_{12}$ (LLZTO) and $LiNi_{0.6}Mn_{0.2}Co_{0.2}O_2$ (NMC) with the addition of a metal oxide coating, Al_2O_3. LLZTO and NMC are mixed together and then infiltrated into porous LLZTO layers. To avoid possible elemental co-diffusion between NMC and LLZTO during sintering, it is required to coat any of the material (NMC or LLZTO) with a thin layer of metal oxide before mixing them together. In this study, Al_2O_3-coated NMC (coated through ALD) was procured to test its efficacy in improving the thermochemical stability of NMC versus LLZTO. However, this requires that the NMC is no longer milled to sub-micron particle sizes since the ALD-coating on the NMC would be destroyed by ball-milling. The as-received particle size of NMC presents its own challenge, as these powders have particle sizes in the range of 10-15 µm; thus, heating at 800°C is no longer sufficient to obtain clean electrochemical impedance spectra when the NMC particle size is large. Therefore, the heating temperature was increased to 1000°C to obtain clear spectra so that accurate comparisons of coated and uncoated NMCs could be made. These EIS results are shown in Figure 16.

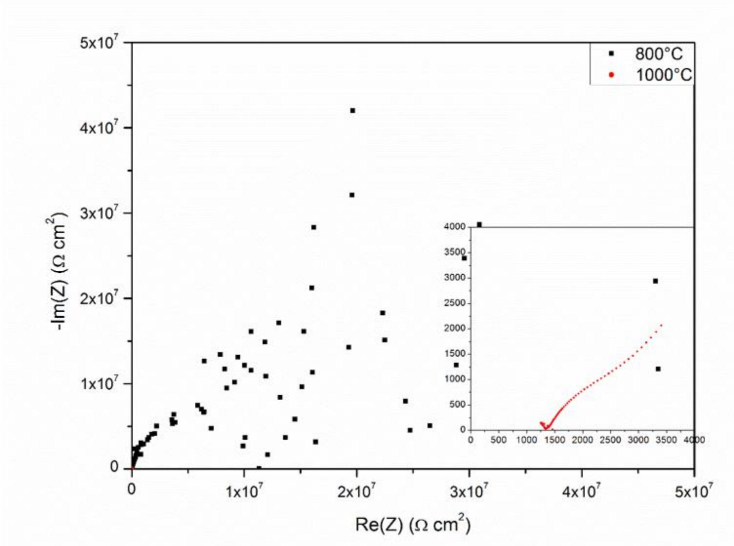

Figure 16. Nyquist plot of un-milled Al_2O_3-coated NMC in composite cathodes sintered at 800°C and 1000°C.

Figure 17 contains EIS results of symmetric cells with composite cathodes of both Al_2O_3 coated and uncoated NMC sintered at 1000°C. The LLZTO is still milled to < 300 nm. From the Nyquist plot (Figure 17a), and the increased peak height from the distribution of relaxation times (DRT) results (Figure 17b), it is clear that the Al_2O_3-coated NMC has significantly higher ASR, suggesting poor Li-ion dynamics at the interface. However, it is suspected that the thickness of the Al_2O_3 layer on the NMC powder is much thicker than what coated the project's tri-layers in previous experiments, since the supplier ran many more ALD cycles than the team's standard, in-house process (50 compared to 15 cycles). A thinner ALD layer will need to be coated on the NMC to make an accurate comparison to previous results since they are inconsistent.

Despite these electrochemical results, XRD data of these same samples are promising. To understand the thermodynamic stability between LLZTO and Al_2O_3 coated and uncoated NMC, the team performed XRD and cross-sectional SEM studies on 800°C and 1000°C co-sintered samples.

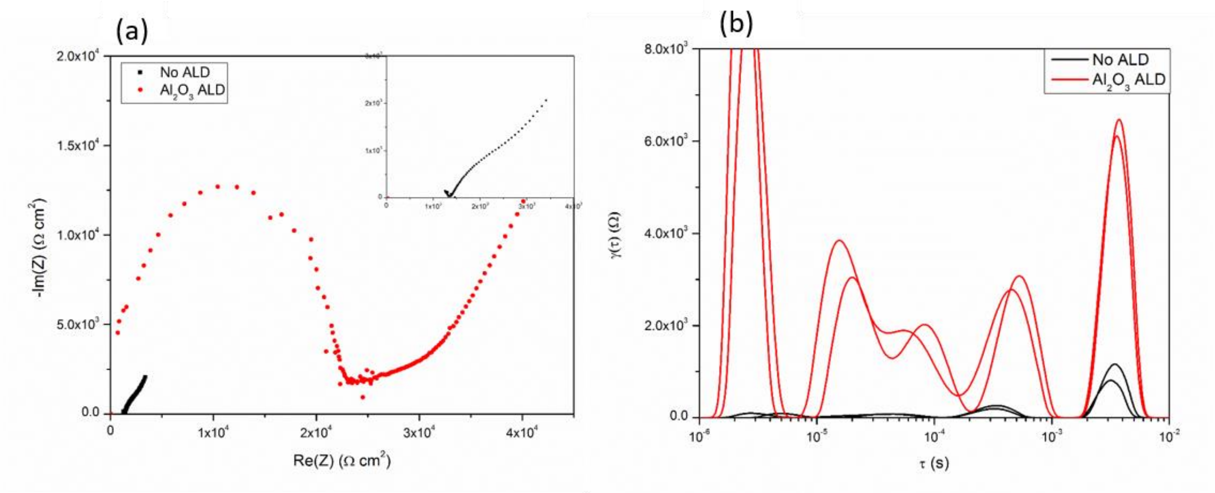

Figure 17. (a) Nyquist plot and (b) distribution of relaxation times analysis of 1000°C co-sintered composite NMC/LLZTO cathodes with and without atomic layer deposition coating the NMC.

Figure 18 contains backscatter SEM images and XRD of the samples sintered at 800°C. The SEM images in Figure 18b-c show that heating at 800°C is insufficient to sinter the nano-sized LLZTO particles together and to NMC particles in the composite cathode, as the brighter LLZTO particles are much smaller than the samples heated at 1000°C (Figure 19b-c). Furthermore, the XRD results in Figure 18a demonstrate no noticeable difference between the samples with or without the Al_2O_3 ALD layer. This implies that the ALD layer may be more effective in protecting NMC at heating temperatures higher than 800°C; however, it is not clear if this because the LLZTO is not sintering at such a low temperature to increase the surface contact and thus lead to an interfacial reaction, or if the ALD layer simply increases the thermochemical stability of the NMC itself.

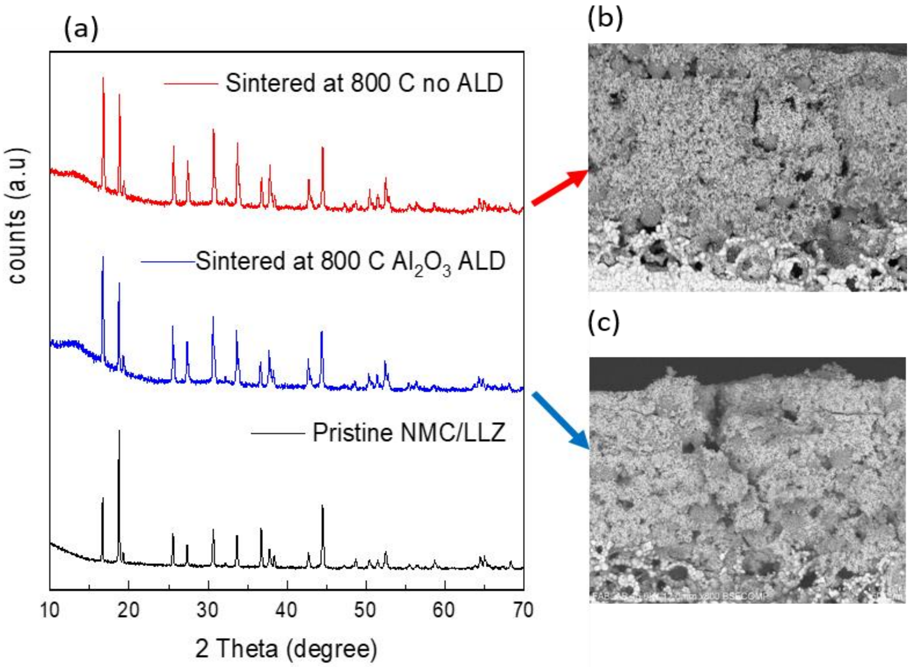

Figure 18. (a) X-ray diffraction spectra of sintered cathodes of NMC and LLZTO with and without atomic layer deposition coating the NMC. Backscatter scanning electron microscopy images of (b) uncoated NMC infiltrated onto the porous LLZTO structure and (c) Al_2O_3-coated NMC infiltrated onto the porous LLZTO structure. These samples were heated to 800°C for 3 hours.

Figure 19 shows that while the NMC peaks seem to become less clear in both samples, particularly the peaks around 38°, the relative intensity between NMC and LLZTO peaks is not maintained in the samples with uncoated NMC. Additionally, the peaks are less sharp than those of the coated NMC, indicating a decrease in relative crystallinity. Backscatter SEM images seem to corroborate this, as the ALD-coated NMC particles retain their original spherical shape more so than the uncoated NMC samples. This suggests that the Al_2O_3 protective layer is effective in slowing the reaction between NMC and LLZTO at 1000°C. The SEM images also provide further insight into the electrochemical results. The uncoated NMC shows more contact between NMC and LLZTO from the increased sintering due to the greater reaction between the two materials. This could explain why the impedance of the uncoated samples is lower than the coated NMC samples. However, one would expect other secondary phases to form and thus be present in the XRD of samples where the reaction occurs to a greater extent.

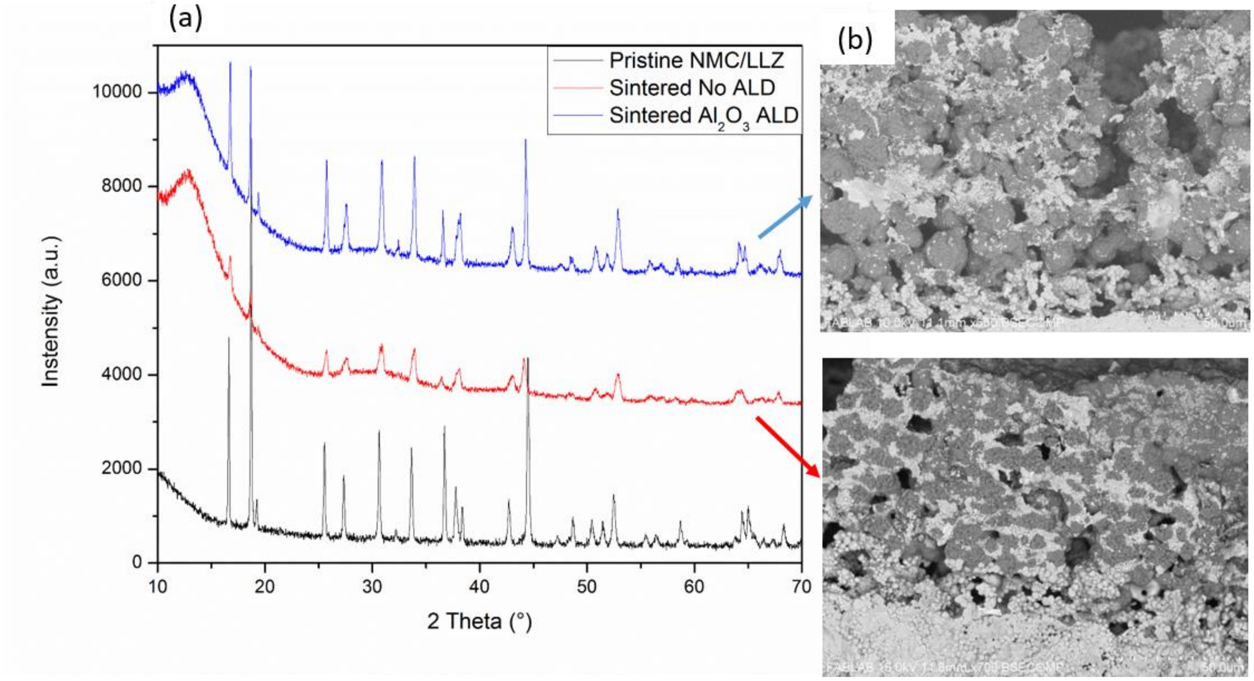

Figure 19. (a) X-ray diffraction spectra of sintered cathodes of NMC and LLZTO with and without atomic layer deposition coating the NMC. Backscatter scanning electron microscopy images of (b) uncoated NMC infiltrated onto the porous LLZTO structure and (c) Al_2O_3-coated NMC infiltrated onto the porous LLZTO structure. These samples were heated to 1000°C for 3 hours.

Patents/Publications/Presentations

Publications

- Neumann, A., T. R. Hamann, T. Danner, S. Hein, K. Becker-Steinberger, E. D. Wachsman, and A. Latz. "Effect of the 3D Structure and Grain Boundaries on Lithium Transport in Garnet Solid Electrolytes." *ACS Applied Energy Materials* 4 (2021): 4786–4804. doi: 10.1021/acsaem.1c00362.
- Nolan, A. M., D. Wickramaratne, N. Bernstein, Y. Mo,* and M. D. Johannes.* "Li^+ Diffusion in Amorphous and Crystalline Al_2O_3 for Battery Electrode Coatings." *Chemistry of Materials* 33, No. 19 (2021): 7795–7804.

Presentations

- Materials Research Society (MRS) Fall Meetings & Exhibits, Virtual (December 6–8, 2021): "A Solid Transformation of Energy Storage"; E. D. Wachsman. Invited.
- World Conference on Solid Electrolytes for Advanced Applications, Webinar (October 25–27, 2021): "A Solid Transformation of Energy Storage"; E. D. Wachsman. Invited.
- 5th Forum of Materials Genome Engineering, Zhengzhou, China, Virtual (December 2021): "Data-Driven Discovery of New Materials for Solid-State Batteries"; Y. Mo. Invited.
- International Battery Materials Association (IBA) 2021 Annual Meeting, Xiamen, China, Virtual (October 2021): "Interfacial Failure of Lithium Metal in Solid-State Batteries: Insight from Large-Scale Atomistic Modeling"; Y. Mo. Invited.
- World Conference on Solid Electrolytes for Advanced Applications, Virtual (October 2021): "Interfacial Failure of Lithium Metal in Solid-State Batteries: Insight from Large-Scale Atomistic Modeling"; Y. Mo. Invited.

Task 1.13 – Development of All-Solid-State Battery Using Anti-Perovskite Electrolytes (Zonghai Chen and Tao Li, Argonne National Laboratory)

Project Objective. The objective of this project is to develop an optimized anti-perovskite electrolyte with a stabilized interface for scalable fabrication of liquid-free SSBs.

Impact. The project will lead to impact on several areas: (1) establishing structure-property relationship of anti-perovskite electrolytes, (2) understanding and quantifying the interaction between the electrolytes and the environment, (3) understanding and mitigating the failure of ASSBs at solid-solid interface, and (4) developing a scalable process for fabrication of ASSBs.

Approach. The project approach is multi-fold: (1) chemistry design: multiple doping at anion sites will be pursued to improve structural stability ionic conductivity and environmental compatibility; (2) interfacial design: surface coating will be deployed to improve the chemical and mechanical stability of solid/solid interface; and (3) process development: a scalable fabrication process based on melt-infiltration or dry lamination will be developed for the fabrication of ASSBs.

Out-Year Goals. The project has the following out-year goal:

- Developing high-performance anti-perovskite electrolytes.
- Accessing the air stability and proton mobility of anti-perovskite electrolytes.
- Stabilizing the solid/solid interface through interfacial engineering.
- Prototyping liquid-free cells using anti-perovskite electrolytes.

Collaborations. This project collaborates with Y. Z. Liu (ANL), W. Q. Xu (ANL), X. H. Xiao (Brookhaven National Laboratory, or BNL), and H. Meng (University of Arkansas).

Milestones

1. Setting up high-throughput (HT) synthesis capability. (Q1, FY 2022; Completed)
2. Optimizing synthesis condition for anti-perovskite electrolytes. (Q2, FY 2022; In progress)
3. Investigating structural stability of doped electrolytes. (Q3, FY 2022)
4. Investigating transport properties of doped electrolytes. (Q4, FY 2022)

Progress Report

The synthesis of anti-perovskite electrolyte is a one-step solid-state reaction. The starting materials are LiOH and lithium halide (LiCl, LiBr, and LiI). Anti-perovskite materials can be easily synthesized by heating the mixture of starting materials at about 300°C under vacuum conditions. Figure 20 shows the evolution of high-energy X-ray diffraction (HEXRD) patterns collected during thermal treatment of Li_3OCl. The *in situ* HEXRD results clearly show that the anti-perovskite material (Li_3OCl) melts at about 280°C. During the cooling processing, anti-perovskite Li_3OCl crystallizes when the temperature is below 280°C.

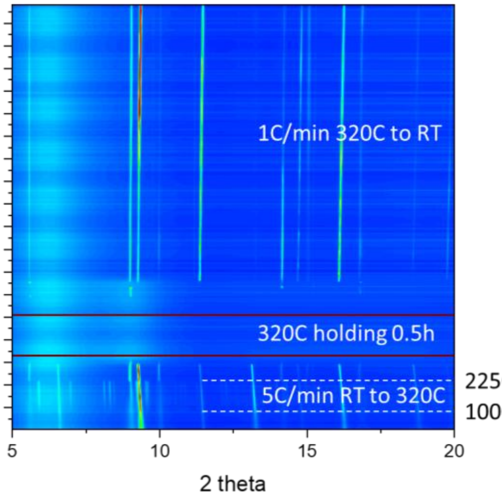

Figure 20. Evolution of high-energy X-ray diffraction patterns during solid-state synthesis of Li_3OCl.

In the lab-scale synthesis, a vacuum oven is used for synthesizing multiple samples simultaneously. However, it was found that the synthesized materials firmly stuck to the crucible wall. This is chemically originated from the strong chemical bonding between the Li_2O moiety and various oxide materials. The chemical interaction between the crucible and the formed electrolyte increases the difficulty in recovering desired materials and partial and unbalanced loss of starting materials due to the interfacial reaction with the crucible, leading to the deviation of desired stoichiometry. To overcome this difficulty, the team has tried crucibles made from different materials (Al_2O_3, quartz, porcelain, and MgO coated Al_2O_3) without any success (Figure 21a-b). Progress was made by using metallic crucibles. They were able to recover the material synthesized in a zirconium crucible. It was found that zirconium was oxidized during the solid-state synthesis (see the color change in Figure 21c); the starting materials were also partially lost due to interaction with the newly formed ZrO_2. Consequently, some impurity phase was observed in the synthesized Li_3OCl (see Figure 22). Alternatively, when an extremely chemically resistive tungsten crucible was used for the synthesis, the material could be easily recovered (Figure 21d), and a pure anti-perovskite material was obtained (see Figure 22).

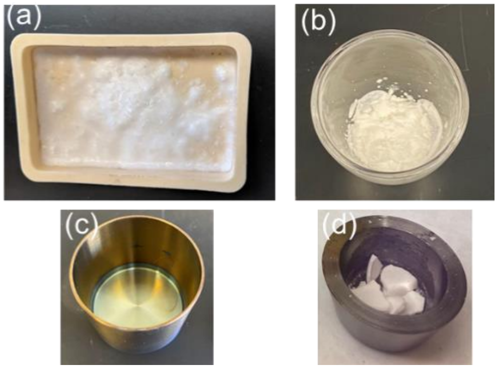

Figure 21. Images showing the interaction between synthesized materials and crucibles made from (a) Al_2O_3, (b) quartz, (c) zirconium, and (d) tungsten.

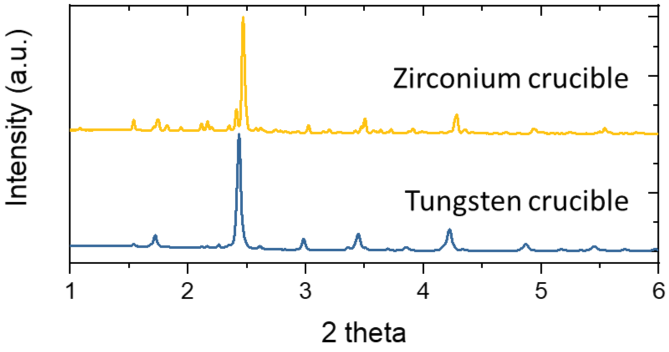

Figure 22. Comparison of high-energy X-ray diffraction patterns of electrolyte materials after synthesis in different crucibles.

To measure the Li^+ conductivity of synthesized electrolytes, a protonated anti-perovskite powder, Li_2HOCl, was cold-pressed into a half-inch pellet, and symmetrical cells using indium as the conducting layers were assembled for EIS measurement. Figure 23a shows the collected EIS results at various temperatures; the extracted Li^+ conductivity at different temperatures is shown in Figure 23b. Although the measured conductivity is consistent with the best-reported results [see Yushin, G., et al. *Advanced Energy Materials* (2017): 1700971], the room-temperature conductivity is still too low. Particularly, there is a sudden drop in Li^+ conductivity at room temperature, resulting from the cubic/tetragonal phase transformation at about 40°C. In the coming quarters, anion doping will be deployed to lock the material in cubic phase, improve the Li^+ conductivity, and suppress the detrimental cubic/tetragonal phase transformation.

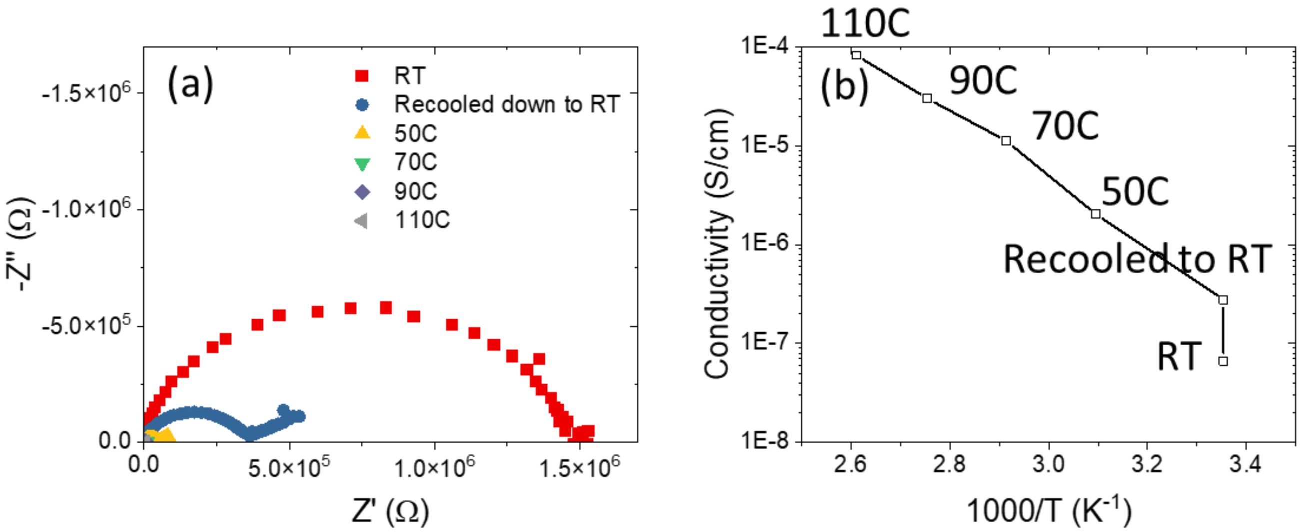

Figure 23. (a) Electrochemical impedance spectroscopy of In/Li_2HOCl/In, and (b) extracted Li^+ conductivity of Li_2HOCl electrolyte at different temperatures.

One of the significant advantages of anti-perovskite electrolyte is that all the elemental components are already at their lowest valence state, and hence the electrolyte will be thermodynamically compatible with metallic lithium. A small amount of Li_3OCl and metallic lithium was sealed in a quartz tube to demonstrate this advantage. The sealed sample was then slowly heated to 220°C and held at 220°C for an hour. The HEXRD patterns of the sample were continuously collected during the experiment. Figure 24 shows that lithium melted at about 180°C. However, the structure of Li_3OCl maintained even being heated and held at 220°C. No chemical reaction between the electrolyte and metallic lithium was observed.

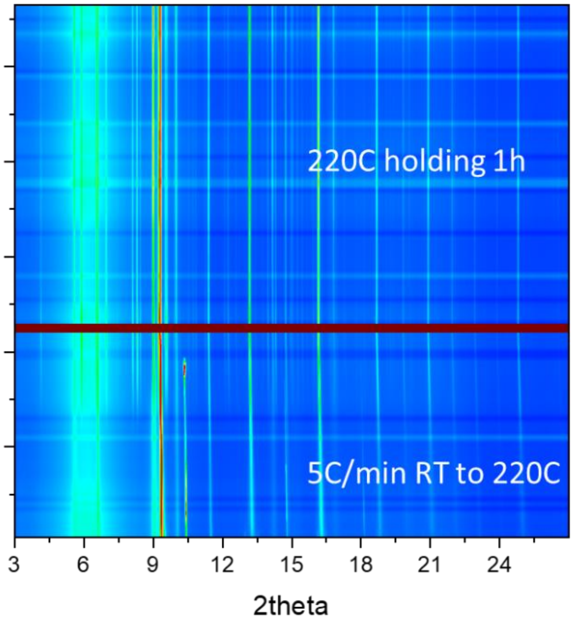

Figure 24. Evolution of high-energy X-ray diffraction patterns showing the interaction between metallic lithium and Li_3OCl electrolyte during heating, showing no reaction up to 220°C.

Patents/Publications/Presentations

The project has no patents, publications, or presentations to report this quarter.

Task 1.14 – Lithium Halide-Based Superionic Solid Electrolytes and High-Voltage Cathode Interface (Jagjit Nanda, Oak Ridge National Laboratory)

Project Objective. The project aims to develop low-temperature solution-based synthesis strategy for high ionic conducting halide-based SE and enable approaches to develop a scalable process for integrating halide-based SE within porous high-voltage Li-ion cathode matrix. Years 1 and 2 aim at developing low-cost, solution-based synthesis routes to produce a halide class of superionic conductor belonging to Li_3MX_6 (where M = Sc, Y, La, Er, In and X = Cl, Br, I) along with enabling electrochemical and structural characterization. Parallel efforts in years 2 and 3 target developing synthesis and processing methods where the high-voltage stable halide-based SEs can be readily infiltrated within the porous cathode structures such as NMC-622, high-voltage Mn-Ni spinel ($LiMn_{1.5}Ni_{0.5}O_4$) and recent fluorinated Mn-rich disorder rock salt cathodes. Years 3 and 4 focus on designing and fabricating thin halide SE separators with a thickness of 50 µm or lower and optimizing the cathode microstructure. Finally, years 4 and 5 will develop approaches for anode-free lithium plating and stripping on alloyed or engineered copper current collectors at relatively higher current densities aimed at improving the volumetric energy density of SSB with a high loading cathode and thin halide SE separator.

Impact. The proposed tasks and metrics aim at addressing the long-term VTO goal for developing ASSBs at ambient temperature with energy density in the range of 500 Wh/Kg and 1000 Wh/L for electric drive vehicles. Advances in scalable processing of superionic SEs, stabilizing electrode-electrolyte interfaces, and promoting long cycle life are all needed to meet the energy density and cost targets for next-generation batteries for EVs.

Approach. The project employs a multi-faceted approach: (1) conduct solution-based synthesis of the metal halide superionic conductor as the platform to enable robust cathode-electrolyte interface (CEI) processing for SSBs, (2) infiltrate pore structures using solution-based processing that deposits high conductivity SEs within cathode pores, and (3) facilitate lithium transport and improve stability using cation doping (divalent to introduce lithium vacancies, and lanthanum to prevent indium redox).

Out-Year Goals. Demonstrate single-layer pouch cell SSB containing a thin halide SE separator coupled with high-voltage cathodes with 70% capacity retention over 300 cycles at 2 mA/cm^2 in an anode free SSB configuration that can attain 1000 Wh/L in prototype cells.

Collaborations. Y. Yao and team at University of Houston (UH) are funded collaborators for halide-based SSB fabrication, testing, and interfacial studies. The project also involves unfunded collaboration with SLAC for XAS and synchrotron-based XRD (SXRD) of SEs.

Milestones

1. Produce gram-scale quantities of Li_3InCl_6 SE using solvent-phase synthesis. (Q1, FY 2022)
2. Obtain phase-pure Li_3InCl_6 thin pellets with ~ 1 mS/cm^{-1} conductivity. (Q2, FY 2022)
3. Utilize neutron diffraction, XPS, Raman, and electron microscopy to characterize Li_3InCl_6 SE. (Q3, FY 2022)
4. Compare structure and Li^+ conductivity of Li_3InCl_6 prepared through solvent-mediated versus mechanochemical; > 5g batch with ionic conductivity in the range of 1 mS/cm^{-1}. (Q4, FY 2022)

Progress Report

Progress for this new project will be reported next quarter.

Patents/Publications/Presentations

The project has no patents, publications, or presentations to report this quarter.

Task 1.15 – Developing an *In Situ* Formed Dynamic Protection Layer to Mitigate Lithium Interface Shifting: Preventing Dendrite Formation on Metallic Lithium Surface to Facilitate Long Cycle Life of Lithium Solid-State Batteries

(Deyang Qu, University of Wisconsin, Milwaukee)

Project Objective. The objective of this project is to research, develop, and test Li-metal-based batteries that implement solid LICs equipped with a formed dynamic protection layer. The proposed project aims to enable safe, long-cycle lithium anodes to achieve cell performance targets of 400 Wh/Kg, over 100 cycles, with 15-year shelf life, and < $100/KWh cost.

Project Impact. Project efforts are to contribute an in-depth understanding of the lithium interface and dendrite growth prevention to the field of Li-metal batteries, which will pave the way for eventual development of high-energy-density, low-cost, and long-lasting lithium batteries. This advancement could be a crucial selling point for the greater adoption of EVs. This project will make possible the translation of fundamental research into practical implementation of high-energy lithium anodes, enabling eventual achievement of cell performance targets.

Approach. The novelty of this approach is that the team intends to mitigate the dendrite problem by creating a dynamic protection layer during the interface shift to prevent dendrite formation throughout battery operation.

Out-Year Goals. The project has three *one-year* goals: (1) *in situ* diagnostic tools are verified; (2) thin SSE and cathode are made; and (3) all-solid-state cells are made.

Collaborations. The PI is the Johnson Control Endowed Chair Professor, who has close and frequent collaboration with Johnson Controls' scientists and engineers. The collaboration enables the team to validate the outcomes of fundamental research in pilot-scale cells. The PI also has been working closely with top scientists at ANL, BNL, LBNL, and PNNL and with U. S. industrial collaborators, for example, GM, Millipore Sigma, and Clarios. In addition, the team works with international collaborators in China, Japan, and South Korea. These collaborations will be strengthened and expanded to give this project a vision with both today's state-of-the-art technology and tomorrow's technology in development, while incorporating feedback from material designers and synthesizers upstream, as well as from industrial end users downstream.

Milestones

1. Coated lithium anode with dendrite suppression demonstrated. Demonstrate effectiveness of inorganic artificial protective layer. (Q1, FY 2022; Completed)
2. Lithium anode with suppressed dendrite growth demonstrated. Demonstrate effectiveness of artificial protective layer. (Q2, FY 2022; In progress)
3. Down select materials and cell fabrication method for final cell build. (Q3, FY 2022; In progress)
4. All-solid-state cell build and test. (Q4, FY 2022; In progress)
5. Dendrite suppression demonstrated; cell performance verified. (Q4, FY 2022; In progress)

Progress Report

In FY 2021, the lithium anodes with different dynamic surface protection layers were put in test in full SSLBs. The team made major progress in the following areas: optimized and finalized test cell for a full SSLB; optimized *in situ* electrochemical optical cell for cross-section view; developed and demonstrated a long-cycle 4.0-V full SSLB. They demonstrated Li/Li symmetric cell with a polarization potential as low as 100 mV and a stable plating/stripping behavior over 1000 hours at 0.2 mA cm^{-2}, 0.2 mAh cm^{-2}. Moreover, $LiNi_{0.8}Co_{0.1}Mn_{0.1}O_2$/Li full solid-state cell delivered a high initial Coulombic efficiency (CE) of > 87%. To the best of the team's knowledge, this was the first case to employ lithium metal as anode in halide-based ASSBs.

Despite the high energy density at the material level and electrode level, the cell-level energy density was still rather unsatisfactory (< 50 Wh kg^{-1}). This was mainly due to the thick SSE pellet (0.5-1 mm). In addition, the pelletizing process itself is limited to lab-scale research due to its high cost and poor practicability. To boost cell-level energy density and render mass production feasible, sheet-type cells have been recognized as a "must-develop" technology.

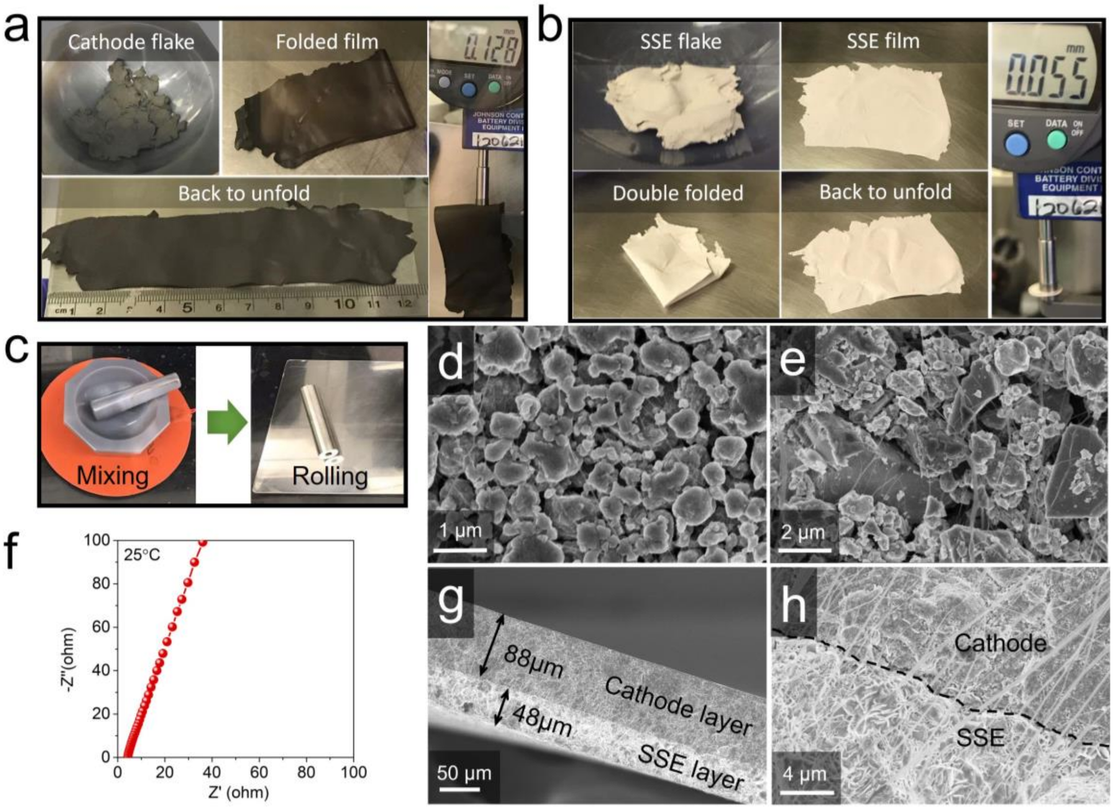

Figure 25. Flexibility test and thickness measurement of the (a) cathode sheet and (b) solid-state electrolyte (SSE) membrane. (c) Schematic illustration of the mixing and rolling process. Top-view scanning electron microscopy (SEM) images of the (d) cathode sheet and (e) SSE membrane before pressing. (f) Ionic conductivity of the SSE membrane after pressing. (g-h) Cross-sectional SEM images.

The team developed a solvent-free, dry-film approach to fabricate thin and flexible SSE with 0.4 wt% fibrous PTFE. The thickness was 55 µm for the SSE membrane (Figure 25b). As illustrated in Figure 25c, the shearing force and elevated operating temperature can trigger fibrillation of PTFE. As a result, all particles were intertwined in the PTFE network like a spider web. PTFE fibrils with nano-sized diameter were observed to be uniformly distributed within the SSE membrane (Figure 25e). The low binder percentage and nano-sized PTFE fibrils would be unlikely to block the conduction pathways within the SSE and cathode sheets. After cold pressing under 370 MPa, the SSE membrane displays an ionic conductivity of 1.4 mS cm^{-1} at 25°C

(Figure 25f), which is slightly lower than the binder-free SSE pellet (1.8 mS cm^{-1}) due to the insulating nature of PTFE. The thickness of SSE membrane film reduced to 48 µm after pressing (Figure 25g), corresponding to a compaction density of 2.6 g cm^{-3}. Notably, the areal resistance of SSE membrane was only 0.39 Ω cm^{-2}, two orders of magnitude lower than that of a binder-free SSE pellet. The PTFE fibril matrix remains intact after compression, which is expected to enhance the overall mechanical integrity of the sheet-type cell (Figure 25h).

Patents/Publications/Presentations

Publication

- Ji, W., X. Zhang, L. Xin, A. Luedtke, D. Zheng, H. Huang, T. Lambert, and D. Qu.* "A High-Performance Organic Cathode Customized for Sulfide-Based All-Solid-State Batteries." *Energy Storage Material* 45 (2022): 680.

Task 1.16 – Polyester-Based Block Copolymer Electrolytes for Lithium-Metal Batteries (Nitash Balsara, University of California, Berkeley)

Project Objective. The project objective is to design and synthesize polyester-based block copolymer electrolytes that can enable full-cell cycling at 1 mA/cm^2 or greater for 300 cycles. The cell comprises Li-metal anode, 4.5 V NMC cathode, and thin separators (20-50 µm) casted from the aforementioned block copolymer.

Impact. PEs offer increased stability in lithium batteries in comparison to more widely used liquid electrolytes (LEs). Block copolymer-based electrolytes containing both soft, ion-conducting domains and rigid, nonconducting domains offer the opportunity to tune both mechanical and electrical properties separately. Most block copolymer electrolytes studied thus far comprise poly(ethylene oxide) (PEO) as the conducting domain. The team hopes to develop polyester-based electrolytes that exhibit much higher transport properties and limiting currents than PEO-based electrolytes. An all-solid full cell with this new block copolymer electrolyte, a Li-metal anode, and an NMC cathode will have much higher energy density than current Li-ion technology.

Approach. The team will begin by synthesizing several series of polyester homopolymers and fully characterizing their blends with lithium salts as PEs in Li-Li symmetric cells. Next, they will make block copolymer electrolytes based on the most promising candidate and measure the electrochemical and mechanical properties thoroughly. Finally, they will assemble full cells with the optimum block copolymer electrolytes together with lithium metal and a 4.5 V NMC cathode.

Out-Year Goals. In the first year, the team will establish an efficient synthesis and characterization platform for polyester electrolytes. Several polyesters will be synthesized, and electrolytes will be made by blending each polymer with lithium salt. Transport properties (such as conductivity and current fraction) and limiting current of resulting electrolytes will be measured in Li-Li symmetric cells. The highest performing PE will be used as the conducting phase in the block copolymer design in the second year.

Collaborations. There are no active collaborations this quarter.

Milestones

1. Establish synthesis platform: synthesize at least two polyester electrolytes. (Q1, FY 2022; Completed)
2. Conductivity: measure conductivity of at least two electrolytes. (Q2, FY 2022; In progress)
3. Symmetric cell characterization: measure salt diffusion coefficient and current fraction of at least two electrolytes. (Q3, FY 2022)
4. Complete characterization: measure thermodynamic factor and thereby complete characterization of at least one polyester electrolyte. (Q4, FY 2022)

Progress Report

New Project

The following milestone has been completed: establish synthesis platform, and synthesize at least two polyester electrolytes.

This quarter, the team developed a general and efficient synthesis platform to make polyesters. Several poly(alkylene malonates) were synthesized through condensation polymerization of dimethyl malonate and the corresponding diol, as shown in Scheme 1. Ethylene glycol, 1,3-propanediol, 1,5-pentanediol, and 1,6-hexanediol were employed individually to make poly(ethylene malonate) (PEM), poly(trimethylene malonate) (PTM), poly(pentylene malonate) (PPM), and poly(hexylene malonate) (PHM). Heat and vacuum are employed for full condensation, but different conditions are required for each monomer. For PPM and PHM, transesterification catalyst Ti(O*i*Pr)$_4$ was used to aid polycondensation reaction at a lower temperature. Molecular weights of these polymers were in the range of 4-10 kDa based on the end group analyses of their ^{1}H nuclear magnetic resonance (NMR) spectra. Gel permeation chromatography (GPC) revealed the polydispersity to be ~ 2 by virtue of condensation polymerization. DSC shows that all these polymers are amorphous and the glass transition temperature (T_g) value decreases with increasing chain length of diol (n). Very high -OH end group functionality (> 95%) is observed in PPM. This feature allows the team to functionalize the chain ends and make block copolymers in the future. More recently, they have been able to make PPM with a molecular weight as high as 35 kDa.

Scheme 1. Synthetic scheme and nomenclature of polyesters made for this project.

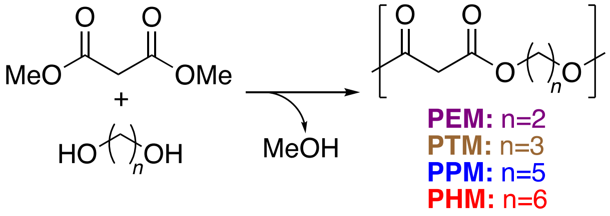

All four polyesters form soluble complex with LiTFSI salt. Blends of 40 wt% LiTFSI and 60 wt% polymer are amorphous. Their T_g values increased compared to homopolymers. The physical properties of these four polymers and blends are summarized in Table 2. The team then examined the T_g of PPM/LiTFSI electrolytes under a wide range of salt concentrations. Figure 26 shows a comparison of T_g data with PEO. While T_g of PEO/LiTFSI blends has a nonmonotonic dependence on salt concentration (r), T_g of PPM/LiTFSI blends increases linearly with increasing r. Moreover, all PPM/LiTFSI blends are fully amorphous. These thermodynamic studies show great promise of these polyester/LiTFSI blends to be electrolytes in lithium batteries.

Table 2. Structural characterization of polyesters made for this project.

Name	M_n (kg mol^{-1})	$Đ$	T_g of pure polymer (°C)	T_m of pure polymer (°C)	T_g of electrolyte (°C)
PEM	3.7	2	-20	NA	0
PTM	10.3	2	-35	NA	-10
PPM	9.6	2	-50	NA	-20
PHM	5.8	2	-60	NA	-25

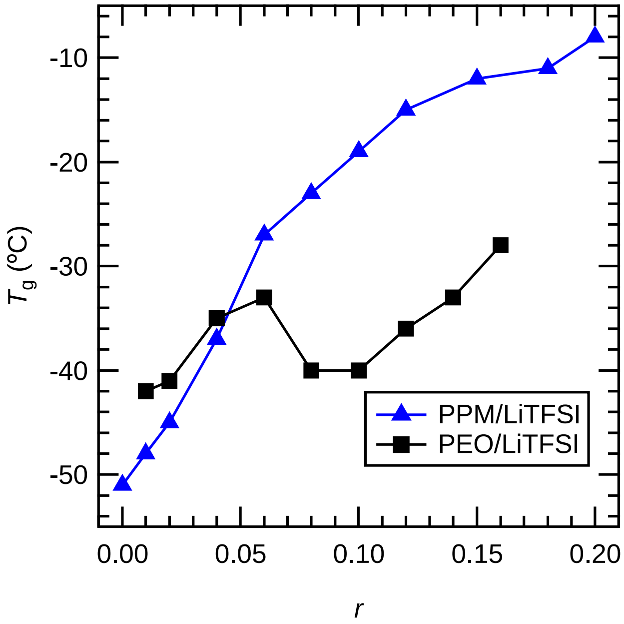

Figure 26. Effect of salt concentration (*r*) on the glass transition temperature of PPM/LiTFSI and PEO/LiTFSI electrolytes.

Next quarter, the team will carefully examine the conductivity of these PEs in Li-Li symmetric cells.

Patents/Publications/Presentations

Publication

- Chakraborty, S., G. K. Sethi, L. Frenck, A. S. Ho, I. Villaluenga, H. Wantanabe, and N. P. Balsara. "Effect of Yield Stress on Stability of Block Copolymer Electrolytes against Lithium Metal Electrodes." *ACS Applied Energy Materials* 5, No. 1 (2021): 852–861. doi: 10.1021/acsaem.1c03288.

Task 1.17 – Advanced Polymer Materials for Batteries
(Zhenan Bao and Yi Cui, Stanford University)

Project Objective. This project will develop new polymer materials for batteries. The team will develop polymer coatings with specific mechanical properties that can accommodate the volume expansion and contraction of the Li-metal anode associated with deposition and stripping (charging and discharging).

Project Impact. The cycling stability and CE of Li-metal electrodes will be increased by implementation of a polymer-based protective layer that functions as an artificial solid electrolyte interphase (SEI) with desired properties. The improved performance will enable further development toward practical utilization of Li-metal anodes with higher cycling efficiency and less susceptibility to dendrite-based failure.

Approach. The project uses soft polymer coatings with dynamic crosslinking to give the resulting polymers liquid-like rheological properties and stretchable and self-healing properties. In previous work, the project has shown that such coatings resulted in uniform deposition/stripping of lithium metal and improved cycling stability of Li-metal electrodes. To understand the design rules for effective polymer coatings, the team chose a few representative polymers to systematically understand structure property relationships. Here, the team investigates the correlation between surface energy of the polymer and exchange current for lithium deposition.

Out-Year Goals. Work will progress toward the correlation between dielectric constant and exchange current. These findings will enable further understanding and development of various polymer coatings for protecting Li-metal anodes.

Collaborations. This quarter, the team is collaborating with J. Qin at Stanford University.

Milestones

1. New lithium anode coating design. Design the polymer chemistry through DFT and contact angle measurement to find salt affinitive and solvent phobic moieties. (Q1, FY 2022; Completed)
2. Characterize the selective transport of salt over solvents for this polymer. (Q2, FY 2022)
3. Characterize the impact of the polymeric coating on lithium deposition morphology and short-term CE. (Q3, FY 2022)
4. Coat thin Li-metal electrodes with the polymeric coating and achieve stable lithium cycling for ≥ 200 cycles at 2.5 mAh/cm^2 capacity and C/3 D/5 current density in lean electrolyte condition. (Q4, FY 2022)

Progress Report

Batteries with Li-metal anode show great potential as the next-generation energy storage devices for their high theoretical energy density (3860 kw kg^{-1}). However, Li-metal batteries suffer from quick capacity fading and short cycle life. This is derived from the unstable interface between lithium metal and the electrolyte.

Specifically, the SEI that forms when lithium metal is in contact with the electrolyte is fragile and cracks during cycling. This inhomogeneity is further amplified throughout battery cycling, resulting in whisker-shaped deposited lithium and capacity fading.

Applying a polymer layer to the lithium anode stabilizes this interface and promotes long-term operation of Li-metal batteries. Polymers are desirable for this application due to their solution processability, programmable mechanical property, and tunable chemical composition. This polymer layer has both physical and chemical interactions with the underlying lithium metal.

Physically, a viscoelastic polymer layer provides mechanical suppression to the growing lithium during the deposition process, which promotes homogeneous deposition of lithium while maintaining uniform coverage of the electrode. By introducing moieties in the polymers that selectively interact with Li^+ or altering the Li^+ solvation environment, one can promote the transport of Li^+ at the interface.

Chemically, a polymer or polymer-based composite layer at the interface reacts with the underlying lithium metal and produces a robust interfacial layer. This process generally aims to produce a "salt derived SEI," which is found to promote stable operation of the lithium anode, when compared with the alternative "solvent derived SEI." However, to sustain this favorable SEI formation reaction, one relies on the limited reservoir of reaction materials in the polymer layer.

Here, the team investigates several siloxane-based polymers with four types of side chains to represent commonly used polymer chemistry in Li-metal battery: (1) glyme, for the application of PEO in SE; (2) pyrrolidinium trifluoromethanesulfonimide (PyTFSI), for electrochemically stable IL-based salt-solvation moieties; (3) perfluorinated chain, for polyvinylidene fluoride (PVDF) or poly(vinylidene fluoride-co-hexafluoropropylene) (PVDF-HFP) based polymer in gel electrolyte (GE) and coating application; and (4) alkyl chain, for widely-used polyethylene chemistry in separator. Siloxane polymers have demonstrated ability to improve the cycling performance of Li-metal anode. Beyond its relative chemical stability with Li-metal anode, the siloxane-based polymer chain is flexible and has a low glass transition point (~ -150°C). The fluid nature of the siloxane backbone offered the team freedom on altering the chemical composition of the polymer via side chain engineering while maintaining the viscoelastic mechanical property of the polymer. Past studies have shown that a flowable interface maintains uniform coverage of Li-metal anode during cycling and is more beneficial than a rigid interface, which can crack and form pin holes.

The team first examined the salt affinities of these polymer side chains with DFT calculation. Figure 27a shows the calculated interaction energy between these side chains and lithium cation. Glyme was known to form coordinated structures with lithium cations, which explains the high interaction energy (356.6 kJ mol^{-1}). The alkyl chain has low interaction energy with Li^+ (131.2 kJ mol^{-1}) due to the non-polar structure. The oxygen and fluorine on the perfluorinated chain forms coordinated structures with Li^+ with moderate interaction energy (223.2 kJ mol^{-1}). The PyTFSI IL side chain also has high interaction energy (355.4 kJ mol^{-1}) with Li^+, attributed to the ionic interactions between the Li^+ and the $TFSI^-$. The interaction energy of Li^+ with the glyme or PyTFSI side chains is nearly half the energy between Li^+ and anion (for example, Li^+-$TFSI^-$, 582.7 kJ mol^{-1}), indicating that these two side chains have limited ability to disassociate Li^+-anion pairing, and their affinity to Li^+ can be extended to their affinity to Li^+-anion salt complex.

Beyond salt affinity, the team further characterized the solvent phobicity of various polymer side chains through contact angle measurements. They dropped 10 µL of either carbonate [1 M $LiPF_6$ ethylene carbonate (EC) / diethyl carbonate (DEC) with 10% fluoroethylene carbonate (FEC); 1 M lithium hexafluorophosphate in

EC and DEC with 10% FEC) or ether [1 M LiTFSI 1,3-dioxolane (DOL) / 1,2-dimethoxyethane (DME), 1 M LiTFSI in DOL/DME) electrolyte to a polymer-coated silica wafer. Classic compound electrolytes were used here to cover a wide range of ether and carbonate solvents. Although the glyme side chain shows affinity to lithium salt, it is also electrolyte philic, demonstrated by the low (< 10°) contact angles for both ether and carbonate electrolyte. In comparison, the other salt affinitive PyTFSI side chain has less attraction to solvents (~ 20° contact angles). Both the alkyl and perfluorinated chains showed higher levels of solvent resistance with contact angles of ~ 40° for ether electrolytes and > 50° for carbonate electrolyte (Figure 27b).

Here, the team identified the PyTFSI side chain as salt affinitive with moderate electrolyte repelling ability. To further increase the solvent repelling capability of the polymer, they replaced 40% of the PyTFSI side chain with the perfluorinated chain. This dual side chain design strategy increased the contact angle from 22° to 36° in ether electrolyte, and from 29° to 45° in carbonate electrolyte, preserving the salt affinity of the polymer while increasing its solvent phobicity (Figure 27c). They named this designer polymer “SAEP” (salt affinitive electrolyte phobic).

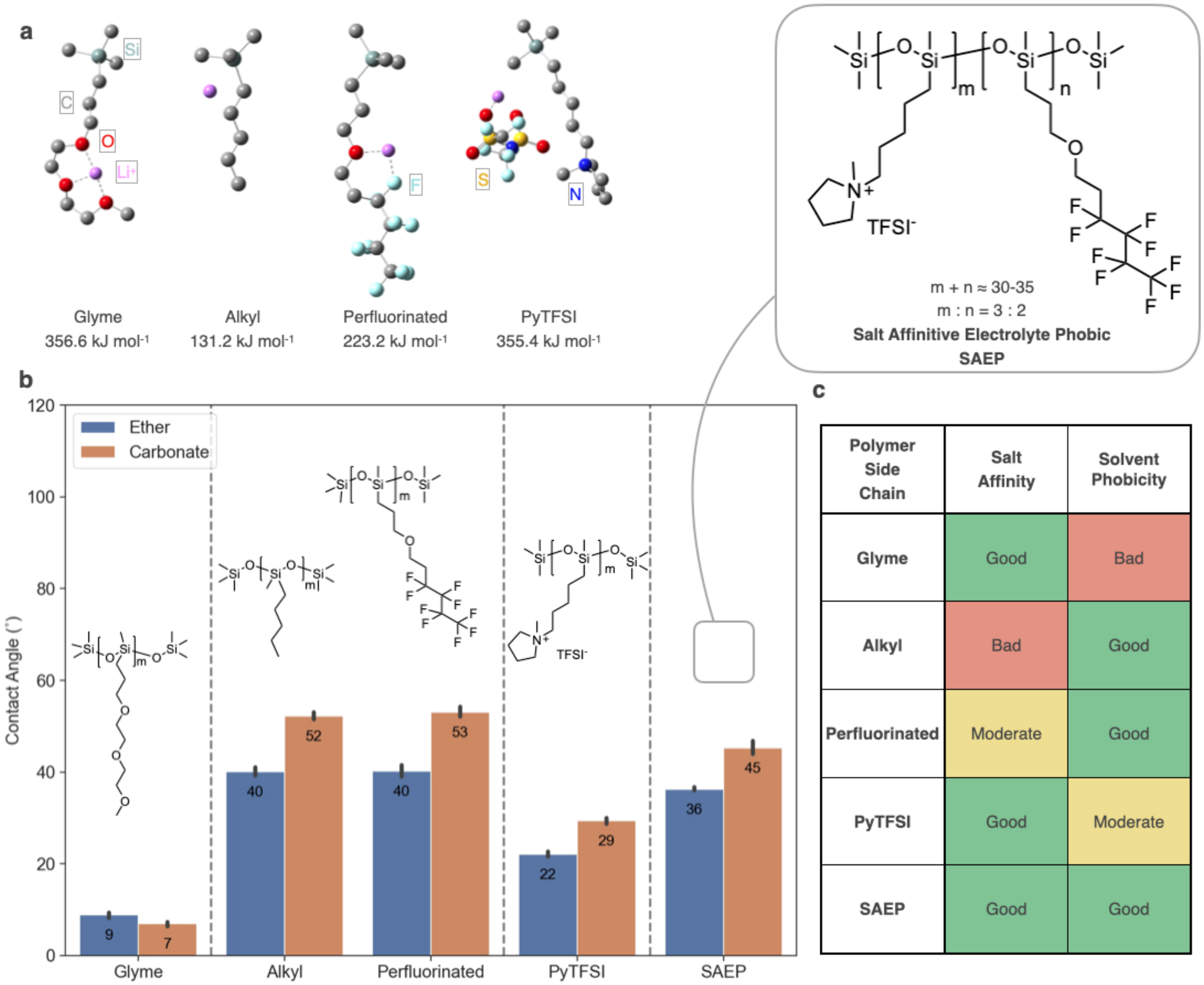

Polymer Side Chain	Salt Affinity	Solvent Phobicity
Glyme	Good	Bad
Alkyl	Bad	Good
Perfluorinated	Moderate	Good
PyTFSI	Good	Moderate
SAEP	Good	Good

Figure 27. Characterization of salt affinity and solvent phobicity. (a) Density functional theory (DFT) based calculation of the Li^+ interaction energy with various polymer side chains. (b) Contact angle measurement of polymer-coated silicon wafer with ether (1 M LiTFSI DME) or carbonate (1 M $LiPF_6$ EC/DEC with 10% FEC) electrolyte. (c) Comparison of salt affinity and solvent phobicity of various polymer side chains.

Patents/Publications/Presentations

Publications

- Yu, Z., P. E. Rudnicki, Z. Zhang, et al. "Rational Solvent Molecule Tuning for High-Performance Lithium Metal Battery Electrolytes." *Nature Energy* 7 (2022): 94–106. doi: 10.1038/s41560-021-00962-y.
- Kim, M. S., Z. Zhang, P. E. Rudnicki, et al. "Suspension Electrolyte with Modified Li^+ Solvation Environment for Lithium Metal Batteries." *Nature Materials* (2022). doi: 10.1038/s41563-021-01172-3.
- Wang, H., Z. Yu, X. Kong, et al. "Liquid Electrolyte: The Nexus of Practical Lithium Metal Batteries." *Joule* (2022). doi: 10.1016/j.joule.2021.12.018.
- Huang, Z., S. Choudhury, N. Paul, J. H. Thienenkamp, P. Lennartz, H. Gong, P. Müller-Buschbaum, G. Brunklaus, R. Gilles, and Z. Bao. "Effects of Polymer Coating Mechanics at Solid-Electrolyte Interphase for Stabilizing Lithium Metal Anodes." *Advanced Energy Materials* (2021). doi: 10.1002/aenm.202103187.

Task 1.18 – Molecular Ionic Composites: A New Class of Polymer Electrolytes to Enable All-Solid-State and High-Voltage Lithium Batteries
(Louis Madsen, Virginia Polytechnic Institute and State University)

Project Objective. Based on a newly discovered class of solid polymer electrolyte (SPE) materials, that is, molecular ionic composites (MICs), the overall objective is to develop solid-state lithium conductors targeted for use in transportation applications. MICs form a mechanically stiff, electrochemically stable, and thermally stable matrix. Specific objectives include the following: (1) development of robust MIC electrolyte thin films (~ 20 µm) to serve as simultaneous nonflammable separators and dendrite-blocking Li^+ conductors, (2) electrochemical quantification of key performance metrics including electrolyte stability, interfacial reactions, and suitability/compatibility with a range of electrode materials, and (3) comprehensive investigation of ion transport mechanisms and electrode-electrolyte interfacial reactivity under practical operating conditions using NMR and synchrotron X-ray analyses.

Project Impact. Commercialization of Li-metal SSBs is hampered by lack of a functional nonflammable SE that can provide high ionic conductivity, wide electrochemical window, favorable mechanical properties to inhibit lithium dendritic growth, and low interfacial resistance. The tunable MIC materials platform has potential to fulfill these requirements with relatively simple fabrication techniques, and thus shows promise for enabling nonflammable SSBs that can be optimized for low cost and high energy density.

Approach. MICs rely on a unique polymer that is similar to Kevlar® in its strength, stiffness, and thermal stability, but with densely spaced ionic groups that serve to form an electrostatic network that permeates mobile ions in the MIC. The team can tailor the ion concentrations and types to yield MIC electrolyte films that are electrochemically compatible with Li-metal anode as well as a range of high-voltage layered cathodes. They are searching the composition space of lithium salts, electrochemically compatible ILs, and polymer [poly(2,2′-disulfonyl-4,4′-benzidine terephthalamide), or PBDT] molecular weight to determine best composition windows for MIC electrolytes. The team is also investigating best methods for casting thin films in terms of temperature, solvent/evaporation conditions, and control over the initial liquid crystalline gel formation point. Concurrently, they are testing MIC films in various electrochemical cells, quantifying transport and structural/morphology parameters with NMR and X-ray techniques, and measuring key mechanical (dynamic mechanical thermal analysis, stress-strain) and thermal [DSC, thermal gravimetric analysis (TGA)] properties.

Out-Year Goals. This year, the team will generate a predictive model to understand the relationship between the mobility of all ions and the MIC synthesis parameters. The team will establish the testing protocol for NMR measurements under operating conditions. The team will study the surface chemistry of the MIC electrolyte before and after cycling. The team will identify methods to mitigate interfacial degradation. The team will test the final project electrolyte in full cell and develop specifications.

Collaborations. The team is collaborating with T. J. Dingemans' group at University of North Carolina, Chapel Hill, in which they are forming composites based on PBDT polymer and carbon materials such as graphene (Gr) oxide and are beginning to develop charged rigid-rod polymers building on the PBDT structure. The team is exploring shear rheology and broadband dielectric spectroscopy collaboration with R. H. Colby at Pennsylvania State University (PSU). They are collaborating with D. Nordlund and Y. Liu at SLAC and S-M. Bak at BNL to conduct synchrotron X-ray studies on MIC films.

Milestones

1. Multivariant analysis of the experimental parameters and electrochemical properties. (Q1, FY 2022; In progress)
2. *In situ* experiments implementing NMR spectroscopy and diffusometry at different cell states of charge. (Q2, FY 2022; In progress)

3. Spectroscopic surface analysis of cathode, anode, and MIC electrolyte after various cycling history. (Q3, FY 2022; In progress)
4. ASR: MIC/Li ≤ 10 Ω cm^2 and cathode/MIC ≤ 50 Ω cm^2 / cells. (Q4, FY 2022; In progress)

Progress Report

Last quarter, the team showed that the MICs made with $Pyr_{13}FSI$ demonstrated enhanced rate capability. To characterize this MIC material in detail, they measured the diffusion coefficients of the IL cation and anion in MICs with 10% PBDT and either 10% or 20% of two different lithium salts. As shown in Figure 28, the diffusion coefficients decrease when increasing the polymer content in the MIC, and when comparing the $Pyr_{13}FSI$ and $Pyr_{14}TFSI$ based MICs, both the cation and anion in $Pyr_{13}FSI$-based MIC show higher diffusion coefficients, indicating that the lithium ion will also likely diffuse faster; this could explain the higher rate capability of the new MICs.

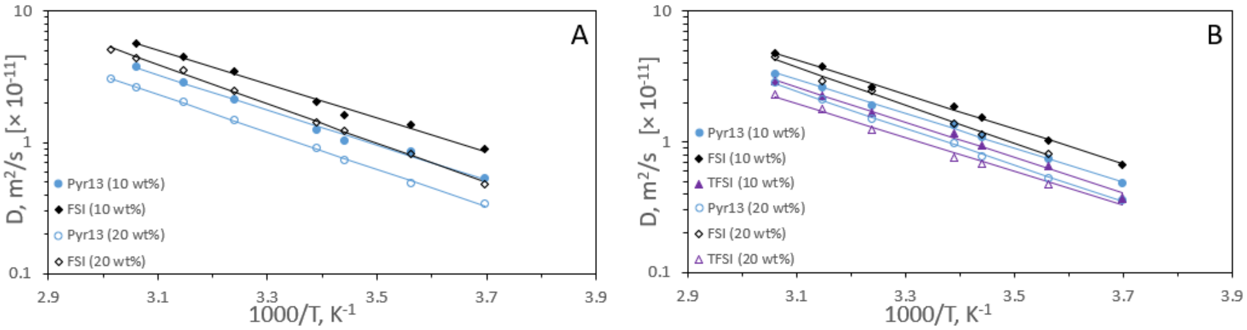

Figure 28. Temperature dependence of diffusion coefficients of $Pyr_{13}FSI$ in molecular ionic composites (MICs) with 10 wt% PBDT and LiFSI or LiTFSI salt. Panel (a) shows the effect of LiFSI wt% (10% or 20%) on diffusion coefficients, while panel (b) shows again the $Pyr_{13}FSI$ ionic liquid (IL), but with LiTFSI at 10 wt% or 20 wt%. In both cases, the diffusion coefficients are a factor of 3 larger than when using $Pyr_{14}TFSI$ IL with these salts. There is also a modestly higher diffusion for the LiFSI salt system as compared to LiTFSI, and only a modest decrease in ion diffusion when using 20 wt% salt as opposed to 10 wt%. Battery cell testing is under way with these optimized systems.

This quarter, they also investigated incorporation of other ILs with systematically varying molecular volume into MICs. This enables the team to understand the general effects of molecular volume in these materials, and thus more rationally modulate conductivity and mechanical properties. They can now make MICs using a large variety of ILs. Figure 29 shows the diffusion coefficients of the IL cation and anion in MICs prepared with a variety of ILs with different molecular volume. The team saw only a slight decrease in diffusion coefficients when comparing the ILs in the MICs to their neat IL counterparts, which agrees well with their previous study that the presence of a moderate amount of PBDT (10 wt%) does not drastically affect the diffusion of the ions. In addition, they also noticed that the size of the cation more dramatically affects the ionic diffusivity significantly, as shown in Figure 29d. When the molar volume of the cation increases, the diffusivity decreases. The team sees that it is due to the cation volume, rather than overall volume, that decreases the diffusivity; this is due to the increase in diffusivity when they change the anion from TfO^- to $TFSI^-$.

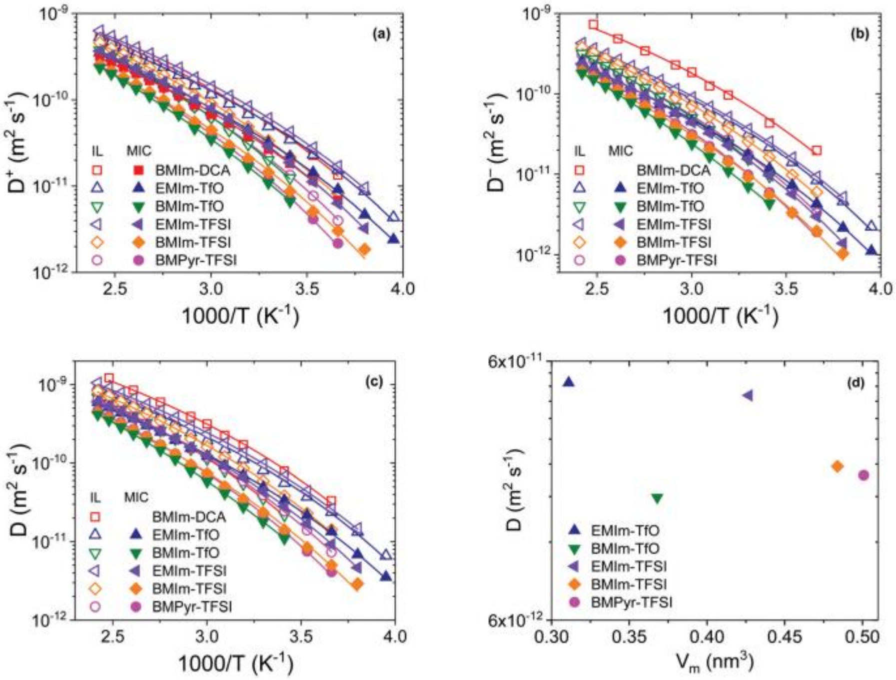

Figure 29. Temperature dependence of the (a) cation diffusion (D^+), (b) anion diffusion (D^-), and (c) ionic diffusivity (D) for neat ionic liquid (open symbols) and molecular ionic composite (MIC, filled symbols) samples, all with 10 wt% PBDT. (d) Ionic liquid molecular volume (V_m) dependence of the MIC ionic diffusivity at 30°C.

Furthermore, the team has progressed toward incorporation of high-energy-density Ni-rich cathode into MIC electrolytes. The electrochemical data show high energy density 558 Wh/kg with good capacity retention (92%) for 50 cycles. The coin cell, Li│MIC│Ni-rich cathode, was cycled between 2.5-4.2 V at 0.33 C-rate. Figure 30 provides an overview of these results. The team is exploring strategies to maintain capacity with higher upper cut off voltage. Compared to conventional PEs, their MICs demonstrated high energy density with good capacity retention.

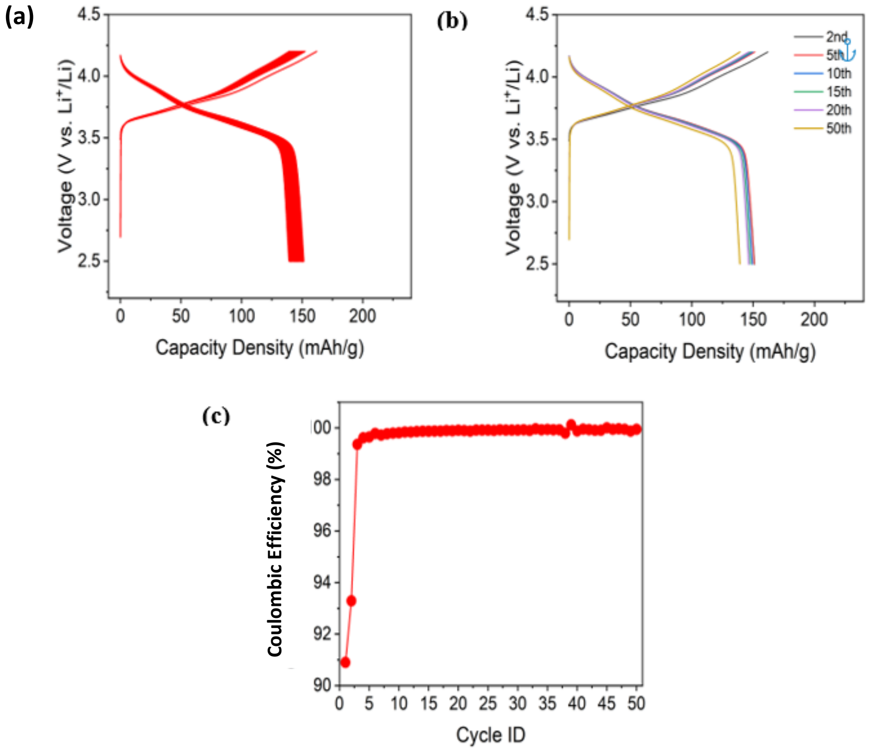

Figure 30. Li/MIC/Ni-rich cathode coin cell cycled at 60°C at C/3. The mass loading of the cathode material is 3.36 mg/cm^2. (a) Galvanostatic charge/discharge profiles at C/3 for 50 cycles. (b) Charge/discharge profiles by different cycle numbers. (c) Coulombic efficiency (%) for 50 cycles.

Patents/Publications/Presentations

Presentation

- 20th Solid-State Proton Conductors (SSPC-20) Conference, Virtual (October 1, 2021): "Effects of Nanoconfinement and Local Molecular Environment on Transport in Polymer Membranes"; L. A. Madsen. Invited.

Task 1.19 – Synthesis of Composite Electrolytes with Integrated Interface Design (Sanja Tepavcevic, Argonne National Laboratory)

Project Objective. This project aims to develop well-controlled, scalable LLZO nanofiber and CPE synthesis processes that will address the manufacturing challenges of current SSEs and demonstrate the fabrication of large-area, thin CPE membranes with outstanding electro-chemomechanical properties.

Impact. The outcome of this proposal will be a transformative manufacturing solution that can create large-area, mechanically and (electro)chemically stable SSEs (0 V to 4.5 V versus Li/Li^+) with Li^+ conductivity of $\geq 10^{-3}$ S/cm at room temperature enabling ≥ 1C charging rates.

Approach. To commercialize all-solid-state lithium-ion battery technology, further advances will require the application of knowledge, concepts, and tools from a variety of fields including materials science, physics, engineering, theory, and interfacial electrochemistry. The team's research philosophy is to establish a synthesis-material characterization-computation cycle that advances synthesis, chemistry, microstructure, interfaces, and transport in CPEs by a coordinated, interdisciplinary approach. The team's diverse expertise will allow them to understand, create, and rapidly scale up composite electrolytes to meet ambitious conductivity, energy, and power density targets.

Out-Year Goals. The innovative design and synthesis of integrated SSE interfaces include the following goals: (1) achieve high room-temperature conductivity by optimizing composite microstructures, synthetically modifying the LLZO-polymer interface, and reducing CPE membrane thicknesses down to 20 µm; (2) create a stable and effective interface between the CPE and metallic lithium that yields low charge transfer resistance and enables high CCD (> 3 mA/cm^2); and (3) modify the CPE-cathode interface to enable the use of different cathodes (LFP, LCO, NMC) and achieve high energy and power density in batteries.

Collaborations. Computational researchers will further help the team to understand and design better ASSBs. They will work closely with L. A. Curtiss, P. Barai, K. Chavan, and V. Srinivasan (ANL) to understand the molecular and mesoscopic characteristics and performance of the team's CPEs.

Milestones

1. Achieve uniform distribution of LLZO nanofibers within CPEs. (Q1, FY 2022)
2. Vary LLZO doping (aluminum, germanium, undoped) to improve conductivity and strength. (Q2, FY 2022)
3. Optimize LLZO nanofibers loading and processing to demonstrate good percolation and maximize conductivity. (Q3, FY 2022)
4. Use computational methods at the continuum level for the understanding of the improved conduction pathways and lithium deposition mechanisms. (Q4, FY 2022)

Progress Report

Progress for this new project will be reported next quarter.

Patents/Publications/Presentations

The project has no patents, publications, or presentations to report this quarter.

Task 1.20 – Polymer Electrolytes for Stable, Low-Impedance, Solid-State Battery Interfaces (X. Chelsea Chen, Oak Ridge National Laboratory)

Project Objective. The overall project objective is to develop stable polymer/cathode and polymer/anode interfaces with low interfacial impedance for integration of a thin solid composite electrolyte into a battery, to achieve chemical stability at the electrodes, high energy density (500 Wh/kg), high rate (1 mA/cm^2), and long cycle life (80% capacity retention for 300 cycles), demonstrated in pouch cells.

Impact. Achieving stable and low impedance interfaces at both the cathode and anode sides is critical to achieve high energy density with excellent safety, lifetime, and cycling efficiency. This project will identify key design strategies that should be used to prepare PE to achieve stable and low impedance polymer/cathode and polymer/Li interfaces and to develop processing procedure to integrate a thin composite electrolyte into a SSB battery. Success will enable DOE technical targets: energy density of 500 Wh/kg with 80% capacity retention for at least 300 cycles.

Approach. The team's main design principle is to use an oxide ceramic as the main ion transporting phase in the electrolyte and a fluorinated polyether-based PE to form optimized interfaces as well as to provide flexibility to the electrolyte membrane. Compared with inorganic electrolytes, PEs are soft and flexible and capable of maintaining good contact at interfaces. However, several technical barriers remain. On the lithium metal side, the interface between PEs and thin-lithium and Li-free anodes is still at an early stage of investigation. Interface optimization using thin-lithium and Li-free designs is crucial to reaching the DOE 500 Wh/kg target. On the cathode side, studies on the polymer/cathode interface are scarce. The interface resistance between polymer (catholyte) and CAM is not well understood. In addition, with a target voltage stability of 0-4.5 V versus Li/Li^+, a polymer with oxidative stability up to 4.5 V is needed. Fluorinated polyethers have the potential to form stable and low impedance interfaces at both the cathode side and the anode side. By systematically examining the effects of fluorine content, polymer chain length and structure, and plasticization on the interfacial resistance with the cathode and the anode, a balance between the desolvation kinetics of Li^+ and diffusion rate will be achieved to optimize the interface ion transport. A fundamental understanding of the origin of interfacial impedance with the cathode as well as Li-metal anode will be developed along the optimization process to generate design rules for polymers with optimized interfaces. The team will also develop a processing procedure to integrate a thin composite electrolyte that was previously developed into a full cell. The composite electrolyte features an interconnected ceramic structure with a thickness of 20 µm. It will be backfilled with the newly developed fluorinated PEs. The mechanical properties of the composite electrolytes will be optimized to accommodate roll-to-roll processing.

Out-Year Goals. In the second and third year of this project, the team will focus on optimizing the cathode/polymer as well as the Li-anode/polymer interface with maximized stability and minimized interfacial impedance. A fundamental understanding of parameters that determine the interfacial impedance and strategies to minimize the interfacial impedance will be developed. The fourth and fifth year of the project will be focused on integration of a thin composite electrolyte into a full cell to achieve high energy density, high rate, and long cycle life, as stated in the overall project objectives. Processing techniques and procedures for electrolyte integration will be investigated to achieve this goal.

Collaborations. Work is conducted by B. Armstrong, S. Kalnaus, R. Sahore, X. Tang, A. Ullman, and X. C. Chen.

Milestones

1. Synthesize fluoropolyether polymers with four fluorine concentrations. (Q1, FY 2022; In progress)
2. Quantify ionic conductivity, Li^+ transference number, oxidative stability, thermal stability, glass transition temperature, and mechanical modulus as a function of fluorine concentration. (Q2, FY 2022; In progress)

3. Optimize conductivity of composite electrolyte with a 3D interconnected structure (at least 5×10^{-5} S/cm at room temperature). Measure flexural strength of the composite electrolyte with three compositions. (Q3, FY 2022)
4. Quantify interfacial resistance and stability between the fluoropolyether polymers and lithium anode from two different sources. (Q4, FY 2022)
5. Build a prototype SSB in a pouch cell using the interconnected composite electrolyte as the electrolyte layer. (FY 2022 Annual Stretch Milestone)

Progress Report

This quarter, the team began synthesis of fluorinated polyethers. Three precursor oligomers were purchased from commercial sources: two hydrogenated polyethers with different molecular weights (P-1000 and P-500), and a fluoro polyether (F-1000). For intellectual property purposes the structure of these precursors is omitted in this report. The molecular weights are used to tune the domain size of the fluorinated sections, and the fluorine content can be adjusted by varying the weight ratios of the fluorinated polyether to the hydrogenated polyether. The synthesis procedure was explored, with results shown in Table 3.

Table 3. Synthesis of fluorinated polyethers with different fluorine contents.

Solvent: Acetonitrile (A), Freon 113 (B), DMF (C)						
Sample	**Composition**	**Li Salt**	**Solvent**	**Temperature for Mixing**	**Dissolves (Yes or No)**	**Membrane Appearance**
1	P-1000	Y	A	RT	Y	Clear
2	P-1000/P-500M (1:1 w/w)	Y	A	RT	Y	Clear
3	F-1000	N	A+B (1:1 v/v)	RT	Y	White
4	F-1000	N	B	RT	Y	Clear
5	F-1000 + P-1000 (3:7 w/w)	N	A+B (1:1 v/v)	RT	N	
6	F-1000 + P-1000 (3:7 w/w)	Y	A+B (1:1 v/v)	RT	N	
7	F-1000 + P-1000 (3:7 w/w)	N	C	RT/70°C	N	
8	F-1000 + P-1000 (3:7 w/w)	Y	C	RT/70°C	N	
9	F-1000 + P-500 (3:7 w/w)	N	A+B (1:1 v/v)	RT	N	
10	F-1000 + P-500 (3:7 w/w)	N	Not Used	RT	N	
11	F-1000 + P-500 (3:7 w/w)	N	B	RT	Y	Hazy/Clear
12	F-1000 + P-500 (3:7 w/w)	Y	B	RT	N	
13	P-500	N	A	RT	Y	Clear
14	P-500	Y	A	RT	Y	Clear

In all membrane synthesis procedures, an initiator was used. Due to the presence of fluorine, fluoro polyether F-1000 is not miscible with the hydrogenated polyethers, without the presence of a solvent (sample 10, Table 3). The team tried three solvents [acetonitrile, trichlorotrifluoroethane (Freon 113), and dimethyl formamide (DMF)] to mixtures of fluoro and hydrogenated polyethers. The hydrogenated polyethers without any fluorine can be dissolved in acetonitrile and DMF. The fluoro polyether can be dissolved in Freon 113. However, the mixture of fluoro and hydrogenated polyethers cannot be dissolved in either DMF (samples 7-8), or a mixture of acetonitrile and Freon 113 (samples 5-6). Further investigation shows that the 3:7 w/w mixture of F-1000 and P-500 can be co-dissolved in Freon 113 if the lithium salt is not mixed in (sample 11).

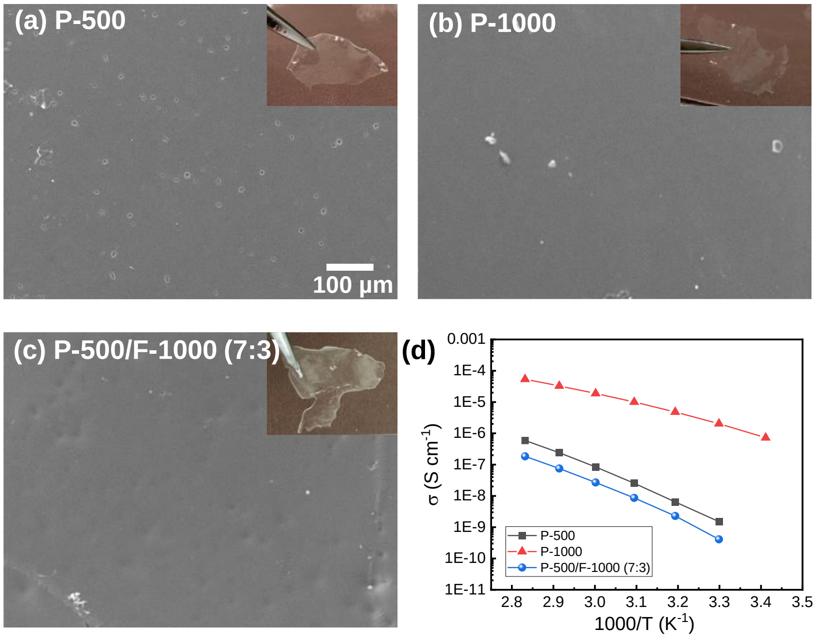

Figure 31. (a-c) Scanning electron microscopy of fluoro and hydrogenated polyether membranes. Inset: physical appearance of the membrane. (a) P-500. (b) P-1000. (c) P-500/F-1000 7:3 w/w. (d) Ionic conductivity of the three membranes as a function of inverse temperature.

Based on the results in Table 3, membranes were obtained by mixing F-1000 and P-500 at 3:7 w/w ratio in Freon 113, while bubbling dry N_2 through the solution. The solution was then cast between two glass plates. Glass cover slips were used to control the gap between the glass plates and the resulting membrane thickness. The solution was cured with the presence of the initiator, and a membrane was thus obtained. Control membranes containing only P-500 and P-1000 using acetonitrile as the solvent were also synthesized. The membrane was gently peeled off the glass plates and dried in a vacuum oven at 80°C overnight. The saltless membranes were subsequently soaked in 1 M lithium salt solution in a mixture of EC and DEC for 24 hours. After infusing the lithium salt, the membrane was dried again in the vacuum oven at 80°C overnight. TGA results show that the Li-salt concentration was 38 wt% in both P-500 and the blend membrane. For P-1000, the lithium salt was blended into the membrane in the solution mixing phase.

The morphology and appearance of the three membranes are shown in Figure 31. P-500 and P-1000 are clear, homogeneous membranes with small surface defects (Figure 31a-b). The blend membrane has hazy parts and clear parts, although SEM did not reveal phase separation of the membrane (Figure 31c). The conductivity of the membranes is shown in Figure 31d; the blend membrane's conductivity is 30 to 50% lower than that of P-500. This is to be expected, as fluoro ether groups do not solvate Li^+ nearly as well as the ethylene oxide groups. On the other hand, the conductivities of P-500 and the blend membrane are much smaller (2 to 3 orders of magnitude) than that of P-1000. Next quarter, efforts will be made toward optimizing membrane preparation procedure and optimizing ionic conductivity.

Patents/Publications/Presentations

The project has no patents, publications, or presentations to report this quarter.

Task 1.21 – Ion Conductive High Li^+ Transference Number Polymer Composites for Solid-State Batteries

(Bryan McCloskey, University of California, Berkeley)

Project Objective. This project seeks to develop polymer-inorganic composites that have an optimal combination of conductivity, processability, and low interfacial resistance at both a Li-metal anode and a porous $Li[Ni, Co, Mn]O_2$ (NMC) cathode. In an effort to enable Li-metal anodes, mechanically rigid solid-state Li^+ conductors, such as LLZO, $Li_{1+x}Al_xTi_{2-x}(PO_4)_3$ (LATP), and Li_2S-P_2S_5 glasses (LPS), have been employed due to their high Li^+ ion conductivity and, when engineered to eliminate interfacial defects, appropriate stiffness to suppress Li-metal dendrite formation. However, for these materials to result in batteries that compete against current commercial cells in terms of energy density and cost per kWh, they would need to be manufactured at no more than 50-µm thickness and cost no more than $5 per square meter. These metrics are daunting for pure thin-film inorganic ion conductors, particularly when a porous, thick cathode also needs to be used to achieve competitive cell energy densities. To overcome these challenges, this project aims to develop polymer-inorganic composites, where high Li^+ transference number PEs serve as a binder for inorganic ion conducting particles.

Impact. By optimizing the composition of this composite electrolyte, the team aims to marry the processability and interfacial mechanical compliance of polymers with the impressive transport properties of inorganic composites, thereby enabling roll-to-roll manufacturing to allow thin (< 50 µm) layers of high-conductivity solid-state conductors to be cost-effectively incorporated into batteries.

Approach. The project approach relies on the following key steps in FY 2022: (1) using monomers with TFSI anions appended to them, synthesize and characterize polyanionic PEs with high Li^+ transference number and conductivity; (2) through systematic material structure-property characterization, understand how to reduce interfacial ion transport impedance between inorganic ion conductors (specifically, thin film inorganic conductors such as LLZTO, LATP, and LPS) and high Li^+ transference number PEs; and (3) characterize electrode-polymer and electrode-inorganic conductor interfacial resistances at a Li-metal anode.

Out-Year Goals. The overall project goal is to develop an optimized polymer-inorganic LIC with superior conductivity (> 1 mS/cm), thin-film processability, and low electrode interfacial impedance. Of particular interest in the out years is development of a process to fabricate thick, porous, and electrochemically stable NMC cathodes using the polymer-inorganic composite as both the binder and electrolyte. The team aims to integrate the optimized high-loading cathode with a 25-µm thin-film polymer-inorganic electrolyte to create an "anode-less" battery with 500 Wh/kg and 80% capacity retention after 300 cycles.

Collaborations. While this project has a single PI, B. McCloskey will leverage the collaborative battery research environment at LBNL and coordinate with other LBNL PIs in the BMR Program for materials and experimental development.

Milestones

1. Establish polymer synthesis by making two neat TFSI-containing polymers. (Q1, FY 2022; In progress)
2. Measure conductivity of two polymers using Li-Li symmetric cells. (Q2, FY 2022)
3. Measure interfacial impedance evolution of polymer in a Li-Li cell. (Q3, FY 2022)
4. Synthesize a series of four copolymers with various ratios of TFSI monomer and a film-forming monomer. (Q4, FY 2022)

Progress Report

Progress for this new project will be reported next quarter.

Patents/Publications/Presentations

The project has no patents, publications, or presentations to report this quarter.

Task 1.22 – Inorganic-Polymer-Composite Electrolyte with Architecture Design for Lithium-Metal Solid-State Batteries
(Enyuan Hu, Brookhaven National Laboratory)

Project Objective. This project targets the following goal: the composite electrolytes will be thin (< 100 μm) and have high Li-ion conductivity ($\geq 10^{-3}$ S/cm at room temperature), low interfacial impedance, and desirable mechanical properties. When used in the SE Li-metal battery, a current density > 1 mA/cm^2 and an aerial capacity of 2-3 mAh/cm^2 can be achieved with more than 300 cycles. The constructed NMC/LiCoO$_2$||composite electrolyte||Li-metal cell can be operated at up to 4.5 V versus Li$^+$/Li. The SE will also be compatible with high loading cathodes in achieving high energy density at the coin or pouch cell level.

Impact. The results of this project will lead to advancement of SSBs, a beyond Li-ion battery option with better safety characteristics and higher energy density. The project will also provide valuable knowledge to U. S. industries in scaling up SSB production for vehicle applications, thus providing solutions to the clean energy strategy.

Approach. The project approaches are as follows: (1) design and synthesize polymer with anion-tether strategy for high transference number, (2) through theories and experiments, design hierarchical inorganic electrolyte for suppressing lithium dendrite penetration, (3) optimize the composite electrolyte composition and structure, (4) use additives for Li-metal anode and $LiNi_xMn_yCo_{1-x-y}O_2$ (NMC) cathode protection, and (5) use synchrotron and cryo-EM characterization to understand the bulk electrolyte and interphases.

Out-Year Goals. The out-year goals are to synthesize single ion conducting SPE with high transference number and conductivity; to design hierarchical inorganic electrolyte with high ionic conductivity and good mechanical/electrochemical stability; and to use synchrotron total scattering to study the structure of ceramic/polymer electrolyte.

Collaborations. This project PI will work closely with co-PI H. Xin of University of California, Irvine, and co-PI X. Li of Harvard University.

Milestones

1. Synthesize single ion conducting SPE with high transference number and conductivity. Achieve formulation optimization to achieved transference number > 0.5. (Q1, FY 2022; In progress)
2. Design hierarchical inorganic electrolyte with high ionic conductivity and good mechanical/electrochemical stability. Develop inorganic electrolytes (sulfides, halides) with ionic conductivity > 1 mS/cm and a hierarchy of voltage stability up to 4.5 V and down to near 0 V in CV tests. (Q2, FY 2022).
3. Optimize composition for plastic hybrid electrolyte. Tune the SPE and inorganic electrolyte composition to enable compatibility. (Q3, FY 2022)
4. Use synchrotron total scattering to study the structure of ceramic/polymer electrolyte. Complete synchrotron pair distribution function (PDF) analysis of the ceramic/polymer electrolyte. (Q4, FY 2022)

Progress Report

Progress for this new project will be reported next quarter.

Patents/Publications/Presentations

The project has no patents, publications, or presentations to report this quarter.

Task 1.23 – Solid-State Batteries with Long Cycle Life and High Energy Density through Materials Design and Integration
(Gerbrand Ceder, University of California, Berkeley)

Project Objective. This project aims to create solid-state Li-metal batteries (SSLMBs) with high specific energy, high energy density, and long cycle life using scalable processing techniques. The team will achieve this by addressing fundamental challenges associated with (1) interfacial reactivity, (2) Li-metal plating, and (3) cathode loading. Addressing these challenges supports the broader VTO goal of SSBs with increased cycle life and energy density.

Impact. Ultimately, this project will develop an understanding of how to prevent interfacial reactions, make uniform Li-metal plating, and increase cathode loading significantly. The knowledge obtained from this project will be used to design SSLMBs with high specific energy of 500 Wh/kg, 80% capacity retention for at least 300 cycles, and CCD > 1 mA/cm^2.

Approach. This project addresses several fundamental challenges and makes the SSLMB competitive, surpassing the specific energy, energy density, and cycle life of Li-ion batteries:

- Create homogeneous lithium deposition on the anode without penetration of lithium metal through the separator to achieve high cycle life and high safety. The team will achieve this with the use of an active buffer layer (ABL) that combines active and inactive components to homogenize lithium plating and to keep the lithium plating potential away from the SE separator.
- Limit chemical reactivity and mechanical decohesion between the SE, carbon, and cathode material in the composite cathode so that high cycle life can be achieved. The team will limit chemical reactivity by protecting the carbon from the SE, by using novel cathode coatings designed to be stable to high voltage and that do not react with the SE, by using novel solid halide catholyte conductors, and by using inorganic/organic solid composite electrolytes in the cathode.
- Achieve high volumetric loading of the active cathode material in the composite cathode to achieve high energy density and high specific energy. The team will achieve high volumetric cathode loading by creating thin highly porous conductor scaffolds that are infiltrated with cathode, by tailored particle size distributions of deformable lightweight conductors, and by the use of organic/inorganic hybrids.
- Create inexpensive materials and processes to fabricate SSBs so that they can be cost-competitive with Li-ion batteries. The team will create solution-processable organic/inorganic hybrids to be used as separator and to blend in the composite cathode; they will use inexpensive, scalable ceramics processing techniques to create high loading composite cathodes.

Out-Year Goals. The ultimate project goal is to develop SSLMBs that achieve high specific energy of 500 Wh/kg, 80% of capacity retention after 300 cycles, and > 1 mA/cm^2 of critical density.

Collaborations. This project collaborates with the following co-PIs: H. Kim, V. Battaglia, G. Chen, M. M. Doeff, G. Liu, M. Scott, M. Tucker, and J. Urban, all at LBNL.

Milestones

1. Demonstration of use of ABL in Li-metal cell with active component other than silver. (Q1, FY 2022; In progress)
2. Integration of NCM into 3D carbon framework with ACM loading > 80 wt%. (Q2, FY 2022)
3. Model studies to assess compatibility of cathode components. (Q3, FY 2022)
4. LPSCl polymer composite glass with 0.1-1 mS/cm. (Q4, FY 2022)

Progress Report

Progress for this new project will be reported next quarter.

Patents/Publications/Presentations

The project has no patents, publications, or presentations to report this quarter.

Task 1.24 – Low-Pressure All-Solid-State Cells
(Anthony Burrell, National Renewable Energy Laboratory)

Project Objective. The goal of this project is to develop ASSBs using four classes of SSEs, and/or electrode modifiers, that can be used to achieve the final 500 Wh/kg cell target. These materials will be down selected using full-cell testing and advanced characterization to achieve cell targets at cell pressures less than 100 psi.

Impact. Many factors limit ASSB performance, and this project seeks to address the interface stability of both the lithium interface and the high-voltage cathode. The combination of multiple ionic conductors coupled is specifically targeted to allow solution processing, and low-pressure cell outcome will enable lower cost deployment of solid-state cells in automotive applications.

Approach. To achieve the goal of low-pressure ASSBs, the team is utilizing three classes of solid ion conductors, sulfide materials, melt-processable lithium carboranes, and multinary metal halides. These materials can be chemically modified to optimize ionic conductivity and voltage stability in single conductor modes or in combinations to effect interface modification for full-cell development. Specifically, the use of flexible ionic conductors at the cathode interface will enable the mechanical effects of cathode expansion and contraction to be mitigated. In combination with the materials discovery work, the project has an extensive characterization team to help determine the impacts of interface, chemical, electrochemical, and mechanical factors on system performance. Full-cell assembly and development, targeting approaches that are readily scalable and compatible with roll-to-roll process, will drive the materials innovation and development.

Out-Year Goals. The out-year goal is demonstration of 2 Ah cells that achieve 500 Wh/kg and lifetimes exceeding 300 cycles at functional pressures below 100 psi.

Collaborations. There is a joint effort for this project between National Renewable Energy Laboratory (NREL), M. Toney at the University of Colorado, and A. Maughan at the Colorado School of Mines.

Milestones

1. Prepare electrochemical cells using lithium carboranes. (Q1, FY 2022; In progress)
2. Prepare electrochemical cells using LiyMClz. (Q2, FY 2022).
3. Prepare electrochemical cells using sulfur-polymer-coated cathodes. (Q3, FY 2022)
4. Demonstrate full-cell design that enables accurate, repeatable internal pressure control for ASSBs. (Q4, FY 2022)

Progress Report

Progress for this new project will be reported next quarter.

Patents/Publications/Presentations

The project has no patents, publications, or presentations to report this quarter.

Task 1.25 – Precision Control of the Lithium Surface for Solid-State Batteries
(Andrew Westover, Oak Ridge National Laboratory)

Project Objective. The overall goal of this project is to understand and engineer the surface and purity of thin Li-metal anodes to enable batteries with an energy density of 500 Wh/kg and a cycle life >300 cycles.

Impact. The knowledge of lithium surface engineering and the implications for cell design of Li-metal-batteries will improve commercialization efforts for SSLMBs. There is very little standard knowledge about variations in the impurity level in different lithium sources, the surface chemistry of different lithium surfaces, and their impact on performance. Furthermore, the strategies developed to engineer the surface of the lithium metal for integration into Li-metal batteries will provide significant performance increases, ideally enabling successful commercialization.

Approach. This project is broken into two parts. First, the team is focused on thoroughly understanding the purity, mechanics, and surface chemistry of multiple lithium sources and how these parameters impact performance. Second, they will focus on intentional engineering of the lithium purity and surface chemistry to control the mechanical properties, electrochemical stability, and electrochemical performance. They will explore three approaches to engineer the surfaces: gas-phase passivation, deposition of thin metal coatings, and deposition of thin inorganic coatings. To test electrochemical performance, they will use standard ceramic and polymer electrolytes to demonstrate the impact of purity and surface chemistry. The program will also employ a range of standard and specialized characterization techniques, including a significant focus on understanding the mechanics of lithium metal using nanoindentation and adhesion measurements using surface probe microscopy.

Out-Year Goals. In FY 2023, the program plans to finish gaining a deep understanding of different lithium sources, purity, and surface conditions, and of how they affect performance in Li-metal cells with both ceramic and polymer electrolytes. In FY 2024 through FY 2027, the primary goal is to develop strategies to carefully control and engineer the surface of lithium metal to optimize performance, enabling batteries that can achieve 500 Wh/kg and cycle for more than 300 cycles at mid-to-high current densities.

Collaborations. The primary collaborator for this project is E. Herbert at Michigan Technological University (MTU), who is focused on mechanical measurements of Li-metal anodes and electrolytes in inert environments. The project also includes R. Sahore, S. Kalnaus, W-Y. Tsai, and R. Sacci of Oak Ridge National Laboratory (ORNL). The team anticipates the BMR program will also foster significant collaborations with other teams who have a complementary focus on lithium metal.

Milestones

1. Obtain lithium sources. (Q1, FY 2022)
2. Conduct chemical characterization of lithium surfaces. (Q2, FY 2022).
3. Conduct nanoindentation of various lithium sources. (Q3, FY 2022)
4. Establish baseline electrochemical performance of multiple lithium sources. (Q4, FY 2022)

Progress Report

Progress for this new project will be reported next quarter.

Patents/Publications/Presentations

The project has no patents, publications, or presentations to report this quarter.

TASK 2 – DIAGNOSTICS

Team Lead: Guoying Chen, Lawrence Berkeley National Laboratory

Summary and Highlights

To meet the goals of the VTO programs on next-generation EVs, low-cost and abuse-tolerant batteries with higher energy density, higher power density, better safety, and longer lifetimes are needed. In pursuit of these goals, high cell operating voltages and demanding cycling conditions are used, which leads to unprecedented chemical and mechanical instabilities in cell components. Successful implementation of promising electrode materials (such as silicon anode and high-voltage cathodes) and new cell chemistry (such as high-energy Li-metal cells combined with SSEs) requires better understanding of fundamental processes, especially those at the interface/interphase of both anode and cathode. Identifying and understanding structure-property-electrochemical performance relationships in materials and various failure modes in cell chemistry are therefore more pressing than ever, not only in guiding battery development activities but also the scale-up efforts needed for commercialization.

Task 2 takes on these challenges by combining model systems, *ex situ*, *in situ*, and *operando* approaches, with an array of state-of-the-art analytical and computational tools. Numerous subtasks are tackling the chemical processes and reactions at the electrode/electrolyte interfaces in Li-metal batteries. Researchers at LBNL use surface- and bulk-sensitive techniques, including FTIR, attenuated total reflectance (ATR)-FTIR, near-field infrared (IR) and Raman spectroscopy/microscopy, and scanning probe microscopy (SPM) to characterize changes in materials and the physicochemical phenomena occurring at the interface of Li-metal electrode. GM is developing *in situ* diagnostic techniques, including atomic force microscopy (AFM), nano-indentor, dilatometer, and stress-sensor, to be combined with atomic/continuum modeling schemes to investigate the coupled mechanical/chemical degradation of the SEI layer as well as the microstructural evolution at the interface/interphase of Li-metal anode. UH is developing multidimensional diagnostic tools, including FIB-SEM, time-of-flight secondary ion mass spectrometry (TOF-SIMS), and in-SEM nanoindentation, to probe structural, chemical, and mechanical evolution at the interfaces of SSLBs. At LBNL, model systems of electrode, SSE, and their interfaces with well-defined physical attributes are being developed and used for advanced diagnostic and mechanistic studies at both bulk and single particle levels. These controlled studies remove the ambiguity in correlating a material's physical properties and reaction mechanisms to its performance and stability, which is critical for further optimization. Subtasks at BNL and PNNL focus on the understanding of fading mechanisms in electrode materials, with the help of synchrotron-based X-ray techniques (diffraction and hard/soft XAS) at BNL and high-resolution transmission electron microscopy (HRTEM) / STEM and related spectroscopy techniques at PNNL. The final subtask at Stanford/SLAC develops and utilizes an integrated X-ray characterization toolkit to investigate and generate insights on SSBs, by tracking the evolution of nanoscale chemistry as well as structure, microstructure, and transport properties. The diagnostics team not only produces a wealth of knowledge key to developing next-generation batteries, they also advance analytical techniques and instrumentation with a far-reaching effect on material and device development in various fields.

Highlight

The UH (Y. Yao) group conducted depth-profiling TOF-SIMS analysis to understand the interfacial reactions between Li-metal anode and Li_3PS_4 glass-ceramic electrolyte. The presence of self-passivation reactions during lithium plating was demonstrated.

Task 2.1 – Characterization and Modeling of Lithium-Metal Batteries: Model-System Synthesis and Advanced Characterization

(Guoying Chen, Lawrence Berkeley National Laboratory)

Project Objective. This project will use a rational, non-empirical approach to design and develop SSE materials and interfaces for next-generation Li-metal batteries. Combining a suite of advanced diagnostic techniques with carefully prepared model-system samples, the project will perform systematic studies to achieve the following goals: (1) obtain understanding on the role of SSE grain and grain boundaries (GBs) on ion conduction and dendrite formation, (2) obtain fundamental knowledge on rate- and stability-limiting properties and processes in SSEs when used in Li-metal batteries, (3) investigate the reactivities between SSE and electrodes, and gain insights on the dynamic evolution of the interfaces, and (4) design and synthesize improved SSE materials and interfaces for safer and more stable high-energy Li-metal batteries.

Impact. The project will focus on fundamental understanding of SSE and relevant interfaces to enable its use in Li-metal batteries. Knowledge gathered from model-system-based studies will guide the design and engineering of advanced materials and interfaces. The use of the non-empirical, rational-design approach will develop high-energy battery systems with improved commercial viability.

Approach. The project will combine model-system synthesis and advanced diagnostic studies to investigate ion conduction and interfacial chemistry of SSE in Li-metal batteries. Single crystalline (SC), polycrystalline (PC), and amorphous model SSE samples with various grain and GB properties will be synthesized. Model interfaces between the SSE and electrodes with controlled properties will also be developed. Both bulk-level and single-grain-level characterization will be performed. Global properties and performance of the samples will be established from the bulk analyses, while the single-grain-based studies will utilize time-resolved and spatially-resolved analytical techniques to probe the intrinsic redox transformation processes and failure mechanisms under battery operating conditions.

Out-Year Goals. In the out years, the project will deliver fundamental knowledge on the role of SSE microstructure in Li^+ conduction and lithium dendrite formation/propagation. Insights on performance-limiting physical properties and phase transition mechanisms as well as dynamic evolution of SSE/electrode interfaces will be obtained. Mitigating approaches, such as use of surface coating or a “buffer layer” in stabilizing SSE/electrode interfaces, will be evaluated. Further, advanced SSE materials and interfaces for improved high-energy Li-metal batteries will be designed and synthesized.

Collaborations. This project collaborates with the following PIs: G. Ceder, K. Persson, M. M. Doeff, B. McCloskey, R. Kostecki, and R. Prasher (LBNL); W. Yang (Advanced Light Source, ALS); D. Nordlund and Y. Liu (Stanford Synchrotron Radiation Lightsource, SSRL); C. Wang (PNNL); and J. Nanda (ORNL).

Milestones

1. Develop SSE/cathode model systems for studying the cathode interfaces. (Q1, FY 2022; Completed)
2. Synthesize SSE model samples and model SSE/cathode interfaces. (Q2, FY 2022; On schedule)
3. Advanced diagnostic studies of SSE/cathode interfaces. (Q3, FY 2022; On schedule)
4. Obtain mechanistic understanding and deliver design strategies to improve SSE/cathode interfaces. (Q4, FY 2022; On schedule)

Progress Report

To investigate ASSB cathode interfaces in a more controlled manner, the team designed model systems with three key elements:

- *Use of Li-metal halide SEs with a general formula of Li_3MCl_6 (M = Sc, In, Y, Er, Yb).* The halides exhibit a high ionic conductivity (> 1×10^{-4} S/cm at room temperature), a wide electrochemical stability window (up to 4.5 V versus Li/Li^+), and excellent ductility, which enables them to be used with 4-V class lithium TM oxide CAMs without coating treatment. This allows diagnostic studies to be performed at the direct interface between the CAM and SE.
- *Use of SC as opposed to PC CAM particles*. Conventional PC samples such as NMCs are large spherical secondary particles made up of sub-micron primary grains with random orientations. This causes prolonged Li^+ diffusion pathways (higher tortuosity) and nonuniform lithium concentration inside the particles, leading to stress and strain and eventual internal cracking along the GBs. In liquid cells, electrolyte permeates into the pores and along the loose GBs to enable utilization of isolated CAMs. In ASSBs, however, cracking and volume change can lead to void formation, contact loss, impedance rise, and capacity fade. Use of SC with controlled particle size can be expected to eliminate intergranular and intragranular cracking associated with volume expansion/contraction during cycling.
- *Design and optimization of CAM SC surface facets for enhanced lithium transport*. It is known that PC particle surfaces are often terminated with various crystalline facets that are not optimized for lithium transport. For NMCs, (003) basal planes are lithium impermeable and their interface with SE can become a bottleneck for lithium transport, increasing overall impedance and limiting rate capability. To this end, SC-based studies enable particle-level surface modification for optimal lithium diffusion.

Figure 32a-b shows SEM images of PC and SC NMC-811 particles, respectively. While the PC sample is made of large secondary particles (~ 10 μm) with many small primary grains (~ 1 μm), the SC sample shows discrete particles in the 3-5 μm size range, largely free of aggregation. ASSB cells consisting of a composite cathode made with SC-NMC-811, Li_3YCl_6 (LYC) and carbon additive, a LYC separator, and a Li-In anode were assembled. Figure 32c-d shows the cross-sectional SEM images of the cell, with the expanded view of the composite cathode as well as its interface with LYC separator shown in Figure 32d. In future work, the team will investigate structural, chemical, and morphological changes associated with electrochemical cycling.

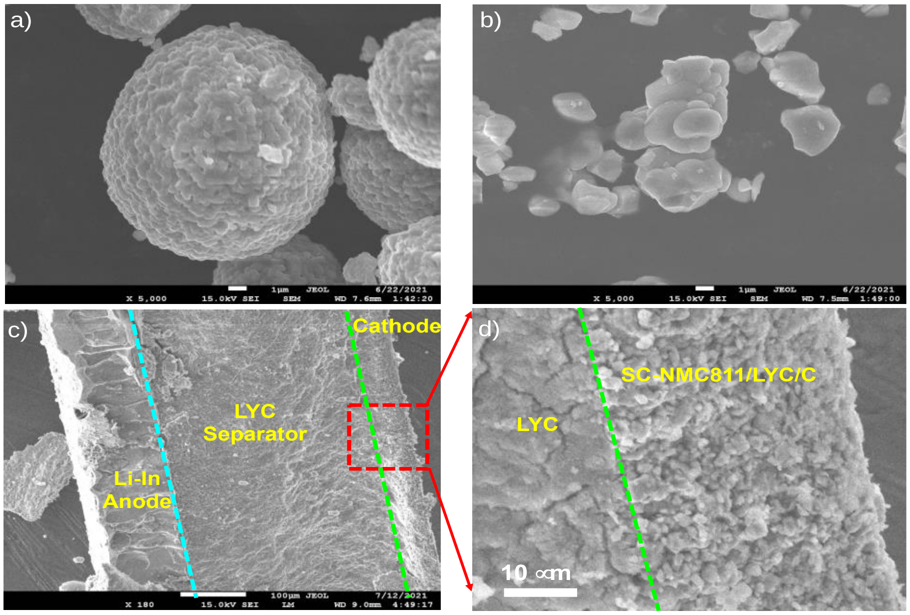

Figure 32. Scanning electron microscopy (SEM) images of as-synthesized cathode particles: (a) PC-NMC-811 and (b) SC-NMC-811. (c-d) Cross-sectional SEM view of an assembled (SC-NMC-811 + LYC + C) | LYC | Li-In solid-state battery cell. Expanded view at the cathode side of the cell is shown in (d).

Patents/Publications/Presentations

Patent

- U.S. Patent Application Ser. No: 63/277,722 (December 2021): “High-Energy and High-Power Composite Cathodes for All-Solid-State Batteries”; S. Kim, Y. Lu, and G. Chen.

Publications

- Li, L., J. Ahn, Y. Yue, W. Tong, G. Chen, and C. Wang. “Fluorination Enhanced Surface Stability of Disordered Rocksalt Cathodes.” *Advanced Materials* (2021). doi: 10.1002/adma.202106256.
- Satish, R., L. Wichmann, M. J. Crafton, J. Ahn, L. Li, B. McCloskey, G. Chen, C. Wang, Y. Yu, W. Tong, and R. Kostecki. “Exposure History and Its Effect Towards Stabilizing Li Exchange Across Disordered Rock Salt Interfaces.” *ChemElectroChem* 8 (2021): 3982. doi: 10.1002/celc.202100891.

Task 2.2 – Interfacial Processes – Diagnostics
(Robert Kostecki, Lawrence Berkeley National Laboratory)

Project Objective. The project objective is to establish specific design rules toward the next generation of low-impedance Li-metal rechargeable batteries that are capable of performing 1000 deep discharge cycles at CE > 99.9% and suppressing lithium dendrite formation at high current densities (> 2 mA/cm^2). This project aims at the following: (1) establishing general rules between Li^+ transport properties in novel liquid/solid electrolytes, and (2) determining the mechanism of the SEI layer (re)formation. The other goal is development and application of far- and near-field optical probes and synchrotron-based advanced X-ray techniques to obtain insight into the mechanism of Li^+ transport and interfacial reactions in lithium/liquid model systems. Through an integrated synthesis, characterization, and electrochemistry effort, this project aims to develop a better understanding of lithium/LE interface so that rational decisions can be made as to their further development into commercially viable Li-metal cells.

Project Impact. Chemical instability and high impedance at the interface of Li-metal electrodes limit electrochemical performance of high-energy-density batteries. A better understanding of the underlying principles that govern these phenomena is inextricably linked with successful implementation of high-energy-density materials in Li-metal-based cells for PHEVs and EVs. New state-of-the-art techniques to identify, characterize, and monitor changes in materials structure and composition that take place during battery operation and/or storage will be developed and made available to BMR participants. The work constitutes an integral part of the concerted effort within the BMR Program, and it supports development of new electrode materials for high-energy, Li-metal-based rechargeable cells.

Approach. The pristine and cycled composite electrode and model thin-film electrodes will be probed using various surface- and bulk-sensitive techniques, including FTIR, ATR – FTIR, near-field IR and Raman spectroscopy/microscopy, and SPM to identify and characterize changes in materials structure and composition. Novel *in situ / ex situ* far- and near-field optical multi-functional probes in combination with standard electrochemical and analytical techniques are developed to unveil the structure and reactivity at interfaces and interphases that determine electrochemical performance and failure modes of materials.

Out-Year Goals. In the out-years, the project aims to achieve the following: (1) understand factors that control performance and degradation processes, (2) unveil structure and reactivity at hidden or buried interfaces and interphases that determine electrochemical performance and failure modes, and (3) propose effective remedies to address inadequate Li-metal-based battery calendar/cycle lifetimes for PHEV and EV applications.

Collaborations. The diagnostic studies will be carried out in sync with other diagnosticians (G. Chen, B. McCloskey, R. Prasher, and L-W. Wang) and theory and computational scientists (G. Ceder and K. Persson).

Milestones

1. Fundamental physicochemical and electrochemical characterization of the considered primary and secondary Li-metal cell chemistries. (Q1, FY 2022; Completed)
2. *In situ* nano-FTIR spectroscopy experimental setup for probing Li/LE interface designed, built, and tested. Preliminary tests and results delivered. (Q2, FY 2022; In progress)
3. Near- and far-field optical and XPS characterization of the baseline Li-metal cell chemistries and relevant interfacial phenomena and processes completed. (Q3, FY 2022; In progress)
4. Correlation of electrolyte chemistry and Li/SEI compositional structure in Li-metal baseline LE and SE systems determined. (Q4, FY 2022; In progress)

Progress Report

This quarter, the team studied the SEI layer on Li-metal anode in a model cell equipped with lithium iron phosphate (LFP) cathode. This allows a steady Li^+ extraction from LFP and subsequent plating on copper current collector under constant potential. By controlling lithium plating, one can also investigate the early SEI formation on lithium. They focused on investigating the SEI components using nano-FTIR spectroscopy in *ex situ* configuration. They assembled a 2-electrode cell with a thin-film copper anode, LFP cathode, and GEN 2 electrolyte. During lithium stripping and plating at current density 25 µA/cm^2, they observed a change in the anode electrode surface morphology, yielding congregated ~ 500 nm nano clusters with different chemical composition, as could be seen in Figure 33a, where the clusters remain less reflective than the flat regions in infrared wavelength range.

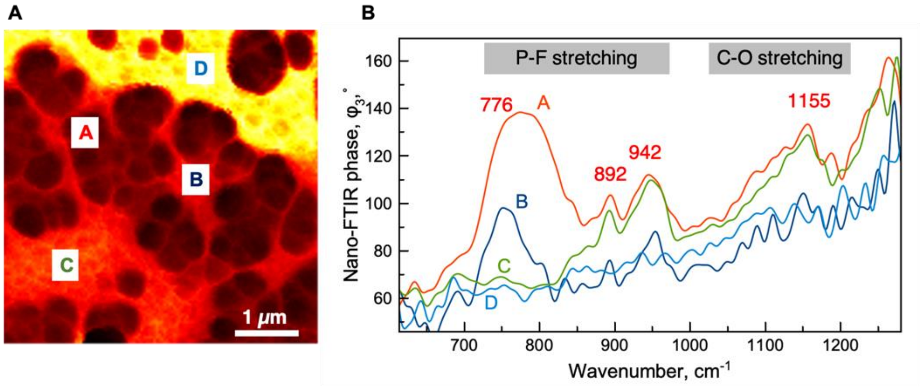

Figure 33. Nano – Fourier transform infrared (FTIR) study of Cu/Li surface after a cycle of plating and stripping lithium. (a) Near-field amplitude image (2nd harmonic) recorded in infrared white light. (b) Nano-FTIR phase φ3 spectra recorded at selected locations A-D.

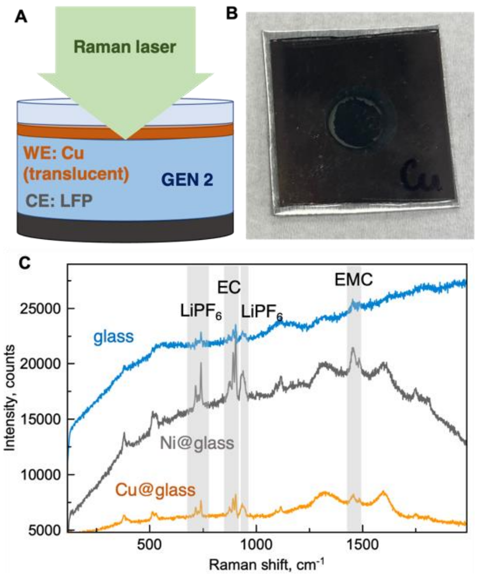

Figure 34. Surface-enhanced Raman spectroscopy (SERS) of the early SEI layer: (a) schematic of *in situ* SERS electrochemical cell. Thin translucent copper film serves as working electrode and SERS substrate, (b) image of assembled 2-electrode electrochemical SERS cell, and (c) *ex situ* SERS spectra of the electrolyte, and the SEI layer on Cu/Li and Ni/Li electrodes.

Nano-FTIR spectra from the clusters (Figure 33b) show the presence of P-F stretching vibrations, where lower frequency corresponds to presence of PF_3 and higher to more oxygen-rich species like PFO_3^{2-}, which is a product of reaction of $LiPF_6$ with carbonate solvent radicals. Interestingly, smaller clusters, located in area “C” in Figure 33a, contain only oxidized PFO_3^{2-} anions. The peak at ~ 1155 cm^{-1} corresponds to C-O stretching vibration of EC.

Next quarter, the team will focus on analyzing different regions of nano-FTIR spectra at copper and nickel current collector surface after lithium plating and stripping.

To get an additional signature of vibrational spectra of the Li/SEI film components, the team employed a surface-enhanced Raman spectroscopy (SERS) approach, where a metal nanostructure enhances Raman signal from molecules in ~ 10-nm radius around the said structure. Although the lateral resolution does not break the optical diffraction limit, this technique is only sensitive to molecules absorbed on the metal surface. When the nanostructured copper acts as a working electrode, it is possible to analyze SEI components in close proximity to the electrode. It should be noted that the spectra of GEN 2 electrolyte both show a strong fluorescence background. With Raman surface-enhanced scattering, spectral features from the SEI film could be seen over the fluorescence background. Figure 34 shows SERS spectra of GEN 2 electrolyte collected through translucent current collector inert to lithium : copper and nickel. Although nickel plasmon resonance occurs in the near UV region, Raman features of GEN 2 electrolyte on nickel electrode were still detected. This could be explained by chemical mechanism of SERS through charge-transfer between metal substrate and electrolyte molecules. Next quarter, the team will focus on investigating lithium stripping and plating via SERS.

Patents/Publications/Presentations

The project has no patents, publications, or presentations to report this quarter.

Task 2.3 – Advanced *In Situ* Diagnostic Techniques for Battery Materials
(Xiao-Qing Yang and Enyuan Hu, Brookhaven National Laboratory)

Project Objective. The primary objective of this project is to develop new advanced *in situ* material characterization techniques and to apply these techniques to support development of new cathode and anode materials with high energy and power density, low cost, good abuse tolerance, and long calendar and cycle life for beyond Li-ion battery systems to power PHEVs and battery electric vehicles (BEVs). The diagnostic studies will focus on issues relating to capacity retention, thermal stability, cycle life, and rate capability of beyond Li-ion battery systems.

Project Impact. The VTO Multi-Year Program Plan describes the goals for battery: "Specifically, lower-cost, abuse-tolerant batteries with higher energy density, higher power, better low-temperature operation, and longer lifetimes are needed for development of the next-generation of HEVs [hybrid electric vehicles], PHEVs, and EVs." The results of this project will be used for development of technologies that will significantly increase energy density and cycle life, and reduce cost. This will greatly accelerate deployment of EVs and reduce carbon emission associated with fossil fuel consumption.

Approach. This project will use a combination of SXRD and pair distribution function (x-PDF) and of neutron diffraction and pair distribution function (n-PDF); X-ray spectroscopies including hard/soft XAS, X-ray photon emission spectroscopy (PES); and imaging techniques including X-ray fluorescence (XRF) microscopy, transmission X-ray microscopy (TXM), and transmission electron microscopy (TEM).

Out-Year Goals. The out-year goals are to develop spectro-tomography, XRD, XAS, and PDF techniques, and to apply these techniques on Li-ion battery cathode, Na-ion battery cathode, and SSE.

Collaborations. The BNL team will work closely with material synthesis groups at ANL (Y. Shin and K. Amine) for the high-energy composite, at PNNL for the S-based cathode and Li-metal anode materials, and with ORNL on neutron scatterings. This project will also collaborate with industrial partners, as well as with international collaborators.

Milestones

1. Complete XRD and X-ray PDF studies on SSE $Li_7P_2S_8I_{0.5}Br_{0.5}$ to understand its degradation mechanism at high voltage. (Q1, FY 2022; Completed)
2. Complete cryo-EM study to understand the positive role of $LiNO_3$ additive in SEI formation on Li-metal anode. (Q2, FY 2022; In progress)
3. Complete many-particle TXM studies on $LiNi_{0.8}Mn_{0.1}Co_{0.1}O_2$ cathode to understand its chemical and morphological heterogeneities at the electrode level. (Q3, FY 2022; In progress)
4. Complete *ex situ* XAS and TXM studies on polymeric sulfur cathode to understand its redox mechanism and morphological evolutions during cycling. (Q4, FY 2022; In progress)

Progress Report

This quarter's milestone was completed. BNL has been focused on developing new diagnostic techniques to study and improve performance of beyond Li-ion batteries such as SSBs. SSE is the key component of SSBs. $Li_7P_2S_8I$ is one type of SE with high ionic conductivity, but poor stability against high-voltage cathode such as NMC-811. Its derivative $Li_7P_2S_8I_{0.5}Br_{0.5}$ (LPSIB) has improved high-voltage stability, but is still not stable against NMC-811 above 4.5 V. The mechanism of such instability has not been clearly understood. Studies were planned in collaboration with D. Lu of PNNL to investigate this issue. x-PDF has been carried out for three samples: pristine LPSIB electrolyte; NMC-811cathode charged to 4.5 V in LE; and a mixture charged to 4.5 V NMC-811 with LPSIB to study the interaction between them. Note that no reaction between NMC-811 and LPSIB was involved for sample #2. Sample #3 is sample #2 reacted with LPSIB. XRD data in Figure 35a show that LPSIB has very few and broad peaks, suggesting that the crystallinity of LPSIB is very low. Charged NMC-811 has the typical layered structure, and all its peaks can be indexed using the $R\bar{3}m$ space group. After mixing with LPSIB, both (003) and (110) peaks for sample #3 show an obvious shift to the lower 2θ, suggesting both *c* and *a* axes lattices are expanded. PDF, as a total scattering technique, can probe both crystalline and amorphous phases and is the ideal tool for structural study of SE. Figure 35b shows the PDF data of LPSIB, and all the peaks in the low "r" region can be accounted for by chemical bonds or indirect correlations. Note that the broadening of peak at around 4Å is due to the anion disorder or paddle wheel rotation effect. The long-range PDF data for LPSIB in Figure 35c confirm that LPSIB has no long range order indicated by the almost flat line in 30-50 Å region. The long-range region data become weaker after NMC-811 4.5 V is mixed with LPSIB, suggesting poorer crystallinity. The short-range PDF data of NMC 4.5 V have peaks at around 1.8 Å and 2.8 Å, corresponding to the TM-O bond and the TM-TM correlation, respectively. Both peaks shift to higher *r* after mixing with LPSIB, suggesting the oxidation state of TM in NMC-811 is reduced. One possible reaction mechanism is that some sulfur atoms replace oxygen atoms in the NMC-811 lattice and bond with TM. This is supported by the intensity ratio between the first and the second peak increasing after mixing.

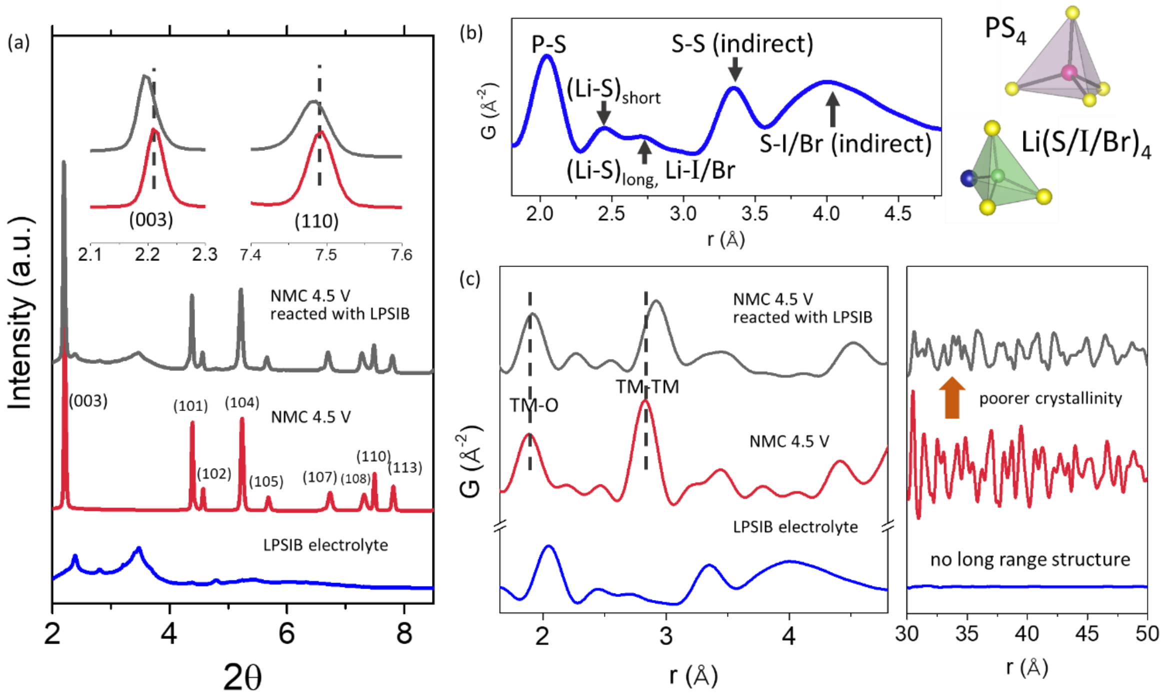

Figure 35. (a) Synchrotron XRD: Sample #1, LPSIB (blue); Sample #2, NMC-811 charged to 4.5 V (red); and Sample #3, which is Sample #2 mixed with LPSIB (black). (b) Short-range PDF data of LPSIB electrolyte with SP_4 and $Li(S/I/Br)_4$ tetrahedra in the structure shown. (c) Short-range and long-range PDF data of all three samples.

Patents/Publications/Presentations

Publication

- Qian, Y., Y. Chu, Z. Zheng, Z. Shadike, B. Han, S. Xiang, Y. Kang S. Hu, C. Cao, L. Zhong, Q. Shi, M. Lin, H. Zeng, J. Wang, E. Hu, C. Weiland, X-Q. Yang, and Y. Deng. "A New Cyclic Carbonate Enables High Power / Low Temperature Lithium-Ion Batteries." *Energy Storage Materials* 45 (2022): 24–32. doi: 10.1016/j.ensm.2021.11.030.

Task 2.4 – Probing Interfacial Processes Controlled Electrode Stability in Rechargeable Batteries (Chongmin Wang, Pacific Northwest National Laboratory)

Project Objective. The main objective is to explore interfacial phenomena in rechargeable Li-ion batteries of both SSE and LE configuration, to identify the critical parameters that control the stability of interface and electrodes as well as SE. The outcome will be establishing correlations between structural-chemical evolution of active components of batteries and their properties. These correlations will provide insight and guidance to battery materials development groups for developing high-performance battery materials.

Project Impact. The proposed characterization work focuses on atomic-level structural and chemical analysis and direct correlation with battery fading properties. The work can be directly used to guide design of electrode materials with tailored microstructure and chemistry for enhanced properties of increasing the energy density of Li-ion batteries and to accelerate market acceptance of EVs, especially for PHEVs as required by the EV Everywhere Grand Challenge.

Approach. The project will use integrated advanced microscopic and spectroscopic techniques, including *in situ* and *ex situ* STEM, environmental STEM, cryo-EM, and *in situ* liquid secondary ion mass spectrometry (SIMS), in collaboration with theoretical modeling, to directly probe the structural and chemical information of active materials in rechargeable batteries. Cryo-STEM with analytical tools, such as EDS and EELS, will be used to gain chemical and electronic structural information at the interface between lithium metal and electrolyte of both solid-state and liquid configuration, which will allow direct correlation between the morphology and chemistry. STEM – high-angle annular dark-field (HAADF) atomic-level imaging and EDS/EELS will be used to probe the interface and bulk lattice stability of cathode and SE in SSB. The work will be in close collaboration with the battery development group within the BMR and U. S.–Germany Collaboration on Energy Storage.

Out-Year-Goals. This project has the following out-year goals:

- Atomic-level multi-scale *ex situ* / *in situ* and *operando* STEM and cryo-STEM investigation on the fading mechanisms of energy-storage materials and devices in the system of both LE and SE; gain a fundamental understanding of electronic and ionic transport characteristics and kinetics in energy-storage system.
- Develop new *in situ* and *ex situ* STEM capability for probing challenging questions related to energy storage technology for both SSE and LE energy storage systems.

Collaborations. This project collaborates with G. Chen (LBNL); J. Nanda (ORNL); Y. Yao (UH); K. Amine (ANL); D. Wang (PSU); A. Manthiram (UT, Austin); W. Tong (LBNL); Y. Cui (Stanford); J. Zhang (PNNL); J. Liu (PNNL); W. Xu (PNNL); X. Jie (PNNL); D. Lu (PNNL); X. Xiao (GM); Y. S. Meng (UCSD); and M. S. Whittingham (State University of New York, Binghamton).

Milestones

1. Measure electronic properties of SEI layer and electrical double layers (EDLs), identifying their effects on electrochemical properties. (Q1, FY 2022; Completed)
2. Identify correlation between electrical properties of SEI layer and lithium structural features, such as how mossy lithium and crystalline lithium form. (Q2, FY 2022)
3. Reveal the nature of reaction product between cathode and S-based SE. (Q3, FY 2022)
4. Measure mechanical properties of SEI layer and its correlation with the lithium morphology. (Q4, FY 2022)

Progress Report

Interfacial reaction between SSEs and electrode constitutes one of the fundamental challenges for advances of rechargeable SSBs. It is often noticed that anode-SE interfacial reaction, coupled with poor contact, results in high interfacial impedance. Although different approaches have been explored for reducing interfacial impedance between SE and anode, the microstructural and dynamic mechanisms of interfacial impedance have not been well understood. The work will use *in situ* TEM to probe lithium transport behavior at the interface between lithium and perovskite-type lithium lanthanum titanate SE: $Li_{3x}La_{2/3-x}TiO_3$ ($0 < x < 0.16$) (LLTO).

The team assembled an *in situ* battery cell within TEM using lithium metal covered with a thin layer of Li_2O and a single nanowire LLTO to *in situ* inject lithium ions into the LLTO, as shown in Figure 36. This enables them to directly *in situ* monitor lithium transport behavior across the interface between lithium and LLTO under TEM, thereby gaining insight as to how lithium ions behave at the interface between lithium and LLTO SE.

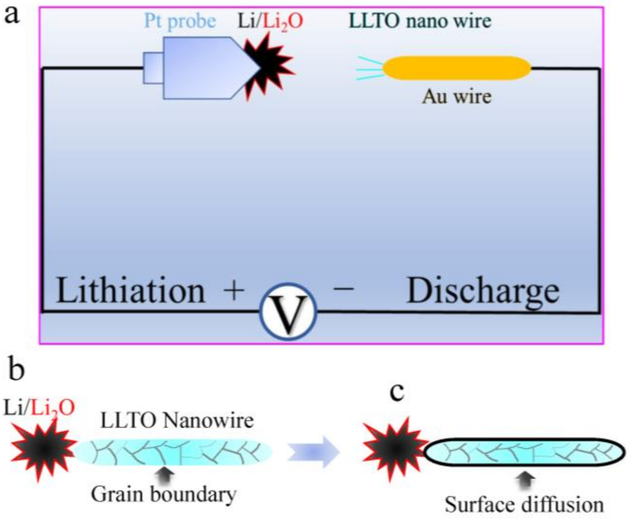

Figure 36. Schematic diagram to illustrate *in situ* transmission electron microscopy (TEM) set up for probing the dynamic reactions between lithium and LLTO. (a) Schematic of *in situ* TEM experimental setup. (b) Poor wetting between lithium and LLTO leads to lithium dendrite growth on the surface of LLTO. (c) Surface diffusion of lithium on LLTO leads to coating of lithium on LLTO.

This effort reveals that during the discharging process, lithium ions will not diffuse into LLTO. Instead, lithium ions behave in two ways. First, as the LLTO nanowire possesses free surface, lithium diffuses on the LLTO surface to form a thin layer to cover the LLTO (Figure 36). Second, lithium ions will be reduced at the

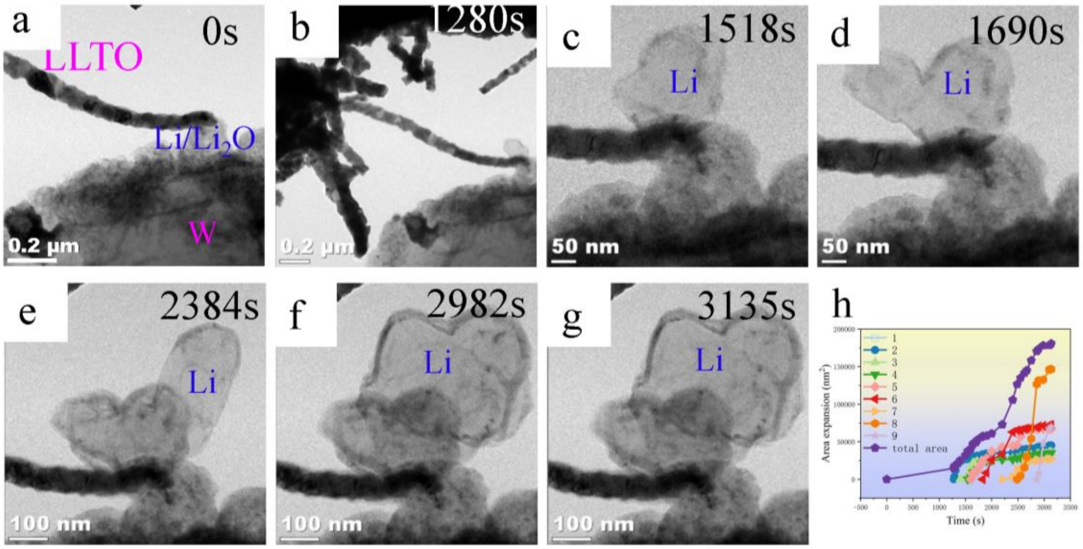

Figure 37. *In situ* transmission electron microscopy (TEM) observation of the dynamic interplay between lithium and LLTO nanowire on *in situ* injection of lithium into LLTO. (a–g) Sequential TEM images showing the dynamic processes of nucleation and growth of lithium dendrite at the interface between lithium and LLTO. (h) The area of lithium dendrite as a function of time, revealing the lithium growth rate during the *in situ* measurement (the numbers represent different areas).

interface between lithium and LLTO to lead to the nucleation and growth of lithium dendrite, as schematically shown in Figure 36. These two features are clearly illustrated by the captured video frames as a function of time, as shown in Figure 37. When a negative potential is applied to the system, Li-ion transport is dominated by surface diffusion at the early stage (Figure 37a-b). With continued biasing, lithium dendrite subsequently nucleates and grows on the surface of LLTO nanowire, as shown in Figure 37b-g. This observation clearly indicates that the high interfacial impedance between lithium and LLTO makes it difficult for lithium ions to diffuse into LLTO. The incubation time for the nucleation of lithium dendrite on the surface of LLTO nanowire is ~ 1000 s (Figure 37b). Following nucleation, lithium dendrite growth is featured by formation of large branches (Figure 37c-g). Quantitatively, the growth velocity of the lithium dendrite can be measured as shown in Figure 37h, indicating initial sluggish growth rate followed by high growth rate. The *in situ* TEM results provide direct structural evolution as to how lithium ions at the interface between lithium and SE behave. The observation that lithium grows as dendrite rather than directly injects into SE indicates that the interface acts as a critical barrier for Li-ion injection into the SE.

In terms of battery operation, it would be expected that lithium ions can be directly injected into the SSE. The present observation clearly reveals that interfacial coupling between lithium and SSE plays a key role for Li-ion transport through the electrolyte. It is apparent that the interface between lithium and SSE acts as a major barrier for Li-ion transport. Interfacial modification appears to be a viable approach for facilitating Li-ion transport into SSE. In follow up work, the team will explore how lithium transports across a modified interface between lithium metal and SE. The combination of *in situ* bias TEM and chemical analysis provides a powerful approach for fundamental investigation of structural and chemical changes during operation of SSBs with high spatial and temporal resolution.

Patents/Publications/Presentations

Publications

- Horstmann, B., J. Shi, R. Amine, M. Werres, X. He, H. Jia, F. Hausen, I. Cekic-Laskovic, S. Wiemers-Meyer, J. Lopez, D. Galvez-Aranda, F. Baakes, D. Bresser, C-C. Su, Y. Xu, W. Xu, P. Jakes, R-A. Eichel, E. Figgemeier, U. Krewer, J. M. Seminario, P. B. Balbuena, C. Wang, S. Passerini, Y. Shao-Horn, M. Winter, K. Amine, R. Kostecki, and A. Latz. “Strategies towards Enabling Lithium Metal in Batteries: Interphases and Electrodes.” *Energy & Environmental Science* 14 (2021): 5289.
- Yang, H., K. Tay, Y. B. Xu, B. Rajbanshi, S. Kasani, J. Bright, C. M. Wang, P. Bai, and N. Q. Wu. “Nitrogen-Doped Lithium Lanthanum Titanate Nanofiber-Polymer Composite Electrolytes for All-Solid-State Lithium Batteries.” *Journal of the Electrochemical Society* 168 (2021): 110507.

Presentations

- Portland State University, Department of Physics, Virtual Seminar (November 1, 2021): “S/TEM beyond Aberration Correction: *In-Situ* and *Operando* S/TEM: Challenges and Opportunities”; C. Wang. Invited.
- 2nd Korea Advanced Institute of Science and Technology (KAIST) Emerging Materials e-Symposium, Virtual (November 15–17, 2021): “Advanced Electron Microscopy and Spectroscopy Diagnosis Guided Design of Materials for Better Batteries”; C. Wang. Invited.

Task 2.5 – Integrated Atomic-, Meso-, and Micro-Scale Diagnostics of Solid-State Batteries (Yi Cui, William Chueh, and Michael Toney; Stanford University / SLAC National Accelerator Laboratory)

Project Objective. By developing a characterization toolkit that tackles length scales (Å to mm), cell pressure (1-100 bars), and dynamics (during synthesis, fabrication, and cycling), the project aims to generate insights to engineer SSBs for deployment in EVs. This interdisciplinary team aims to achieve this objective by merging a broad range of characterization approaches as well as modeling to track the evolution of nanoscale chemistry and structure, microstructure, and transport.

Project Impact. The project will have an impact in several areas: (1) accelerate rational design of coatings and artificial SEIs in SSBs; (2) inhibit the root causes leading to cell shorting, and enable high current cycling; (3) accelerate design of cathode coating and composite electrode architectures; and (4) reduce degradation and variability during SSB manufacturing via composition and surface engineering.

Approach. The project has a multi-fold approach that will encompass the following: (1) resolve nanoscale structure and chemistry of SEIs via cryo-TEM; (2) track SE and lithium microstructure evolution in 3D via X-ray micro and diffraction tomography; (3) visualize nanoscale ionic and electronic transport at GBs via conducting AFM; (4) map current distribution in cathodes via scanning TXM; and (5) monitor nanoscale SE evolution with gas impurity via *in situ* environmental TEM.

Out-Year Goals. The project will develop an integrated characterization toolkit to characterize SSBs within a single cycle and over hundreds of cycles, spanning a wide range of relevant length scales.

Collaborations. Project collaborations include work with SSRL, ALS, and Advanced Photon Source (APS) synchrotron light sources.

Milestones

1. Quantify the effect of microindentation pressure on fracture formation of LLZO SE using *in situ* electrochemical SEM. (Q1, FY 2022; Completed)
2. Quantify the degree of H/Li exchange for acid-treatment LLZO before and after heat treatment. (Q2, FY 2022; In progress)
3. Characterize the chemical nature of the Ag-LLZO interface via cryo-TEM. (Q3, FY 2022; In progress)
4. Characterize lithium plating on LLZO coated with 5 metallic electrodes using *in situ* electrochemical SEM. (Q4, FY 2022; In progress)

Progress Report

Recently, electronic conductivity has been investigated as an origin of sub-surface lithium deposition in oxide SEs. In principle, partial electronic conductivity in bulk or interfacial (for example, at GB) regions of the SE will lead to electrochemical reactions occurring within the electrolyte. Indeed, there have been reports of subsurface lithium plating as well as lowered bandgap in GBs. Another popular hypothesis is internal or near-surface porosity, which has been investigated theoretically.

The team is exploring the role of surface microstructural defects in subsurface lithium plating. An important first step is to systematically and repeatably introduce such defects to SEs, such as LLZO. There are several important considerations. First, due to the extreme reactivity of LLZO with water vapor and CO_2, the surface mechanical treatment must be conducted in an inert environment. Second, because each individual defect is different, they should be introduced and characterized locally. Crucially, a statistical approach is needed. The team has examined diamond scribing, laser ablation, FIB milling, and indentation. To characterize the effect of these mechanical modification methods, they used a microprobe to plate lithium locally and examine the electrochemistry (specifically, resistance toward plating and critical potential for fracture). These characterizations were performed inside an *in situ* SEM setup developed by the team.

For diamond scribing and laser ablation, the feature size is large, on the order of tens to hundreds of microns. These dimensions are larger than the size of the microprobe tip. As such, they are less suitable. Moreover, the team found that these methods led to significant increase in plating resistance, indicating that they are not representative of a typical LLZO surface for plating. Among the approaches examined, indentation appears to be most suitable. While indentation does not produce noticeable change in the surface microstructure, nanomechanical testing suggests plastic deformation and possibly microstructure at the forces the team used. Importantly, they observed that lithium plating and fracture behavior depend strongly on the indentation forces, confirming that the indentation is indeed modifying the surface behavior of LLZO. They are now systematically investigating the effect of mechanical modifications caused by indentation.

Patents/Publications/Presentations

Publication

- McConohy, G. "Interfacial Degradation of Ceramic Solid Electrolytes in High Energy Density Batteries." Materials Science & Engineering, Stanford University (2022). Ph.D Thesis.

Presentations

- Max Planck Institut fuer Eisenforschung, Virtual (November 9, 2021); W. C. Chueh.
- Stanford U. S. – China Climate & Energy Roundtable, Virtual (October 9, 2021); W. C. Chueh.
- University of California, Berkeley (UCB), Department of Materials & Engineering (October 7, 2021); W. C. Chueh.
- UCB, Berkeley Sensor & Actuator Center, Virtual (October 4, 2021); W. C. Chueh.

Task 2.6 – Fundamental Understanding of Interfacial Phenomena in Solid-State Batteries (Xingcheng Xiao, General Motors)

Project Objective. The project objective is to develop a comprehensive set of *in situ* diagnostic techniques combined with atomic/continuum modeling schemes to investigate and understand the coupled mechanical/chemical degradation associated with dynamic interfacial phenomena in SSBs. Specifically, *in situ* observations and characterizations of lithium plating-stripping processes, lithium dendrite formation, interphase formation, and the induced interfacial stresses, as well as the mechanical and electrochemical properties of interfaces and interphases, are paramount. The study will provide useful guidelines for optimizing cell structure design and engineering interfaces and interphases to enable SSBs.

Project Impact. The project will provide fundamental understanding of the dynamic interfacial phenomena and the coupled mechanical and chemical degradation. In addition, it will establish a critical guideline to design safe and durable SSBs with energy density > 500 wh/kg for EV applications.

Approach. The multi-scale *in situ* diagnostic tools, including AFM, nanoindentation, dilatometer, stress sensors, and pressure cells, will be used to investigate mechanical behavior and microstructure evolution at interface/interphase during lithium plating and stripping. The information (along with Li-ion transport properties and microstructure evolution obtained using the advanced spectroscopic ellipsometry, and *in situ* TEM) will be correlated with electrochemical performance toward high cycle efficiency and dendrite-free SSBs. The goal of this understanding is to develop strategies for surface and interface engineering, apply them to commercially available SEs (including powder, pellets, and foils), and assemble SSBs for further validation and optimization, eventually extending cycle life for EV application.

Out-Year Goals. The project seeks to develop SSB model systems to capture critical mechanical properties and probe the coupled mechanical-chemical degradation by further developing comprehensive *in situ* diagnostic tools. All results obtained from these *in situ* studies, combined with advanced *postmortem* analysis and modeling, will be correlated with the cycling stability of SSBs. The *in situ* tools developed will be applied to the following two periods to deeply understand the coupled mechanical and chemical degradation of interface/interphase.

Collaborations. The co-PIs involved in experiments and simulation will be as follows: B. W. Sheldon and Y. Qi (Brown University), and Y-T. Cheng and A. Seo (University of Kentucky).

Milestones

1. Artificial interlayer can regulate mechanical/chemical properties of interfaces. (Q1, FY 2022; Completed)
2. Artificial interphase has good ionic conductivity and chemical stability. (Q2, FY 2022)
3. Model to predict the governing mechanical and material properties of interfaces responsible for failures. (Q3, FY 2022)
4. Pouch cells of SSBs with optimized interlayers with energy density > 350 Wh/kg and cycle life> 500 cycles. (Q4, FY 2022)

Progress Report

Predicted CCD for Li/Li_2O, Li/LiF, and Li/LLZO Interfaces using Analytical Model

Table 4 lists the CCD ($\frac{\Delta N}{N_1} = 10^{-6}$) predicted for Li/$Li_2O$, Li/LiF, and Li/LLZO interfaces. The predicted CCD here is consistent with the team's previous kinetic Monte Carlo (KMC) simulations considering the hopping events for Li/Li_2O and Li/LiF. Although the CCD for LLZO is higher than the experimental values by 2 orders of magnitude, the LLZO surface in experiments is normally covered with some Li_2CO_3 (not a flat surface), which limits the measured CCD.

Table 4. $k_{f,2}$ and predicted critical current density for Li/Li_2O, Li/LiFm, and Li/LLZO interfaces using Equation 6 without creep effects.

	Li_2O	LiF	LLZO
$k_{f,2}$ (s^{-1})	3.31e10	3.76e3	2.14e8
CCD (A/cm^2)	43.0	4.88e6	0.277

Figure 38 shows i_c at different stack pressure for Li/Li_2O, Li/LiF, and Li/LLZO interfaces using Equation 10 assuming $\frac{\Delta N}{N_1} = 10^{-6}$. For the lithiophilic Li/Li_2O interface (wetting angle 0°), no stack pressure is required to reach a current density of 10 m A/cm^2. In contrast, for the lithiophobic Li/LiF interface (wetting angle 108.7°), a stack pressure ~ 4 MPa is necessary to achieve the goal of 10 m A/cm^2. For another lithiophilic interface (Li/LLZO, wetting angle 60.2°), the stack pressure is not necessary to reach a stripping current density of 10 m A/cm^2. As the Li/LLZO is not as lithiophilic as the Li/Li_2O, the CCD is smaller than that of the Li/Li_2O interface, but larger than that of the Li/LiF interface, suggesting that the analytical model captures the trends of CCD among different Li/SE interfaces.

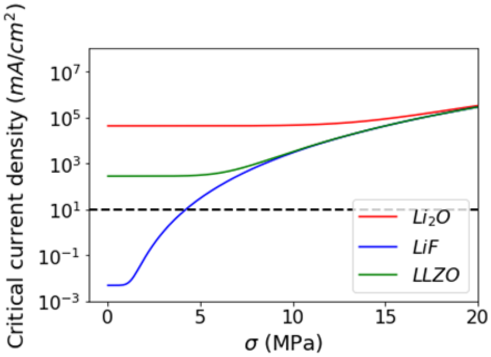

Figure 38. Predicted critical current density at different stack pressures for Li/Li_2O, Li/LiF, and Li/LLZO interfaces considering lithium hopping and creep-induced lithium flux.

Nanoindentation along Li-Rich LLZTO Cross-Section

Environmental nanoindentation was performed along a Li-rich cross-section of LLZTO SE. A LLZTO pellet was cycled until failure in a Swagelok type cell with Li-metal foil as both electrodes. After disassembly of the cell, the LLZTO pellet was fractured into two halves, exposing a metallic Li-rich cross-section as shown in Figure 39a. One half of the LLZTO pellet was taken to SEM and imaged. The lithium microstructure can be seen in Figure 39b. The other half of the LLZTO pellet was mounted in epoxy and lightly polished to provide a smooth surface for safe nanoindentation along the Li-rich cross-section. Figure 39c shows the mounted and polished LLZTO cross-section. 120 indents were made along the cross-section in a 3 × 40 matrix, as shown by the overlaying groupings of A, B, and C in Figure 39c. Nanoindentation was performed in an Ar-filled glovebox to minimize exposure to air and the growth of any passivation films. The elastic modulus of the entire cross-section was 117.60 ± 18.11 GPa, while the hardness was 5.41 ± 1.63 GPa. A statistical t-test showed that results for both mechanical properties were not statistically significant compared to the surface nanoindentation results of the same pellet prior to electrochemical cycling. If the excess lithium shown in the cross-section was to influence the mechanical properties of the pellet, then group A would show the most change, as it covers the most Li-rich area. Group B covers a lower percentage of Li-rich area, while group C does not cover any of the lithium morphology. However, when comparing the mechanical properties between all three groups, there was no significant difference. Figure 39d compares the elastic modulus among the three groups. If the excess lithium does influence the mechanical properties of the LLZTO pellet, then it must be localized and does not extend far into the pellet. Thus, the mechanical polishing method used in this project could remove the influence of the lithium metal. More precise measurements of local mechanical properties, such as AFM-based indentation, and better sample preparation methods will be used to properly perform nanoindentation of a cross-section.

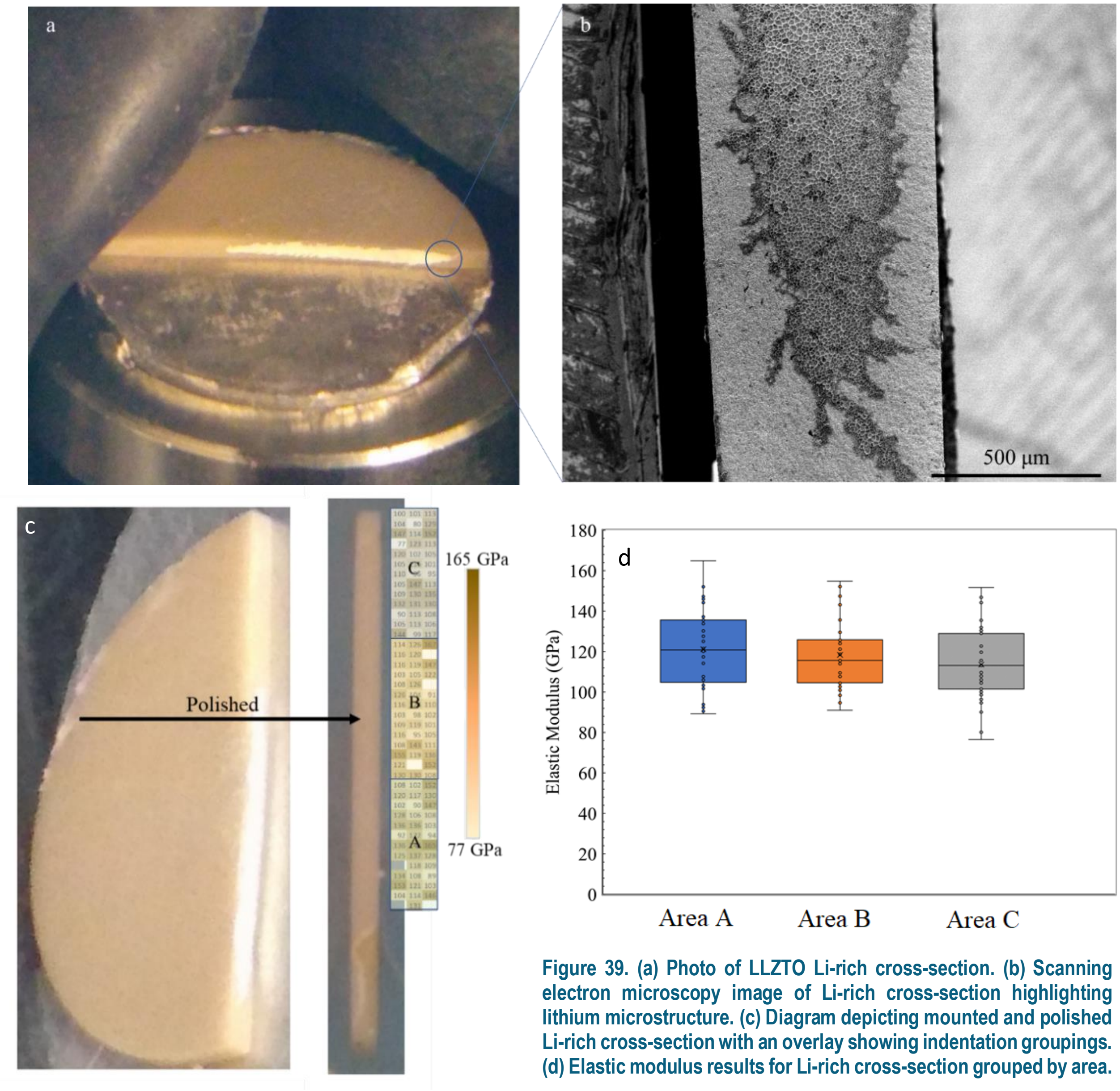

Figure 39. (a) Photo of LLZTO Li-rich cross-section. (b) Scanning electron microscopy image of Li-rich cross-section highlighting lithium microstructure. (c) Diagram depicting mounted and polished Li-rich cross-section with an overlay showing indentation groupings. (d) Elastic modulus results for Li-rich cross-section grouped by area.

Patents/Publications/Presentations

Publication

- Meyer, A., X. Xiao, M. Chen, A. Seo, and Y. T. Cheng. “A Power-Law Decrease in Interfacial Resistance Between $Li_7La_3Zr_2O_{12}$ and Lithium Metal after Removing Stack Pressure.” *Journal of The Electrochemical Society* 168, No. 10 (October 2021): 100522.

Presentations

- The Electrochemical Society (ECS), Meeting Abstracts, MA2021-02 365 (2021): “An Investigation of Chemo-Mechanical Phenomena in All-Solid-State Lithium Metal Batteries Using In-Situ Curvature Measurements”; J. H. Cho, K. J. Kim, S. Chakravarthy, X. Xiao, J. L. M. Rupp, and B. W. Sheldon.
- MRS Fall Meetings & Exhibits (December 2021): “In-Situ Curvature Measurements Using LLZO Solid Electrolyte”; J. H. Cho, K. J. Kim, S. Chakravarthy, X. Xiao, J. L. M. Rupp, and B. W. Sheldon.

Task 2.7 – Multidimensional Diagnostics of the Interface Evolutions in Solid-State Lithium Batteries (Yan Yao, University of Houston)

Project Objective. The project objective is to develop a platform combining FIB-SEM tomography, TOF-SIMS, and in-SEM nanoindentation-based stiffness mapping for structural, chemical, and mechanical characterizations in SSLBs. Assessment of the influence of cell design and testing conditions (that is, external pressure, current density, and temperature) on the evolutions of interfaces will be performed.

Project Impact. The consolidated in situ structural–chemical–mechanical diagnostic platform established in this project will provide unprecedented insights into the failure mechanisms of SSLBs.

Approach. Space- and time-resolved structural, chemical, and mechanical characterizations of the cathode-electrolyte and anode-electrolyte interfaces will be performed on lithium ASSBs using FIB-SEM, TOF-SIMS, and in-SEM nanoindentation. Tasks include the following: (1) development of solid-state cell thin stacks and test-cell configurations that are suitable for *in situ* characterizations; (2) quantitative characterization and *in situ* tracking of interfacial voids formation within composite cathode and electrolyte layer; (3) identification and *in situ* tracking of the chemical composition, spatial distribution, and mechanical properties of electrolyte decomposition products at the lithium- and cathode-electrolyte interfaces; and (4) visualization, chemo-mechanical properties detection, and *in situ* tracking of lithium dendrites grown within the SE layer.

Out-Year Goals. In the out years, the project will develop thin-stack solid-state cells, micro-cells, in-SEM nanoindentation, and testing protocols. The correlation between structural evolution, electrolyte decomposition, and interfacial resistance increase will be investigated.

Collaborations. The UH team (Y. Yao, Z. Fan, and Y. Liang) works closely with the Rice University team (J. Lou and H. Guo).

Milestones

1. Multi-scale structural investigations. (Q1, FY 2022; Completed)
2. Composition and spatial distribution study. (Q2, FY 2022; Completed)
3. Selected region mechanical property probing. (Q3, FY 2022; Completed)

Progress Report

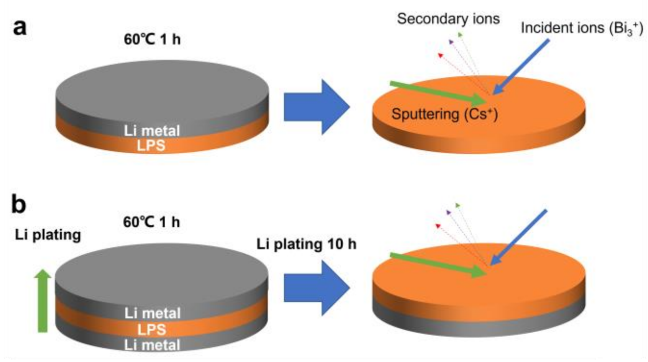

Figure 40. (a) Schematic illustration of the preparation of pristine LPS. (b) Schematic illustration of the preparation of plated LPS.

The team conducted TOF-SIMS analysis to understand the interfacial reactions between lithium anode and Li_3PS_4 (LPS) glass-ceramic electrolyte. As shown in Figure 40, a "pristine LPS" sample was prepared by stacking lithium foil onto an LPS pellet, heating at 60°C for 1 hour, then carefully peeling off the lithium foil. In comparison, a "plated LPS" sample was obtained after charging a Li|LPS|Li symmetric cell at 0.28 mA cm^{-2} for 10 hours and then peeling off the lithium foil at the negative side. TOF-SIMS measurements were performed using a TOF-SIMS NCS (ION-TOF GmbH); the samples were transferred from the glovebox using an air-free transfer vessel. Depth profile analysis was conducted by Cs^+ sputtering to acquire spatial–chemical information across the interface between lithium and LPS for both samples.

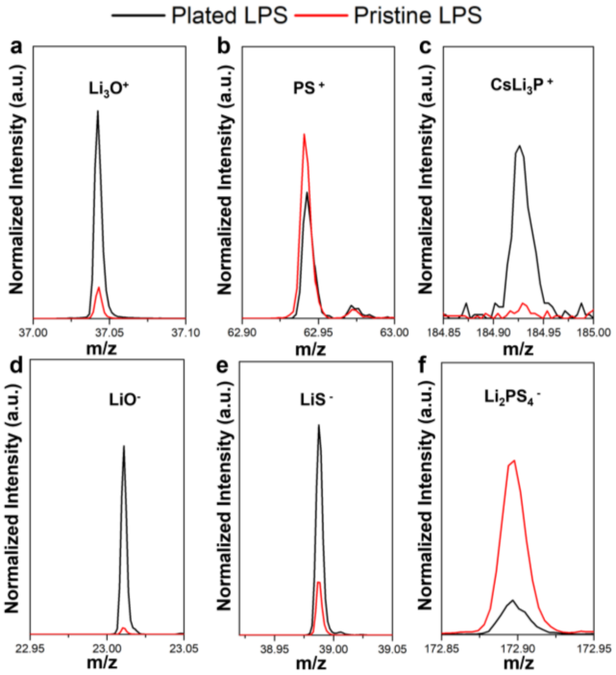

Figure 41. (a-c) Mass spectra of pristine LPS and plated LPS in positive polarization mode. (d-f) Mass spectra of pristine LPS and plated LPS samples in negative polarization mode.

The mass spectra of pristine LPS and plated LPS were collected to identify the chemical evolution of the LPS electrolyte during lithium plating. As shown in the high-resolution spectra measured in positive polarization mode (Figure 41a-c), obvious peak intensity increases occurred at m/z of ~ 37.04 (Li_3O^+) and ~ 184.93 ($CsLi_3P^+$). The Li_3O^+ peak can be ascribed to the plated lithium metal near the surface of the sample pellet. Formation of $CsLi_3P^+$ fragment is due to the combination of Cs^+ and Li_3P fragments during Cs^+ sputtering, representing the formation of reduced electrolyte product Li_3P. The PS^+ fragment represents the LPS electrolyte, and the slight decrease of the PS^+ intensity in plated LPS indicates the decomposition of LPS at the interface. The decomposition product of LPS can also be observed in the negative polarization mode shown in Figure 41f. The $Li_2PS_4^-$ peak ascribed to LPS shows a dramatic decrease in plated LPS. Similarly, the increase of LiO^- peak in Figure 41d further proves the existence of plated lithium metal at the interface. The LiS^- peak supposedly representing another reduction product Li_2S was also observed in Figure 41e.

To further understand the distribution of plated lithium metal, LPS, and interfacial reduction products across the interface on the plated LPS, the TOF-SIMS spectra were collected during prolonged Cs^+ sputtering. The depth profile of various secondary ions is shown in Figure 42. For pristine LPS (Figure 42a), slight decrease of the intensity of Li_3O^+ and $CsLi_3P^+$ peaks were observed at the beginning of the Cs^+ sputtering, which may imply the minor reactions happened between lithium and LPS during their contact at 60°C. The intensity of the peaks became relatively stable once the Cs^+ sputtered away the surface layer.

For the plated LPS, variation of Li_3O^+, PS^+, and $CsLi_3P^+$ can be observed across the interfacial layer shown in Figure 42b. The much higher Li_3O^+ intensity in this sample compared to that in Figure 42a indicates the existence of plated lithium metal at the surface. The fragment of $CsLi_3P^+$ in Figure 42b remained stable throughout the interfacial layer and dropped significantly into the LPS phase. In contrast, LPS related species were negligible at the surface of the interfacial layer, but rapidly increased to the similar level of pristine LPS. The depth profile data demonstrated the self-passivation reaction between lithium anode and LPS electrolyte during lithium plating. The team is further characterizing and monitoring the evolution of the interfacial layer to better understand the extent of interfacial reactions, their impact on interfacial resistance, and electrode performance.

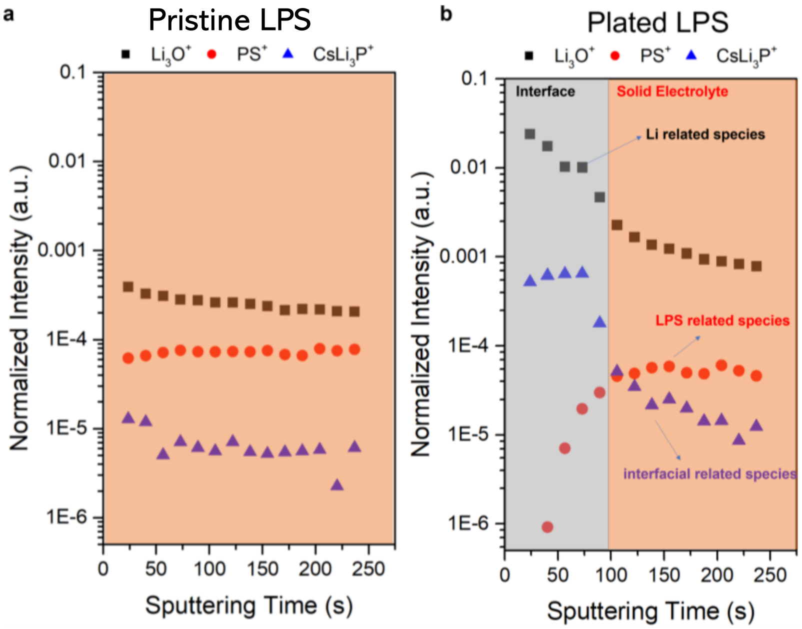

Figure 42. Depth profile of Li_3O^+, PS^+, and $CsLi_3P^+$ fragments in (a) pristine LPS and (b) plated LPS.

Patents/Publications/Presentations

Presentations

- Institute of Electrical and Electronics Engineers (IEEE) Nanotechnology Materials and Devices Conference (NMDC), Online (December 12–15, 2021): “Next-Generation Batteries for Electric Transportation and Stationary Energy Storage.” Invited.
- UT, Arlington, Materials Science and Engineering, Virtual (October 22, 2021): “Next-Generation Batteries for Electric Vehicles and Stationary Storage”; Y. Yao. Invited.
- Iowa State University, Materials Science and Engineering, Virtual (October 4, 2021): “Next-Generation Batteries for Electric Vehicles and Stationary Storage”; Y. Yao. Invited.

TASK 3 – MODELING

Team Lead: Venkat Srinivasan, Argonne National Laboratory

Summary and Highlights

Achieving the performance, life, and cost targets outlined by VTO will require moving to next-generation chemistries, such as higher capacity Li-ion intercalation cathodes, silicon and other alloy-based anodes, Li-metal anode, and sulfur cathodes. However, numerous problems plague development of these systems, from material-level challenges in ensuring reversibility to electrode-level issues in accommodating volume changes, to cell-level challenges in preventing cross talk between the electrodes. In this task, a mathematical perspective is applied to these challenges to provide an understanding of the underlying phenomenon and to suggest solutions that can be implemented by the material synthesis and electrode architecture groups.

The effort spans multiple length scales, from *ab initio* methods to continuum-scale techniques. Models are combined with experiments, and extensive collaborations are established with experimental groups to ensure that the predictions match reality. Efforts also focus on obtaining parameters needed for the models, either from lower-length scale methods or from experiments. Projects also emphasize pushing the boundaries of the modeling techniques used to ensure that the task stays at the cutting edge.

A major focus of the effort is around Li-metal-based SSBs. While these chemistries hold promise, numerous challenges such as reactivity, conductivity, and mechanical stability prevent their commercialization. Mathematical models are ideal to provide the guidance and insights needed to solve these issues.

In the area of Li-metal anodes, the focus is on understanding how materials can be designed to prevent dendrite growth using continuum modeling approaches, combined with calculations on mobility in solid conductors. The results are used to guide materials development by providing the properties needed to prevent dendrites, while also achieving the energy and power goals. Models examine the role of the SEI on the morphology of the dendrite and describe the mechanical-electrochemical coupled effects that are critical for dendrite formation. Finally, efforts are focused on discovery of new solid ion conductors with properties that far exceed existing materials. The focus is on using these models as a guide before embarking on extensive experimentation.

Lithium metal with SEs will be paired with cathode materials, often intercalative in nature. Models are being developed to examine the solid-cathode interface in Li-metal based systems, where side reactions and interface debonding issues are known to limit cycling. These models are being used to understand how to prevent chemo-mechanical failure at the interface. Coatings, an effective strategy for high-voltage operation, are being explored with the aim of providing a rational design approach for new coating materials. In addition, focus is paid to porous electrodes with cathode particles to predict the impact of heterogeneities on electrode behavior.

Highlight. There has been increasing interest in utilizing polymer-ceramic composite materials as a means of protecting Li-metal anodes from dendrites. These materials hold the promise of providing the mechanical stability advances of hard materials with the processibility of soft materials. While much attention has been paid to the interface between the polymer and the ceramic, the Srinivasan group has shed light on the need to carefully examine the interface between the composite and lithium metal. Due to the different materials properties of the two phases, the Li-metal interface undergoes nonuniform reaction, thereby leading to regions of enhanced lithium deposition, which then become hot spots for dendrite growth. Using meso-scale models, the group was able to shed light into this phenomenon and suggest approaches that can minimize the heterogeneous rate of deposition.

Task 3.1 – Characterization and Modeling of Lithium-Metal Batteries: First-Principles Modeling and Machine Learning
(Kristin Persson, Lawrence Berkeley National Laboratory)

Project Objective. This project supports VTO programmatic goals by developing next-generation, high-energy cathode materials and enabling stable cathode operation at high voltages through target particle morphology design, functional coatings, and rational design of electrolytes. The end-of-project goals include the following: (1) understanding of the factors that govern charge transport in nonaqueous, superconcentrated LEs, (2) critical surface and coating design and optimization strategies that will improve cycling of Li-ion battery cathodes by reducing cathode degradation from oxygen loss, and (3) simulation and machine learning (ML) of the early formation of the SEI on Li-metal electrodes.

Project Impact. This project is aimed at providing fundamental insights into the atomistic mechanisms underlying surface reactivity and performance of Li-ion cathode materials and electrolytes, with the ultimate goal being to suggest improvement strategies, such as coatings, surface protection, novel electrolyte formulations, and particle morphology design. Transport modes as a function of solvent and salt concentrations will be clarified, and a data-driven reaction network framework will be designed and implemented to predict early SEI formation on lithium metal.

Approach. First-principles calculations, both static and dynamic approaches, are used to model SSE material thermodynamics and kinetics. LEs are modeled through coupled classical molecular dynamics (CMD) and first-principles methods to accurately capture solvation structure as well as reactivity of the liquid system. The reaction network is built on large-scale first-principles data, using graph theory and ML models.

Out-Year Goals. Electrolyte work will be aimed toward understanding the atomistic interactions underlying performance of lithium electrolytes, specifically elucidating conductivity (as a function of salt concentration) and impact on the charge transport mechanisms at play. Amorphous coatings will be evaluated based on ionic transport metrics and thermodynamic stability. The reaction network will be tested against known interfacial species forming on lithium metal in $LiPF_6$/EC electrolytes.

Collaborations. This project is highly collaborative between BMR PIs G. Chen (LBNL), G. Ceder (UCB), and R. Kostecki (ANL). Improved coating formulations will be examined by Chen and Ceder, and interfacial reactivity insights will be corroborated by Kostecki.

Milestones

1. Correlate electrolyte chemistry and Li/SEI compositional structure determined for Li-EC-based electrolyte. (Q1, FY 2022; In progress)
2. Determine sensitivity of molecular dynamics (MD) parameters to diluent effect on transport in at least one superconcentrated electrolyte. (Q2, FY 2022; In progress)
3. Develop HT infrastructure for MD simulations. (Q3, FY 2022, In progress)
4. Determine chemistry and structural motifs that control cathode amorphous coating performance, screening over 50,000 compositions. (Q4, FY 2022; In progress)

Progress Report

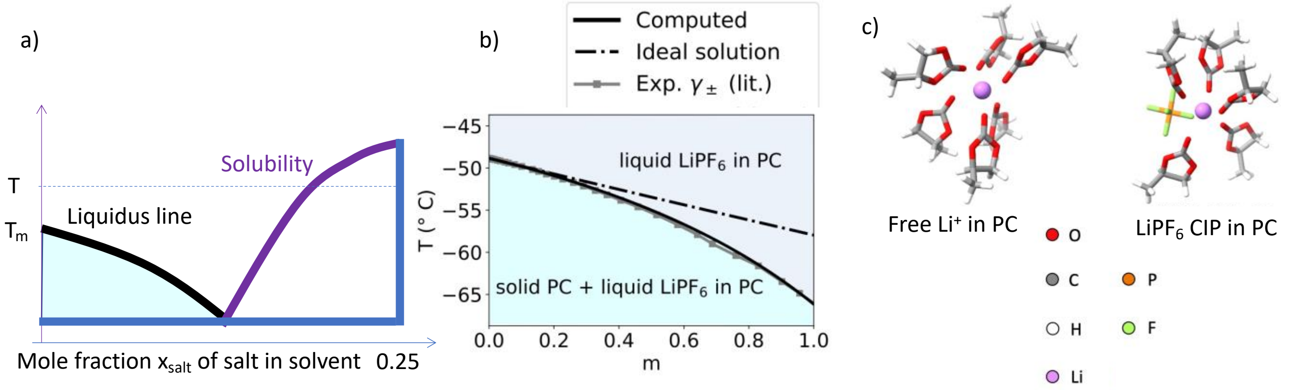

Figure 43. (a) Schematic representation of the liquidus line (black) for a eutectic phase diagram. The line in purple shows the solubility; for example, at a temperature T, the salt will not be soluble past the solubility line. (b) Computed liquidus line based on activity coefficients calculated from the physical-chemical model developed. (c) Sample structures of relevant species in solutions for the studied carbonate electrolyte, $LiPF_6$ in PC. These are the free Li^+ and contact-ion pair (CIP).

One of the principal design obstacles of superconcentrated electrolytes is the *a priori* prediction of salt solubility, which is an open problem of physical chemistry. This problem is directly related to the electrolyte phase diagram construction (see Figure 43a). The team developed a physical-chemical model that is intended for the dilute-to-moderate concentration range (up to ~ 1 molal) as a preliminary effort to addressing this open problem. This allows computation of the liquidus lines for selected carbonate electrolytes (for example, $LiPF_6$ in PC) via calculation of the activity coefficients, and with certain assumptions regarding the eutectic composition and the glass transition, and knowing neat solvent properties (see Self et al., 2021). CMD simulations, first principles calculations, and theoretical expressions are employed. The physical-chemical model computes the activity coefficients via accounting of solvent-ion and ion-ion interactions. These are quantified via Debye-Huckel theory, ion-pairing, the Born solvation equation, and solvent entropic effects. The team finds that these contributions are all significant. These are all interrelated; for example, the quantity of ion-pairing dictates the concentration-dependent dielectric constant, a quantity on which the Born solvation equation and Debye-Huckel theory are dependent. The dielectric increment of specific solvated species in solution (Figure 43c, free and $LiPF_6$ contact-ion pair species) is calculated via CMD simulations. Moreover, to account for ion-pairing, electronic structure calculations are used to find the association constant between such species. It is found that for test carbonate solutions, the herein developed physical-chemical model properly reproduces the activity coefficients and the relevant liquidus lines, as shown in Figure 43b.

Patents/Publications/Presentations

Publication

- Self, J., et al. "A Theoretical Model for Computing Freezing Point Depression of Lithium-Ion Battery Electrolytes." *Journal of the Electrochemical Society* 168 (2021): 12.

Task 3.2 – Electrode Materials Design and Failure Prediction (Venkat Srinivasan, Argonne National Laboratory)

Project Objective. The main project objective is to develop computational models for understanding the various degradation mechanisms for next-generation Li-ion batteries. This year's goal is to use the continuum-based mathematical model to estimate the conduction pathway through the SEs and investigate interfacial stability between Li-metal electrodes and SEs during deposition and dissolution of lithium under externally applied currents. Electrolytes comprising of soft polymers, hard ceramics, and a combination of the two in the form of polymer-ceramic composites, will be investigated. SEs are expected to enable high-energy-density and liquid-free, safe, next-generation Li-ion batteries, while combined with thin Li-metal anodes. During charge, lithium dendrites are observed through the SEs, which are supposed to occur because of the non-uniform current distribution at the Li/electrolyte interface. Due to their lack of conformability, hard-ceramic-based SEs (such as LLZO and LATP) are expected to experience loss of electrochemically active surface area during lithium plating and stripping, which can eventually lead to current focusing and subsequent dendrite growth. Sulfide-based soft ceramics (LPS and LPSCl), and/or polymer-ceramic composite electrolytes are expected to maintain better contact with the Li-metal electrode because of their higher deformability. The possibility of stabilizing the lithium deposition with composite electrolytes consisting of PEO-based soft-polymer matrix and LLZO type hard ceramic fillers will be studied. Proper conduction pathways through the polymer and ceramic domains, and their influence on the effective conductivity of the SE, will be elucidated. Other soft SEs, such as SEO polymer and sulfide-based soft ceramics, will be investigated for their capability to stabilize the lithium deposition on metallic anodes.

Project Impact. Findings from this research will give a better understanding of the ion transport mechanism within the polymer and ceramic domains of the composite SEs, and will help elucidate the factors influencing the deposition of lithium at the electrode/electrolyte interface.

Project Approach. In the present project, mesoscale models are developed based on mass conservation, charge balance, and force balance relations at the continuum level to describe the physical processes occurring in the electrochemical systems during charge and discharge, which is then compared with the experimental observations for appropriate validation. The models are then used to provide insights and guidance for strategizing new design concepts and materials for the stabilization of Li-metal anodes.

Out-Year Goals. In this project, a computational framework will be presented that can capture the ionic transport through composite electrolytes and predict lithium deposition at the electrode/electrolyte interface.

Collaborations. This project collaborates with L. A. Curtiss, A. T. Ngo, S. Tepavcevic, and Y. Zhang at ANL.

Milestones

1. Investigate the current, focusing on the interface between Li-metal electrode and polymer/ceramic composite electrolyte. (Q1, FY 2022; Completed)
2. Elucidation of ion transport mechanism through the polymer and ceramic phases in a composite electrolyte. (Q2, FY 2022; In progress)
3. Deciphering the influence of stress state on the exchange current density experienced by lithium metal electrodes in contact with SPEs during lithium deposition and stripping processes. (Q3, FY 2022)
4. Understanding the impact of GBs in soft inorganic SEs on the lithium deposition process and subsequent dendrite growth. (Q4, FY 2022)

Progress Report

Investigate the Current Focusing at the Interface between Li-Metal Electrode and Polymer/Ceramic Composite Electrolyte. From a macroscopic standpoint, composite electrolytes containing ceramic fillers and polymer matrix are expected to demonstrate high enough mechanical stiffness capable of preventing growth of lithium dendrites as well as show large enough deformability that can maintain good contact between the electrode and electrolyte domains (see Figure 44a). Microscopically, the polymers and ceramics demonstrate very different ionic conductivities, exchange current densities, and mechanical properties. The Li-metal anode can possibly see both the polymer and ceramic domains (as shown in Figure 44b), or just the polymer region (depicted in Figure 44c), depending on the adopted synthesis procedure. Transport of charge and ions in the electrode and electrolyte, and evolution of mechanical stress due to deposition of metallic lithium, have been solved in detail. Current focusing observed within the polymer domain is depicted in Figure 44d as a function of the elastic modulus of the soft polymer matrix. It is evident from the red squares that when the lithium electrode can see both polymer and ceramic domains, major current focusing occurs in the ceramics. If the lithium sees only polymer, current focusing occurs in the polymer with much smaller magnitude (see the cyan and blue lines in Figure 44d).

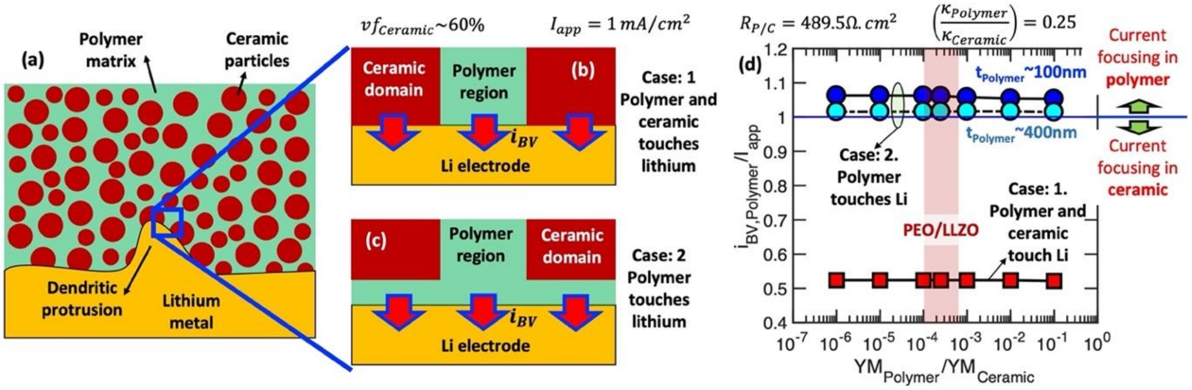

Figure 44. (a) Schematic representation of the polymer/ceramic composite in contact with lithium metal. The brown domains are ceramics, and the green region is the polymer. (b) Zoomed-in view at the electrode/electrolyte interface where both polymer and ceramic touch the lithium electrode. (c) Zoomed-in view of the composite-electrolyte/Li-metal interface where only polymer touches the electrode. (d) Current focusing within the polymer as a function of its elastic modulus. When both polymer and ceramic touch lithium (red squares), major current focusing is observed in the ceramics. When only polymer touches lithium (blue and cyan circles), current focusing is reduced substantially and occurs at the polymer domains.

Experimental observations reveal that the majority of the cell fabrication procedures lead to only polymers seeing the lithium electrode. A phase map between the polymer layer thickness and the polymer/ceramic interfacial resistance is depicted in Figure 45a, where it is clearly shown that increasing the thickness of the polymer layer at the electrode/electrolyte interface and decreasing the interfacial resistance between polymers and ceramics can help to stabilize the lithium deposition process. In the literature, several ceramic particles have been incorporated with PEO polymers for constructing composite electrolytes, such as LLZO, LATP, and Li_6PS_5Cl, and the current focusing experienced by each of them is depicted in Figure 45b. Due to the smaller interfacial resistance (~ $5\Omega.cm^2$), the sulfide-based ceramic particles (Li_6PS_5Cl) tend to stabilize the lithium deposition most effectively. Analyzing stability of lithium deposition at the Li/electrolyte interface completes this quarter's milestone.

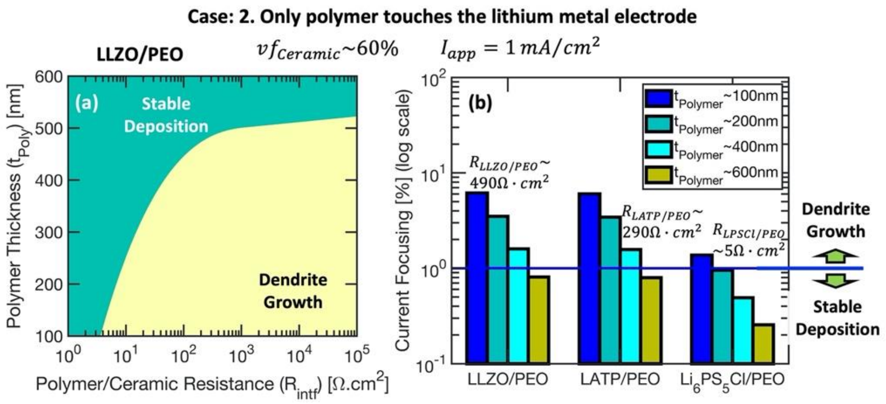

Figure 45. In general, only the polymer sees the lithium electrode. (a) Phase map between polymer-layer thickness and polymer/ceramic charge transfer resistance indicating domains of stable deposition (green) and regions with dendrite growth (yellow). (b) Current focusing at the polymer region for LLZO/PEO, LATP/PEO, and Li_6PS_5Cl/PEO composite electrolytes with different thickness of the polymer layer at electrode/electrolyte interface.

Patents/Publications/Presentations

The project has no patents, publications, or presentations to report this quarter.

Task 3.3 – Modeling of Amorphous Solid-State Conductors (Gerbrand Ceder, University of California, Berkeley)

Project Objective. SSBs are promising to achieve high energy density. The project objective is to determine the design principles needed to create SSEs with high Li-ion conductivity, while also achieving stability against common Li-ion cathodes and Li-metal anodes.

Project Impact. The project will lead to understanding the factors that control Li-ion motion in crystalline and amorphous solids and will develop strategies to create stable interfaces against lithium metal and high-voltage cathode materials. The understanding of such processes is necessary to determine design principles to develop reliable ASSBs.

Approach. HT computation is used to screen suitable SE with high electrochemical stability and high ionic conductivity, by incorporating nudged elastic band (NEB) and an AIMD method. Meanwhile, DFT is used to calculate bulk elastic constants of materials, surface energies, and interface decohesion energies of GBs. Thermodynamic interface stability is assessed from *ab initio* computed grand potential phase diagrams in which the lithium voltage can be controlled. Kinetic limits for SE decomposition are assessed by topotactic lithium insertion and removal from the SE.

Out-Year Goals. Future goals include the following: (1) gain insight into what creates high Li-ion conduction in sulfide and oxide solids, and (2) develop stable, processable solid-state conductors that can be applied in ASSBs.

Collaborations. There are no collaborative activities this quarter.

Milestones

1. Investigate lithium diffusion mechanism in activated network structures. (Q1, FY 2022; Completed)
2. Diffusion network analysis in low-density structures. (Q2, FY 2022; In progress)
3. Detailed lithium transport modeling in one novel conductor. (Q3, FY 2022; In progress)
4. Stability analysis of novel LIC. (Q4, FY 2022; In progress)

Progress Report

Oxy-Argyrodite Framework Exhibiting High Ionic Conductivity

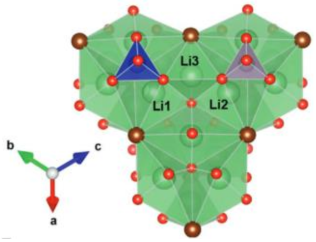

Figure 46. The crystal structure of $Li_{6+1/4}Si_{1/4}P_{1-1/4}O_5Br$. Li1 and Li2 are the lithium sites in the stoichiometric structure, and Li3 is the site where additional lithium is stuffed.

Last quarter, the team successfully identified the topology of activated diffusion networks, as inspired by NASICON and garnet frameworks. The three topological features of the diffusion network of NASICON and garnet frameworks were used to perform HT screening to find novel SEs that contain these frameworks. One of the identified candidates is Li_6PO_5Br with the oxy-argyrodite structure. Argyrodite sulfides can reach ionic conductivity > 10 mS/cm.[1] However, due to the 20% smaller lattice constant[2] and smaller polarizability of oxygen, the oxygen analogue Li_6PO_5Br is a poor ionic conductor with an activation energy that is 330 meV higher than its sulfide counterpart.[2] The team finds nonetheless that this framework can be activated by stuffing extra lithium in the interstitial tetrahedral 16e (Li3 in Figure 46), reducing the activation energy to 199 meV. The *ab initio* predicted room-temperature ionic conductivity is expected to reach up to 3.2 mS/cm. The extra lithium face-shares with two 24-g Li-ions, facilitating the inter-cage diffusion.[3] The team's analysis reveals that high ionic conductivity can be reached in the oxide-type of argyrodite framework, and that the diffusion network of argyrodites resembles that of NASICONs.

Novel $LiM(SeO_3)_2$ Framework Resembling Diffusion Network of NASICONs

While the oxy-argyrodites framework is a well-known conductor in the sulfides form, $LiM(SeO_3)_4$ framework is a completely novel framework that was discovered from the team's HT screening. $LiGa(SeO_3)_2$[4] and lithium stuffed $Li_{1+1/4}Mg_{1/4}Sc_{1-1/4}(SeO_3)_2$ are predicted to have room-temperature ionic conductivity exceeding 0.1 mS/cm. Several structural factors make this framework highly similar to that of NASICON. First, the lithium ions in the pristine form reside in highly distorted tetrahedral sites (Figure 47a), similar to the distorted 6b octahedral lithium site in stoichiometric NASICON $LiTi_2(PO_4)_3$. Secondly, similar to the NASICON framework, $LiM(SeO_3)_2$ framework possesses a 3D homogeneous transport path. Lastly, it has a low-energy intermediate site (site X, Figure 47b), which allows the bridging of neighboring lithium ions to facilitate their diffusion. These features make the $LiM(SeO_3)_2$ framework an intriguing candidate for in-depth investigation.

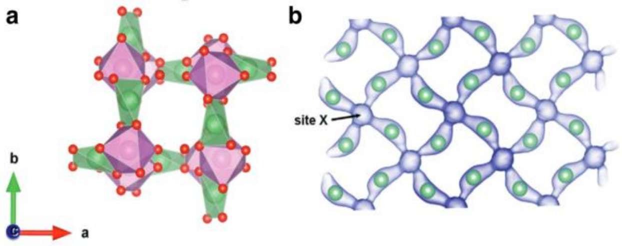

Figure 47. (a) Crystal structure of $LiGa(SeO_3)_2$. Green and pink polyhedrons represent the coordination environment of lithium and gallium, respectively. (b) Isosurface of Li-ion probability density from *ab initio* molecular dynamics simulation at 1000 K.

References

[1] Adeli, P., et al. *Angewandte Chemie International Edition* 58 (2019): 8681–8686.
[2] Kong, S., et al. *Zeitschrift Für Anorganische Und Allgemeine Chemie* 636 (2010): 1920–1924.
[3] Klerk, N., et al. *Chemistry of Materials* 28 (2016): 7955–7963.
[4] Lee, D., et al. *Inorganic Chemistry* 52 (2013): 5176–5184.

Patents/Publications/Presentations

Publications

- Tu, Q., T. Shi, S. Chakravarthy, and G. Ceder. "Understanding Metal Propagation in Solid Electrolytes due to Mixed Ionic-Electronic Conduction." *Matter* 4, No. 10 (2021): 3248–3268.
- Xiao, Y., K. Jun, Y. Wang, L. J. Miara, Q. Tu, and G. Ceder. "Lithium Oxide Superionic Conductors Inspired by Garnet and NASICON Structures." *Advanced Energy Materials* 11, No. 37 (2021): 2101437.

Task 3.4 – *In Situ* and *Operando* Thermal Diagnostics of Buried Interfaces in Beyond Lithium-Ion Cells
(Ravi Prasher, Lawrence Berkeley National Laboratory)

Project Objective. Transport at various interfaces in beyond Li-ion cells will play a major role in electrochemical performance and reliability. It has not yet been possible to thermally profile a Li-metal cell during operation to provide a spatially resolved map of thermal transport properties throughout the cell. The objective of this research is to create a metrology capable of spatially resolved *in operando* thermal property profiling, and then to relate thermal property to the quality of electrodes and interfaces, and to use the developed thermal metrology to understand electrochemical processes in Li-metal batteries, such as dendrite growth, interface kinetics, and ionic transport.

Project Impact. Characterizing electrochemical processes in Li-metal cells such as lithium deposition and dendrite growth at interfaces is of great significance for understanding and enhancing their electrochemical performance and reliability. *In situ* and *operando* micro electrothermal sensors can provide significant information regarding the impact of buried interfaces as a function of time, material, voltage, current, temperature, etc. Therefore, it is important to develop *operando* micro electrothermal sensors and develop models relating those signals to electrochemical performance for beyond Li-ion cells. The physics-based model relating thermal and electrochemical properties based on these measurements can facilitate future design of Li-metal batteries.

Approach. To accomplish project goals, the team will utilize an in-house adapted 3-omega (3ω) technique to probe thermal properties of a Li-metal cell while it is in operation, without affecting the operation of the cell. The 3ω sensors will be deposited and fabricated on Li-metal cells based on previous learning on 3ω sensor fabrication. The characteristic depth of the thermally probed region is defined by the wave's "thermal penetration depth," $\delta_p = \sqrt{D/2\omega}$, where D is the sample's thermal diffusivity, and 2ω is the heating frequency of the thermal wave. By depositing the project's 3ω sensors on the battery's outer surface and adjusting ω, the team controls δ_p to span the full range from the top to the bottom layer, thereby noninvasively probing the thermal transport in subsurface layers and interfaces within the bulk of the battery. Thermal transport can be related to quality of the interfaces. By doing concurrent thermal transport and electrochemical performance measurements, the team plans to relate thermal transport to electrochemical performance. As frequency-based thermal measurement techniques provide excellent spatial resolution within the cell, the team also plans to study heat generation at the electrolyte – Li-metal interface and to relate the thermal signals to the interface kinetics and ionic transport. The frequency dependence of heat generated due to transport resistance is different from that due to kinetic resistance. The team plans to utilize this difference to separate the contributions of kinetic and transport resistance at the interface, which will enable understanding of interface kinetics and transport at the Li-metal – SSE interface.

Out-Year Goals. The project will design, build, and implement the adapted 3ω metrology to examine thermal properties and a general frequency-dependent thermal metrology to examine heat generation. This will involve developing and testing the metrology itself along with accompanying theory, designing compatible battery samples, and applying the technique to live cells. The team will measure thermal transport properties of battery materials provided by collaborators. Combined with the electrochemical performance measurement, this will provide significant information relating the thermal signal to the electrochemical process.

Collaborations. This project collaborates with two LBNL groups: V. Battaglia's for cell assembly for 3ω studies, and R. Kostecki's for pristine battery active material growths for studies of thermal signals related to electrochemical process.

Milestones

1. Identification of theoretical model relating the interface morphology to thermal contact resistance (TCR). (Q1, FY 2022; Completed)
2. Measured change to TCR/morphology with cell cycling correlated with EIS. (Q2, FY 2022)
3. *Ex situ* characterization of interface morphology to validate the theory relating the morphology to TCR. (Q3, FY 2022)
4. Effect of temperature on TCR and self-heating study of thermally insulated LLZO cycling. (Q4, FY 2022)

Progress Report

This quarter, the team measured TCR at the Li-metal – LLZO electrolyte interface of a lithium-LLZO-lithium symmetric cell using previously designed 3ω sensors as a function of applied external pressure. Based on the TCR versus pressure data, they identified an appropriate theoretical model based on contact mechanics and interface thermal transport to describe the morphology of the lithium deposition at the lithium-LLZO interface. To describe the interface resistance, they have chosen the elastoplastic contact conductance model developed by M. R. Sridhar and M. M. Yovanovich (*Journal of Heat Transfer*, 118, 1996). The model combines the effects of interface heat transfer; contact mechanics determined the morphology of the interface and external pressure. The advantage of this model over other existing models is that this model does not pre-assume elasticity or plasticity of lithium deformation at the interface; therefore, the results are independent of whether the local deformations are elastic or plastic. With this model, there is a single parameter fitting to describe the measured TCR as a function of pressure. From the fitting (shown in Figure 48), they obtained the best fit TCR versus pressure data for lithium roughness of 3.4 μm at the interface.

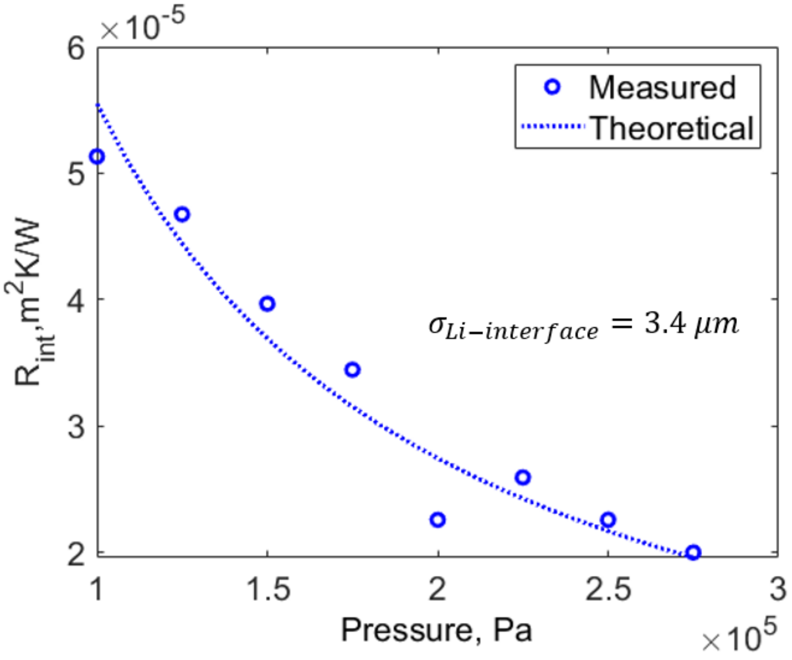

Figure 48. Measured thermal contact resistance at the lithium-LLZO interface as a function of external pressure. The best fit roughness of deposited lithium at the interface is obtained for the lithium roughness of 3.4 μm at the interface.

Next quarter, the team will compare the TCR versus pressure results with the electrochemical interface resistance obtained from EIS. Additionally, for the previous TCR data as a function of number of cell cycles, they will use the one-parameter fitting model to extract interface roughness as a function of number of cycles.

Patents/Publications/Presentations

The project has no patents, publications, or presentations to report this quarter.

Task 3.5 – Multi-Scale Modeling of Solid-State Electrolytes for Next-Generation Lithium Batteries (Anh Ngo, Larry A. Curtiss, and Venkat Srinivasan, Argonne National Laboratory)

Project Objective. This project is part of a multi-scale modeling effort to obtain an in-depth understanding of the interaction of the electrode and the SE aimed at developing highly efficient SSE batteries for vehicle applications. Input parameters needed for mesoscale (continuum) level calculations are being obtained from atomistic calculations including DFT and CMD simulations. This atomistic input will enable a multi-scale computational procedure for SSEs that is capable of successfully capturing the physicochemical aspects during charge and discharge process, including lithium transport mechanisms, interfacial phenomena during the insertion and extraction of lithium ions, and mechanical deformation of SSE.

Project Impact. A major safety concern experienced with commercially available Li-ion batteries under some scenarios is leakage of the LE, which can potentially catch fire. Replacement of the LE is necessary to decrease the fire hazard and improve safety associated with present-day Li-ion batteries. In addition, use of SEs provides a path to prevent dendrites in Li-metal anodes, thereby leading to batteries with significantly higher energy density. The impact of this project will be to help in development of good SSEs as a replacement for the commercially used organic LEs to improve safety and energy density in Li-ion batteries.

Approach. Parameters needed for mesoscale modeling of grain interior, GB, and electrode-electrolyte interface will be calculated by DFT-based calculations along with Monte Carlo (MC) and MD simulations. The calculations will be used to determine properties of the electrode with the SE as well as in GB regions of the SE. This will include calculations of structure, stability, ionic conductivity, Young's modulus, fracture toughness, exchange current density, and other properties.

Out-Year Goals. The out-year goals of this work are to calculate other properties such as fracture toughness and include other SSEs and coatings in the multi-scale modeling.

Collaborations. This project collaborates with Y. Cui at Stanford.

Milestones

1. Determine the stable phase of $Li_7P_3S_{11}$ amorphous/disordered glass-ceramic SSE and S-C cathode / $Li_7P_3S_{11}$ interface. (Q1, FY 2022; Completed)
2. Conduct AIMD study of an electrochemical interface between S-C cathode / amorphous $Li_7P_3S_{11}$ interface. (Q2, FY 2022; Initiated)
3. Investigate Li-ion transport of the S-C cathode / amorphous $Li_7P_3S_{11}$ interface. (Q3, FY 2022; Initiated)
4. Compute the exchange current density associated with charge transfer from amorphous $Li_7P_3S_{11}$ glass-ceramic SSE to the S-C cathode. (Q4, FY 2022; Initiated)

Progress Report

Li-S batteries have been under investigation for several decades due to the low-cost S-based cathode materials and demonstration of high specific capacity. In a LE system during the discharge process, the reduction reaction between lithium and sulfur occurs through a multistep process. The sulfur gets dissolved into the LE and forms polysulfide chains of various lengths before reacting with the lithium cations. These negatively charged polysulfide chains can easily migrate and diffuse through the LE toward the anode side and react with the lithium electrode surface to form a passivation layer that can effectively minimize capacity and enhance resistance of the cell. This detrimental shuttling of polysulfide chains can substantially limit the performance of Li-S batteries with LEs. To prevent this polysulfide shuttling mechanism, SEs have been invoked that can potentially prevent the dissolution of negatively charged polysulfides into the SE and their movement toward the anode during the discharge process.

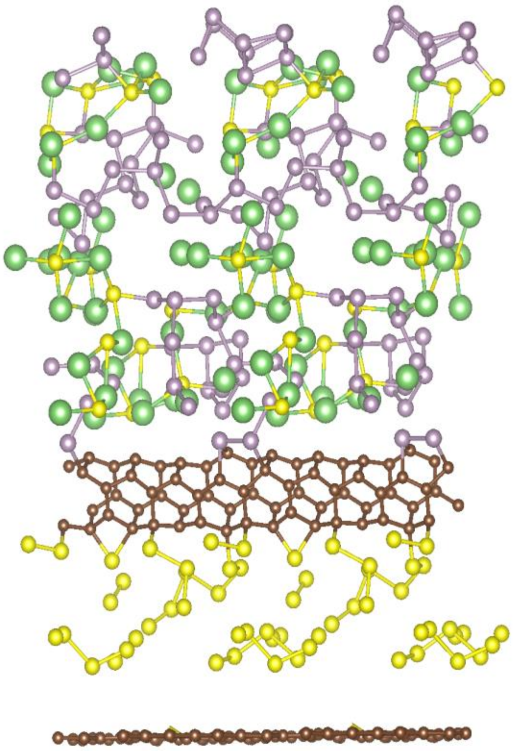

Figure 49. Snapshots of the optimized interface between S-C cathode and $Li_7P_3S_{11}$ amorphous glass-ceramic SSE.

Successful operation of an electrochemical Li-S cell depends not only on the reaction between lithium and sulfur, but also on various ion and charge transfer processes occurring within the bulk of the electrode and electrolyte materials and at their interfaces. To understand the impact of these transport mechanisms, and their impact on overall cell resistance, mesoscale simulations of Li-S cells conducted at larger length scales are necessary. Since most of the bulk and interfacial phenomena occurring within an electrochemical cell are usually taken into consideration in the continuum-level simulations, it is always easier to compare the model predictions from larger length scales with the experimental observations. However, the large-scale simulations require various parameters, such as ionic conductivity in the bulk, reaction rate constants at the interface, and equilibrium potentials where electrochemical reactions occur, as input to the model. All these material and interface specific thermodynamic and transport parameters can be estimated using calculations conducted at atomistic length scales. Hence, for successfully predicting the performance curve and understanding the various reaction pathways in Li-S batteries with SEs, development of a multiscale computational framework is necessary.

As an initial part of this study, the team investigated the possible $Li_7P_3S_{11}$ amorphous phases to determine the best structures that are closest to experimental findings. The simulation boxes were built following the same molar ratios as the experimental setup. For this, all atoms were initially arranged randomly inside the simulation box. To take the experimental finite temperature into account, they performed AIMD simulations using the Vienna *Ab Initio* Simulation Package (VASP). A time step of 1 *f*s was used for integration of the equations of motion and a 10^{-6} eV energy convergence criterion. An NVT-ensemble simulation was employed. The structures were heated to 1000 K at 70 K/ps, held at 1000 K for 3 ps, and then cooled at the same rate to the target room temperature. All further calculations start after the runs of AIMD trajectories. The interfacial supercell between S-C cathode and $Li_7P_3S_{11}$ SSE was constructed. The lattice mismatch between two materials is ~ 5.2 % mean absolute strain.

The team is now performing a series of AIMD calculations to investigate the stability of the interface and Li-ion transport channels.

Patents/Publications/Presentations

The project has no patents, publications, or presentations to report this quarter.

Task 3.6 – First-Principles Modeling of Cluster-Based Solid Electrolytes (Puru Jena, Virginia Commonwealth University)

Project Objective. The objective of the project is to use cluster-ions, which are stable atomic clusters that mimic the chemistry of individual atoms, as the building blocks of new SEs for Li-ion batteries and the corresponding battery system. The advantages of using cluster-ions to replace elemental ions is that the size, shape, and composition of the former can be tailored to achieve higher superionic conductivity, electrochemical stability, and charge transfer across the solid-state ions (SSIs) than the conventional materials. More specifically, the goal is to develop superior SEs based on cluster-ions and to model these SEs and their interfaces with electrodes, especially with the Li-metal anode, for successful integration into high-performance SSBs for EVs. The team will model and screen cluster-based solid electrolytes (CSEs) that, compared to conventional SEs, have low activation energies, practical room-temperature ionic conductivities, wide electrochemical stability windows, and desired mechanical properties that, for example, can inhibit the Li-metal anode dendrite growth. They will provide a fundamental understanding of the ionic conduction mechanism in the newly developed CSEs and will identify means to further improve property metrics via chemical and defect engineering. The team will model the interfacial properties, such as the structural, chemical, electrochemical, and ion/charge transfer properties, between the CSEs and electrodes at the atomic level, as well as find the interfacial coating materials with desired properties. Based on accumulated data from modeling, they will establish links between the basic parameters of the cluster-ions and the bulk/interface properties, which can directly guide experiments. Meanwhile, the team will work closely with experimentalists in the BMR Program to complement the project's theoretical efforts and to guide them in focused development of the predicted CSEs and the interfaces.

Project Impact. The proposed project will open a new avenue for guiding experiments in the synthesis of SSBs equipped with CSEs and capable of operating over a wide temperature range. Modeling and understanding of the ionic conduction of CSEs and their interfacial properties with electrodes, especially with Li-metal anode, will enrich current battery science and also train the future workforce in SSB development for next-generation EVs by supporting postdoctoral fellows.

Approach. This project will employ multi-scale theoretical methods and computational techniques.

Out-Year Goals. The out-year goals involve modeling development of new CSE materials and database.

Collaborations. The team is working with J. Nanda of ORNL, Y. Wu of Ohio State University (OSU), and D. Mitlin of UT, Austin, on SEs.

Milestones

1. Completing phase analysis for interfaces between the CSE and electrodes. (Q1, FY 2022; Completed)
2. Modeling structural, chemical/electrochemical, and transport properties of CSE interfaces. (Q2, FY 2022)
3. Identifying potential coating materials and modeling electrolyte-coating-electrode interfaces. (Q3, FY 2022)

Progress Report

This quarter, the team has carried out phase analysis on the interface of anode (Li-metal) / electrolyte and the interface of cathode/electrolyte. The intrinsic electrochemical windows of the studied CSEs are evaluated. The decomposition phases at the electrode/electrolyte interfaces are identified at different cell voltages. Also identified are the possible chemical reactions at the interfaces and their reaction energies that measure the driving force for the reactions to occur. Commonly used cathode materials as well as coating materials of cathodes are considered. For each studied SE, the compatible cathode and coating materials are identified.

It is well-known that lithium sulfides are featured by high ionic conductivities at the low (room) temperature and small intrinsic electrochemical windows, as exemplified by $Li_{10}GeP_2S_{12}$ (LGPS) and argyrodite Li_6PS_5Cl. Therefore, it is important to have favored decomposition phases that are electronically insulating and Li-ion conductive at the electrode/electrolyte interphases. These decomposition phases effectively form a passivation layer to protect the SE from being reduced against Li-metal anode and oxidized by the cathode. Figure 50 shows the calculated intrinsic electrochemical windows of the CSEs in the database. In each case, the column bar is colored according the reaction energy that measures the driving force for such a reaction to happen (that is, the less negative the reaction energy, the better). Several features of the CSEs are observed in the Figure. First, many CSEs have small intrinsic electrochemical windows as the known lithium sulfides. Second, nearly all the CSEs exhibit significantly smaller reaction energies than those of the well-known LGPS and lithium argyrodite. Third, $Li_6POS_4(SH)$, especially, nonstoichiometric $Li_{3.33}SB_8H_8$ and $Li_{2.83}SB_5H_5$, show relatively large intrinsic electrochemical windows compared to the others.

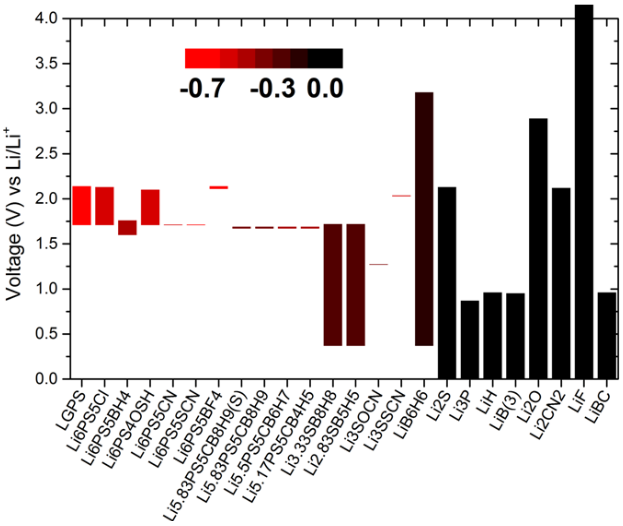

Figure 50. Evaluated intrinsic electrochemical windows of the solid electrolytes and of their decomposed lithium binary compounds. Each column bar is colored according to the corresponding reaction energy (eV/atom).

Table 5 summarizes the decomposition phases of the CSEs at the Li-metal anode and the cathode interfaces, compared to those of the LGPS and the lithium argyrodite. The decomposition phases at the Li-metal side are found to be electronically insulating and lithium conductive. They have large intrinsic electrochemical windows, as shown in Figure 50. At a high cell voltage on the cathode side, the decomposition phases are also electronically insulating. These decomposition phases can effectively “shield” the SEs from further decomposition, leading to larger overpotentials that significantly expand their electrochemical windows.

Table 5. Identified decomposition phases at the anode/electrolyte (0 V) and the cathode/electrolyte (5 V) interfaces.

Solid Electrolytes	Li-Metal Side (0 V)	5 V
LGPS	$Li_{15}Ge_4$, Li_3P, Li_2S	GeS_2, P_2S_7, S
Li_6PS_5Cl	Li_3P, Li_2S, LiCl	SCl, P_2S_7, S
Cluster-Based Solid Electrolytes	LiB, Li_3P, Li_2S, LiH, Li_2O, Li_2CN_2, ...	BPS_4, H_2S, BP, P_2S_7, PH_3O_4, S_8O, ...

For the studied CSEs, the compatible cathode and coating materials that are unlikely to react with the SEs are identified, as shown in Table 6. Compared to the LGPS and lithium argyrodite, most CSEs can be coupled with more cathode and coating materials without reacting with them and forming mixing phases at the interfaces.

Table 6. Cathode and cathode-coating materials that are unlikely to react with the solid electrolyte at a high voltage of 5 V.

Solid Electrolytes	Coupled Cathodes	Coupled Coating
$Li_{10}GeP_2S_{12}$ (LGPS)	Li_2S, $LiVS_2$, $LiTiS_2$	Li_2SiO_3 (-0.04), Li_3PO_4
Li_6PS_5Cl	Li_2S, $LiVS_2$, $LiTiS_2$	Li_2SiO_3 (-0.06), Li_3PO_4 (-0.06)
$Li_6PS_5BH_4$	Li_2S, $LiVS_2$, $LiTiS_2$, $LiFePO_4$	Li_2SiO_3 (-0.07), Li_3PO_4 (-0.07)
Li_6PS_4OSH	Li_2S, $LiVS_2$, $LiTiS_2$, $LiFePO_4$, $LiMnO_2$, $LiCoO_2$	Li_2SiO_3, Li_3PO_4
Li_6PS_5CN	Li_2S, $LiVS_2$, $LiTiS_2$, $LiFePO_4$, $LiMnO_2$, $LiCoO_2$	Li_2SiO_3, Li_3PO_4
Li_6PS_5SCN	Li_2S, $LiVS_2$, $LiTiS_2$, $LiFePO_4$, $LiMnO_2$, $LiCoO_2$	Li_2SiO_3, Li_3PO_4
$Li_6PS_5BF_4$	$LiNiO_2$ (mixing energy: -0.96)	Li_3PO_4 (-0.12)
$Li_{5.83}PS_5CB_8H_9$	Li_2S, $LiTiS_2$	Li_2SiO_3
$Li_{5.5}PS_5CB_6H_7$	Li_2S, $LiVS_2$, $LiTiS_2$, $LiNiO_2$ $LiFePO_4$	Li_2SiO_3
$Li_{5.17}PS_5CB_4H_5$	Li_2S, $LiVS_2$, $LiTiS_2$ $LiFePO_4$	Li_2SiO_3, Li_3PO_4
$Li_{3.33}SB_8H_8$	Li_2S, $LiVS_2$, $LiTiS_2$	Li_2SiO_3
$Li_{2.83}SB_5H_5$	$LiVS_2$, $LiTiS_2$ $LiFePO_4$	Li_2SiO_3, Li_3PO_4
LiB_6H_6	Li_2S, $LiVS_2$, $LiTiS_2$	$LiTaO_3$

The above study is based on a thermodynamic system that is open to a lithium reservoir (Li-metal anode), assuming that lithium transport dominates the kinetics at the interfaces. The phase diagram at the electrode/electrolyte interfaces is established based on the calculated grand potentials of all the considered phases with chemical potential of lithium as the variable. At the anode (Li-metal) / electrolyte interface, lithium has the highest chemical potential, which is equal to the total energy per atom of the lithium metal. The SE tends to uptake lithium from the anode. At the CEI, lithium has the smallest chemical potential, which is lowered by the charged cell voltage. The SE tends to give away its lithium at the cathode side.

Patents/Publications/Presentations

Presentation

- Progress update meeting (January 12, 2022).

Task 3.7 – Predictive Engineering of Interfaces and Cathodes for High-Performance All-Solid-State Lithium-Sulfur Batteries
(Badri Narayanan, University of Louisville)

Project Objective. The primary project goal is to leverage data-driven methods and ML strategies to develop accurate multi-physics models for ASSLSB materials that can capture electrochemical and transport phenomena over atomic-to-mesoscopic length/timescales; these models will be rigorously validated by synthesis and advanced characterization experiments. The team will leverage the predictive power of these models, alongside synthesis/characterization experiments and battery fabrication, to address longstanding issues at the electrode/electrolyte interfaces in ASSLSBs. The project's proposed technology involves the following: (1) halide-doped solid sulfide electrolytes that can concurrently provide high Li^+ ion conductivity and suppress dendrite growth; (2) novel mesoporous cathode composed of interconnected carbon nano-cages (CNCs) co-infiltrated with sulfur and sulfide electrolyte, which hold potential to allow high sulfur loading and optimal ion/electron pathways; and (3) functionalization of sulfide electrolyte with ILs to improve physical contact and minimize impedance at the CEI.

Project Impact. ASSLSBs remain far from commercialization due to poor understanding of fundamental electrochemical/chemical and transport processes that occur at the interfaces, especially at atomic to mesoscopic scales. Successful development of proposed predictive models (at multiple scales) will bridge this knowledge gap and will advance fundamental understanding of reaction chemistry, kinetics, charge transfer, and dendrite growth at electrified SSIs. This will enable predictive design of effective strategies to mitigate interfacial problems in ASSLSBs, including poor interfacial contact, interfacial impedance to Li^+ ion transport, and poor electron/ion conduction within cathodes. Ultimately, the fundamental knowledge gained will lead to development of high-performance ASSLSBs that meet DOE targets of specific energy (350 Wh/kg @C/3), sulfur loading (> 6 mg/cm^2), and high cycle life (1000).

Approach. The project brings together innovative solutions in multi-scale materials modeling, electrolyte synthesis, fabrication of cathode architecture, and electrolyte functionalization to overcome the issues at electrode/electrolyte interfaces in ASSLSBs. The central idea is to employ a data-driven and ML-based approach to develop accurate multi-physics battery models at atomic-to-mesoscopic scales. This approach overcomes critical problems with existing model development methods by foregoing the need for pre-defined functional forms, introducing deep-learning technique to describe reactivity, and employing optimization methods that do not require human intuition. Multi-scale simulations based on the newly developed models will provide insights into electrochemical phenomena at electrode/electrolyte interfaces.

Out-Year Goals. In Year 3, the goal is to optimize the composite cathode, functionalize CEI, and understand interfacial reactions to design ASSLSBs with high-sulfur loading (> 4 mg/cm^2) and good capacity retention (~ 1000 mAh/g, 100 cycles @C/10).

Collaborations. The team collaborates with the groups under A. Ngo and L. A. Curtiss at ANL for quantum simulations of battery systems; they plan to collaborate with J. Nanda at ORNL for advanced spectroscopic *in situ* characterization of interfaces.

Milestones

1. Optimize cathode architecture to achieve good sulfur utilization at high sulfur loading. (Q1, FY 2022; Completed)

2. Develop composite cathodes and optimize CEI to achieve good electrochemical performance at high sulfur loading using insights from simulations and experiment. (Q2, FY 2022; In progress)

3. Utilize reactive MD and advanced sampling to gain insights into defect chemistry, microstructural evolution, and interfacial processes. (Q3, FY 2022; In progress)
4. Fabricate batteries that meet performance metrics. (Q4, FY 2022; In progress)

Progress Report

This quarter, the team progressed on (1) optimizing the architecture of S-C cathodes along with their integration in solid-state Li-S coin cells that provide good cyclability at high sulfur loading, and (2) further optimization of their reactive force field (ReaxFF) to enhance its predictive capability for transport properties.

Optimization of Cathode Architecture

In Year 2, the team employed water-based binder chemistry, mesoporous cathode architecture composed of interconnected CNCs, and porous aluminum collectors to achieve stable cycling of solid-state Li-S batteries at high sulfur loading (> 4 mg/cm^2). Using this engineered cathode, and functionalizing interface between cathode and $Li_6PS_5F_{0.5}Cl_{0.5}$ SSE with ionic liquid [40 μL 2 M LiTFSI in 1:1 N-butyl-N-methyl pyrrolidinium (Pyr_{14}) : DOL], they achieved capacity retention of ~ 93% after 100 cycles. Nevertheless, these batteries showed low capacities ~ 140 mAh/g after 100 cycles. Even while using conventional (liquid) ether electrolytes, these cathodes could provide initial discharge capacity of ~ 300 mAh/g, which indicates the need to engineer the cathode architecture. Electrical conductivity measurements of fabricated cathodes showed that electronic conductivity at high sulfur loading (~ 4 mg/cm^2: ~ 0.95 S/cm) drops to less than half the value at low sulfur loading (~ 1 mg/cm^2: 2.25 S/cm); this is most likely to be the cause of low capacity.

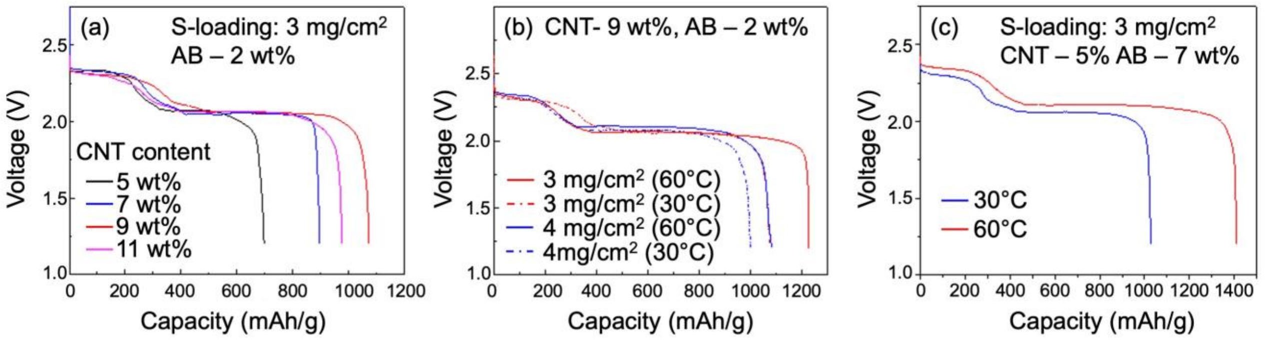

Figure 51. Effect of varying amounts of acetylene black (AB) and multiwalled carbon nanotube (CNT) in super-P cathode on the electrochemical performance of Li-S coin cell with lithium anode and conventional liquid electrolyte (1 M LiTFSI in 1:1 DOL:DME). As shown, discharge curves for batteries with super-P cathode containing (a) different amounts of CNT and 2 wt% AB operated at 30°C and S-loading of 3 mg/cm^2, (b) optimized composition 9 wt% CNT and 2 wt% AB at different S-loading [3 mg/cm^2 (red), 4 mg/cm^2 (blue)] and operating temperatures [30°C (dotted line), 60°C(solid line)], and (c) optimized composition 5 wt% CNT and 7 wt% AB at S-loading of 3 mg/cm^2 and two operating temperatures [30°C (blue), 60°C(red)]. All batteries are cycled at C/10.

This quarter, the team optimized the cathode architecture for high sulfur loading using super-P carbon, water-based binder 0.5 wt%. They systematically investigated the effect of adding acetylene black (AB) and multi-walled carbon nanotube (CNT) on the percolation of carbon network in the cathode, and in turn, its electrical conductivity. To de-couple the effect of interfacial processes, they tested the performance of cathodes containing different amounts of AB/CNT using Li-S coin cells with lithium anode and conventional ether electrolyte, 1 M LiTFSI with DME in DOL, (DME/DOL = 1/1 vol%) with $LiNO_3$ as an additive (Figure 51).

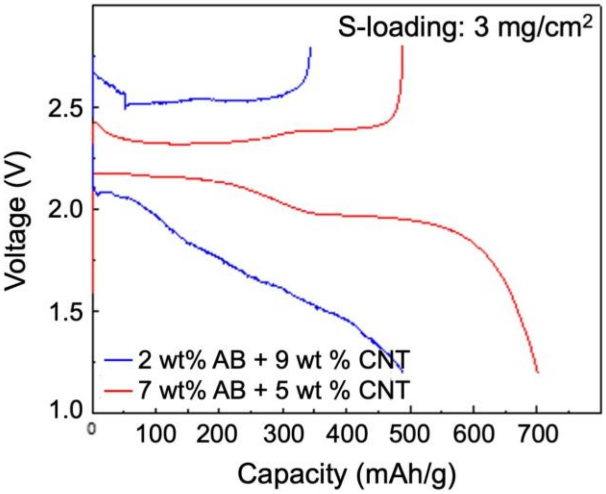

Figure 52. Discharge curve for solid-state Li-S battery made up of lithium anode, $Li_6PS_5F_{0.05}Cl_{0.5}$ solid-state electrolyte, and super-P cathode with sulfur loading of 3 mg/cm^2 and two optimized compositions, namely 2 wt% AB + 9 wt% CNT (blue) and 7 wt% AB + 5 wt% CNT (red). Both batteries are cycled at C/10.

Indeed, the team finds that addition of AB and CNT in the cathode significantly enhances discharge capacity of the batteries. For example, Figure 51a shows that when increasing the CNT content from 5 wt% to 9 wt%, the discharge capacity increases by ~ 53% (5 wt% CNT: 698 mAh/g; 9 wt% CNT: 1073 mAh/g). Note the capacity drops with further increase in CNT content; for example, at 11 wt% CNT, capacity drops to 976 mAh/g). Similarly, they found that addition of AB also increases discharge capacity. Importantly, the new cathode architecture (with super-P carbon, AB, and CNT) retains good electrochemical performance at high sulfur loading, as well. For instance, two optimized cathode compositions, namely 2 wt% AB + 9 wt% CNT (Figure 51b) and 7 wt% AB + 5 wt% CNT (Figure 51c), show good discharge capacity (~ 1000 mAh/g) at sulfur loading of 4 mg/cm^2 at 30°C. These batteries show even better discharge capacity when operated at high temperature (60°C), with values of ~ 1100 mAh/g for CNT-rich cathode (2 wt% AB + 9 wt% CNT; Figure 51b), and ~ 1400 mAh/g for AB-rich cathode (7 wt% AB + 5 wt% CNT; Figure 51c). Finally, they also tested performance of the two optimized cathodes at sulfur loading of 3 mg/cm^2 with SSE (Figure 52). They fabricated coin cell with these optimized cathodes, lithium anode, and $Li_6PS_5F_{0.5}Cl_{0.5}$ electrolyte; they also functionalized the CEI with their optimized IL [40 μL of 2 M LiTFSI in PYR:DOL (1:3)]. The cathode with 7 wt% of AB + 5 wt% of CNT showed an initial discharge capacity ~ 700 mAh/g, while the cathode with 2 wt% of AB + 9 wt% of CNT showed initial discharge capacity of ~ 500 mAh/g; this is a substantial improvement (3-5 times) over their earlier cathode architectures. Efforts are under way to investigate the cycling characteristics of these batteries and also to incorporate SSE in these cathodes at high sulfur loading to improve ionic conduction and cycling behavior.

Enhancing Predictive Power of ReaxFF for Transport Properties

In Year 2, the team had extended their ReaxFF to account for electrode/electrolyte interfaces. They also demonstrated that the newly developed ReaxFF can accurately predict (a) lattice parameters (within ~ 1% of DFT), (b) heat of formation (~ within 15 meV/atom of DFT), and (c) elastic constants (within ~ 20% of DFT); see Figure 52. Additionally, the predicted interfacial energies for various Li|SSE, S_8|SSE, and Li_2S|SSE interfaces are within 0.2 J/m^2 of DFT values; the atomic charges in the interface are close to Bader charges predicted by DFT calculations.

This quarter, the team optimized the ReaxFF parameters further by training against trajectories from AIMD simulations to enhance its predictive power for transport properties. Using this optimized ReaxFF, they calculated the lithium diffusivity of the three LiPS systems [namely, Li_3PS_4 (orthorhombic), *low-temperature* (*LT*) Li_7PS_6 (orthorhombic), and *high-temperature* (*HT*) Li_7PS_6 (cubic) systems at various temperatures (600 K, 700 K, and 800 K) using CMD simulations. For each of these temperatures, they initially equilibrated the system using NPT (that is, constant number of atoms, pressure, and temperature) ensemble for 1 ns before starting the production run of 2 ns using NVT (that is, constant temperature, constant volume ensemble). The diffusivity of lithium is obtained from the slope of the mean square displacement (MSD) of lithium versus time following the Einstein relationship; the lithium diffusivity is then used, in turn, to calculate the ionic conductivity of lithium using the Nernst-Einstein relation (Figure 53).

For Li_3PS_4, the calculated value of activation energy is found to be 0.346 eV/atom, which is in close agreement to several previous experimental measurements in the range of 0.32-0.47 eV/atom (Figure 53a). Similarly, the extrapolated conductivity at 300 K for Li_3PS_4 is found to be 1.517×10^{-5} Scm^{-1} (Figure 53a), in reasonable agreement with experiments ($10^{-5} – 10^{-4}$ Scm^{-1}). Activation energy for lithium conduction in *LT*- Li_7PS_6 is found to be 0.259 eV, in good agreement with experimental value of 0.33 eV. *LT*-Li_7PS_6 is known for sluggish diffusion of lithium ions with experiments reporting lithium conductivity of 10^{-6} S/cm; indeed, the newly developed ReaxFF also predicts slow diffusion in *LT*-Li_7PS_6 (1.683×10^{-5} Scm^{-1}). On the other hand, *HT*-Li_7PS_6 shows much faster lithium diffusion with ReaxFF predicted conductivity at room temperature of 5.018×10^{-4} Scm^{-1} (experimental value: of 0.59×10^{-4} Scm^{-1}). The team is employing this optimized ReaxFF to perform CMD simulations to advance the fundamental understanding of (1) the effect of GBs and extended defects on Li-ion conduction in SSEs, and (2) long-time nanoscale dynamics of evolution of electrified interfaces, including chemical reactions, rates, composition of SEI/CEI, ion-transport across interfaces, and effect of electric field.

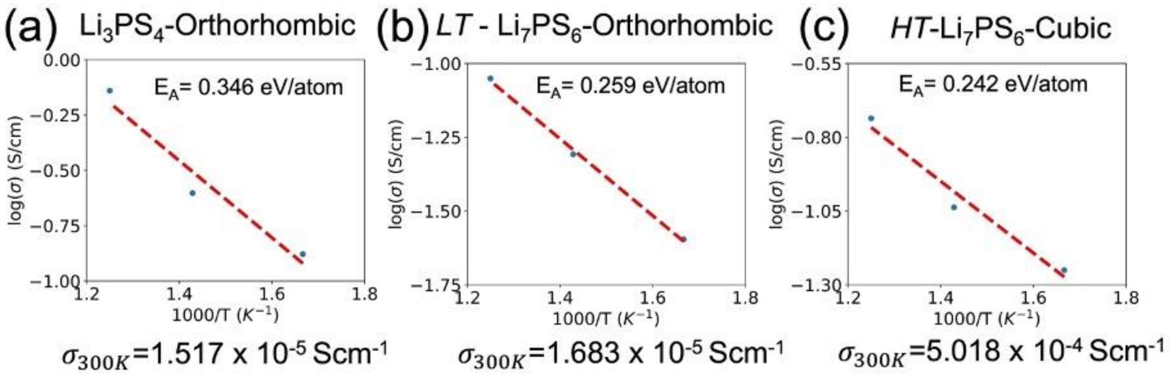

Figure 53. Temperature dependence of Li-ion conductivity (σ) for (a) Li_3PS_4 (orthorhombic), (b) *low-temperature* Li_7PS_6 (orthorhombic), and (c) *high-temperature* Li_7PS_6 (cubic) obtained using classical molecular dynamics simulations employing the newly developed reactive force field. E_A and σ_{300K} are the activation energies, and the extrapolated room-temperature conductivities are calculated using the slope and intercepts of each semi log plot.

Patents/Publications/Presentations

Publication

- Narayanan, B. “Computational Modeling of Battery Materials.” In *Encyclopedia of Energy Storage*, 1st Edition, edited by L. Cabeza. United Kingdom: Elsevier, 2021. doi: 10.1016/B978-0-12-819723-3.00156-6.

Task 3.8 – Predicting the Nucleation and Evolution of Interphases in All-Solid-State Lithium Batteries (Sabrina (Liwen) Wan, Lawrence Livermore National Laboratory)

Project Objective. The goal of this project is to develop and apply a suite of new computational tools to predict early-stage formation of metastable interphases in SSBs. To achieve this goal, this project focuses on meeting three primary objectives corresponding to different regimes within the early-stage interphase formation: (1) identify chemical motifs for pre-nucleation; (2) predict possible interphase structures; and (3) model the kinetics of interphase formation.

Project Impact. Degradation of SSE and formation of undesired secondary interphases at the solid electrolyte/electrode interfaces are some of the key issues that limit SSB technology from practical applications. The computational tools developed in this project will allow modeling of nucleation and formation of interphases with quantum-level accuracy as well as significantly improved efficiency compared to currently available methods. Completion of this project will also provide valuable insights into the correlation between local chemistry and interphase formation, which can be used to inform design of interfacial structures to lower interfacial resistance and to extend cycling life of SSBs.

Approach. The project approach centers on close integration of *ab initio* simulations, ML, and stochastic methods to probe chemistry and nucleation across broad ranges of time and length scales. First, the team will identify chemical motif, which acts as chemical precursor for pre-nucleation based on ML and large-scale AIMD simulations. Second, they will predict possible interphase structures based on stochastic minimizations of population-weighted chemical motifs identified from the MD simulations. Third, they will model the kinetics of interphase formation and evolution using kinetic Monte Carlo (KMC). To test the general applicability of the proposed computational methods, the team considers various commercially viable SE and cathode materials, including cubic LLZO and LiPON SEs, and LCO and LFP cathodes. These materials also represent a range of degrees of stability arising from their intrinsic properties—in particular, LiPON|LCO, LLZO|LCO, and LLZO|LFP are expected to form stable, less stable, and reactive interfaces, respectively.

Out-Year Goals. The future goal is to predict practical strategies either (1) to facilitate formation of the desired interphase that allows for fast Li^+ diffusion and is stable on cycling, or (2) to suppress formation of undesired interphase to reduce interfacial impedance of ASSBs.

Collaborations. There are no collaborative activities this quarter.

Milestones

1. Establish a library of meta-stable interphase structures. (Q1 FY 2022; In progress)
2. Identify initial phase transformation pathways. (Q2, FY 2022; In progress)
3. Obtain lowest energy phase transformation pathways. (Q3, FY 2022; In progress)
4. Extract phase transformation kinetics as a function of composition. (Q4, FY 2022; On schedule)

Progress Report

AIMD Simulations of Interfaces. To sample the interfacial structure and chemistry, the team has performed high-temperature AIMD simulations, and results of the LLZO|LCO and LiPON|LCO interfacial systems are summarized in Figure 54. As expected from previous thermodynamic analysis, the LiPON|LCO interface is found more stable than the LLZO|LCO interface. Figure 54 plots the evolution of density distribution of cobalt, lanthanum, and phosphorus during the AIMD simulations. Significant cobalt and lanthanum interdiffusion is observed for the LLZO|LCO interfaces, which can lead to interfacial degradation and/or nucleation and formation of secondary phases at the interfaces. Detailed post-structural analysis reveals that along with cobalt diffusion at the interfaces, its coordination number (CN) is reduced, for example, from CoO_6 to CoO_4, which implies the unique chemical environment of cobalt at the interfaces. In contrast, less structural and chemical evolution is observed at the LiPON|LCO interfaces, as shown in Figure 54b. The team is performing coordination environment analysis of cobalt and phosphorus at the interfaces to quantify the degrees of interdiffusion and variations of their local chemistry.

Global Minimization to Identify Possible Interphase Structures. Based on insights the team obtained from the AIMD simulations regarding the structural and chemical evolution of the LLZO|LCO interfaces, they identified and constructed various precursors or nucleation seeds that may lead to formation of secondary phases at the interfaces. Last quarter, they have focused on prediction of meta-stable $LaCoO_3$ phases by sampling

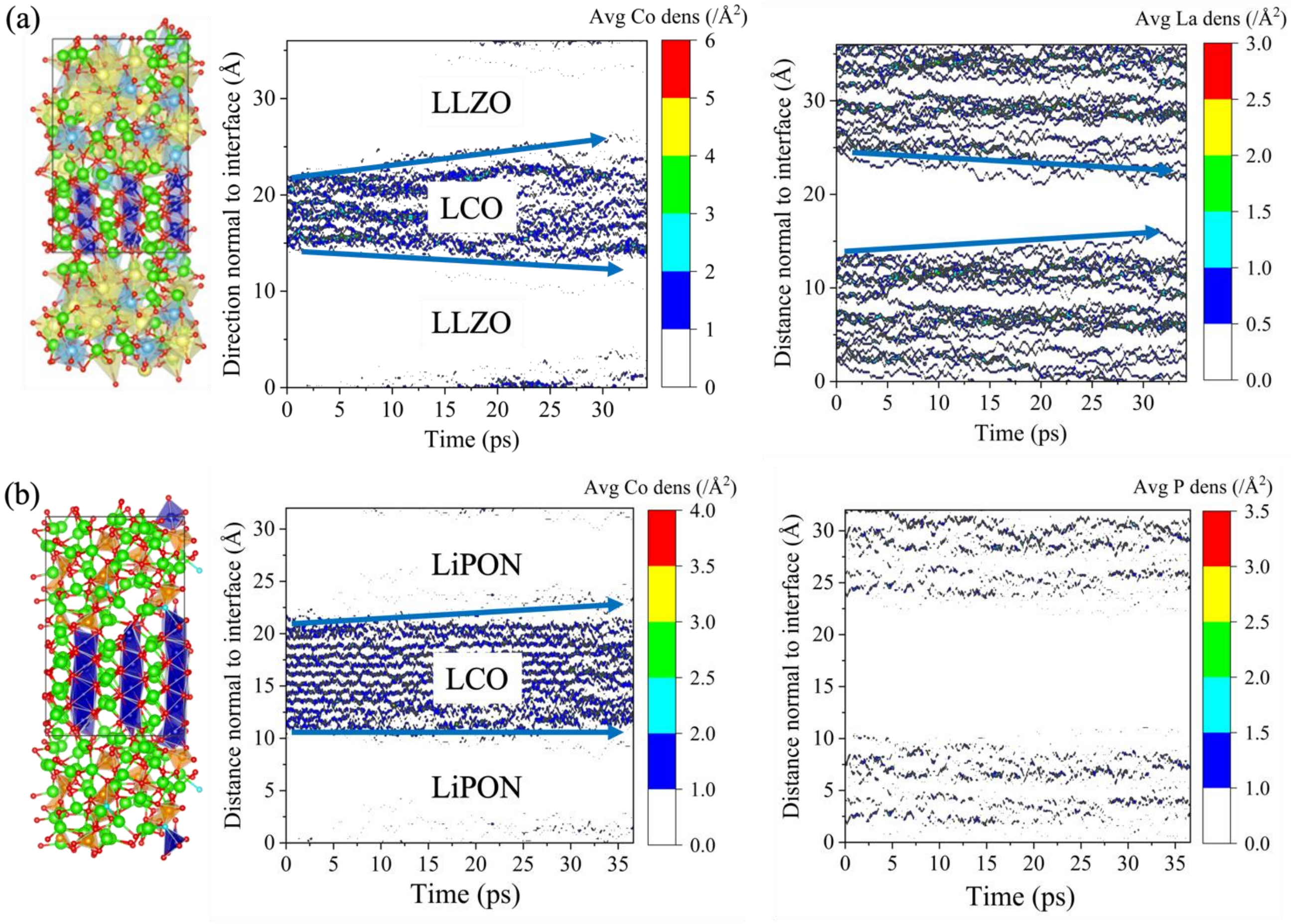

Figure 54. Average number density (/Å²) evolution of cobalt, lanthanum and cobalt, phosphorus ions at the (a) LLZO(001)|LCO(100) and (b) LiPON|LCO(100) interfaces. The lithium, lanthanum, zirconium, cobalt, phosphorus, nitrogen, and oxygen ions are represented by green, yellow, sky-blue, blue, orange, cyan, and red spheres, respectively, in the structural representation of the LLZO(001)|LCO(100) and LiPON|LCO(100) interface.

the potential energy surfaces of La-Co-O_3 precursors constructed based on the unique chemical environment observed from AIMD simulations. They have performed atomic mapping between various, low-energy candidate meta-stable phases of $LaCoO_3$ and extracting the activation energies for phase transformation. This quarter, they applied the same methodology and expanded the search to include more compositions as possible interfacial degradation products. Figure 55 demonstrates a list of initial nucleation seeds they created for $LaCoO_3$, $Li_{1.5}La_{0.5}CoO_3$, $Li_{1.5}LaCo_{0.5}O_3$, and $LiCoO_2$, based on which they began to scan potential energy surfaces using the Basin Hopping approach as introduced and described in previous quarters. Figure 56a/c shows examples of the survey of potential energy surfaces of $LaCoO_3$ and $Li_{1.5}La_{0.5}CoO_3$, and Figure 56b/d provides representative structures for each of the compositions during the structure search. It is obvious that incorporation of lithium into $LaCoO_3$ has a significant impact on its structure as well as its relative stability. This quarter, the team has been developing an algorithm to map the atomic positions in different crystal structure for phase transformation, and they are working on extracting the kinetics of such phase transformation following different transformation pathways.

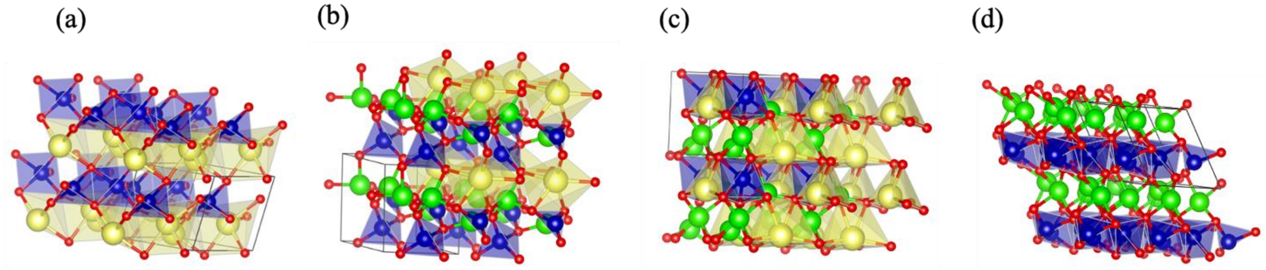

Figure 55. Generated precursor or nucleation seeds for secondary phase formation at the LLZO|LCO interfaces. (a) $LaCoO_3$, (b) $Li_{1.5}La_{0.5}CoO_3$, (c) $Li_{1.5}LaCo_{0.5}O_3$, and (d) disordered $LiCoO_2$. The lithium, lanthanum, cobalt, and oxygen atoms are represented by green, yellow, blue, and red spheres, respectively.

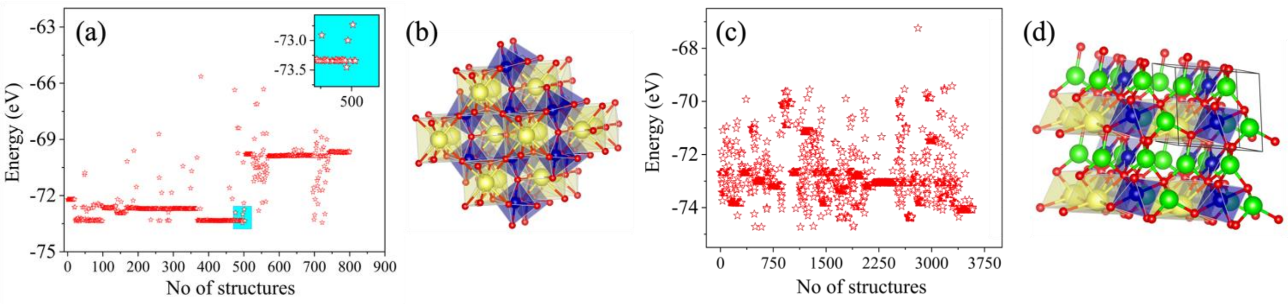

Figure 56. Surveys of potential energy surfaces of (a) $LaCoO_3$ and (c) $Li_{1.5}La_{0.5}CoO_3$ with representative structures shown in (b) and (d). The lithium, lanthanum, cobalt, and oxygen ions are represented by green, yellow, blue, and red spheres, respectively.

Patents/Publications/Presentations

Presentation

- MRS Fall Meetings & Exhibits, Virtual (December 6–8, 2021): "Development of Machine-Learning Force Fields for Complex Materials Systems in Energy Applications"; K. Kim, A. Dive, A. Grieder, N. Adelstein, S. Y. Kang, L. F. Wan, and B. Wood.

Task 3.9 – Design of Strain Free Cathode – Solid-State Electrolyte Interfaces Using Chemistry-Informed Deep Learning
(Hakim Iddir, Argonne National Laboratory)

Project Objective. The main objective of this project is to use state-of-the-art ML techniques and high-performance computing (HPC) to model complex oxide materials that will allow the team to develop cathode – SE interfaces that exhibit minimal or no strain as well as provide chemical stability at the interface between the cathode material and the SSE. A deep understanding and control of the cathode/SSE interface (including its chemical and mechanical stability) is needed to develop an effective SSB. The active cathode material changes volume during cycling, particularly at high task state of charge (SOC). This volume change leads to strained interfaces triggering loss of contact and delamination, and hence reduction/elimination of electron and ion transport pathways. The increased strain could also generate cracks within the SSE, creating new paths for lithium dendrite growth channels. These structural changes degrade the electrochemical performance of the battery. Several strategies have had limited success in alleviating these drawbacks, including mixed SSE, buffer layers between the cathode and the SSE, and dopants to improve chemical stability of the interface. These approaches, although promising, could not resolve issues with both the chemical and mechanical stability of the interface. In this project, the team proposes a new approach that takes advantage of well-established ML techniques and HPC to screen for candidate dopants of high-Ni-content NMC cathodes that would both reduce the volume expansion and the chemical reactivity (mixing) at the interface, with minimum impact on electrochemical performance and energy density of the cathode.

Project Impact. Structure-property relationships are at the heart of most fundamental scientific approaches. However, the link between structure and property remains a challenge in the materials science of complex systems, such as the oxides that form battery components. In particular, the chemical and mechanical stability of the cathode-SSE interface presents a challenge to development of SSBs. High-performance DFT calculations provide the necessary framework to understand such systems. Unfortunately, given the limited number of atoms and time scales accessible by the method, along with the myriad calculations required to achieve satisfactory results, the computational cost of simulating all the possible configurations of a multicomponent oxide is prohibitive. In this work, the team augments the DFT data with ML (especially deep learning) techniques that allow them to access the large system sizes and longer time scales necessary to build thermodynamic models. They focus on understanding the nature of benchmark $Li_{1-\alpha}Ni_{1-x-y-z}Mn_xCo_yM_zO_2$ structures (M dopant, α, x, y, $z < 1$), their volume change with lithium content, the nature and concentration of the dopants, and chemical stability of the SSE-cathode interface. The DFT and ML approach will provide new cathode compositions that will reduce the strain of the SSE-cathode interface and hence improve its mechanical and chemical stabilities.

In this project, the team aims at developing a methodology that will allow them to explore and expand the configurational space using HPC approaches in a systematic and efficient way. The methodology will encompass DFT, AIMD, MD, and ML. The methodology will also take advantage of various software already developed at ANL and at other DOE laboratories (for example, Balsam) to automate, manage, and control the large number of calculations needed to achieve the project goal.

Approach. All calculations will be performed by spin-polarized DFT as implemented in VASP. After geometry optimization within the DFT+U framework, electronic relaxation will be performed using a single-point calculation with the hybrid functional HSE06. For production calculations, they will use the message-passing interface (MPI) parallelized version of VASP.

Exploration of the potential energy surface is needed to predict the structure of solid materials and interfaces. Such calculations are infeasible using MD or DFT calculations alone. Thankfully, the potential energy surface of a system can be represented by the sum of the energies of the local neighborhoods surrounding each atom. This enables the use of ML surrogate models trained with DFT calculations to capture the energies in local neighborhoods. The input to the ML surrogate must be a unique representation of the system under study. Consequently, the local environment of each ion is described using a local environment descriptor that renders the atomic configuration invariant to rotations, translations, and permutations of the atoms. In recent years, several different descriptors have come to prominence with advantages and disadvantages. Once the ML surrogate is trained, the total energy and forces over all the ions of any structural configuration can be determined. Such information can be used for atomistic simulations, namely, MD and MC.

In this project, the team proposes to use the open-source DeepMDkit python/C++ package to construct the ML potential energy surface and FFs. The promise of DeepMDkit in this work is to provide near-DFT accuracy at orders-of-magnitude lower computational expense, comparable to traditional MD simulations. Efficiency in training is facilitated through integration with TensorFlow and MPI / graphics processing unit support.

One of the challenges of developing ML potential energy surface is achieving accurate predicted forces and energies across the entire configurational space, while minimizing the total number of calculations required for training. In recent years, active learning has been highlighted for its ability to target training examples most likely to improve the model quality or to achieve some other objective (that is, maximizing a predicted material property). DP-GEN, an open-source python package based on DeepMDkit, implements a similar active learning scheme with HPC support, and has been employed to construct ML potential energy surface with accuracy approaching DFT and sometimes exceeding embedded atom potential for experimentally measured properties of interest. In this work, the team proposes to leverage DeepMDkit and DP-GEN to efficiently generate ML potential energy surfaces for cathode-electrolyte systems including a variety of dopants.

Out-Year Goals. One out-year goal involves developing a DFT-trained ML model on NMC/LLZO interface, ready to use for large screening of new cathodes, SSE compositions, and cathodes/SSE interfaces. A second is to provide fundamental understanding on critical parameters limiting performance and stability of the cathode/SSE interface and hence of the SSB.

Collaborations. Project collaborators include J. Croy, C. Johnson, and E. Lee from ANL Chemical Sciences and Engineering Division for the synthesis phase of the project.

Milestones

1. Determine cationic distribution in $LiNi_{0.8}Mn_{0.1}Co_{0.1-y}X_yO_2$ (NMCX) for X in (Ti, Zr, Al, Fe, Ca, Mg, Y, W, Nb, B, La). (Q1, FY 2022; Completed)
2. Determine elemental segregation, volume changes, and phase transformation during charging of doped (including fluorine anionic substitution) NMC-811 using the developed DFT-trained ML model. (Q2, FY 2022)
3. Determine doped NMC-811-LLZO interface reactivity and structural stability. (Q3, FY 2022)
4. Screen for compositions with low interfacial strain, and elemental mixing (NMCX-LLZO). (Q4, FY 2022)

Progress Report

The cathode volume change on delithiation is the leading cause of cathode-SEI strain. To design doping strategies that minimize strain, the distribution of the dopant and effect on the cation arrangements must be determined. In previous reports, the team has shown their strategy to understand the distribution of elements and the subsequent volume change on delithiation. They have chosen NMC-811 as the baseline cathode material, given its widespread use and favorable electrochemical properties. They have tested titanium, zirconium, aluminum, iron, calcium, magnesium, yttrium, tungsten, niobium, boron, and lanthanum as dopants and candidates for cobalt substitutes. Anionic substitutions (fluorine on oxygen sites) are being tested. As an example of the collected data, Figure 57 shows the energy landscape for Zr-doped NMC-811, where zirconium is substituting a third of the cobalt sites. The lowest energy configuration presents uniformly distributed Mn-Co or Mn-Zr pairs. The highest energy configuration shows Zr-Mn-Co clusters and some Li/Ni anti-site defects in contiguous layers. They also collected data for zirconium substituting two thirds, and all cobalt sites. All calculations have been performed using the R2SCAN + D3 functional and Van der Waals correction, which have been demonstrated previously to offer very accurate structural and energetic features for cathode materials. All data produced are being used to train the ML potential that would be used to further explore the cation distributions in much larger simulation cells. The ML fitting is being performed using DeepMDkit as indicated in previous reports.

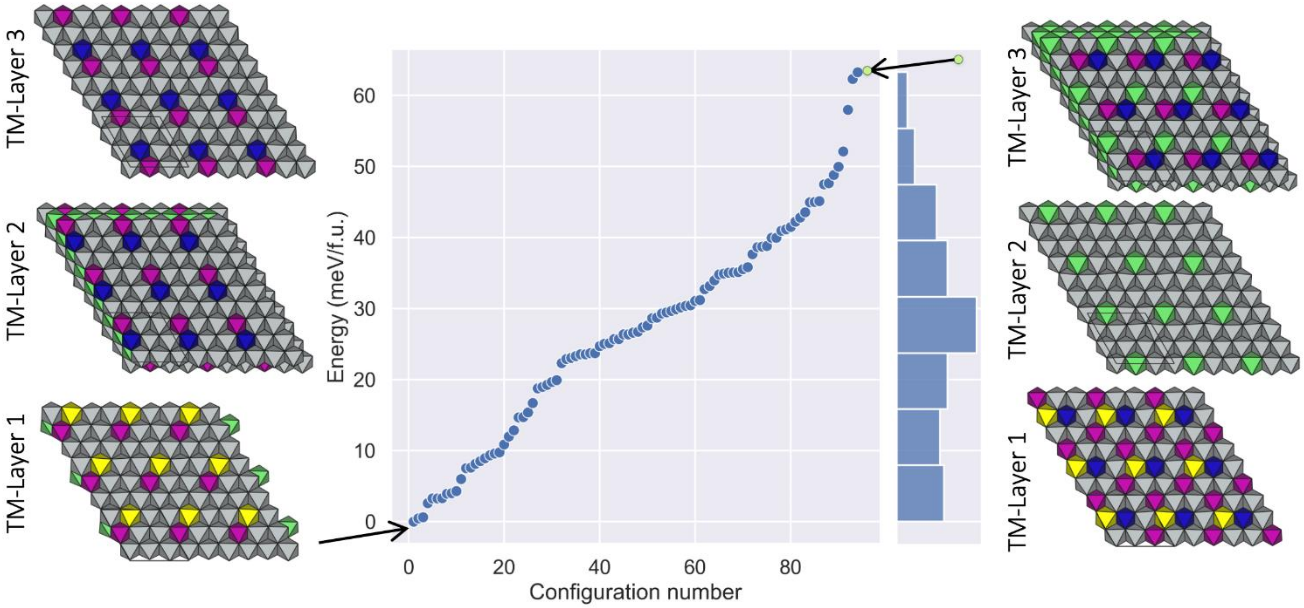

Figure 57. Zr-doped (1/3 of cobalt sites) NMC-811 energy distribution for several random cationic configurations. Insets show top view of three transition-metal layers in the simulation cell for the lowest and highest energy configurations. Purple, blue, grey, yellow, and green tetrahedrons represent manganese, cobalt, nickel, zirconium, and lithium sites.

The project team is developing two Bayesian optimization strategies to identify low energy configurations of dopants in the NMC-811 structure. The first leverages the technology described in Garcia et al. (2021), wherein each member of an ensemble of MLFFs is trained with a subsampling with replacement of the dataset. This provides an estimate of the uncertainty propagated to the energy predictions from the variability of the MLFF parameters. By selecting configurations that best balance high uncertainty and low energy, configurations with potentially very low energies can be identified. The downside of this approach is that each evaluation of the MLFF takes enough time that it limits the number of total configurations that can be explored. In the second approach, a Gaussian process (GP) surrogate is built for the MLFF and is tuned using an active learning approach. This GP surrogate can then be employed to evaluate the energies of a much larger number of configurations than with the MLFF alone. A methods paper is in development that introduces these approaches in detail and demonstrates finding low-energy configurations for two dopants.

Using the DFT data to estimate volume change for the baseline cathode material, some differences with the previous work on $LiNiO_2$ (LNO) volume change (see publications) are observed. Specifically, the distribution of vacancies in NMC-811 follows a solid solution model without any apparent clustering (see Figure 58). Hence, only one phase is being observed at high SOC (highly delithiated system). The volume change, however, remains similar for NMC-811 and $LiNiO_2$. The c-lattice parameter for LNO decreases by 8%, while for NMC-811 it decreases by 7.5%.

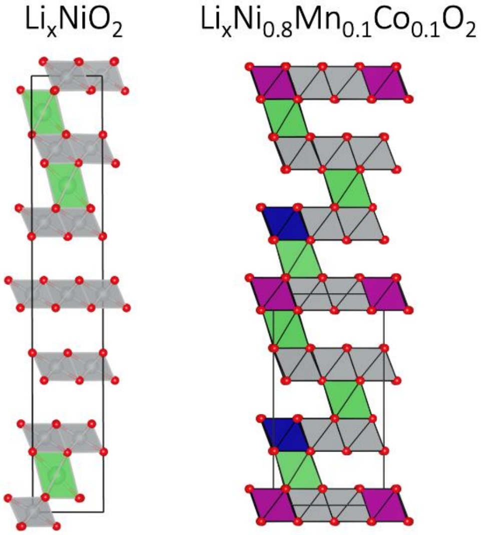

Figure 58. Side view of schematic simulation cells comparing LNO and NMC-811 lowest energy lithium distribution (lithium content: x = 0.12). Purple, blue, grey, and green tetrahedrons represent manganese, cobalt, nickel, and lithium sites. Small red spheres represent oxygen ions.

Patents/Publications/Presentations

Publication

- Garcia, J. C., J. Gabriel, N. H. Paulson, J. Low, M. Stan, and H. Iddir. “Insights from Computational Studies on the Anisotropic Volume Change of Li_xNiO_2 at High States of Charge ($x < 0.25$).” *The Journal of Physical Chemistry C* 125, No. 49 (2021): 27130–27139. doi: 10.1021/acs.jpcc.1c08022.

Task 3.10 – Tackling Solid-State Electrochemical Interfaces from Structure to Function Utilizing High-Performance Computing and Machine-Learning Tools

(Shinjae Yoo, Feng Wang, and Deyu Lu, Brookhaven National Laboratory; Nongnuch Artrith and Alexander Urban, Columbia University)

Project Objective. This project aims at elucidating the structural evolution and other dynamic properties of the interphases at the SSIs in SSBs under processing and electrochemical cycling conditions that strongly impact cell performance. By leveraging synergies of first-principles theory, HPC, ML, and computational/experimental spectroscopy, this project involves a comprehensive investigation of SE systems and SSIs that may enable the practical use of lithium anodes and high-nickel NMC cathodes in SSBs. Specific project objectives are as follows: (1) develop realistic atomic-scale structure models of the heterostructural SSIs, (2) determine the impact of structural evolution on stability and transport properties of SSIs, and (3) identify the coating/doping chemistry that may stabilize SSIs during formation and electrochemical cycling.

Project Impact. Interfacial properties and the dynamical evolution of interphase structures are crucial for the stability and performance of SSBs. This project will lead to fundamental understanding of current materials limits and will identify key materials parameters for optimizing the performance of SSBs. By corroborating atomic-scale theory with experiment, the project will identify structure–property relationships of the heterostructural SSIs in SSB systems that are relevant for EVs. The outcomes of this project will therefore accelerate development of high-energy-density, safe SSBs for EVs.

Approach. Accurate ML potentials will be trained on an extensive database from DFT calculations to simulate the structure evolution and electrochemical properties of the SSIs. Using a second ML model, key physical descriptors will be extracted from EELS and XAS measurements. This spectral fingerprinting will enable the automated interpretation of spectroscopy measurements, thereby bridging between atomistic modeling and experiment. An experimental platform will be developed to integrate experimental/computational spectroscopy and modeling of SSIs. In combination, the two ML models and the spectroscopic data will facilitate the construction of a physics-based model to unravel the structure-property relationships of the SSIs.

Out-Year Goals. The project will progress toward establishing dynamic composition-structure-property relationships for interface stability and transport within and across the electrochemical SSIs in SSBs. The ML approach will be further developed to a general model for thermodynamic and transport properties of dynamic heterostructural electrochemical interfaces and will eventually be applied to the practical SSB systems.

Collaborations. The project is collaborating with Y. Du at BNL.

Milestones

1. Determine electrochemical stability of LPS/Li interfaces during cycling through spectroscopy characterization aided by ML, data-analysis, and modeling. (Q1, FY 2022; Completed)
2. Analyze impact of halide-substitution on chemical and electrochemical stabilities of LPS-X (X = Cl, Br, I) systems in contact with lithium metal. (Q2, FY 2022; In progress)
3. Identify key limitations to interfacial stability of LPS and LPS-X systems in contact with lithium metal through combined computational/experimental investigations. (Q3, FY 2022; In progress)
4. Establish doping/coating-based approaches for enabling long cycling stability of the LPS-X based half and full cells at high current density. (Q4, FY 2022; In progress)

Progress Report

This quarter, the team used a combination of electrochemical, spectroscopic, and computational techniques to identify the sequence of the LPS redox reactions and their microscopic structural characteristics. It was found that LPS electrolytes start to oxidize at ~ 2.5 V versus Li^+/Li, where sulfur atoms lose lithium neighbors during delithiation. During deep delithiation at voltages above 3.6 V, under-coordinated sulfur atoms in LPS form bridging sulfur bonds and so give rise to a structurally different interphase that is electrochemically active and participates in lithiation and delithiation reactions in the following cycles. If LPS is not deeply delithiated (that is, below 3.4 V), the formed interphase affects the subsequent reactions less. Additional experimental evidence was also obtained on the change in the local phosphorus environment during the lithiation process, likely due to formation of P-P or Li-P bonds. These findings provide insights into the electrochemical stability of LPS/Li interfaces during cycling.

Cyclic Voltammetry Study of the Electrochemical Stability of LPS

The team first measured the chemical stability and redox reaction of LPS in the LPS-C | LPS | Li-In cells using CV experiments. To focus on the intrinsic redox reaction of LPS, they employed an LPS-C composite working electrode consisting of LPS particles and carbon black. The battery used an LPS pellet as the SE and Li-In alloy as the counter/reference. More details on this setup can be found in last quarter's report. CV experiments were conducted for the LPS-C composite, as shown in Figure 59 under the voltage sweep rate of 0.1 mV/s. Figure 59a-b shows the CV curves for the scan ranges of 0-5 V and 0-3.4 V, respectively. Both experiments started with an anodic scan, that is, an increase in the voltage from the open-circuit voltage (OCV) to 5 V (Figure 59a) or 3.4 V (Figure 59b) versus Li^+/Li. The team defines one cycle as the voltage sweep OCV → 5 V → 0 V → OCV. They note that in both experiments, the curve from the 1st cycle is different from the curve in the 2nd cycle; however, the voltage curves after the 2nd cycle are similar (not shown here). This implies that the redox reactions in the 1st cycle are different from the following cycles.

In Figure 59a, the team first observes a large current bump, denoted as (a), which starts at ~ 2.5 V and has a maximum current at ~ 3.6 V. Here, they use the term "bump" instead of "peak" because of the relative large broadness as compared to common CV sweep peaks. This bump is indicative of an oxidative decomposition reaction, likely associated with the delithiation of LPS. During the reverse scan from 5 V to 0 V, the current decreases as the voltage decreases. At ~ 2.4 V, the current becomes negative and its amplitude increases as the voltage decreases. The negative current corresponds to the lithiation reaction. In the sweep from 0 V to 5 V, the current turns positive at about 0.7 V. There are two positive current bumps at ~ 1.35 V (b) and 3.25 V (c), respectively, indicating two different delithiation reactions. They note that the bump at 3.25 V (c) is at a different position from the 3.6 V bump (a). This means that the delithiation reactions of the 1st and 2nd cycles are different, which may be caused by the composition change of the LPS after the 1st cycle.

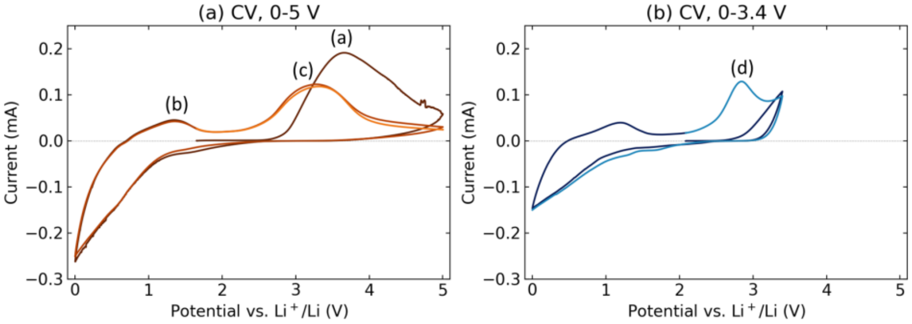

Figure 59. Cyclic voltammetry experiments of LPS-C | LPS | Li-In cells under the voltage scan rate of 0.1 mV/s. (a) Experiment starts with anodic sweep from open-circuit voltage to 5 V versus Li^+/Li, then reverses the scan to 0 V. (b) Experiment starts with anodic sweep, but to 3.4 V instead of 5 V, and then reverses to 0 V.

In the second measurement, as shown in Figure 59b, they only scan the voltage to a maximum of 3.4 V. The LPS does not undergo the decomposition reaction as in Figure 59a. From 3.4 V to 0 V, the current becomes negative at ~ 2.4 V, but the current amplitude is smaller than that in the 5 V experiment. They note that the bump at (d) occurs at a lower voltage than (c) and has a narrower width. This means that (d) in this experiment with a narrow voltage range (0-3.4 V) is indicative of a different reaction than (c) in the first experiment with a wide range (0-5 V).

From the CV experiments, they draw the following conclusions. First, the onset of LPS oxidation is at ~ 2.5 V versus Li$^+$/Li. Second, the 1st redox cycle is different from the 2nd and following cycles. Third, the reactions are different depending on the voltage range and whether the threshold at 3.6 V is passed in the 1st cycle affects subsequent reactions. To further investigate, they performed XAS experiments as well as first-principles calculations on delithiated LPS structures.

XAS to Resolve LPS Redox Reactions

The team performed XAS experiments of phosphorus and sulfur K-edge in fluorescence mode at the NSLS-II TES (8-BM) beamline. As shown by the markers in Figure 60c and Figure 61c, the measured samples (A1-A5 and B1-B5) were cycled to different stages, disassembled and sealed with Kapton tape and polyester film in the glovebox, and then transferred to the helium chamber at the beamline. The measured data of the pristine LPS for phosphorus K-edge X-ray absorption near-edge spectroscopy (XANES) (Figure 60a and Figure 61a) and sulfur K-edge XANES (Figure 60b and Figure 61b) are consistent with those reported in the literature.[1] Figures 60 and 61 show the evolution of the spectra during CV experiments at the ranges of 0-5 V and 0-3.4 V, respectively.

In the experiment with the 0-5 V voltage range, the phosphorus K-edge XANES white line at 5 V in the 1st cycle (curve A1) decreases and broadens as compared to the pristine LPS; in the sulfur K-edge spectrum, a peak of 2470.5 eV appears, which has been attributed to the formation of bridging sulfur bonds[2-3] and is consistent with the XANES simulation results in the previous report. From A1 to A2, phosphorus XANES shows a higher intensity between 2150 eV and 2153 eV in A2, while interestingly the change in the sulfur spectrum is marginal. At the end of the 1st cycle (A3), phosphorus XANES shows a higher intensity at the white line; the 2470.5 eV peak in the sulfur XANES decreases and the spectral shape shows a three-peak feature, similar to the pristine spectrum, but with a higher intensity in the second peak region. In the 2nd cycle, the team observes a large change in the phosphorus and sulfur spectra after the 3.25 V bump. A new peak of 2148.5 eV appears in the

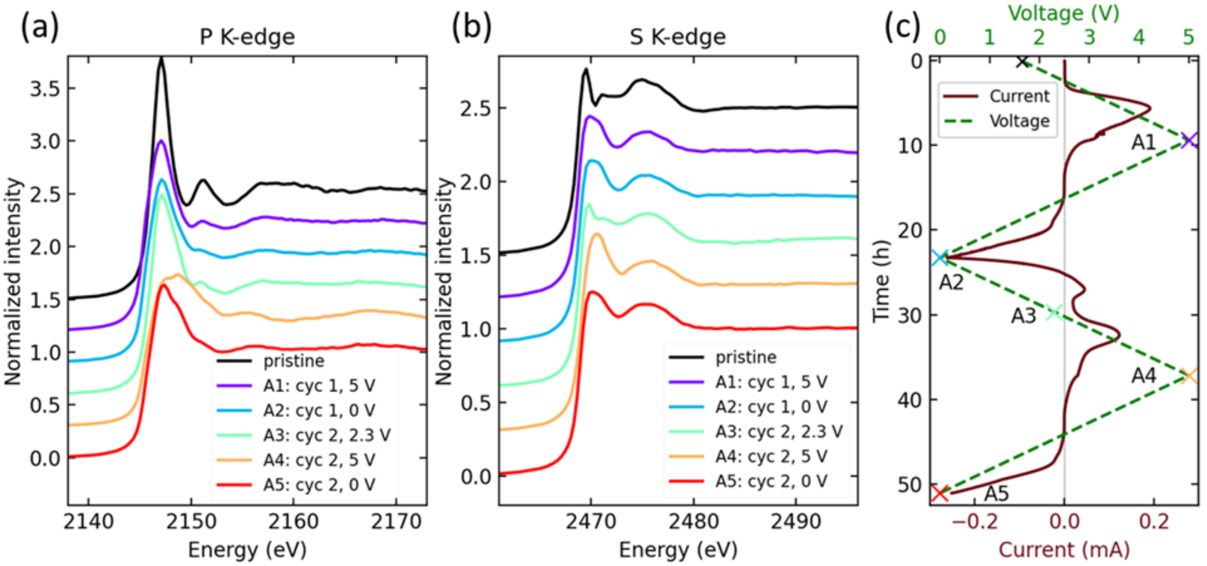

Figure 60. Experimentally measured X-ray absorption near-edge spectra of the phosphorus K-edge (a) and sulfur K-edge (b) of LPS from the cyclic voltammetry (CV) experiment within 0-5 V scanning range. (c) Current (red solid line) and voltage (green dashed line) profiles from the CV experiment. Spectra in (a) and (b) are vertically shifted for clarity. Markers in (c) indicate the states of the samples that were prepared for X-ray absorption spectroscopy measurement. The voltage sweep rate is 0.1 mV/s.

phosphorus spectrum, which could be the origin for the broadening of the white line in curve A1. The 2470.5 eV peak of sulfur exceeds the intensity of the original 2469.5 eV white line peak and becomes the dominant feature. In the last sample (curve A5), both peaks of 2148.5 eV of phosphorus and 2470.5 eV of sulfur spectrum decrease.

In the experiment with the 0-3.4 V voltage range, the XANES spectra exhibit quite different behavior. As compared with the pristine material, at B1 (3.4 V in the 1st cycle) the white line intensity of phosphorus spectrum decreases a bit without broadening, while the sulfur spectrum overall shows little change. Details about this slight change can be found in the next section. Combining the pristine, B1, and A1 curves, they can see a gradual evolution of the phosphorus and sulfur K-edge XANES spectra during the first oxidation (OCV → 3.4 V → 5 V), where the intensity of the phosphorus white line first decreases and then broadens as the intensity further decreases, as well as a slow emergence of the 2470.5 eV peak in sulfur spectra.

Starting from curve B2, the experiment with the 0-3.4 V voltage range proceeds along a different path from that with the 0-5 V voltage range. First, the phosphorus spectra do not show the white line broadening or the new peak of 2148.5 eV during the entire sweep. The team only observed intensity fluctuations of the white line peak and the 2151 eV peak during cycling. Second, a shoulder peak at 2143.5 eV appears in curve B2, remains in curve B3 but with a decreased intensity, disappears in curve B4, and finally reappears in curve B5. They hypothesize that the shoulder peak could be due to the formation of P-P bond or Li-P bond formation during lithiation. The P-P bond[1] could be formed due to the loss of sulfur in LPS during lithiation, as the result of the formation of Li-S compounds. In this process, the P-S bond breaks and the P-P bond is formed between two adjacent PS_4^{3-} tetrahedra to form the $P_2S_6^{4-}$ local structural motif. During the delithiation process (B2→B3→B4), when this P-P bond breaks, the shoulder peak disappears in the phosphorus XANES spectra. The Li-P bond formation is due to the lithium insertion near phosphorus sites in the LPS structure. The data analysis is still ongoing to determine which hypothesis is correct. Third, the change in the sulfur spectra is much smaller than in the experiment with the 0-5 V voltage range. The sulfur spectra only show a shape change in the second peak and very slight intensity variation in the third peak. Finally, comparing A5 and B5, although both were measured at 0 V in the 2nd cycle, they show different XANES spectra in both phosphorus and sulfur. The same applies to A2 and B2.

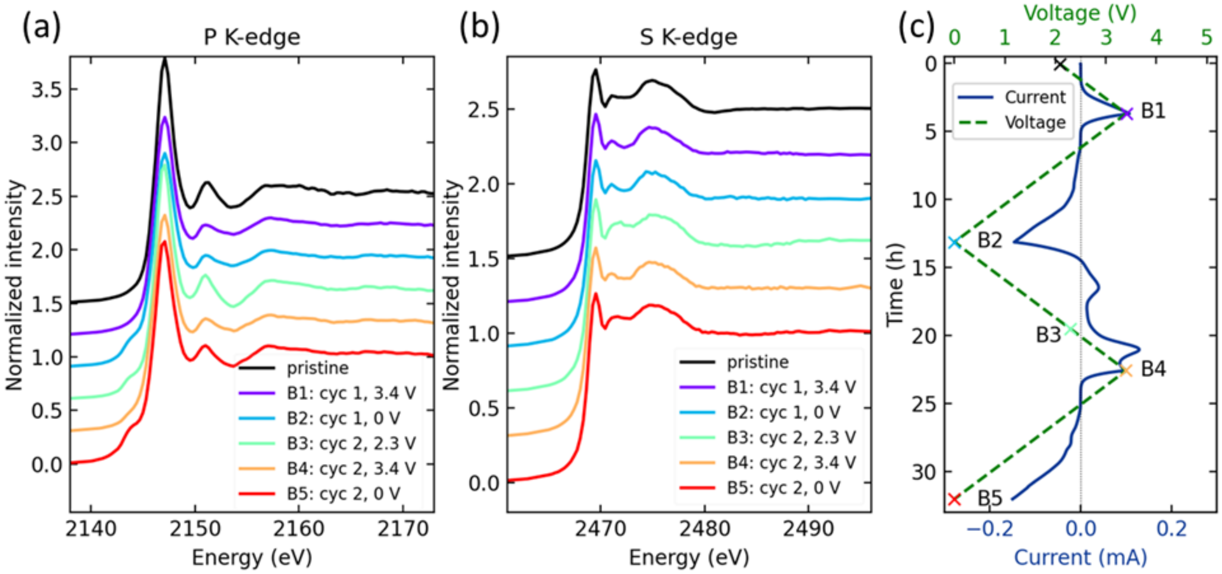

Figure 61. Experimentally measured X-ray absorption near-edge spectra of the phosphorus K-edge (a) and sulfur K-edge (b) of LPS from the cyclic voltammetry (CV) experiment within 0-3.4 V scanning range. (c) Current (blue solid line) and voltage (green dashed line) profiles from the CV experiment. Spectra in (a) and (b) are vertically shifted for clarity. Markers in (c) indicate the states of the samples that were prepared for X-ray absorption spectroscopy measurement. The voltage sweep rate is 0.1 mV/s.

First-Principles Study of Sulfur K-Edge XANES Spectra

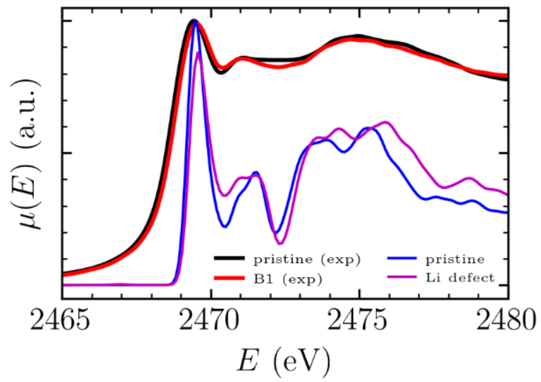

Figure 62. Simulated sulfur K-edge X-ray absorption near-edge spectra of pristine and Li-defect β-LPS (bottom) compared with experimental references (top).

To interpret sulfur K-edge XANES spectra during delithiation, the team performed first-principles calculations. They first generated representative atomic structures of delithiated LPS by removing a single lithium atom from a supercell of β-LPS of 48 lithium atoms, which corresponds to ~ 2% delithiation. This concentration is close to that calculated from the measurement at 3.4 V (B1 in Figure 61b), assuming that the observed current is proportional to the extracted amount of lithium. The sulfur K-edge XANES spectrum was averaged over all sulfur sites in the relaxed structure using the core hole potential method described in the team's FY 2021 Q2 report. The comparison between theory and experiment is shown in Figure 62. Spectral features of the simulation are overall consistent with experiments, which show small changes during the early delithiation. Trends between the experimentally delithiated (B1) and pristine spectra are well reproduced, including a similar white line peak intensity and slightly lower intensity at the dip at ~ 2472.5 eV. However, the agreement is not perfect. For example, the overall post-edge intensity is higher in the calculated lithium defect spectrum compared to the pristine LPS, though this is not seen in the experiment. The small discrepancy is likely caused by the fact that the team did not exhaustively sample lithium defect structures and that their spectral simulation does not include temperature effects. Work is in progress to disentangle different contributions (for example, the change of sulfur charge state and local coordination environment) using detailed electronic structure analysis. The physical understanding from this study will provide guidance to identify relevant local structure motifs from the LPS spectral database the team developed (see details in the FY 2021 Q2 report) and build ML models to capture the structure-spectrum correlation.

In summary, comparing the two sets of XAS spectra data, the team concludes the following. First, bridging sulfur bonds are likely formed during the first oxidation at 3.6 V. Second, the subsequent reaction processes of LPS show a dependence on the maximum voltage, in particular, whether the LPS has been oxidized to above the threshold of 3.6 V. When the LPS is delithiated to 5 V, a new layer likely forms at the LPS surface, and the reactions during the reverse scan to 0 V will mainly occur on this new layer instead of the pristine LPS beneath it. During the 5 V → 0 V scan, the experiment measures the redox reaction of this newly formed layer; during the scan from 3.4 V to 0 V, the reaction process is different, likely involving the formation of Li-P bonds or P-P bonds in $P_2S_6^{4-}$ local structure motifs. Results from this study reveal that the redox reactions of LPS differ depending on the reaction voltage ranges. This suggests that the electrode-electrolyte interface reactions are different for cathode materials with different working potentials. In future studies, XPS experiments will be conducted to determine the valence changes during the redox reactions and to gather more information to aid in data interpretation.

References

[1] Li, X., et al. "Totally Compatible P_4S_{10}+n Cathodes with Self-Generated Li^+ Pathways for Sulfide-Based All-Solid-State Batteries." *Energy Storage Materials* 28 (2020): 325–333.

[2] Koerver, R., et al. "Capacity Fade in Solid-State Batteries: Interphase Formation and Chemomechanical Processes in Nickel-Rich Layered Oxide Cathodes and Lithium Thiophosphate Solid Electrolytes." *Chemistry of Materials* 29, No. 13 (2017): 5574–5582.

[3] Swamy, T., X. Chen, and Y-M. Chiang. "Electrochemical Redox Behavior of Li Ion Conducting Sulfide Solid Electrolytes." *Chemistry of Materials* 31, No. 3 (2019): 707–713.

Patents/Publications/Presentations

Publication

- Guo, H., Q. Wang, A. Urban, and N. Artrith. "AI-Aided Mapping of the Structure-Composition-Conductivity Relationships of Glass-Ceramic Lithium Thiophosphate Electrolytes." Online: http://arxiv.org/abs/2201.11203.

Presentations

- MRS Fall Meetings & Exhibits, Virtual (December 6, 2021): "Shedding Light on the Sulfide Electrolytes/ Electrode Interphases in Solid-State Batteries via Integrated Computation and Spectroscopy"; C. Cao, M. R. Carbone, H. Guo, S. Liu, Y. Du, S. Bak, T. Xiao, N. Artrith, A. Urban, D. Lu, S. Yoo, and F. Wang.
- MRS Fall Meetings & Exhibits, Virtual (December 6, 2021): "Structure-Composition-Conductivity Relationships of Glass-Ceramic Lithium Thiophosphates Electrolytes"; H. Guo, Q. Wang, A. Urban, and N. Artrith.

Task 3.11 – Integrated Multiscale Model for Design of Robust, Three-Dimensional, Solid-State Lithium Batteries
(Brandon Wood, Lawrence Livermore National Laboratory)

Project Objective. This project is developing and applying multiscale, multiphysics models that connect composition, microstructure, and architecture to mechanical integrity in 3D SSBs. The models integrate multiple computational methods, informed and validated through collaborations with complementary experimental efforts. The project scope addresses three objectives: (1) develop multiphysics, multiscale chemomechanics models; (2) assess interface- and microstructure-induced mechanical failure thresholds; and (3) simulate chemomechanical evolution under battery operating conditions.

Impact. This project will deliver multiscale, multiphysics models that connect composition, microstructure, and architecture to mechanical integrity in 3D SSBs. The tools will be used to examine common interfaces in commercially viable electrolyte and cathode materials and to provide design principles for maintaining mechanically robust operation. The modeling framework will address the shortcomings of existing modeling strategies that either lack coupling of the multiphysics nature of various processes active in 3D batteries or fail to incorporate processes at different length scales to understand function. Connections will be made to understand the limits of operability and to co-optimize ionic conductivity and mechanical robustness in solid electrolyte-cathode matrix composites.

Approach. The project approach integrates atomistic, mesoscale, and continuum simulation methods to predict chemomechanical properties of interfaces in ceramic (LLZO) and halide-based SEs. Both internal GBs and interfaces with $LiCoO_2$ (LCO) and NMC cathode materials are considered. The project is aligned along three tasks, each of which uses simulations to probe a different fundamental length scale relevant to the performance of 3D-SSB architectures. First, atomic-scale interfacial properties are computed using DFT and ML approaches. These include local bond strength and mechanical response, as well as stress distributions associated with formation of cracks. Second, using digital reproductions of 3D electrodes and electrolytes, the local stress distributions and stress hotspots in SEs and cathode-electrolyte composites are computed within a mesoscale model. Third, materials performance is coupled to cycling conditions within an operating device by incorporating phase-field models that can simulate rate-dependent fracture likelihood under cycling and extract microstructure-fracture-transport relationships.

Out-Year Goals. The team will focus on the following out-year goals: use *ab initio* methods to generate models for GBs and CEIs; compute local bond strength and mechanical response of model interfaces; reconstruct microstructures of electrodes and electrolytes using phase-field models; and develop a phase-field model for cathode-induced volume evolution on cycling.

Collaborations. This project collaborates with N. Adelstein from San Francisco State University on atomistic diffusion modeling, and J. Ye from Lawrence Livermore National Laboratory (LLNL) on 3D printing of SSB materials. They also partner with T. Danner and A. Latz from Deutsches Zentrum für Luft- und Raumfaurt (DLR) on impedance modeling and electro-chemo-mechanical interface models, with P. Zapol from ANL on modeling of interfaces in LLZO, and with D. Fattakhova-Rohlfing from Forschungszentrum Jülich (FZJ) and E. Wachsman from UMD on properties of LLZO with varying densities and microstructures as part of the U. S.–Germany partnership on SSB research.

Milestones

1. Complete atomistic CEI models. (Q1, FY 2022; In progress)
2. Determine composition profiles of CEIs. (Q2, FY 2022)

3. Set up model for local stress mapping. (Q3, FY 2022)
4. Train ML force fields (FF) for disordered interfaces. (Q4, FY 2022; In progress)

Progress Report

Progress for this new project will be reported next quarter.

Patents/Publications/Presentations

The project has no patents, publications, or presentations to report this quarter.

TASK 4 – METALLIC LITHIUM

Team Lead: Jagjit Nanda, Oak Ridge National Laboratory

Summary and Highlights

The use of a metallic lithium anode is required for advanced battery chemistries like Li-ion, Li-air, and Li-S to realize dramatic improvements in energy density, vehicle range, cost requirements, and safety. However, use of metallic lithium with liquid and solid polymer or ceramic electrolytes has so far been limited due to parasitic SEI reactions and dendrite formation that eventually short circuit the battery. Adding excess lithium to compensate for such losses negates the high-energy-density advantage of a Li-metal anode and leads to further concern for battery safety. For a long lifetime and safe anode, it is essential that no lithium capacity is lost either (1) to physical isolation by roughening, dendrites, or delamination processes, or (2) to chemical isolation from side reactions. The key risk, and current limitation, for this technology is the gradual loss of lithium over the cycle life of the battery.

BMR, Battery500, and other DOE programs are addressing this challenge with many innovative and diverse approaches. Key to all is the need for a much deeper analysis of the degradation processes and new strategies to maintain a dense, fully connected lithium and a dendrite-free electrolyte so that materials can be engineered to fulfill the target performance metrics for EV application, namely 1000 cycles and a 15-year lifetime, with adequate pulse power. Projecting the performance required in terms of just the lithium anode, this requires a high rate of lithium deposition and stripping reactions, specifically about 30 µm of lithium per cycle, with pulse rates up to 10 and 20 nm/s (15 mA/cm^2) charge and discharge, respectively, with little or no excess lithium inventory. This is daunting in the total mass and rate of material transport that must be achieved without failures. Researchers are typically working toward cycling of full cells with relevant and balanced capacities for the lithium anode, including developing various pre-lithiation methods for other high-capacity anodes like silicon using measures of CE, interface resistance, and post-cycling observation of the disassembled cell components to assess stability of the Li-metal anode and chosen electrolyte.

Highlight

The highlights for this quarter are as follows:

- The Stanford-SLAC team (Y. Cui) has designed a new solvent-free dry *in situ* prelithiation method in which prelithiation reagents are added directly to the electrode in the assembly step, to prevent the concern of solvent compatibility. Further, there is no need to extract the inserted lithium foil after prelithiation, and thus it prevents cell reassembly and reduces electrolyte waste. They have demonstrated this concept on silicon anode.
- The PNNL Team (W. Xu) has demonstrated that morphology of the separator that is in direct contact with lithium metal plays a dominant role on lithium deposition behavior and, consequently, cycling performance of Li||NMC-622 cells. The polyethylene-polyimide / three-dimensional ordered microporous (3DOM) dual separator-based cells exhibit much longer cycle life compared to the single-layer polyethylene-based cells.

Task 4.1 – Lithium Dendrite Prevention for Lithium Batteries (Wu Xu and Ji-Guang Zhang, Pacific Northwest National Laboratory)

Project Objective. The objective of this project is to enable lithium (Li) metal to be used as an effective anode in Li-metal batteries with good thermal stability and safety. The investigation in FY 2022 will focus on the following aspects: (1) continuing evaluation of separators with high thermal stability in Li-metal batteries, (2) developing 3D-structured, lightweight, flexible current collectors for Li-metal anode and Li-metal batteries, and (3) obtaining mechanistic insight on Li-metal deposition/stripping behavior.

Project Impact. Lithium metal is an ideal anode material for next-generation, high-energy-density, rechargeable batteries. However, the application of Li-metal anode has been hindered by concern for safety and short cycle life. The safety concern regarding Li-metal batteries mainly arises from lithium dendrite growth and electrolyte flammability; the short cycle life is largely associated with the high reactivity of lithium metal with electrolyte and the lithium loss due to formation of SEI and electrochemically inactive or "dead" lithium during cycling. Although much progress has been achieved in suppressing lithium dendrites and increasing lithium CE in LEs in recent years, the intrinsic problems of Li-metal anode still exist. This fiscal year, the PNNL team will continue to evaluate the effectiveness of separators with high thermal stability in improving the thermal stability of Li-metal batteries. Meanwhile, the team will develop 3D porous current collectors for Li-metal anode to suppress lithium dendrite growth, increasing the utilization of lithium metal and consequently extending the cycle life of Li-metal batteries. The success of this project will increase safety and cycle life of lithium batteries and accelerate market acceptance of EVs, as required by the EV Everywhere Grand Challenge.

Approach. The approach will encompass the following areas: (1) continue comparative evaluation of separators with high thermal stability in Li||NMC-622 cells during cycling and heating process, (2) develop current collectors with 3D structure for Li-metal anode to suppress lithium dendrite growth, increase lithium utilization, and extend cycle life of Li-metal batteries, and (3) conduct mechanistic studies on lithium deposition behavior to lay groundwork for future improvement of Li-metal batteries.

Out-Year Goals. The long-term goal of the proposed work is to enable Li-metal and Li-ion batteries with a specific energy of > 350 Wh/kg (in cell level), 1000 deep-discharge cycles, 15-year calendar life, and less than 20% capacity fade over a 10-year span to meet the goal of the EV Everywhere Grand Challenge.

Collaborations. This project collaborates with C. Wang of PNNL on characterization by TEM/SEM; K. Xu and M. Ding of U. S. Army Research Laboratory (ARL) on DSC measurements; and B. Polzin of ANL on coated electrode sampling.

Milestones

1. Evaluate thermal properties of polyimide and polyethylene separators in Li||NMC cells during heating. (Q1, FY 2022; Delayed due to the approval process for operation safety of the accelerating rate calorimetry (ARC) tests.
2. Evaluate cell performance and thermal properties of other separators in Li||NMC cells. (Q2, FY 2022)
3. Fabricate 3D-structured current collectors and characterize their physical properties; elucidate influencing factors on lithium deposition/stripping behavior by *in situ* characterization. (Q3, FY 2022)
4. Evaluate effect of new separator and 3D-structured current collector on cycling performance of Li||NMC cells. (Q4, FY 2022)

Progress Report

Last quarter, the long-term cycling performances of Li||NMC-622 cells using a single-layer polyethylene separator (20-µm thick) and the polyethylene – polyimide / 3DOM dual separator (where the polyethylene is 7-µm thick and the 3DOM polyimide is 11-µm thick) were compared. The polyethylene-polyimide/3DOM dual separator based cells exhibit much longer cycle life compared to the single-layer polyethylene-based cells. To understand whether this improvement originates from the polyimide/3DOM, an electrospun polyimide separator (hereinafter polyimide/electrospun) was fabricated as a reference for polyimide/3DOM. The morphologies of the 20-µm polyethylene, 7-µm polyethylene, polyimide/3DOM, and polyimide/electrospun separators are summarized in Figure 63a-c. It is seen that 3DOM polyimide and electrospun polyimide have significant difference in morphology. Moreover, 20-µm polyethylene has a different morphology than 7-µm polyethylene (used in polyethylene-polyimide dual separators). The 20-µm polyethylene separator exhibits larger pore size and wider distribution of pore size.

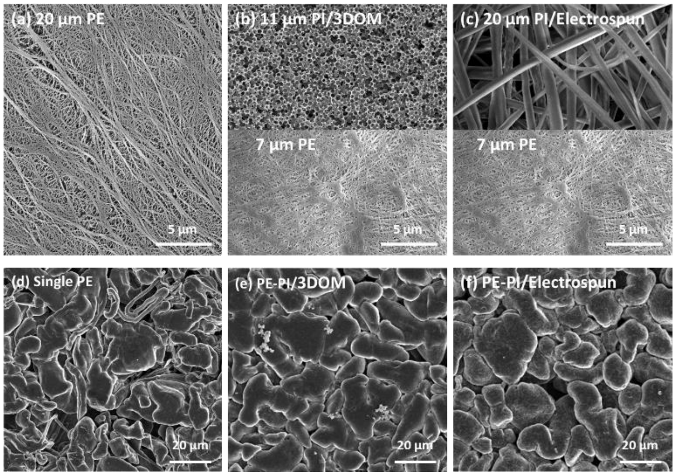

Figure 63. Morphologies of (a) single-layer polyethylene separator (20 µm), (b) 3DOM polyimide and 7 µm polyethylene, and (c) electrospun polyimide and 7 µm polyethylene. (d-f) Morphologies of lithium deposited on copper with separators (a), (b), and (c), respectively, at current density of 0.4 mA cm^{-2} for 10 hours.

When using these separators in Li||Cu cells to check lithium morphologies deposited on copper substrates (in the cells using dual separators, the 7-µm polyethylene is in contact with copper), they lead to different lithium deposits. As shown in Figure 63d, most lithium deposits exhibit a granular morphology with sporadic dendrites when the 20-µm polyethylene is used. However, after using the dual separators with 7-µm polyethylene, dendritic lithium is no longer observed. Lithium deposits exhibit similar morphologies in both dual separator cells, despite the polyimide membranes having significantly different morphologies. It suggests that the morphology of lithium deposited on copper substrate is mainly determined by the separator, which is in direct contact with the copper substrate.

To prove this hypothesis, Li||NMC-622 cells using these separators were built where polyethylene was in direct contact with lithium electrode in all cells. As shown in Figure 64a, after substituting the 3DOM polyimide with electrospun polyimide in the polyethylene-polyimide dual separator, the cycling performance of Li||NMC-622 cells shows almost no difference, even though the two polyimide separators have significantly different morphologies. It indicates that the morphology of the polyimide separator in direct contact with positive electrode has minimal influence over long-term cycling performance. Because the two polyethylene-polyimide dual separators share the same 7-µm polyethylene separator, they exhibit very similar long-term cycling performance. To further prove that the separator in direct contact with lithium is more influential over cycling performance, Li||NMC-622 cells using

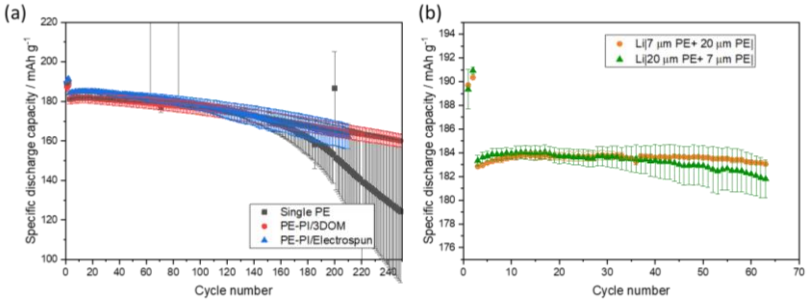

Figure 64. (a) Room-temperature cycling performance of Li||NMC-622 coin cells with three separators shown in Figure 63a-c. (b) Room-temperature cycling performance of Li||NMC-622 coin cells with two dual separators. The cells contained 50-µm thick lithium, 4.2 mAh cm^{-1} NMC-622, 75 µL DME-LHCE (LiFSI:DME:TTE = 1:1.1:3 by mol.), and were cycled between 2.5-4.4 V with C/10 charge and C/5 discharge after three formation cycles at C/10, where 1C = 4.2 mA cm^{-2}.

polyethylene (7 μm) – polyethylene (20 μm) and polyethylene (20 μm) – polyethylene (7 μm) dual separators were built. As shown in Figure 64b, after switching the polyethylene separator that is in direct contact with lithium, the cycling performance of Li||NMC-622 cells is changed. The team infers from all evidence that the morphology of the separator in direct contact with lithium plays a dominate role on lithium deposition behavior and, consequently, cycling performance of Li||NMC-622 cells.

Patents/Publications/Presentations

Publication

- Jia, H., X. Cao, J-G. Zhang, and W. Xu.* "Electrolytes for Lithium-Ion and Lithium Metal Batteries." In *Encyclopedia of Energy Storage*, 1st Edition, edited by L. Cabeza. United Kingdom: Elsevier, 2021. doi: 10.1016/B978-0-12-819723-3.00106-2.

Presentation

- MRS Fall Meetings & Exhibits, Virtual, (December 6, 2021): "Development of PEO-Based Polymer-in-Salt Electrolytes for High-Voltage Lithium Metal Batteries"; H. Wu, P. Gao, H. Jia, J-G. Zhang, and W. Xu.

Task 4.2 – Prelithiation for High-Energy Lithium-Ion Batteries (Yi Cui, Stanford University)

Project Objective. Prelithiation of high-capacity electrode materials is an important means to enable those materials in high-energy batteries. This study pursues three main directions: (1) development of facile and practical methods to increase 1st-cycle CE of anodes, (2) synthesis of fully lithiated anode to pair with high-capacity, Li-free cathode materials, and (3) prelithiation from the cathode side.

Project Impact. Prelithiation of high-capacity electrode materials will enable those materials in the next generation of high-energy-density Li-ion batteries. This project's success will make high-energy-density Li-ion batteries for EVs.

Approach. Silicon electrode film will be prepared by coating the slurry of silicon nanoparticles (NPs), carbon black, and binder mixture on copper foil through a doctor-blading method. The silicon electrode film will be prelithiated by pressing a Li-metal foil on top of it and heating it in an argon glovebox for a certain time. Then, Li_xSi electrode film can be obtained by removing the redundant lithium foil through a peeling-off approach. The redundant lithium foil is reusable for the next prelithiation. The structure, morphology, and other properties can be analyzed by SEM, TEM, XPS, Raman spectroscopy, XRD, etc. In the first year, the team aims to fabricate Li_xSi freestanding electrode film and improve its air stability. In the second year, the team aims to improve the electrochemical stability in full cells.

Out-Year Goals. Materials containing a large quantity of lithium will be synthesized for pre-storing lithium ions inside batteries. Materials and processes will be developed to be compatible with battery electrode and cell fabrication. First-cycle CE of anodes will be improved and optimized by prelithiation materials. Materials for prelithiation from the cathode side will be developed.

Collaborations. This project engages in collaboration with the following: BMR PIs; SLAC: M. Toney *(in situ* X-ray); and Stanford: W. Nix (mechanics).

Milestones

1. Demonstrate a new solvent-free dry prelithiation strategy through *in situ* prelithiation. (Q1, FY 2022; Completed)
2. Demonstrate that the *in situ* prelithiation strategy can delicately control the prelithiation amount. (Q2, FY 2022; In progress)
3. Demonstrate that the *in situ* prelithiation strategy can achieve uniform prelithiation. (Q3, FY 2022)
4. Investigate the prelithiation kinetics in the *in situ* prelithiation strategy. (Q4, FY 2022)

Progress Report

Substantial improvements on energy density of Li-ion batteries require development of high-capacity electrodes. Silicon anodes that have high theoretical capacities (3579 mAh/g)—ten times higher than the conventional graphite anodes (372 mAh/g)—hold great potential for application in high-energy Li-ion batteries. However, silicon anodes exhibit a low initial CE of 50-80%, which means 20-50% of battery capacity will be lost after 1st cycle due to side reactions. Therefore, a strategy to compensate for the initial active lithium loss and improve initial CE is urgently needed to prevent battery capacity degradation.

In previous reports, the team has presented Li-rich compounds for both anode and cathode prelithiation. However, the challenge associated with anode prelithiation is the high reactivity of prelithiation materials, which then have difficulty surviving multiple processing steps during battery electrode fabrication. Here, the team designs a new solvent-free dry method for prelithiation through *in situ* prelithiation. Prelithiation reagents are added to the battery in the assembly step, to prevent the concern of solvent compatibility.

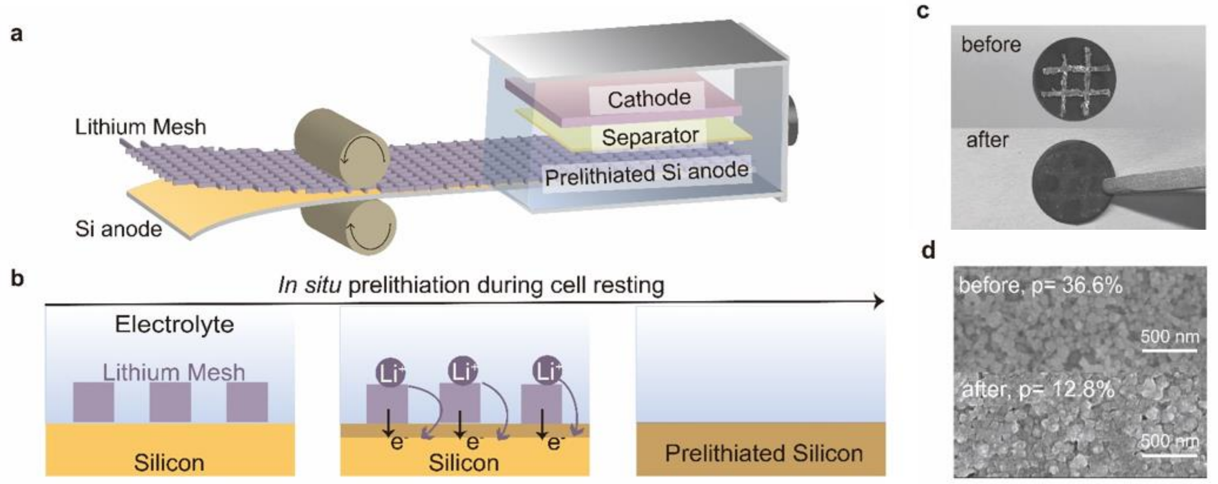

Figure 65. (a) Schematic of *in situ* prelithiation process that applies a layer of lithium mesh on silicon anode in battery fabrication. (b) The mechanism of *in situ* prelithiation reaction based on shorting mechanism. (c) Digital photos of the silicon anode before (upper) and after (bottom) 24-hour *in situ* prelithiation by lithium mesh. (d) Scanning electron microscopy images of the silicon anode before (upper) and after (bottom) 24-hour *in situ* prelithiation by lithium mesh.

The *in situ* prelithiation is achieved by applying a layer of lithium mesh on the silicon anode in battery fabrication (Figure 65a). After assembly, the lithium mesh in direct contact with the silicon anode is surrounded by electrolyte, which creates conditions for shorting reaction between the silicon anode and the lithium mesh. As illustrated in Figure 65b, electrons can transport from the lithium mesh directly to the silicon anode by the Si-Li contact points, while Li^+ ions can flow from lithium to silicon through electrolyte. Considering that batteries congenitally require a resting period after assembly for electrolyte wetting, the team's prelithiation approach utilizes this resting period to achieve *in situ* prelithiation during battery resting. The highlight of *in situ* prelithiation is no need to extract the inserted lithium foil after prelithiation, thus preventing cell reassembly and reducing electrolyte waste. However, this strength also requires insertion of the correct amount of lithium in cell assembly. Commercially available 25-μm thick lithium foils provide 5 mAh cm^{-2} capacity, much beyond the desired prelithiation amount. Therefore, the team uses patterned lithium mesh here to provide the desired prelithiation amount. As shown in Figure 65c, lithium mesh inserted is fully consumed after *in situ* prelithiation, illustrating prelithiation completes after a 24-hour simultaneous resting and prelithiation period. SEM characterizations display that silicon particles expand and sinter into each other after a 24-hour resting period, with the porosity of silicon electrode decreasing from 36.6% to 12.8% (Figure 65d). These phenomena indicate silicon lithium alloying and demonstrate successful prelithiation.

Patents/Publications/Presentations

The project has no patents, publications, or presentations to report this quarter.

TASK 5 – LITHIUM-SULFUR BATTERIES

Team Lead: Prashant Kumta, University of Pittsburgh

Summary

The collected work of the projects in this Task encompasses the following areas:

- Conducting focused fundamental research on the mechanism of "shuttle effect" inhibition for rechargeable Li-S batteries.
- Developing electrode and electrolyte systems that can mitigate the "shuttle effect" so the low self-discharge and long cycle life can be achieved.
- Synthesizing sulfur composite materials with an emphasis on polymer sulfur composite materials.
- Developing creative electrode-making processes to improve processability and aerial capacity; for example, polymeric sulfur composites may not be suitable for the traditional slurry casting process.
- Developing a novel S_xSe_y cathode material for rechargeable lithium batteries with high energy density and long life, as well as low cost and high safety.
- Delivering an electrochemically responsive self-formed hybrid LIC as a protective layer for Li-metal anodes, enabling them to cycle with high efficiency.
- Developing high-energy, low-cost Li-S batteries with long lifespan.

Highlights. The highlights for this quarter are as follows:

- Y. S. Meng's group at UCSD initiated a new project, Task 5.6, focused on developing high energy density (> 500 Wh/kg) and low cost (< 65$/kWh) Li-S pouch cells using the hexaazatrinaphthylene (HATN) polymer-S composite (HATN-S) electrode. They have benchmarked the electrochemical performance of HATN-S as the baseline and new electrolyte systems. They claim that HATN-S enabled porosity reduction from 50.9% to 29.8%, reducing excess electrolyte. Initial results of the cathode seem to indicate higher capacity retention and longer cycle life than S-C electrodes. The system still shows capacity fade within the first 100 cycles. They plan to modify the localized high concentration electrolyte (LHCE) system with introduction of suitable diluents to enhance the transport of polysulfides. They have also conducted detailed TGA to separate loss of sulfur and Li_2S, as well as titration gas chromatography (TGC) to quantify lithium loss, and they claim that sulfur loss is more predominant than lithium in Li-S cells. The team plans to perform a detailed analysis of these losses in this novel system. The results of this work will have a profound impact on development of high-energy-density Li-S cells. Moreover, development of practical and commercially feasible systems portends significant value to the battery community and society at large.
- D. Wang's group at PSU initiated a new project, Task 5.8, focused on developing a new soluble-polysulfide-free sulfur cathode with a high sulfur content (> 50 wt%) and high discharge specific capacity (> 700 mAh/g) based on the weight of the whole cathode, new functional polymer binders enabling Li-ion transport, and trapping of residual lithium polysulfides. The goals are to demonstrate performance of the sulfur electrode at high electrode capacity (> 7 mAh/cm^2), low N/P ratio (< 2), and low electrolyte/sulfur (E/S) ratio (< 2.5 µL/mg). They also plan to fabricate prototype pouch cells of Li-S with predicted energy density of 400 Wh/kg and 80% capacity retention over 300 cycles using conventional electrolyte and Li-metal anodes with a protective layer developed by the team. Use of these new sulfur-composite active materials and functional polymer binders will enable Li-S batteries with high energy density and long cycle life. Meeting these goals will result in increased adoption of EVs and PHEVs, reducing petroleum consumption. Furthermore, successful demonstration of this work will lay the foundation for continued and escalated adoption and growth of Li-ion batteries.

- P. Kumta's group at the University of Pittsburgh, Pennsylvania, initiated a new project, Task 5.7) focused on developing a Li-S pouch cell with cell capacity of > 300 mAh and energy density ≥ 500 Wh/kg, and with cycling stability of over 1000 cycles @ C/3 rate, cycle life of 100 cycles at C/3, and ≤ 20 % fade in energy @ C/10-C/3 rates with a cost of ≤ $80/kWh under lean electrolyte conditions of E/S of 4 μL/mg. The team plans to achieve these goals by identification of effective electrocatalysts and LICs lowering the activation barriers, and by developing new *in situ* synthesis of electrocatalysts and LICs dispersed in the complex carbon-based framework materials (CFM) and sulfur nanocomposite architecture. These novel architectures will enable sulfur contents ≥ 90 wt%, demonstrating areal capacities ~ 15 mAh/cm^2 areal capacity of sulfur electrode with sulfur loading of ≥ 10 mg/cm^2. Together with the novel sulfur architectures, the team plans to develop lithium-containing structurally isomorphous alloys (Li-SIAs) exhibiting area capacities of ~ 15 mAh/cm^2 @ C/3 rates and cycle life ≥ 1000 cycles. Finally, the team also plans to identify new electrolyte additives and develop new optimal electrolyte compositions that will stabilize the cathode and anode interfaces by developing stable SEIs that will prevent polysulfide-related corrosion of the anode while promoting optimal Li-ion conductivities of ~ 10^{-2}S/cm and polysulfide dissolution of < 1ppm. Results of this work, if successful, will have a profound impact on the scientific and technological development of high-energy-density Li-S batteries for EVs and PHEVs and for a plethora of portable and consumer electronic devices.
- The Task 5.1 group led by K. Amine at ANL continued work on microporous carbon with double-end binding (DEB) sites as sulfur host [3D-ordered microporous sulfur host (3D-OMSH)/ZnS, Co-N-C/S cathode] by fabricating pouch cells of high sulfur loading under lean electrolyte conditions. They utilized *in situ* SXRD to reveal reaction mechanisms operational in the 3D-OMSH/ZnS, Co-N-C/S cathode during charge and discharge at C/10 rate. They show the formation of Li_2S during discharge with also formation of Li_2S_2. During charging process, they observe the disappearance of Li_2S, while they did not observe formation/decomposition of crystalline Li_2S_2. Furthermore, they demonstrate with use of UV-visible spectroscopy that Li-polysulfides are trapped effectively by the DEB sites, with the separator color remaining unchanged in contrast to the normal C/S electrode. They also fabricated 80 mm × 60 mm pouch cells with 100 mg sulfur as well as 200 mg sulfur. The 100-mg sulfur loaded pouch cell cycled at 200-mA/g current exhibited a specific capacity of > 800 mAh/g with a capacity retention of 80.32% and CE > 98% for 60 cycles with low E/S of 4 μL/mg. For the 200 mg loaded sulfur pouch cells, the cells demonstrated stable capacity of 175 mAh for 20 cycles, indicating the need for protection of the lithium metal to avoid Li-polysulfide related corrosion of the anode, which is planned for in the team's continued studies. Results of the work show continued promise of the DEB catalytic function of the ZnS, Co-N-C sulfur cathode hosts for achieving high-capacity sulfur electrodes.
- Task 5.2 led by D. Lu and J. Liu's group at PNNL demonstrated a 3D pore-scale electrode model to understand electrolyte propagation in the high loaded and tortuous sulfur electrodes and their combined effect on sulfur reactions. They utilized the 3D flow simulation to provide new insights on optimization of materials and electrode architectures validated by micro-CT and materials analysis. They utilized two particle sizes of sulfur, 20 μm called small particle cathode (SPC) and large particle cathode (LPC) comprising 90 μm to fabricate two electrodes with identical thickness of 120 μm and porosities. They demonstrated that the SPC electrode exhibits more barriers to wetting due to narrow and even closed pores. The LPC electrode, on the other hand, revealed much better wetting with only a small portion of air trapped inside the electrodes to the tune of ~ 3.5%, while the SPC electrode shows 11.1% air fraction at the separator-electrode interface. The multiple flow simulation from the 3D pore-scale electrode model suggests that using large particle stacking layers facilitates wetting of high sulfur loaded electrodes (> 4mg/cm^2) and dense sulfur electrodes with porosity of 45%. They also measured tortuosity of 2.01 and 1.16 for the SPC and LPC, respectively, indicating the lower tortuosity of LPC contributing to better electrolyte wetting inside dense sulfur electrodes, which is vital for improving sulfur utilization rate and yielding enhanced reaction kinetics.

- Task 5.3 led by Y. Cui's group at Stanford reports on the continuing studies on ASSLSBs exploring the reaction mechanism of redox mediators (RMs). They have studied that during charging the oxidized RM, RM_{ox}, chemically oxidizes Li_2S to form Li-polysulfides, while the RM_{ox} is reduced to reduced RMs (RM_{red}). The RM_{red} in turn, is electrochemically oxidized to the initial state of RM_{ox}, giving electrons to the current collector. The RMs shuttle electrons between current collectors and Li_2S, which would have remained inactive. Their electrochemical studies of ASSLSBs indicate two criteria for selection of effective RMs such as solubility in the SPEs and higher potential to Li_2S. They studied three different RMs, and the cyclic voltammograms (CVs) of the RMs versus lithium metal in PEO/LiTFSI SPEs demonstrated that 1,5-bis(2-(2-(2methoxyethoxy)ethoxy)ethoxy) anthra-9,10-quinone (AQT) exhibited very clear oxidation and reduction potentials matching that of Li_2S, while lithium iodide (LiI) and anthraquinone-2-carboxylic acid (AQC) exhibited very weak redox peaks or even absence of any significant peaks in the CV plots. The result therefore confirms that AQT could be a potentially useful RM for oxidizing Li_2S in ASSLSBs using Li_2S cathodes. Results of these studies show the promise for reversibly using Li_2S as a high-energy-density cathode in ASSLSBs.
- Task 5.4 led by E. Hu's group at BNL, in partnership with D. Qu at UWM, conducted studies using a new organosulfur cathode based on their earlier studies using mass spectrometry (MS) coupled with high performance liquid chromatography (HPLC) identifying dissolved polysulfide ions in various electrolytes. Based on their studies, they had identified that short-chain-length polysulfide ions, for example, S_4^{2-} and S_3^{2-}, are much less reactive to lithium than the longer-chain polysulfide ions. They also observed that the sulfur : polymer ratio must be limited to avoid the presence of elemental sulfur to prevent soluble polysulfide formation. Such low sulfur containing organosulfur compounds tend to be soluble in organic LEs, but could be promising in an ASSLSB. They therefore used dipentamethylenethiuram hexasulfide (PMTH) as a representative cathode material in an ASSLSB comprising a 10-electron reaction corresponding to a theoretical capacity of 597 mAh/g. The system shows a discharge capacity of ~ 600 mAh/g at 82 mA/g current at 25°C retaining 80% of its capacity for 250 cycles at $0.12 mA/cm^2$. The system shows a single pair of redox peaks at ~ 1.65 V / 3.1 V, implying direct conversion between the charged and discharged state of the organosulfur, PTMH cathode. They also conducted rate capability studies, with the system demonstrating a reversible capacity of ~ 341 mAh/g at 1.2C rate. Microscopy studies showed that the cathode underwent minimal volumetric variation, and the cathode interface also remained almost unchanged. These studies show the potential of the organosulfur cathode in ASSLSBs.
- Task 5.5 led by G. Liu's group at UCB continued to study use of amphiphilic hydrofluoroethers (HFEs) in electrolytes for Li-S batteries by forging a collaboration with G. Nagy and W. Heller at the Neutron National Science User facility of ORNL. They plan to use small angle neutron scattering (SANS) to estimate scattering lengths and study the micelle structure of the electrolytes. With the estimated calculation of scattering lengths based on the available molecular structures for scattering length density of the different components in the system, they estimate each sample would take ~ 1-2 hours to perform one full scan. They plan to run 4-8 samples for the one-day proof-of-concept experiments, utilizing different ratios of the solvent, 1,1,2,2-tetrafluoroethyl-2,2,3,3-tetrafluoropropyl ether (TTE) with two of the amphiphilic additives [1,1,1,2,2,3,3,4,4-nonafluoro-6-(2-methoxyethoxy)hexane (F_4EO_2) and 1,1,1,2,2,3,3-heptafluoro-4-(2-methoxyethoxy)butane (F_3EO_1)] selected as the most effective additives with the TTE solvent and lithium salt of LiTFSI. The goal is to identify the correct neutron scattering experimental parameters to identify the micelle/cluster formation in the electrolyte due to the presence of the amphiphilic electrolyte additives, with the hope of using neutron scattering techniques to characterize the electrolyte and polysulfide interaction in Li-S batteries. Results of these studies will demonstrate the effectiveness of using neutron scattering to identify the fundamental reaction mechanisms in Li-S batteries.

Task 5.1 – Novel Chemistry: Lithium Selenium and Selenium Sulfur Couple (Khalil Amine, Argonne National Laboratory)

Project Objective. The project objective is to develop novel S_xSe_y cathode materials and advanced LEs for rechargeable lithium batteries with high energy density and long life, as well as low cost and high safety.

Project Impact. Development of a new battery chemistry is promising to support the goal of PHEV and EV applications.

Approach. The dissolution of lithium polysulfides in nonaqueous electrolytes has been the major contribution to the low energy efficiency and short life of Li-S batteries. In addition, insulating characteristics of both end members during charge/discharge (sulfur and Li_2S) limit their rate capacity. To overcome this problem, sulfur or Li_2S is generally impregnated in a carbon-conducting matrix for better electronic conductivity. However, this makes it difficult to increase the loading density of practical electrodes. It is proposed to solve these barriers using the following approaches: (1) partially replace sulfur with selenium, (2) nano-confine the S_xSe_y in a nanoporous conductive matrix, and (3) explore advanced electrolytes with suppressed shuttle effect.

Out-Year Goals. This new cathode will be optimized with the following goals:

- A cell with nominal voltage of 2 V and energy density of 600 Wh/kg.
- A battery capable of operating for 500 cycles with low capacity fade.

Collaborations. This project engages in collaboration with the following: C. Sun and X. Zuo of APS at ANL, Y. Liu of the Center for Nanoscale Materials at ANL, and L. Cheng of the Materials Science Division at ANL.

Milestones

1. Fabrication of single-layer Li-S pouch cell with stable cycle life and *in situ* diagnostics. (Q1, FY 2022; Completed)
2. TOF-SIMS studies on the cycled lithium metal and sulfur cathode. (Q2, FY 2022; In progress)
3. Development of 1 Ah Li-S pouch cell with a cell energy density of > 300 Wh/kg and stable cycle life. (Q3, FY 2022; In progress)
4. Optimization of Li-S pouch cells: cell-level diagnostic, electrolytes, and interlayer optimization. (Q4, FY 2022; In progress)

Progress Report

In FY 2021, the team designed and synthesized a macroporous carbon with DEB sites as sulfur host (3D-OMSH/ZnS, Co-N-C/S cathode) for high-energy Li-S batteries. Excellent electrochemical performance in coin-cell configuration was achieved, and the underlying mechanism was investigated by DFT calculation. In FY 2022, the team will further evaluate electrochemical performance in practical pouch cells under high sulfur loading and lean electrolytes condition.

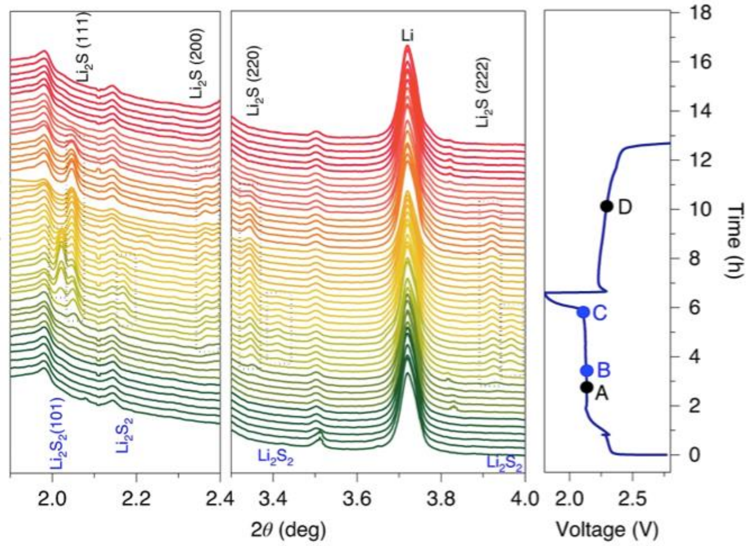

Figure 66. Charge/discharge curve of the 3D-OMSH/ZnS, Co–N–C/S cathode at 0.1 C and the corresponding *in situ* high-energy X-ray diffraction (HEXRD) patterns. Points A/D and B/C indicate the critical voltage point of the appearance/disappearance of Li_2S (marked by the black boxes in HEXRD) and Li_2S_2 (marked by the blue boxes in HEXRD), respectively.

First, the team used *in situ* SXRD to reveal the reaction mechanism of the 3D-OMSH/ZnS, Co-N-C/S cathode during charge/discharge at C/10. As shown in Figure 66, four peaks located at 2.05°, 2.37°, 3.35°, and 3.92° can be assigned to the Li_2S crystalline phase, which started to emerge at the same DOD (Point A, 2.14 V). The peak intensities for the solid Li_2S keep increasing with further lithiation to 1.8 V, suggesting the continuous precipitation of Li_2S during discharge. Moreover, four XRD peaks at ~ 2.02°, 2.18°, 3.40°, and 3.96°, which appeared slightly later (Point B, 2.13 V) than that for Li_2S and then disappeared (Point C, 2.10 V) during further discharge, can be attributed to the solid Li_2S_2 intermediates. This is consistent with the previous observation of Li_2S_2 and resolves the debate on the existence of Li_2S_2 during charge/discharge of Li-S batteries. During the charging process, the peak intensities assigned to Li_2S gradually decrease and completely disappear after charge beyond point D, 2.30 V. In addition, the formation/decomposition of the crystalline Li_2S_2 intermediate that was observed during discharge did not occur during charge, which is due to the fast and efficient conversion of solid Li_2S_2 to liquid LiPSs by the DEB sites.

Furthermore, *in situ* UV-visible (UV-vis) spectroscopy characterization during discharge of the 3D-OMSH/ZnS, Co–N–C/S cathode directly confirmed no migration of LiPS species on the lithium anode side, indicating no LiPS shuttling or lithium metal corrosion. As shown in Figure 67a, during the discharge of the cell with KB/S cathode at 0.1 C (discharge curve is shown on right), the team identified a very sharp peak located at the wavelength of 535 nm after being discharged to 1.8 V, suggesting a large amount of diffusion of Li_2S_6 to the anode side. Moreover, other polysulfide species S_8^{2-}, S_4^{2-}, and S_2^{2-} located at the wavelengths of 570 nm, 510 nm, and 450 nm, respectively, were also identified, indicating a severe shuttle effect in the KB/S cathode. The digital photograph of the test cell (inset of Figure 67a) shows a clear color change of the separator to dark brown, further revealing the polysulfides to prevent their diffusion to the lithium anode side. The digital photograph of the cell after being discharged to 1.8 V (inset of Figure 67b) shows that the color of the separator remained unchanged, confirming the capability of relieving the shuttle effect by the 3D-OMSH/ZnS, Co-N-C host material.

Given the excellent coin-cell performance of the 3D-OMSH/ZnS, Co–N–C/S cathode, the team further fabricated a pouch cell with 100-mg sulfur loading in a single-piece cathode of this material with dimensions of 80 mm × 60 mm. To assemble the 100-mg sulfur loading pouch cell, they added 135 mg 3D_OMSH/ ZnS,Co-N-C/S (or 3D-OMSH/ZnS), 17 mg Ketjenblack, and 17 mg PVDF binder to a suitable amount of of N-methyl-2-pyrrolidone (NMP). The resulting slurry was casted on the surface of aluminum foil. The aluminum foil was cut to be 60 mm × 80 mm. After baking on a hot plate for 3 hours, the cathode was transferred into a 60°C vacuum oven overnight. The aluminum tab was riveted on the as-prepared cathode, and a nickel tab was riveted on the Cu-foil current collector. After that, lithium foil (60 mm × 80 mm) with a thickness of 0.1 mm was placed on the copper foil. Then, the team stacked a layer of electrolyte-soaked Celgard 2400 on the surface of the lithium foil, followed by the cathode on top of the Celgard 2400 separator, and injected 0.4 mL electrolyte (E/S = 4 μL/mg) into the stack. Then, the package was sealed under vacuum.

To assemble the 200-mg sulfur loaded pouch cell, two pieces of lithium foil (60 mm × 80 mm, 0.1-mm thickness) were placed on both sides of the copper foil, and two pieces of as-prepared 100-mg sulfur loading cathode were applied in the 200-mg sulfur loaded pouch cell. All other assembling processes were the same as the case of the 100-mg sulfur loaded pouch cell. The E/S ratios in all 200-mg sulfur loading pouch cells were controlled to be 10 μL/mg).

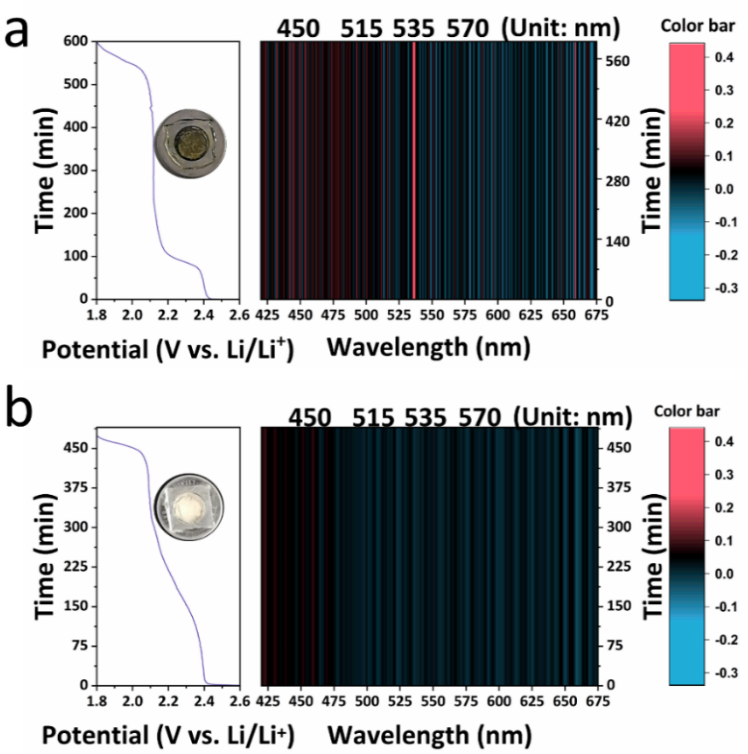

Figure 67. *In situ* UV-visible spectroscopy observations and corresponding discharge curves of (a) KB/S and (b) 3D-OMSH/ZnS, Co-N-C/S cathodes at 0.1 C. Inset of (a): digital photograph of *in situ* cell of KB/S cathode after testing; inset of (b): digital photograph of *in situ* cell of 3D-OMSH/ZnS, Co-N-C/S cathode after testing. Color bars indicate the derivative of reflectance, with pink corresponding to a positive number and blue corresponding to a negative number.

As shown in Figure 68, the as-prepared 100-mg-level pouch cell was cycled at a current density of 200 mA g^{-1}. The cell exhibited a specific capacity of > 800 mA h g^{-1} with a capacity retention rate of 80.32% and high CE of > 98% for 60 cycles, even with a relatively low ratio of E/S = 4 μL/mg (Figure 68a). Note that in earlier studies, the intrinsic high reactivity of lithium metal with conventional ether-based electrolyte was responsible for the fluctuation of CE. However, the shuttle effect of the LiPS and the associated lithium metal corrosion, which have been often ignored in coin-cell tests with thick lithium electrodes, could also result in rapid cell degradation of pouch cells with limited lithium. Pouch cells with 200-mg sulfur using different host materials were thus fabricated and tested for comparison. As shown in Figure 68b, the Li–3D-OMSH/ZnS, Co–N–C/S pouch cell still demonstrates stable cycle life and CE close to 100% within 20 cycles. By contrast, the Li-3D-OMSH/ZnS/S pouch cell even with minor LiPS shuttle effect exhibits continuous capacity fading and lower CE in pouch cells despite its stable cycle life in coin cells.

These results show that lithium metal protection is necessary to enable long cycle life of Li-S pouch cells. Meanwhile, reducing E/S ratio and increasing areal sulfur loading are necessary to further increase the practical cell energy density. The team will continuously optimize the energy density and cycle of Li-S pouch cells and report on it in coming quarters.

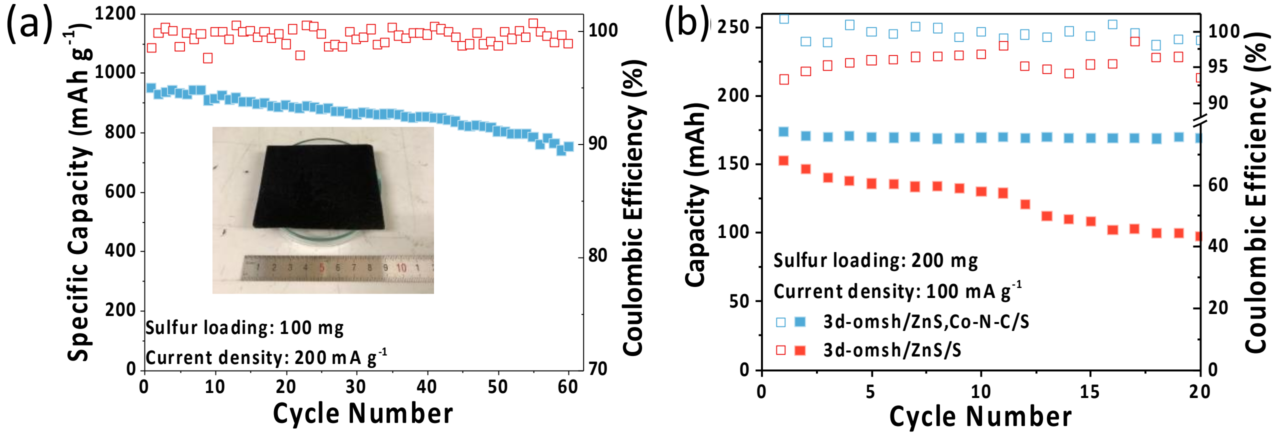

Figure 68. (a) Capacity retention of 100-mg-sulfur pouch cell using 3D-OMSH/ZnS, Co–N–C/S cathode with an E/S ratio of 4 μl/mg. Inset: digital photo of the as-prepared 6 cm × 8 cm cathode. (b) Cycling performance of 200-mg-sulfur pouch cells using 3D-OMSH/ZnS/S and 3D-OMSH/ZnS, Co–N–C/S cathodes with an E/S ratio of 10 μl/mg.

Patents/Publications/Presentations

The project has no patents, publications, or presentations to report this quarter.

Task 5.2 – Development of High-Energy Lithium-Sulfur Batteries (Dongping Lu and Jun Liu, Pacific Northwest National Laboratory)

Project Objective. The project objective is to develop high-energy, low-cost Li-S batteries with long lifespan. All proposed work will employ thick sulfur cathode (≥ 4 mg/cm^2 of sulfur) at a relevant scale for practical applications. The diffusion process of soluble polysulfide out of thick cathode will be revisited to investigate cell failure mechanism at different cycling. The fundamental reaction mechanism of polysulfide under the electrical field will be explored by applying advanced characterization techniques to accelerate development of Li-S battery technology.

Project Impact. The theoretical specific energy of Li-S batteries is ~ 2300 Wh/kg, which is almost three times higher than that of state-of-the-art Li-ion batteries. The proposed work will design novel approaches to enable Li-S battery technology and accelerate market acceptance of long-range EVs required by the EV Everywhere Grand Challenge.

Approach. The project proposes the following approach: (1) to identify and address key issues of applying high-energy sulfur cathodes including materials, binders, electrode architectures, and functional electrode additives, (2) to advance the mechanism study of sulfur cathode and electrolyte by using *in situ* / *ex situ* techniques and custom-designed hybrid cell setup, and (3) to verify effectiveness of the new approaches with coin/pouch cells by using high-loading electrodes (> 4 mg/cm^2), limited lithium (< 200% lithium excess), and lean electrolyte (E/S < 4 µL/mg).

Out-Year Goals. This project has the following out-year goals:

- Fabricate Li-S pouch cells with thick electrodes to understand sulfur chemistry/electrochemistry in environments similar to those witnessed in real application.
- Leverage the Li-metal protection project funded by the DOE and PNNL advanced characterization facilities to accelerate development of Li-S battery technology.
- Develop Li-S batteries with a specific energy of 400 Wh/kg at cell level, 1000 deep-discharge cycles, improved abuse tolerance, and less than 20% capacity fade over a 10-year period to accelerate commercialization of EVs.

Collaborations. This project engages in collaboration with the following: X-Q. Yang (BNL), M. Cai (GM), J. Bao (PNNL), P. Khalifah (BNL), and Z. Liu (Thermo Fisher Scientific).

Milestones

1. Build 3D electrode models to understand electrolyte transport and sulfur reactions in high-loading and low-porosity sulfur electrodes. (Q1, FY 2022; Completed)
2. Optimize S/C material and electrode architecture to realize sulfur utilization > 1100 mAh/g in high loading electrode (> 4 mg S/cm^2) with sulfur content > 70% and porosity < 35%. (Q2, FY 2022; In progress)
3. Study impacts of electrode architecture and topography on sulfur utilization rate and cell cycling. (Q3, FY 2022)
4. Process high-loading (> 4 mg/cm^2) and dense (< 35% porosity) sulfur electrodes at a relevant scale for pouch-cell fabrication. (Q4, FY 2022)

Progress Report

This quarter, a 3D pore-scale electrode model was built to understand electrolyte propagation in the high-loaded and tortuous sulfur electrodes and its effect on sulfur reactions. The 3D flow simulation provides new insights on the optimization of materials and electrode architectures, which was validated by micro-CT and materials analysis. In the pore-scale model, the electrode and electrolyte infiltration were simulated using the discrete element method and multiple flow simulation, respectively. To investigate the effects of particle size on electrolyte wettability, SPC (particle size of 20 µm) and LPC (particle size of 90 µm) models were generated with the same electrode porosity (Figure 69a/e). Both the electrodes have a thickness of 120 µm to mimic the thick electrode; the SPC has 6-8 layers of particles (Figure 69a), whereas the LPC has 1-2 layers of particles (Figure 69e). At the initial wetting stage, driven by gravity and surface tension, the added electrolyte will flow through the voids and diffuse into the electrode pores, pushing the air outside the electrode. After reaching steady state, air is still observed occupying a portion of the pore channels due to non-uniform electrolyte flow and surface tension, which is dictated by material/electrode properties. While the SPC electrode has more challenges in wetting due to narrow and even closed pores, the LPC, in contrast, reveals a much better wetting with only a small portion of the air trapped inside the electrode. Accordingly, the nonuniform wetting effect of SPC and LPC was quantified. The electrode volume (ϵ_d) is set at a constant value of 0.55, which consists of loaded S (ϵ_s) and the carbon materials volume (ϵ_c). The volume fraction of the electrolyte and air was calculated by the cross-section average distribution profile along the thickness direction from the 3D pore-scale model. As shown in Figure 69f, for LPC, at the separator-electrode interface (x = 25 µm), the electrode is fully wetted without trapped air. Starting from x = 50 µm, the air volume begins to increase slightly and reaches the maximum volume fraction of 8.2% at x = 85 µm (bottom of electrode). The average air fraction inside the LPC is only 3.5%, revealing the electrolyte can access most of the pores. In contrast, the SPC electrode has 11.1% air fraction at the separator-electrode interface. The air volume increases along the electrode thickness direction and reaches a plateau around 23% at x > 60 µm. The average air fraction in SPC is nearly 50% (Figure 69b). The multiple flow simulation from the 3D pore-scale electrode model suggests that using large particles to reduce particle stacking layers is helpful in facilitating the wetting of high-loading electrodes. Experimentally, carbon particles of different sizes were synthesized to fabricate high-loading (> 4 mg/cm^2) and dense sulfur electrodes (porosity 45%). The structures of SPC and LPC were studied using X-ray micro-CT. Three phases—S/C particles, binder/carbon additives, and voids—were separated and colored yellow, grey, and blue, respectively (Figure 69c/g). Consistent with the simulation results, small particles tend to form a compact layer in SPC and generate horizontally aligned pores along the plane direction (Figure 69c, top and cross-sectional view), blocking electrolyte infiltration. The micro-CT results of the LPC indicate that large particles form a

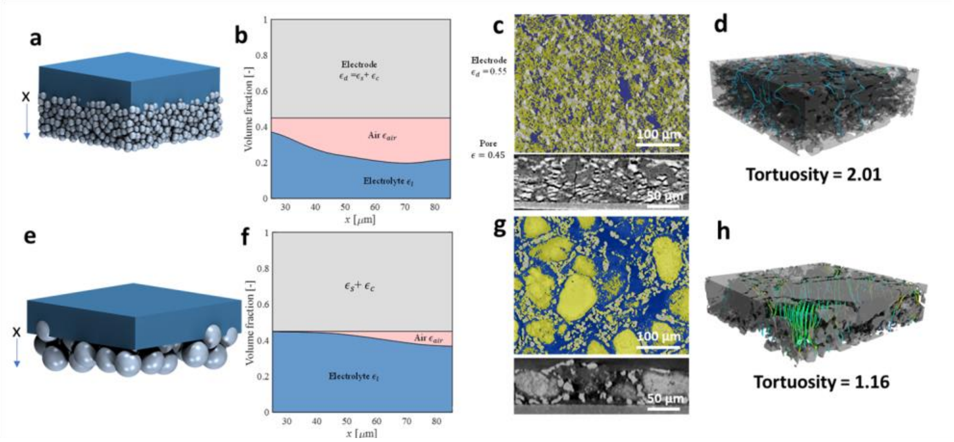

Figure 69. 3D pore-scale models for (a) small particle cathode (SPC) and (e) large particle cathode (LPC). The electrolyte and air distribution along the electrode depth x for (b) SPC and (f) LPC. Top and cross-sectional view of micro-computed tomography images of (c) SPC and (g) LPC. Tortuosity and flow path of (d) SPC and (h) LPC.

single-particle-layer electrode with through-pores formed perpendicularly across the electrode (Figure 69g). The measured electrode tortuosity of SPC and LPC are 2.01 and 1.16, respectively, along the perpendicular direction. The lower tortuosity indicates better electrolyte wetting inside the dense electrodes, which is critical to improving sulfur utilization rate and reaction kinetics.

Patents/Publications/Presentations

The project has no patents, publications, or presentations to report this quarter.

Task 5.3 – Nanostructured Design of Sulfur Cathodes for High-Energy Lithium-Sulfur Batteries (Yi Cui, Stanford University)

Project Objective. The charge capacity limitations of conventional TM oxide cathodes are overcome by designing optimized nano-architectured sulfur cathodes. This study aims to enable sulfur cathodes with high capacity and long cycle life by developing sulfur cathodes from the perspective of nanostructured materials design, which will be used to combine with Li-metal anodes to generate high-energy Li-S batteries. Novel sulfur nanostructures as well as multi-functional coatings will be designed and fabricated to overcome issues related to volume expansion, polysulfide dissolution, and the insulating nature of sulfur.

Project Impact. The capacity and cycling stability of sulfur cathode will be dramatically increased. This project's success will make Li-S batteries to power EVs and decrease the high cost of batteries.

Approach. The approach involves three main efforts:

- Advanced nanostructured sulfur cathodes design and synthesis, including (1) engineer empty space into sulfur cathode to solve the problem of electrode volume expansion, (2) develop novel sulfur nanostructures with multi-functional coatings for confinement of S/Li polysulfides to address issues of active materials loss and low conductivity, (3) develop/discover optimal nanostructured materials that can capture the polysulfide dissolved in the electrolyte, (4) develop space-efficiently-packed nanostructured sulfur cathode to increase volumetric energy density and rate capability, and (5) identify interaction mechanism between sulfur species and different types of oxides/sulfides, and find optimal material to improve capacity and cycling of sulfur cathode.
- Structure and property characterization, including *ex situ* SEM, XPS analysis, and *in operando* XRD and optical microscopy.
- Electrochemical testing including coin cells and pouch cells as well as a set of electrochemical techniques.

Out-Year Goals. The cycle life, capacity retention, and capacity loading of sulfur cathodes will be greatly improved (200 cycles with 80% capacity retention, > 0.3 mAh/cm^2 capacity loading) by optimizing material design, synthesis, and electrode assembly.

Collaborations. This project collaborates with the following: BMR PIs; SLAC: M. Toney *(in situ* X-ray); and Stanford: W. Nix (mechanics) and Z. Bao (materials).

Milestones

1. Designing redox mediators to facilitate Li_2S activation for ASSLSBs. (Q1, FY 2022; Completed)
2. Understanding redox chemistry in ASSLSBs using *operando* XAS measurements. (Q2, FY 2022; In progress)
3. Demonstrating cycling performance of ASSLSBs with designed RMs. (Q3, FY 2022; In progress)
4. Enabling ASSLSBs with high area capacity and high energy density. (Q4, FY 2022; In progress)

Progress Report

The reaction mechanism of redox mediators (RMs) in ASSLSBs is shown in Figure 70a, which is considered as a two-step process involving electrochemical and chemical reactions. During charging, oxidized RMs (RM_{ox}) chemically oxidize Li_2S to lithium polysulfides, while RM_{ox} is reduced to reduced RMs (RM_{red}) (step A, chemical reaction). RM_{red} in turn is electrochemically oxidized to the initial state of RM_{ox} by giving electrons to current collectors (step B). RMs shuttle electrons between the current collectors and isolated Li_2S, which would have otherwise remained inactive. The charging voltage of the cell is determined by the electrochemical step (step B). Therefore, the team proposes that reduced charge polarization and improved sulfur utilization for ASSLSBs can be realized by choosing an appropriate RM, as shown in Figure 70b. Two criteria are paramount for effective RMs: (1) they should be soluble in SPEs, and (2) they should have a redox potential slightly higher than that of Li_2S. The team selected three typical RMs originally developed in liquid electrolytes (LEs) to examine their electrochemical properties in SPEs, including 1,5-bis(2-(2-(2methoxyethoxy)ethoxy)ethoxy) anthra-9,10-quinone (AQT), anthraquinone-2-carboxylic acid (AQC), and LiI. RMs are first mixed with PEO/LiTFSI electrolytes in acetonitrile solution, and then drop casted on the carbon paper as the electrodes. Figure 70c-e shows CV curves of the RM electrodes versus lithium metal in PEO/LiTFSI SPEs. Compared with LiI and AQC, AQT showed the most favorable redox potentials, matching that of Li_2S oxidation and best redox reversibility.

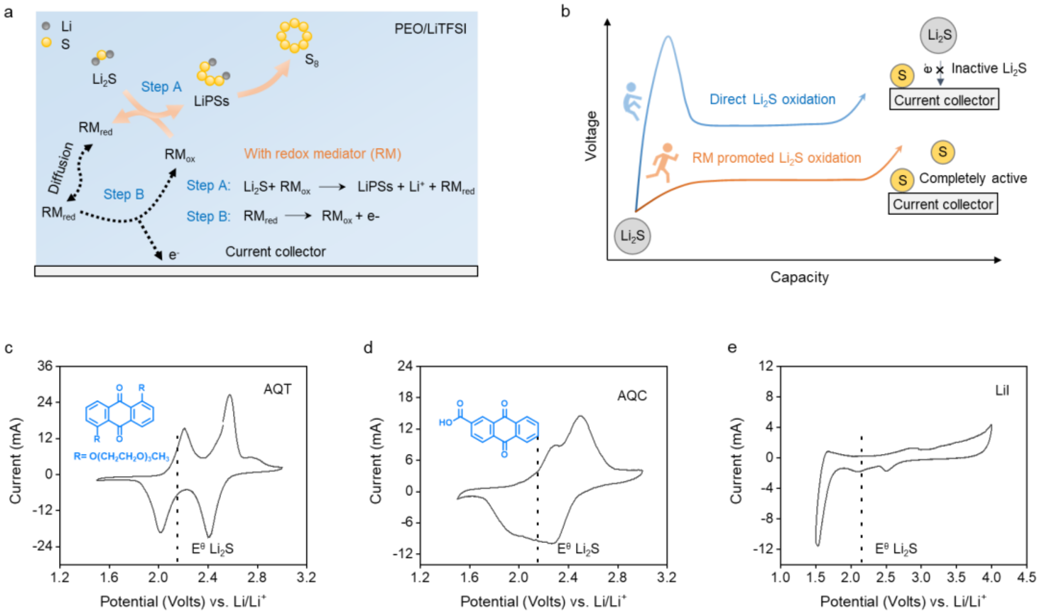

Figure 70. Designing redox mediators (RMs) for all-solid-state lithium-sulfur batteries (ASSLSBs). (a) Proposed reaction scheme of the RMs for ASSLSBs. Effective RMs solubilized in the solid polymer electrolyte (SPE) shuttle electrons between current collectors and the surfaces of isolated Li_2S particles. During the charging process, RM_{ox} chemically oxidizes Li_2S to polysulfides, while RM_{ox} is reduced to RM_{red} (step A, chemical reaction). RM_{red} diffuses toward the current collector and is oxidized to the initial state of RM_{ox} near the current collector surface (step B, electrochemical reaction). The light blue color indicates the SPEs. (b) Schematic 1st charge profiles of ASSLSBs with (orange line) and without (blue line) RM. A high charging voltage (~ 4 V versus Li^+/Li) is necessary to activate Li_2S in the 1st charge process. Li_2S is directly converted to elemental sulfur through a two-phase transformation. Grey: Li_2S particles; and yellow: sulfur. (c-e) Cyclic voltammogram curves and chemical structure of (c) AQT, (d) AQC, and (e) LiI in PEO/LiTFSI SPEs at a scan rate of 0.1 mV s^{-1}. The dotted line is the equilibrium potential of Li_2S (~ 2.15 V versus Li^+/Li).

Patents/Publications/Presentations

The project has no patents, publications, or presentations to report this quarter.

Task 5.4 –Investigation of Sulfur Reaction Mechanisms
(Enyuan Hu, Brookhaven National Laboratory; Deyang Qu, University of Wisconsin, Milwaukee)

Project Objective. The primary objectives are as follows:

- To optimize and down select polymeric sulfur electrode. The team will focus on the overall dissolution of polysulfide in an electrolyte and effectiveness of polymeric sulfur electrodes.
- To develop small organosulfur materials for all SE Li-S batteries.
- To continue developing alternative anode materials having low reactivity with dissolved polysulfide ions.
- To continue investigating the interaction of polysulfides in the cathode solid phase.

Project Impact. The results of this project will be used for development of technologies that will significantly increase energy density and cycle life and will reduce the cost of beyond Li-ion battery systems. This will greatly accelerate deployment of EVs and reduce carbon emission associated with fossil fuel consumption and help in the direction of building the U. S.-based energy storage manufacture chains.

Approach. The team will first down select the cross-linked polymerized sulfur compounds, in which sulfur are attached to the conductive backbone with covalent bonds; therefore, the polysulfides can be immobilized within the matrix. They will also explore the small organosulfur molecules in ASSLSBs. They will continue exploring alternative anode materials that can cycle well and do not react with dissolved polysulfide and sulfur in the electrolyte to mitigate the “shuttle effect.” In addition, they will continue to engage in fundamental *in situ* electrochemical investigations of the sulfur redox mechanisms to guide material and engineering designs. They will also continue optimizing alternative electrode fabrication processes.

One-Year Goals. The interim goal is to develop a Li-S battery with S-containing cathode of 600-800 mAh/g capacity with mitigation of the “shuttle effect.”

Collaborations. The PI works closely with beamline scientists at synchrotron facilities to develop novel Li-S characterization tools. The PI and co-PI collaborate closely with top scientists at ANL, LBNL, and PNNL, as well as U. S. industrial collaborators at GM, Duracell, Clarios, etc. The PI and co-PI also collaborate with scientists in China, Japan, and South Korea. These collaborations will be strengthened and expanded to give this project a vision on both today’s state-of-the-art technology and tomorrow’s technology in development, with feedback from the material designer and synthesizers upstream and from industrial end users downstream.

Milestones

1. Selection of small organosulfur compounds and complete design of all-solid-state testing. (Q1, FY 2022; Completed)
2. Complete initial testing of prelithiated tin anode. Complete initial testing of small organo-sulfur molecules in ASSLSB. (Q2, FY 2022; In progress)
3. Complete testing of full Li-S cell with alternative prelithiated anode. Complete synthesis of potential polymeric sulfur materials. (Q3, FY 2022; In progress)
4. Complete testing full cell with selected polymeric sulfur, small organosulfur cathodes, and alternative anode. (Q4, FY 2022; In progress)
5. Complete the investigations of sulfur redox reaction mechanism in the solid phase in cathode and the interplay between dissolved polysulfide ions in electrolyte and sulfide compounds in the solid. Complete and continue testing of polymeric sulfur cathode, small organosulfur cathode, and alternative anode in full cell format. (Annual Milestone; In progress)

Progress Report

In the past few years, the team has successfully developed a mass spectrometry – high-performance liquid chromatography (MS-HPLC) technique for the quantitative and qualitative identification of dissolved polysulfide ions in various electrolytes. Coupled with an *in situ* electrochemical method, the changes in the dissolved polysulfides during the battery operation can be determined. The mechanisms for the sulfur redox reaction, which includes the equilibrium between dissolved polysulfide ions and elemental sulfur, were revealed. As a result, the continuous decay of capacity during cycling, the "shuttle-effect," and the high self-discharge during storage were better understood. With the *in situ* analytical method, the team also revealed that the short-chain-length polysulfide ions, for example, S_4^{2-} and S_3^{2-}, are much less reactive with lithium than the longer-chain polysulfide ions. To mitigate the problem caused by the soluble long-chain polysulfides in a Li-S battery, sulfur/organic polymer materials were synthesized as alternative cathode materials instead of elemental sulfur (S_8). The team has exhausted many sulfur / organic polymer materials last year. However, the sulfur-to-polymer ratio must be limited to a certain value to avoid the existence of elemental sulfur, for example, 4:1 S_8:PAN ratio. In addition, a substantially low discharge voltage was also observed. To mitigate the problem, this quarter, they tried to explore small organo-sulfur compounds. Such organo-sulfur compounds are highly soluble in LE; thus, they have attracted little attention as Li-S cathode. But if used in an all-solid-state lithium cell, the small organo-sulfur compound demonstrated high reversibility, high capacity, and potential to operate at room temperature.

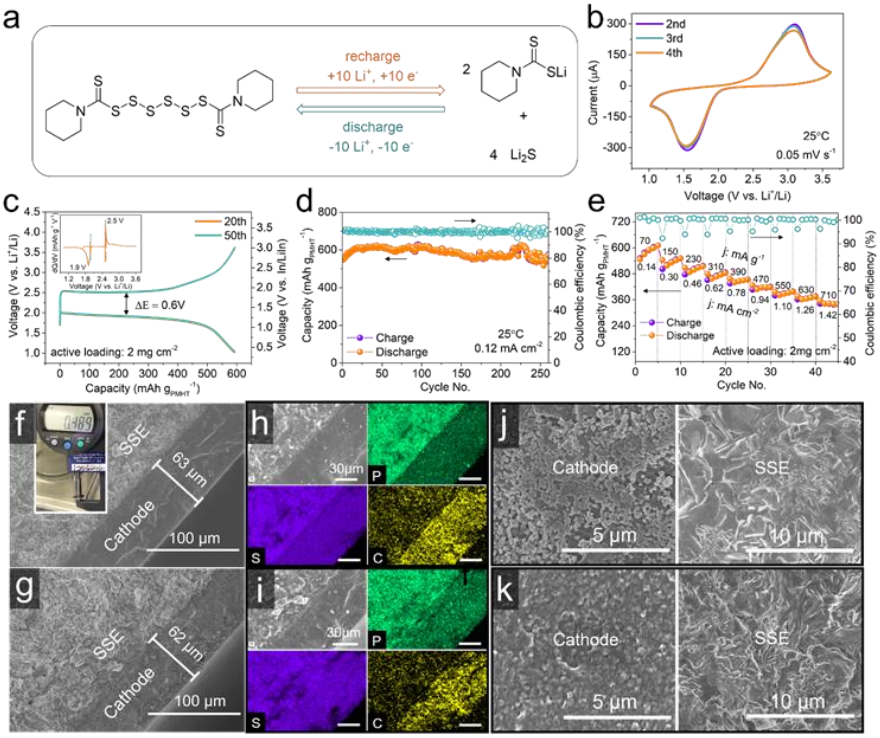

Figure 71. (a) Conversion reaction mechanism of PMTH molecule. (b) Cyclic voltammetry profiles at 0.05 mV s^{-1}. (c) Galvanostatic voltage profiles and corresponding dQ/dV curves. (d) Cycling performance at 0.1 C and (e) rate performance at 25°C. Cross-sectional scanning electron microscopy (SEM) images of the cathode-SSE pellet (f) before (inset is the thickness measurement) and (g) after cycling. Energy dispersive spectroscopy mapping of cathode|SSE interface (h) before and (i) after cycling. Top-view SEM images of cathode and SSE surface (j) before and (k) after cycling.

Dipentamethylenethiuram hexasulfide (PMTH) was selected as a representative cathode material. A discharge capacity of ~ 600 mAh g^{-1} was obtained under 82 mA g^{-1} at 25°C. The cell retained 80% of its capacity for 250 cycles at 0.12 mA cm^{-2}. On cycling, an electrochemically reversible CEI was revealed. The redox chemistry of PMTH cathode involves ten-electron transfer (Figure 71a), corresponding to a theoretical capacity of 597 mAh g^{-1}. CV profiles in Figure 71b display only one pair of redox peaks occurring at ~ 1.65 V / 3.1 V, implying a direct conversion between the charged state (PMTH) and the discharged state (Li_2S + $NC_6S_2H_{10}Li$), which is different from the multi-staged redox mechanism in LEs. Figure 71c shows galvanostatic charge-discharge voltage profiles at the 20th and 50th cycles. An attainable capacity of ~ 595 mAh g^{-1} at 82 mA g^{-1} was demonstrated, corresponding to a nearly full material utilization. The inset dQ/dV curves display a pair of highly reversible redox. Figure 71e displays the rate performance from 0.12C (70 mA g^{-1}, 0.14 mA cm^{-2}) to 1.2C (710 mA g^{-1}, 1.42 mA cm^{-2}). A reversible capacity of ~ 341 mAh g^{-1} was delivered at 1.2C, corresponding to 57% of the capacity at 0.12C. The thickness of the cathode and the SSE is ~ 63 µm and ~ 420 µm before cycling (Figure 71f). After cycling, cathode thickness remains almost unchanged (Figure 71g). EDS mappings in Figure 71h-i display that the cathode interface remains in intimate contact except for becoming less distinguishable after cycling. Top-view SEM images in Figure 71j-k exhibit almost no crack formation for both the cathode and the SSE layer throughout cycling, indicating a moderate volumetric variation during repetitive conversion process.

Patents/Publications/Presentations

The project has no patents, publications, or presentations to report this quarter.

Task 5.5 – New Electrolytes for Lithium-Sulfur Battery (Gao Liu, Lawrence Berkeley National Laboratory)

Project Objective. The project objective is to develop new electrolytes, additives, and electrode compositions for Li-S battery with high ion-conductivity, stable toward polysulfide, and promoting the polysulfide affiliation with the electrode substrate to prevent polysulfide dissolution.

Project Impact. This work will address the high cost and low energy density of Li-ion rechargeable batteries. The emerging Li-S batteries could feature both high energy density and low cost. This project enables applications of the low-cost, abundant sulfur element as a major chemical component for electrical energy storage. This project will develop new approaches for electrolytes and electrode compositions of Li-S rechargeable batteries.

Approach. This project aims to develop new electrolytes and additives for Li-S battery. The properties of the ideal electrolyte for sulfur electrode would be high ion conductivity, stable toward polysulfide, and promoting the polysulfide affiliation with the electrode substrate to prevent polysulfide dissolution. The project is designed to first understand the electrode substrate interaction with the polysulfides in different electrolytes. This will lead to better understandings of the polysulfide nucleation and precipitation mechanisms in common electrolytes. The second stage of the project will focus on chemically modifying the structures of the solvent and salt electrolyte molecules to increase electrolyte stability and ionic conductivity, to prevent polysulfide dissolution, and to promote polysulfide precipitation.

Out-Year Goals. The team will also investigate the contribution of Li-metal electrodes to overall Li-S battery performance and will develop methods to stabilize Li-metal surface.

Collaborations. This project collaborates with J. Guo and C. Zhu (ALS/LBNL), A. Minor (National Center for Electron Microscopy (NCEM) at LBNL/UCB), G. Nagy and W. Heller (Neutron National Science User Facility/ORNL), and P. B. Balbuena, Texas A&M University.

Milestones

1. Synthesize and formulate amphiphilic electrolytes using combination solvents, salts, and ILs. (Q1, FY 2022; Completed)
2. Optimize sulfur positive electrode to balance ionic and electronic conductivity, as well as dissolution and precipitation properties. (Q2, FY 2022; In progress)
3. Implement at least one strategy to stabilize Li-metal anode electrode. (Q3, FY 2022; In progress)
4. Combine the electrolyte, sulfur electrode, and lithium metal stabilization strategies to achieve stable cell cycling. (Q4, FY 2022)

Progress Report

Two amphiphilic additives, F_3EO_1 and F_4EO_2, were identified as the most effective additives in combination with TTE and lithium salts to form the amphiphilic electrolytes for Li-S batteries. The two amphiphilic additives were synthesized and purified in 10-mL scale to be used for Li-S battery research.

The team also successfully forged a collaboration with G. Nagy and W. Heller at the Neutron National Science User Facility at ORNL this quarter. They have developed a successful one-day proof-of-concept proposal to use neutron scattering techniques to characterize the structure features of this unique amphiphilic electrolyte system. SANS is often used for micelles-related studies. There should be reasonable contrast between (Li,H) and (C,F,N,O,S) atom groups. The scattering lengths of lithium and hydrogen are negative at natural isotopic abundance, while the other elements are all positive. The negative scattering lengths are a unique feature of neutrons and can be explored for much improved scattering results to understand the micelle structure detection and characterization. Working with neutron beamline scientists, they determined the Extended Q-range SANS Diffractometer (EQ-SANS, beamline 6, Spallation Neutron Source) is a proper equipment setup to conduct proof-of-principle experiments. Furthermore, an initial assessment was made based on the available molecular structures for the scattering length density (SLD) of the different components in the system. To initially assess possible contrasts, the calculation used officially reported numbers and reasonable assumptions (that is, $C_5H_4F_8O$ density is 1.53 g/cm^3 and SLD is 2.752; outer layer of micelle is C_8F_{17} and density of C_8F_{18} is 1.77 g/cm^3) to get SLD of 3.798. The inner micelle core is $C_9O_4H_{19}$, and the density of polyethylene glycol (PEG) is 1.125 g/cm^3 to get SLD of 0.424. The salt structure is $LiC_2F_6NO_4S_2$ with density of 1.33 g/cm^3 to obtain SLD of 2.332. Depending on the ratio of the last two components, the innermost layer SLD will be between c.a. 0.5 and 2. Therefore, the estimated hours to perform one full scan for one sample would be 1-2 hours. Therefore, 4-8 samples are planned for the one-day proof-of-concept experiments, as in Table 7. The samples will be formulated and prepared in January 2022 and are due to be shipped in February 2022. The experiments will be conducted by the beamline scientist of ORNL in March 2022, with detailed experimental conditions provided by LBNL. The purpose of the proof-of-concept experiments is to identify the correct neutron scattering experiment parameters based on the baseline Sample 3 identified by the team, and to use the conditions to test a few relevant samples to identify the micelle/cluster formation in the electrolyte due to the presence of the amphiphilic electrolyte additives of F_3EO_1 and F_4EO_2. Results will be used to develop a comprehensive user proposal to use neutron scattering techniques to characterize the electrolyte and polysulfides interaction in the Li-S chemistry.

Table 7. Eight samples: Samples 1-4 are first priority, and Samples 5-8 are addressed as time permits. Sample 3 is suggested as an initial test sample to determine the experimental conductions.

Sample No.	Sample Descriptions	Sample No.	Sample Descriptions
1	Neat F_4EO_2	5	F_4EO_2:TTE = 1:5
2	F_4EO_2:TTE = 1:1 (v/v)	6	F_4EO_2:TTE = 1:5 0.5M LiTFSI
3	F_4EO_2:TTE = 1:10	7	F_3EO_1:TTE = 1:5
4	F_4EO_2:TTE = 1:10 0.5M LiTFSI	8	F_3EO_1:TTE = 1:5 0.5M LiTFSI

Patents/Publications/Presentations

The project has no patents, publications, or presentations to report this quarter.

Task 5.6 – Strategies to Enable Lean Electrolytes for High Loading and Stable Lithium-Sulfur Batteries (Y. Shirley Meng, University of California, San Diego)

Project Objective. The project aims to develop high energy density (> 500 Wh/kg) and low cost (< 65 $/kWh) Li-S pouch cells.

Impact. The project focuses on addressing the fundamental bottleneck in enabling high-energy-density Li-S batteries. These have been identified as the need to reduce LE excess and enable high areal loading electrodes. The challenges are overcome via the use of a dense polymer-S electrode composite, which significantly reduces electrode porosity in conventional C-S systems while improving capacity retention. These capabilities, combined with project collaborator Ampcera's material scaling and collaborator GM's pouch prototyping capability using thin lithium metal, will result in breakthroughs in next-generation Li-S battery chemistries that meet the energy density (> 500 Wh/kg) and cost goals (< $65/kWh) of this project.

Approach. Novel electrode architectures using hexaazatrinaphthylene polymer-S composite (HATN-S) electrode will be explored to reduce the porosity and increase the active loading of the composite electrode. Additionally, advanced electrolyte systems and optimization of Li-metal anode will be applied to further increase energy density of the Li-S pouch cell. If successful, the proposed HATN-S electrode should have less than 20% porosity with high areal capacities of > 15 mAh cm^{-2}, which will enable lean electrolyte conditions < 2 g/Ah in the full Li-S pouch cell.

Out-Year Goals. The out-year goals involve demonstration of baseline cell chemistries with reduced cathode porosity and increased cathode areal loading pairing with limited electrolyte and lithium inventory. The conventional electrode drying process (solvent evaporation) limits sulfur loading in the electrode. Thus, the HATN-S electrode will be prepared by optimizing the electrode architecture to increase sulfur loading and reduce electrode porosity. The electrolyte system will be optimized to reduce lithium usage (low N/P ratio) and improve cell stability.

Collaborations. Project collaborators include GM and Ampcera. This quarter, the work has been accomplished by UCSD, with Ampcera and GM starting preparations for synthesis of HATN monomer and polymer, and the thin lithium metal.

Milestones

1. A benchmark performance metric of 80% capacity retention of HATN-S electrodes was achieved after 200 cycles using baseline electrolyte system. (Q1, FY 2022; Completed)
2. Process synthesis to demonstrate HATN-S electrode with reduced porosity and increased areal loading. (Q2, FY 2022; In progress)
3. Demonstrate cyclability of optimized HATN-S electrode with limited electrolyte and lithium inventory. (Q3, FY 2022; In progress)
4. Demonstrate stable cycling of optimized HATN-S electrode, which should be able to cycle with limited electrolyte (< 2 g/Ah) and low N/P ratios (< 1.2). (Q4, FY 2022; In progress)

Progress Report

Introduction

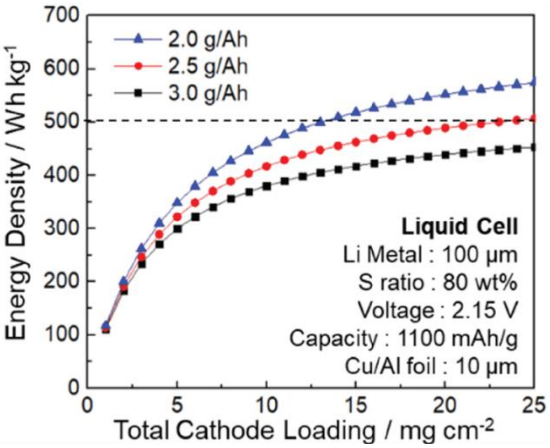

Figure 72. Calculated cell energy densities of Li-S with different electrolyte excess.

The project objective is to develop high-energy-density (> 500 Wh/kg) and low-cost (< 65 \$/kWh) Li-S pouch cells. Figure 72 and Table 8 below summarize the metrics required to reach the goals. To that end, the team will explore novel electrode architectures using the HATN-S electrode to reduce porosity and increase active loading of the composite electrode. Additionally, advanced electrolyte systems and the optimization of Li-metal anode will be applied to further increase energy density of the Li-S pouch cell. If successful, the proposed HATN-S electrode should have less than 20% porosity with high areal capacities of > 15 mAh cm^{-2}, which will enable lean electrolyte conditions < 2 g/Ah in the full Li-S pouch cell.

This quarter, major activities include benchmarking the electrochemical performance of HATN-S electrodes in the baseline and new electrolyte systems. A benchmark performance metric of 80% capacity retention was achieved after 200 cycles. On top of this, the reduced porosities of the HATN-S composite electrode were also characterized and compared against the baseline carbon sulfur (C-S) composite electrodes; the team found that the HATN-S composite enabled porosity reduction from 50.9% to 29.8%, potentially enabling significantly reduced excess electrolyte. Finally, quantitative characterization analysis was used to demonstrate feasibility of separating lithium and sulfur inventory losses within pristine and cycled cells, in efforts to investigate root causes of capacity fade.

Table 8. Cost breakdown of Li-ion battery versus proposed Li-S battery chemistries.

Material for Li-Ion Battery with NMC-622	Unit Price (\$/kg)	Material Cost (\$/kWh)	Material for HATN Polymer – S-based cell	Unit Price (\$/kg)	Material Cost (\$/kWh)
Graphite	12.30	12.93	Li metal	50.00	9.14
Electrolyte	25.00	19.74	Electrolyte	25.00	23.8
Separator	62.50	3.26	Separator	62.50	3.26
Aluminum	2.22	0.15	Aluminum	2.22	0.15
Copper	8.22	8.07	Copper	Not Required	Not Required
NMC-622	27.00	47.39	Sulfur Cathode	**< 16.80 (Target)**	**< 8.00 (Target)**
Manufacturing Cost	20% of Overall Cost		Manufacturing Cost	20% of Overall Cost	
Total	**\$114.44/kWh**		Total	**< \$65/kWh (Target)**	

Performance Benchmarking

The capacity and stability of the HATN-S electrode with baseline and new electrolyte systems were demonstrated. In Figure 73, the performance of this composition is shown over the first 200 cycles in commercially available ether-based formulation [1 M LiTFSI in a DOL/DME mixture (1:1, v/v) with 2 wt% $LiNO_3$, baseline]. Compared to the conventional C-S composite electrode, the HATN-S material displayed significantly higher capacity retention and longer cycle life. However, the majority of its capacity fade still occurs within the first 100 cycles, an observation consistent with various studies reported in the literature. While various hypotheses have been proposed to identify the root causes of this phenomenon, detailed quantitative analysis has not yet been conducted to address this challenge. As such, the later sections will detail initial results in characterizing sulfur and lithium inventory losses to identify causes of initial capacity fade.

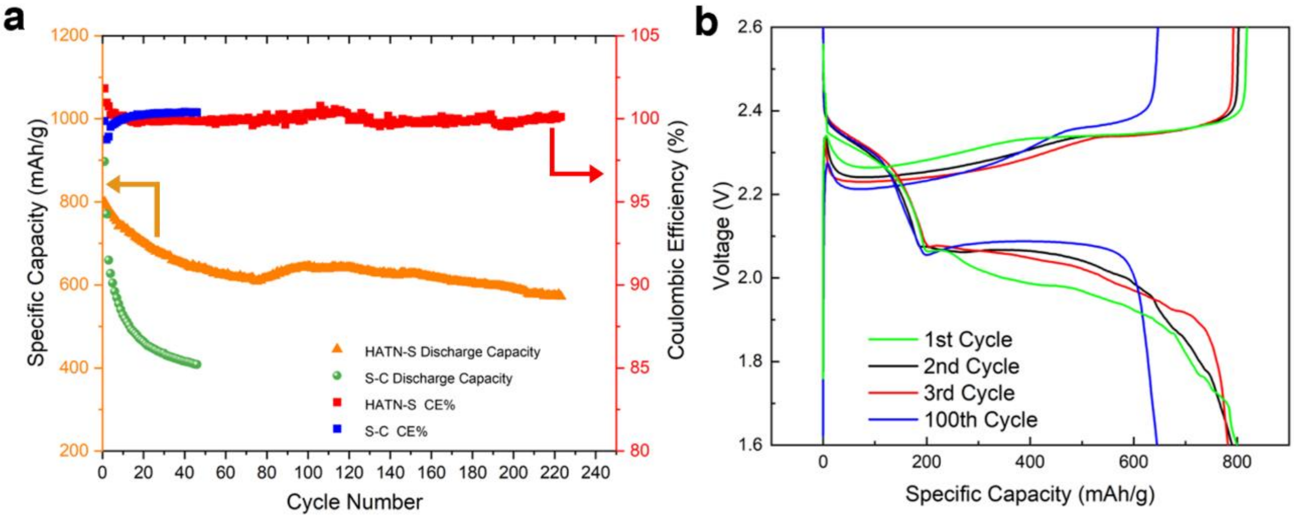

Figure 73. (a) Cycling performance of the HATN-S electrode. (b) Cycling voltage profiles of the HATN-S electrode.

In efforts to improve performance, alternative electrolyte compositions were also explored. One promising electrolyte candidate previously reported in the literature was investigated: localized high concentration electrolyte (LHCE), first developed by PNNL researchers in 2018. By mixing a highly concentrated electrolyte with an inert diluent that can mix well with the solvent but does not solvate the salt, LHCEs developed by PNNL show extraordinary performance when coupled with Li-metal anode (Figure 74a-b). The Li||Cu made with LHCE (LiFSI:DME:TTE with 1:1.2:3 molar ratio) exhibits around 99% CE when cycled at 0.5 mA/cm^2 for 1 mAh/cm^2. It is noted that the small CE fluctuation is originated from the temperature sensitivity. The lithium plated with LHCE also shows large granular morphology with diameters of 20 µm. These results indicate that LHCE can work well with Li-metal anode. However, when S-C composite electrode cells are assembled with LHCE, the resulting voltage profile shows a large polarization during the 1st cycle. As a result, only limited capacity can be delivered by the cells (Figure 74c). One possible reason for the large polarization is that the diluent used in the LHCE, TTE, cannot fully dissolve the polysulfides formed during the first stage of discharge of Li-S cells, causing the high impedance for the continuous lithiation of the sulfur particles. As such, while the LHCE is highly promising for the Li-metal anode, it needs to be modified to enable compatibility with the sulfur cathode. In future work, the team will focus on finding suitable diluent for the LHCE so that it can be incorporated into the Li-S system.

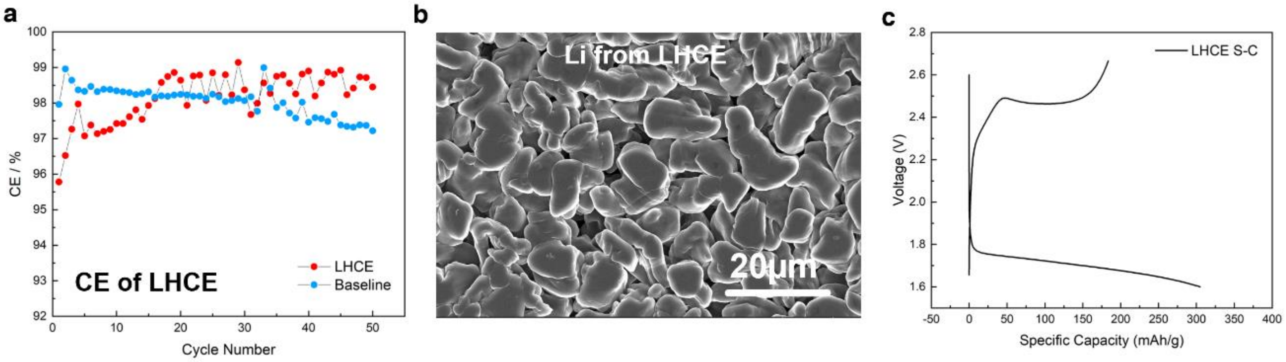

Figure 74. (a) The Li||Cu cycling Coulombic efficiency of localized high concentration electrolyte (LHCE) and baseline electrolyte. (b) The dense lithium plating morphology of LHCE. (c) Voltage profile of S-C composite electrode cycling in LHCE.

Reducing Porosity in Electrodes

One main cause for the large electrolyte excess used in the Li-S system is the high intrinsic porosity in the S-based composite electrodes. The large porosity in the composite electrode translates into extra electrolyte needed to provide good wetting and ionic contact for cycle performance. As shown in Figure 72, to reach the project goal of 500Wh/kg, the E/S ratio needs to be lowered to 2-2.5 g/Ah, which is unprecedented in the field to date. Based on theoretical calculations, the porosity of the HATN-S electrode will need to be lowered to 20% to meet the 500 Wh/kg goal.

Using the HATN polymer, elemental sulfur is well-bonded to the polymer backbone with good sulfur chemical affinity during the synthesis process, which results in formation of highly dense HATN-S particles. As shown in Figure 75, with similar loading of 1.5 mg/cm^2, the thickness of the HATN-S electrode (~ 15.6 µm) is much less than that of the conventional S-C electrode (~ 20.0 µm). Additionally, porosity of the HATN-S electrode (29.8%) is reduced by more than 20% compared to the traditional S-C electrode (50.9%). The enlarged FIB/SEM images (Figure 75c-d) further show that the HATN-S particles are highly dense, unlike the nano-porous S-C particles. However, the current porosity of HATN-S is still about 10% higher than the target goal (20%). More work, such as optimization of composite processing and dry electrode fabrication, will be done to further decrease porosity of the HATN-S electrode.

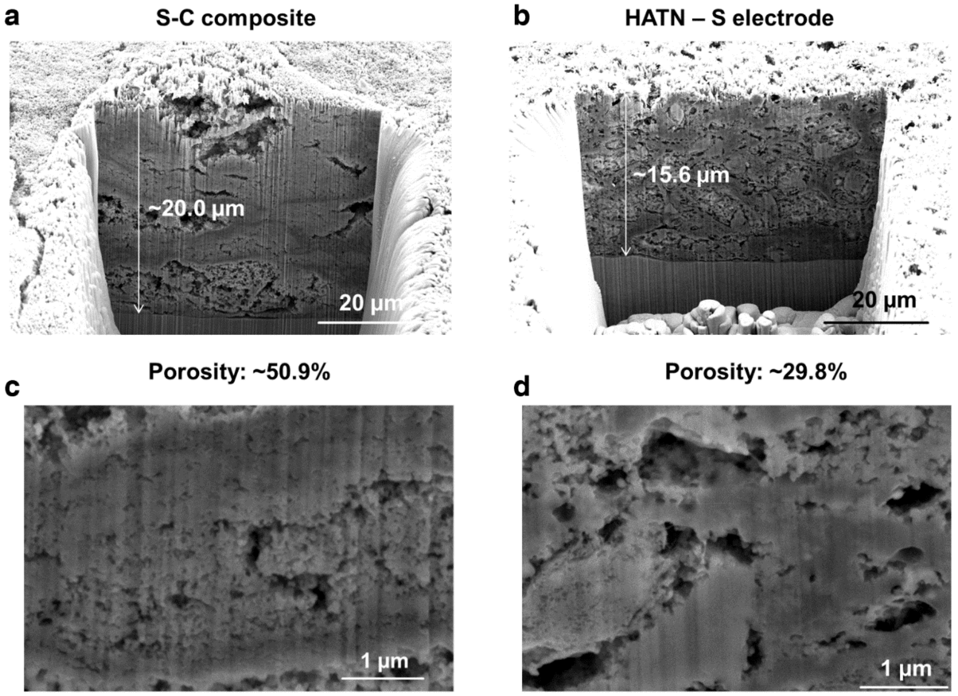

Figure 75. Cryo – focused ion beam / scanning electron microscopy images of (a) S-C composite electrode and (c) its zoom-in image. (b) HATN-S electrode and (d) its zoom-in image.

Quantifying Li_2S and Sulfur Inventory Losses

Capacity fade observed in Li-S battery chemistries can be attributed to several possible sources including sulfur inventory losses as a result of irreversible Li_2S formation, polysulfide dissolution losses, and lithium inventory losses as a result of trapped lithium or SEI accumulation. Each respective root cause would require different engineering solutions. As a result, it is vital for the team to conduct quantitative analysis to identify the bottleneck in each of these sources of capacity loss. To quantify and separate inventory losses from S / Li_2S, TGA tools can be employed by utilizing the large physical property differences between sulfur and Li_2S. Table 9 below summarizes the properties of interest.

Table 9. Physical properties of sulfur and lithium sulfide.

	Melting Point	Boiling Point
Sulfur	115.21°C	444.6°C
Lithium Sulfide	938°C	1372°C

To validate the TGA tool, a series of controlled reference experiments was first conducted. As shown in Figure 76, four reference powders were measured using TGA to validate the method for quantifying elemental sulfur in the electrode. All samples were sealed in aluminum pan, and the TGA measurement was conducted under argon environment. At a fixed heating temperature of 300°C, the sulfur powder can be successfully vaporized completely, while the Li_2S powder retained nearly all its mass after the heating process (Figure 76a-b), validating the tool's ability to separate contributions from sulfur and Li_2S, respectively. PVDF and super P powders, which are used in the electrode making, also show good stability during heating under argon environment. Thus, the team believes that mass loss contributions can be eliminated from these inactive additives.

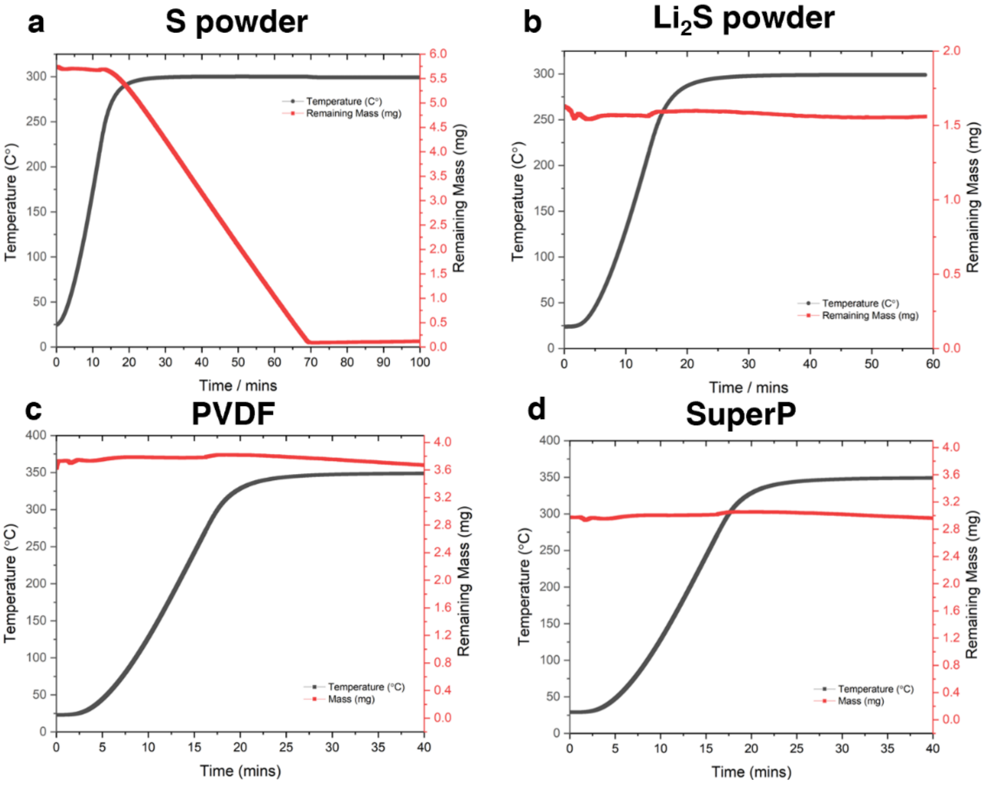

Figure 76. Thermal gravimetric analysis curves of (a) elemental sulfur powder, (b) Li_2S powder, (c) PVDF powder, and (d) super-P conductive carbon powder.

As previous results have shown that TGA is a valid tool for quantifying sulfur mass, the team proceeded to conduct analysis on the electrode materials. First, TGA measurement on the S/Li_2S mixture was conducted, to verify whether the TGA-measured sulfur mass matches the balance-measured sulfur mass. To exclude human bias during the measurement process, the balance measurement and the TGA measurement of the sample powders are conducted by two individuals. The results are only compared after all measurements are completed. As shown in Figure 77a, the TGA-measured sulfur mass is quite close to the balance-measured sulfur mass, with an error of 3.9%, which supports the validity of the methodology.

Subsequently, the team proceeded to quantify the sulfur content in the pristine HATN-S electrode by using the TGA method. Figure 77b shows that the loading of the sulfur in the pristine HATN-S electrode is 2.49 mg, which is also close to the balance-measured sulfur mass (2.58 mg). The sulfur mass in the HATN-S electrode after the first 3 cycles is also quantified by TGA (Figure 77c). After the first 3 cycles, only 89.4% of sulfur mass is retained, indicating that there is more than 10% of active material loss during the formation cycles. After 10 cycles, the HATN-S electrode lost another 4% of the active sulfur mass. Results so far show that the loss of active sulfur mass is significant during the first 10 cycles. As the rate of sulfur loss is non-linear, additional quantification will be done at further cycle numbers to study their trends. In the future, more work will also be done to control the active sulfur mass loss, such as electrolyte and electrode engineering.

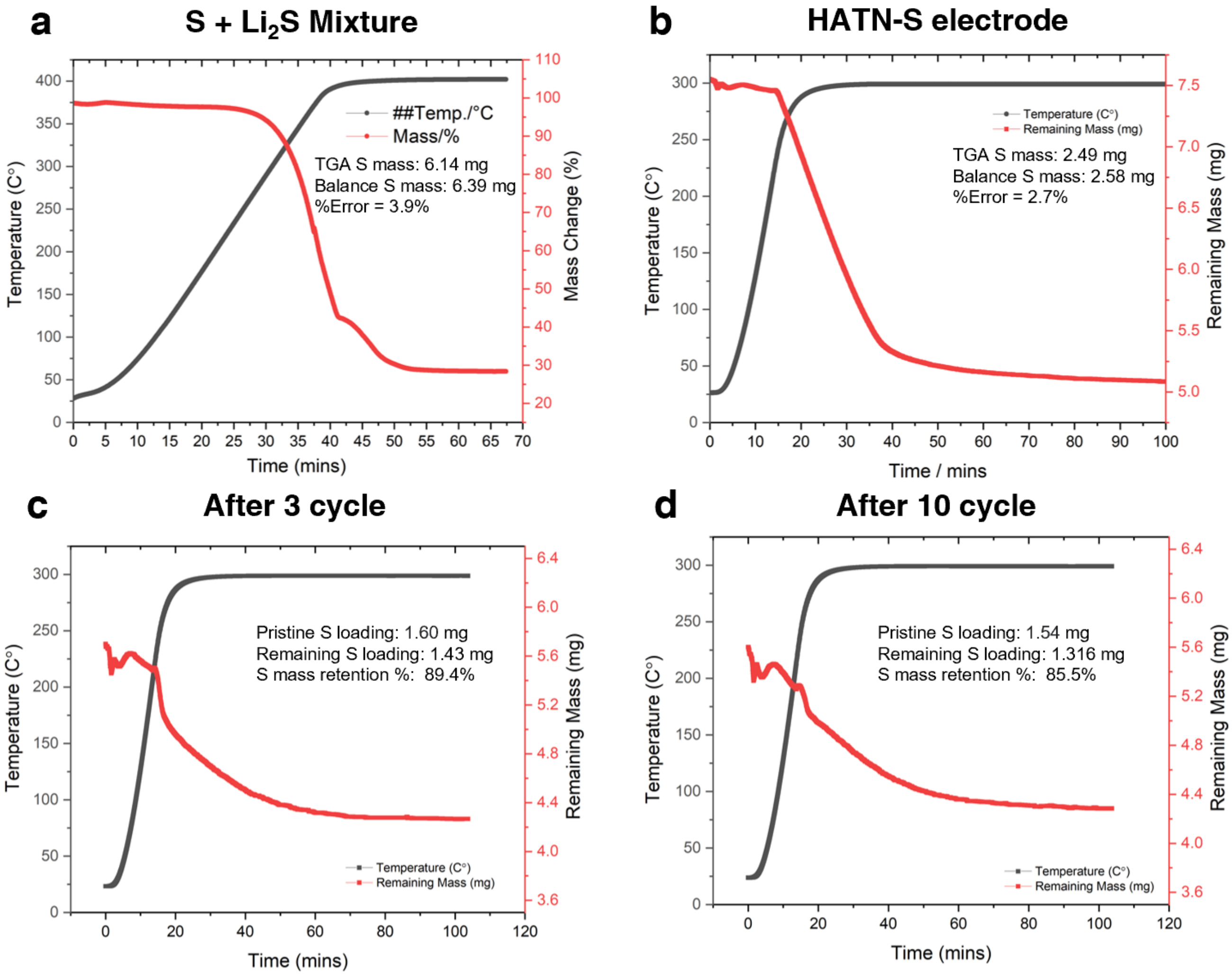

Figure 77. Thermal gravimetric analysis curves of (a) elemental sulfur + Li_2S powder mixture. (b) HATN-S pristine electrode. (c) HATN-S electrode after 3 cycles. (d) HATN-S electrode after 10 cycles.

Quantifying Lithium Inventory Losses

Beyond sulfur mass losses, lithium inventory loss might be another reason for the capacity fade in the Li-S system. Previously, the team has successfully developed the TGC method to quantify the metallic lithium mass in the cycled electrodes. The TGC method has been expanded recently to accommodate the Li-S system. A new calibration curve with a range up to 2.5 mg of lithium is established for measuring larger quantities of lithium used in this project. With the new calibration curve, the remaining metallic lithium mass in the cycled Li-metal electrode from Li-S cells can be quantified.

Figure 78 shows the lithium inventory quantification after 3 and 10 cycles in the HATN-S cells. After 3 cycles, the lithium mass retention is about 91%, which indicates that about 9% of lithium has been converted to SEI Li^+. The loss of metallic lithium can be attributed to several reasons: (1) native oxides layers during lithium metal manufacturing and transportation; (2) SEI formation during lithium plating, and (3) reaction with lithium polysulfides. However, after 10 cycles, only another 2% of metallic lithium is lost after cycling, which is lower than the rate of sulfur inventory loss quantified by TGA. These initial results indicate that capacity fade in the Li-S cells is likely due to sulfur mass losses instead of lithium metal losses. However, more work needs to be done to study the lithium and sulfur inventory losses over longer cycles.

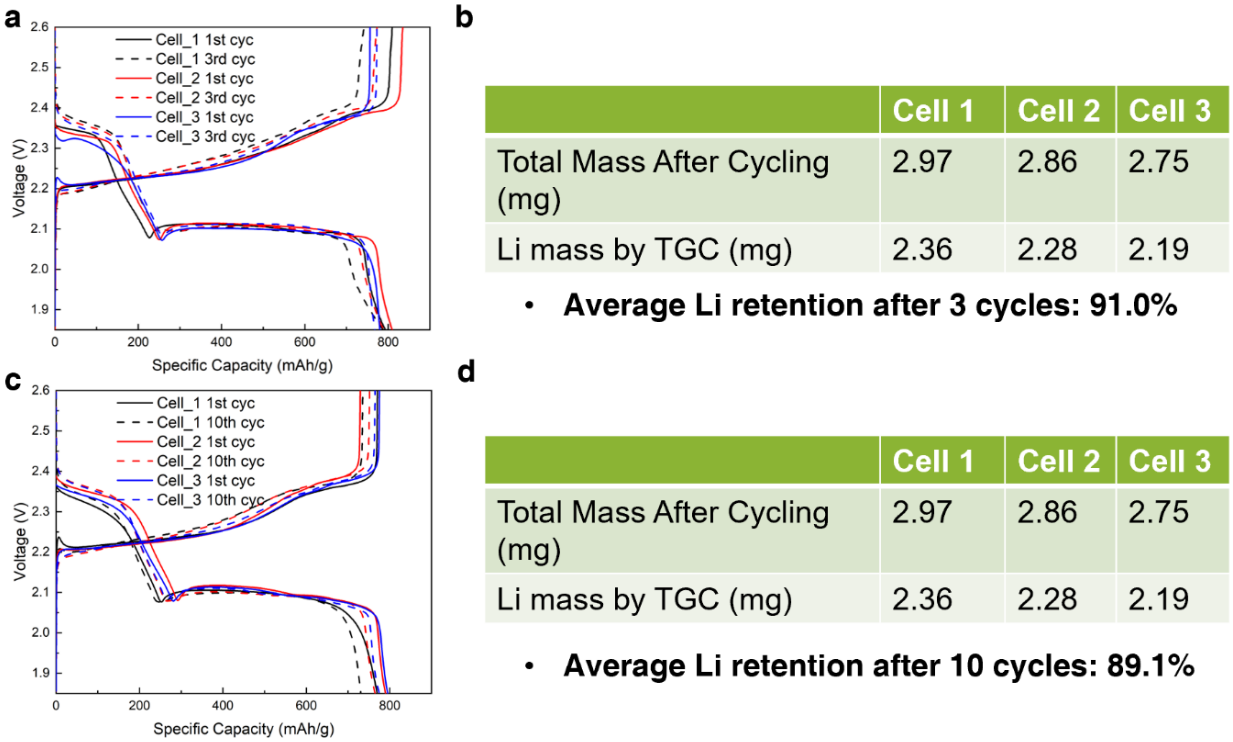

	Cell 1	Cell 2	Cell 3
Total Mass After Cycling (mg)	2.97	2.86	2.75
Li mass by TGC (mg)	2.36	2.28	2.19

- **Average Li retention after 3 cycles: 91.0%**

	Cell 1	Cell 2	Cell 3
Total Mass After Cycling (mg)	2.97	2.86	2.75
Li mass by TGC (mg)	2.36	2.28	2.19

- **Average Li retention after 10 cycles: 89.1%**

Figure 78. Titration gas chromatography analysis of lithium inventory. Voltage profiles of HATN-S cells for the (a) first 3 cycles and (c) first 10 cycles. The lithium inventory quantification of HATN-S cells after (b) 3 cycles and (d) 10 cycles.

Patents/Publications/Presentations

The project has no patents, publications, or presentations to report this quarter.

Task 5.7 – New Engineering Concepts to High-Energy-Density Lithium-Sulfur Batteries (Prashant Kumta, University of Pittsburgh)

Project Objective. The major objectives of this project are to develop a Li-S pouch cell with a cell capacity > 300 mAh with energy density ≥ 500 Wh/kg, ≥ 750 Wh/L with cycling over 1000 cycles @C/3 rate, cycle life of 1000 at C/3 and ≤ 20% fade in energy @ C/10-C/3, and ≤ $80/kWh. To achieve the proposed objectives, the following major goals will be successfully attained over the first year of the project: (1) identification of effective electrocatalysts and LICs lowering the activation barrier; (2) *in situ* synthesis of electrocatalysts and LICs dispersed complex CFM and sulfur nanocomposite with sulfur content ≥ 90 wt%; (3) ~ 15 mAh/cm^2 areal capacity of sulfur electrode with sulfur loading ≥ 10mg/cm^2; (4) Li-SIA of ≥ 1000 cycles with 15 mAh/cm^2 areal capacity @C/3 rate; and (5) identification of optimal electrolyte compositions giving Li$^+$ conductivities ~ 10^{-2} S/cm and polysulfide dissolution < 1 ppm.

Impact. The work from this project will have a strong impact on development of high-energy-density Li-S batteries. The results of this work will lead to new knowledge on identification and generation of high-capacity sulfur cathodes and dendrite-free Li-metal anodes using scalable synthesis and fabrication approaches. Both fundamental and applied knowledge will be gathered from the study. Systematic characterization will provide new scientific insights into the mechanisms contributing to the corresponding response in coin-cell and pouch-cell formats. Results of this work also will likely have an impact on other fields such as electrocatalysts for water splitting and fuel cells and other fields engaged in electrochemistry. Plans are also in place to engage under-represented minority undergraduate students to gain research experience in various aspects of the project. With new materials identified as the project is executed, opportunities will emerge for filing invention disclosures, provisional and non-provisional patent applications. The training and opportunities presented by this project to undergraduate and graduate students as well as postdoctoral research associates will foster next-generation work force training, equipping workers with the necessary skillsets to transform the quality of life all over the globe by generating high-energy-density systems that can be deployed in EVs as well as in laptops, and cell phones including innumerable portable and wireless devices opening the doors to a new green and sustainable energy environment improving overall quality of life.

Approach. Work involves executing a theory-driven study directed at identification of electrocatalysts for efficient conversion of polysulfides to Li_2S during the forward discharge process and backward charge process to elemental sulfur and lithium. Also, first-principles computational approaches will be applied to identify solid-state LICs with conductivity > 10^{-4} S/cm. Employing expertise in the PI's laboratory, suitable low-temperature (< 240°C) scalable synthesis techniques will be used to generate theoretically identified electrocatalysts and LICs. Low polysulfide solubility and stable SEI forming electrolytes will then be prepared from commercially available solvents, additives, and salts. The effectiveness of the electrocatalysts and LICs to improve the polysulfide to Li_2S transformation kinetics and the ability to achieve the targeted specific capacity by trapping polysulfides, including desired structural transformation during charging/discharging, will be assessed; accordingly, suitable modification of electrocatalysts and LICs will be performed to generate the ideal microstructures. Suitable modification if required of lithium alloy as anode will also be performed by alloying with other metals to improve the Li-ion diffusivity kinetics and the Gibbs-Thomson parameter. The scalable approaches developed will be further refined to optimize sulfur utilization in the cathode, engineer the surface and bulk structure of the novel Li-SIA and lithium multicomponent alloy (Li-MCA) anodes to yield the desired areal capacity with optimal CE, and finally optimize the electrolyte structure to minimize and eliminate polysulfide dissolution with desired Li$^+$ conductivities. Finally, the developed systems will be scaled up, fabricated, and tested in pouch-cell configurations.

Out-Year Goals. The following goals will be achieved in subsequent years: (1) determine optimal cell component design parameters such as electrode thickness and porosity exhibiting minimal polarization while maintaining cathode capacity ≥ 1500 mAh/gS; (2) demonstrate excellent cycle life of > 1000 cycles with > 80% capacity retention; (3) electrochemically test cells with dendrite-free Li-alloy anodes comprising Li-SIA and Li-MCA of areal capacity of ~ 15 mAh/cm^2; (4) electrochemically test cells with modified electrolytes at charge-discharge rages of C/3 as well as other C-rates of C/10-C/3; (5) fabricate > 300 mAh pouch cell giving energy density of greater or equal to 500 Wh/kg at C/3 rate and demonstration of acceptable performance at other C-rates of C/10-C/3; and (6) demonstrate cyclability of a minimum of 1000 charge/discharge cycles with < 20% fade rate for operation in -40^{o}C to +40^{o}C temperature ranges with temperature measured external to the pouch cell.

Collaborations. The project involves collaboration with G. E. Blomgran of Blomgren Consulting Services, Ltd.

Milestones

1. Computational identification of electrocatalysts and LICs will be completed: 80% lower activation barrier of polysulfide to Li_2S transformation and a 10-times improvement of reaction kinetics will be achieved. (Q1, FY 2022; In progress, April 2022)
2. Synthesis and characterization of ~ 20-nm-sized electrocatalysts and LICs homogeneously dispersed in the CFM/S will be completed. Dendrite-free growth study will be completed, and ≥ 1000 cycles cyclability tests @C/3 rate will be completed for dendrite-free anode technology innovation. (Q2, FY 2022; In progress, June 2022)
3. Modified electrolyte with high Li-ion conductivity (~ 10^{-2} S/cm) and minimum polysulfide solubility (< 1 ppm) will be achieved. (Q3, FY 2022; In progress, September 2022)
4. Electrochemical characterization of the system will be completed, and targeted cathode capacity of > 1500 mAh/gS (> 15 mAh/cm^2) will be achieved @ C/3 rate poised to be scaled up. (Q4, FY 2022; In progress, December 2022)

Progress Report

Progress for this new project will be reported next quarter.

Patents/Publications/Presentations

The project has no patents, publications, or presentations to report this quarter.

Task 5.8 – Development of Lithium-Sulfur Battery Cells with High Energy Density and Long Cycling Life (Donghai Wang, Pennsylvania State University)

Project Objective. The objective of this project is to develop a new soluble-polysulfide-free sulfur cathode with a high sulfur content (> 50 wt%) and high discharge specific capacity (> 700 mAh g^{-1}, based on the weight of the whole cathode), and demonstrate the performance of the sulfur electrode at high electrode capacity (> 7 mAh cm^{-2}), low N/P ratio (< 2), and low E/S ratio (< 2.5 µL mg^{-1}). Prototype Li-S pouch cells with predicted energy density of 400 Wh kg^{-1} and 80% capacity retention for over 300 cycles using conventional electrolyte and Li-metal anodes with a protective layer developed by the team will be demonstrated.

Impact. This project aims to develop new sulfur composite active materials and functional polymer binders that enable polysulfide-free, high-performance, low-cost sulfur cathode. The use of these high-performance and low-cost sulfur cathodes, in turn, enables Li-S batteries with high energy density and long cycle life. Such Li-S batteries, made using the developed cathodes paired with a Li-metal anode, can lead to 50% greater energy density than conventional Li-ion batteries. Meeting the technical targets will potentially develop high-energy-density lithium batteries, promote increased adoption of EVs and PHEVs, and reduce petroleum consumption in the transportation sector by helping battery-powered vehicles become accepted by consumers as a reliable source of transportation.

Approach. The overall approach will focus on synthesizing and optimizing a novel polysulfide-free sulfur composite active material and functional binders. Specifically, approaches to realize the project objectives include the following: (1) development of novel polysulfide-free sulfur composite active materials, (2) development of new functional polymer binders to facilitate Li^+ transport and trap residual lithium polysulfide; and (3) diagnostics, characterization, theoretical simulation, and cell tests on the developed materials in Li-S batteries.

Out-Year Goals. The out-year goals are as follows: (1) develop new sulfur composite active materials, and (2) conduct characterization, simulation, and performance tests on material and electrode levels. The *Go/No-Go Decision* will be demonstration of Li-S batteries using the developed sulfur composite active materials with an initial discharge specific capacity > 600 mAh g^{-1} (based on cathode weight) at an areal capacity of 4 mAh cm^{-2} and E/S ratio < 8 µL mg^{-1}.

Collaborations. PSU will collaborate with the University of Illinois at Chicago (UIC) on theoretical simulation.

Milestones

1. Demonstrate sulfur cathode using sulfur composite active material (generation 1) with an initial discharge capacity > 500 mAh g^{-1} (based on cathode weight), at E/S ratio < 10 µL mg^{-1}. (Q1, FY 2022; In progress)
2. Demonstrate sulfur cathode using sulfur composite active material (generation 2) with an initial discharge capacity > 500 mAh g^{-1} (based on cathode weight), at E/S ratio < 10 µL mg^{-1}. (Q2, FY 2022; In progress).
3. Demonstrate sulfur cathode using sulfur composite active material (generation 1) with an initial discharge capacity > 600 mAh g^{-1} (based on cathode weight), at E/S ratio < 10 µL mg^{-1}. (Q3, FY 2022; In progress)
4. Demonstrate sulfur cathode using sulfur composite active material (generation 2) with an initial discharge capacity > 600 mAh g^{-1} (based on cathode weight), at E/S ratio < 10 µL mg^{-1}. (Q4, FY 2022; In progress)

Progress Report

Progress for this new project will be reported next quarter.

Patents/Publications/Presentations

The project has no patents, publications, or presentations to report this quarter.

TASK 6 – LITHIUM-AIR BATTERIES

Team Lead: Ji-Guang Zhang, Pacific Northwest National Laboratory

Summary and Highlights

The Task objective is to develop rechargeable Li-O_2 batteries with long-term cycling stability through in-depth research on more stable electrolytes and highly efficient catalysts for air electrodes, protection of Li-metal anodes, and deeper understanding on the oxygen reduction reaction (ORR) and oxygen evolution reaction (OER) mechanisms behind the electrochemical performance of Li-O_2 cells.

Highlights. The highlights for this quarter are as follows:

- The ANL team studied the functioning mechanism of the SEI layer and its role as a cathode for a Li-O_2 battery. They found that the functioning mechanism of the SEI layer depends on formation of soluble species that can diffuse to and oxidize the Li_2O_2, that is, a soluble catalyst. However, the SEI layer cannot contribute significantly to charge/discharge capacity after the 1st charge cycle.
- The team at ANL/UIC developed a novel co-catalytic system comprised of tin sulfide (SnS) nanoflakes (NF) / reduced graphene oxide (rGO) as a solid catalyst and a dual functional additive that provides a liquid phase catalyst as well as an anode protection. They discovered that SnS NF catalysts embedded with rGO show an excellent catalytic activity during the discharge and charge of Li-O_2 batteries.
- The UIC group explored a Li-air battery based on a CO_2 reactant. They discovered a novel combination of transition metal dichalcogenide alloy structure as a cathode catalyst and a bi-functional RM that works in synergy with IL-based electrolyte to operate the battery at high rates. The battery is capable of operating under 0.3 mA/cm^2 and high capacities of 0.3 mAh/cm^2 (corresponding to 3000 mAh/g) up to 100 cycles.

Task 6.1 – Lithium-Air Batteries
(Khalil Amine, Larry A. Curtiss, and Jun Lu; Argonne National Laboratory)

Project Objective. This project will develop new cathode materials and electrolytes for Li-air batteries for long cycle life, high capacity, and high efficiency. The goal is to obtain critical insight that will provide information on the charge and discharge processes in Li-air batteries to enable new advances to be made in their performance. This will be done using state-of-the-art characterization techniques combined with state-of-the-art computational methodologies to understand and design new materials and electrolytes for Li-air batteries.

Project Impact. The instability of current nonaqueous electrolytes and degradation of cathode materials limits performance of Li-air batteries. The project impact will be to develop new electrolytes and cathode materials that are stable and can increase energy density of electrical energy storage systems based on lithium.

Approach. The project is using a joint theoretical/experimental approach for design and discovery of new cathode and electrolyte materials that act synergistically to reduce charge overpotentials and increase cycle life. Synthesis methods, in combination with design principles developed from computations, are used to make new cathode architectures. Computational studies are used to help understand decomposition mechanisms of electrolytes and how to design electrolytes with improved stability. The new cathodes and electrolytes are tested in Li-O_2 cells. Characterization, along with theory, is used to understand the performance of materials used in the cell and to make improved materials.

Out-Year Goals. The out-year goals are to find catalysts that promote discharge product morphologies that reduce charge potentials and to find electrolytes for long cycle life through testing and design.

Collaborations. This project engages in collaboration with K. C. Lau (UC at Norridge), Y. Wu (OSU), and R. Shahbazian-Yassar (UIC).

Milestones

1. Design functionalized cathodes to achieve high electrochemical performance of Li-O_2 batteries. (Q1, FY 2022; Completed)
2. Characterize cathode materials and investigate electrochemical behaviors. (Q2, FY 2022)
3. Gain understanding of the processes of ORR and OER of these materials and reveal the possible parasitic reactions. (Q3, FY 2022)
4. By understanding the effects, engineer new catalysts with improved catalytic performance and suppressed side reactions. (Q4, FY 2022)

Progress Report

Last quarter, the team summuarized their finding of a new metal-free catalyst platform for enabling low overpotential charge of Li-O_2 batteries across various current densities and types of carbon-based substrate materials. This platform was based on what is traditionally called SEI, which is an organic/inorganic interphase that is formed by the reduction of electrolyte components. This quarter, the team specifically studied the functioning mechanism of the SEI layer and its role as a cathode for a Li-O_2 battery.

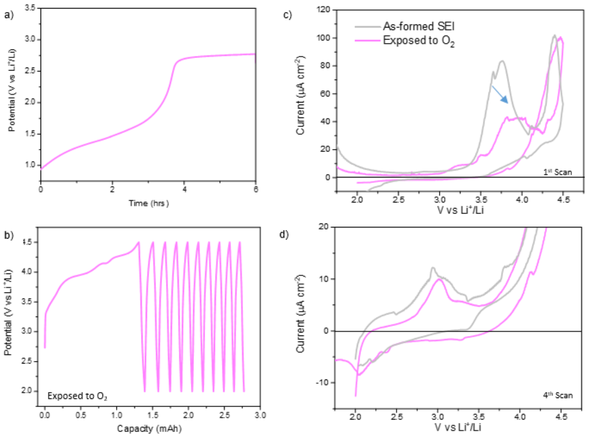

Figure 79. (a) Open circuit potential of SEI versus lithium metal (reference electrode) when exposed to O_2 gas. (b) Cycling profile of the SEI versus Li-metal cell in argon atmosphere *after* exposing the SEI to O_2. Cyclic voltammograms (CVs) of the pristine SEI and SEI exposed to O_2 gas (c) 1st scan and (d) 2nd scan, indicating the relatively reversible CV current peak at ~ 3.0 V versus Li^+/Li.

They discovered profound properties in the ether-based SEI layer when exposed to O_2 gas. As shown in Figure 79a, the open-circuit potential was measured while the SEI was exposed to and allowed to rest in an O_2 atmosphere over 6 hours. It was apparent that the potential of the SEI changed drastically during this process (stabilizing after ~ 4 hours). A constant current charge revealed (Figure 79b) a multi-plateau voltage profile followed by almost no capacity contribution from continued cycling after the 1st charge. This eliminates the possiblity that the SEI layer can contribute significantly to charge/discharge capacity after the 1st charge cycle. A similar conclusion was reached the 1st and 4th cycle of CV (Figure 79c-d, respectively) where the large initial irreversible peak at ~ 3.75 V decreased drastically from the 1st to 4th cycle. However, a small peak at ~ 3.0 V remained, indicating that there is a reversible eletrochemical process derived from the SEI layer, which likely contributes to its catalytic function.

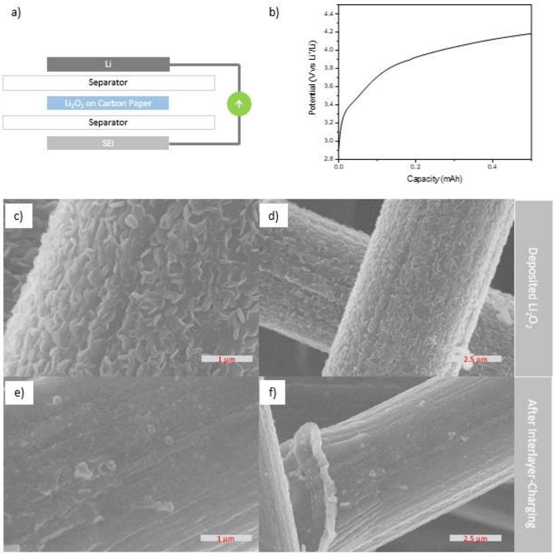

Figure 80. (a) Schematic of interlayer-based electro-chemical cell developed for studying the catalyst. (b) Constant current charging profile of the bare SEI-based cathode. Deposited Li_2O_2 over the surface on a carbon paper gas diffusion layer (GDL), (c) high and (d) low magnification. Scanning electron microscopy of the carbon paper GDL after charging in an interlayer position (no electrical contact to circuit) at (e) high and (f) low magnification.

To determine if the charging benefit of using the SEI is derived from a direct SEI-Li_2O_2 contact mechanism or a solution mechanism between SEI-derived soluble species, the team designed what they refer to as an interlayer cell. Ths main feature of this cell is that the interlayer is not electronically connected to the circuit of the battery (Figure 80a). They pre-deposited Li_2O_2 onto a carbon paper (Figure 80c-d) and used it as the interlayer. With the O_2-exposed SEI as the cathode, they charged the cell (voltage profile shown in Figure 80b), and found that the Li_2O_2 content decreased substantially (Figure 80e-f). This is strong evidence that the functioning mechanism of the SEI layer is based on formation of soluble species that can diffuse to and oxidize the Li_2O_2, that is, a soluble catalyst. Future studies will dive deeper into which species are present and also the role of the SEI layer on the deposition kinetics and mechanism of Li_2O_2.

Patents/Publications/Presentations

Publication

- Plunkett, S. T., C. Zhang, K. C. Lau, M. R. Kephart, J. G. Wen, D. Y. Chung, D. Phelan, Y. Ren, K. Amine, S. Al-Hallaj, B. P. Chaplin, H-H. Wang, and L. A. Curtiss. “Electronic Properties of Ir_3Li and Ultra-Nanocrystalline Lithium Superoxide Formation.” *Nano Energy* 90 (2021): 106549.

Task 6.2 – Lithium Oxygen Battery Design and Predictions
(Larry A. Curtiss / Anh Ngo, Argonne National Laboratory; Amin Salehi-Khojin, University of Illinois, Chicago)

Project Objective. The objective of this work is to develop new materials for Li-O_2 batteries that give longer cycle life and improved efficiencies in an air environment. New electrolyte blends and additives will be investigated that can reduce clogging and at the same time promote the cathode functionality needed to reduce charge overpotentials. New cathode and anode materials will be investigated that can work in conjunction with the electrolytes to improve cycle life in the presence of air components.

Project Impact. Li-air batteries are considered as a potential alternative to Li-ion batteries for transportation applications due to their high theoretical specific energy. The major issues with the existing Li-O_2 systems include degradation of the anode electrode, reactions with air components, clogging of the cathode, and electrolyte instability. Thus, this project is using a comprehensive approach to improve cycle life and efficiency through developing new materials for electrodes, anodes, and electrolytes that work in synergy.

Approach. The experimental strategy is to use cathode materials based on two-dimensional (2D) transition metal dichalcogenides (TMDs) that the team has found to be among the best ORR/OER catalysts. These cathode materials will be combined with new electrolyte blends and additives that work in synergy to reduce charge potentials and increase stability of the Li-air system. DFT and AIMD simulations are used to gain insight at the electronic structure level of theory of the electrolyte structure, and function both in bulk and at interfaces with the cathode, anode, and discharge product. CMD is used to obtain understanding at longer length and time scales of processes occurring in the electrolyte and growth mechanisms of discharge products. The team will also utilize a HT screening strategy based on experiment and theory to develop a large database of properties and outcomes of electrolyte combinations that can be analyzed using ML to predict electrolytes and additives with the best performance.

Out-Year Goals. The out-year goals are to find electrolytes that give high capacities and long cycle life in an air atmosphere using HT screening.

Collaborations. This project engages in collaboration with R. Assary, J. G. Wen, and S. Tepavcevic of ANL; B. Narayanan of University of Louisville; T. Li of Northern Illinois University; and F. Khalili-Araghi and R. Klie of UIC.

Milestones

1. Investigation of a highly active tin sulfide (SnS)-based catalyst for high-rate Li-O_2 battery performance. (Q1, FY 2022; Completed)
2. Computational studies of the active sites and electronic structure of the SnS catalyst. (Q2, FY 2022)
3. Development of new electrolyte RMs that work with the SnS catalyst to decrease charge potentials and computational studies. (Q3, FY 2022)
4. Investigation of new Li-anode coatings for longer life Li-O_2 batteries with high rates. (Q4, FY 2022)

Progress Report

Li-air batteries are considered as strong candidates for the next-generation energy storage systems designed for electrical transportation. However, low cyclability and low current rates are two major drawbacks that hinder these batteries from further realization. These issues necessitate discovery of novel electrocatalysis processes to significantly enhance the formation and decomposition of the discharge products on battery cycling. The team is working on a novel co-catalytic system comprised of SnS NF / rGO as a solid catalyst and a dual functional additive that provides a liquid phase catalyst as well as anode protection. The goal of this work is to develop a co-catalytic process that enables operating the battery at high current rates up to 1 mA/cm^2. It is found that the catalytic activity of SnS NFs / rGO catalyst for both ORRs and OERs occurring during discharge and charge, respectively, far exceeds that of state-of-the-art catalysts from carbon, noble metal, and TMD families.

Thus far, cathode materials such as platinum, palladium, iridium, and oxides like Pb/BiRO, Cr_2O_3, $MnCo_2O_4$, and 2D materials such as MoS_2 have been reported to exhibit improved redox process during discharge and charge processes. However, these studies are generally limited to low current densities (for example, < 0.1 mA/cm). To operate the batteries at much higher rates, in this work, the team discovered that SnS NF catalysts embedded with rGO show an excellent catalytic activity during discharge and charge.

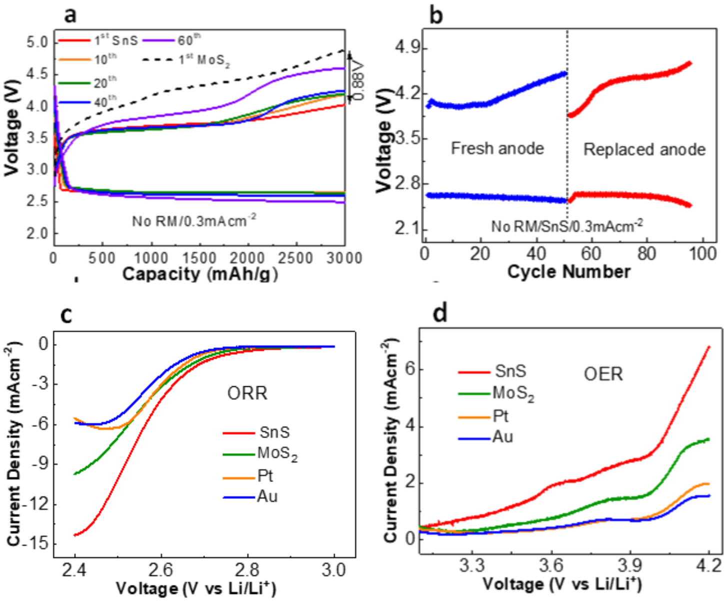

Figure 81. (a) Galvanostatic cycling results of Li–air cell with SnS/rGO and MoS_2 cathodes at the current density of 0.3mAcm^{-2}. No redox mediator was used for both batteries. The dashed black line represents the charge potential of MoS_2 at the 1st cycle. (b) Cycle numbers versus charge/discharge potential for the fresh (blue) and replaced (red) lithium anode after 50 cycles of operation of the tin sulfide (SnS) catalyst. (c-d) Linear sweep voltammetry results of SnS/rGO nanoflakes (NFs), MoS_2 NFs, gold nanoparticles (NPs), and platinum NP electrodes under oxygen reduction reaction and oxygen evolution reaction with a sweeping rate of 10 mV/s.

To evaluate the galvanostatic cycling performance of SnS catalysts, Swagelok battery cells were assembled in an Ar-filled glovebox with both oxygen and humidity levels less than 0.1 ppm. The battery is composed of a Li-metal foil anode, a porous glass-fiber separator, SnS/rGO cathode, and 30 µL of dimethylsulfoxide (DMSO) / 1-ethyl-3-methylimidazolium tetrafluoroborate (EMIM) – BF_4 (volumetric ratio of 9:1) electrolyte. Galvanostatic cycling results of the battery cells at current density of 0.3 mA/cm^2 with capacity of 3000 mAh/g (corresponding areal capacity of 0.3 mA/cm^2) are illustrated in Figure 81a. Results indicate that the battery with SnS/rGO electrode shows a charge potential of ~ 4 V at the 1st cycle, which remained below 4.3 V for 40 cycles. The battery operates up to 60 cycles before reaching the cut-off potential of 4.6 V. However, the battery with 2D MoS_2 catalyst can only run one cycle with the charge potential of 4.9 V, shown in black dashed line in Figure 81a. This is consistent with the lower catalytic activity of MoS_2 compared to SnS in Figure 81c-d. Results for platinum and gold activities are also given in these figures for comparison. To rule out the effect of lithium anode poisoning in the cyclability of the SnS-based system, they replaced the lithium anode with a fresh one after 50 cycles; results are shown in Figure 81b. It is found that the SnS catalysts are still functional for another 45 cycles at the same cut-off range, confirming stability of the catalyst and justifying the necessity of anode protection for longer battery operation.

In future work, the team will develop and characterize a new additive for this new SnS catalyst to reduce the charge potential in the voltage profiles in Figure 81a-b. This will involve a liquid catalyst that can be oxidized at a lower potential and then act as a catalyst to decompose the Li_2O_2. In addition, an additive is needed to provide lithium anode protection for longer cycling life. Failure of the anode is evidenced by the results in Figure 81b. An additive is needed that can operate for synergy with the SnS catalyst at high rates.

Patents/Publications/Presentations

Publication

- Majidi, L., A. Ahmadiparidari, N. Shan, S. K. Singh, C. Zhang, Z. Huang, S. Rastegar, K. Kumar, Z. Hemmat, A. T. Ngo, P. Zapol, J. Cabana, A. Subramanian, L. A. Curtiss, and A. Salehi-Khojin. "Nanostructured Conductive Metal Organic Frameworks for Sustainable Low Charge Overpotentials in Li-Air Batteries." *Small* 18, No. 4 (2021). doi: 10.1002/smll.202102902.

Task 6.3 – Development of a High-Rate Lithium-Air Battery Using a Gaseous CO_2 Reactant (Amin Salehi-Khojin, University of Illinois, Chicago)

Project Objective. The main objective of this project is to develop a novel strategy to enable operation of Li-CO_2 batteries at high-capacity high-rate with a long-cycle-life. The experiments will be performed in both Swagelok and pouch cells. In the former case, the team will use: (1) a novel co-catalyst system comprised of inexpensive and earth-abundant TMD materials that work in synergy with IL-based electrolytes to enhance efficiency of reactions during discharge and charge processes, (2) a solution-based catalyst (RM) to reduce charge overpotential and increase energy efficiency of the battery, (3) high porosity cathode electrodes to increase electrode surface area, gas permeability, stability, electrical conductivity, and lifetime of battery operation, and (4) SEI layer to protect the anode against oxidation without affecting the ionic transport of Li^+ species in the system. At the pouch-cell level, the team will design and construct a stackable pouch cell to deliver a capacity of > 200 mAh.

Impact. Li-air batteries are considered as a potential alternative to Li-ion batteries for transportation applications due to their high theoretical specific energy. Most work in this area focuses on use of O_2 as the reactant. However, newer concepts for using gaseous reactants, such as CO_2 that has a theoretical specific energy density of 1,876 Wh/kg, provide opportunities for further exploration. This project will produce a thorough understanding of key chemical and electronic parameters that govern the operation of Li-CO_2 batteries in realistic conditions. Achieving the project objectives will generate a library of fundamental properties of TMD- and IL-based electrolytes with the most promise for Li-CO_2 battery applications. The methodologies employed, and the insight generated, will also be valuable beyond advancing the field of Li-CO_2 batteries.

Approach. The above targets will be achieved through an integrated approach based on materials synthesis, testing, characterization, analysis, and computation. The team will synthesize catalysts and test them in cells along with developing new electrolytes and additives. These cathode materials with new electrolyte blends and additives will work in synergy to reduce charge potentials and increase battery stability. DFT and AIMD simulations will be performed to understand battery operation and make predictions of new materials for the Li-CO_2 battery.

Out-Year Goals. The out-year goals are to find novel 2D catalysts and IL-based electrolytes that give high capacities and long cycle life in a CO_2 atmosphere.

Collaborations. This project collaborates with L. A. Curtiss (ANL), F. Khalili-Araghi (UIC), A. Subramanian (UIC), and Z. Huang (Stockholm University).

Milestones

1. Successful synthesis and characterization of bulk and 2D forms of six alloy TMDs for electrocatalysis and battery experiments. (Q1, FY 2022; Completed)
2. Successful exfoliation of TMD alloys with desired lateral sizes for battery experiments. (Q2, FY 2022; Initiated)
3. Initiation of electrolyte blend development and characterization for battery experiments. (Q3, FY 2022)
4. Charge transfer properties of different TMD alloys. (Q4, FY 2022)

Progress Report

Most current research in energy storage for EVs and flights focuses on incremental advances in Li-ion batteries. In recent years, research has also focused on new concepts that go beyond Li-ion batteries, with many challenges in making the new concepts feasible. Considerable effort has been spent on batteries based on chemical transformations, including Li-S and Li-air batteries based on oxygen (Li-O_2), with the latter having the highest theoretical energy density (3500 Wh/kg). Another chemical transformation involving air components that has been less studied is batteries based on a CO_2 reactant, that is, the Li-CO_2 battery. Such a battery has a theoretical energy density of 1876 Wh/kg.

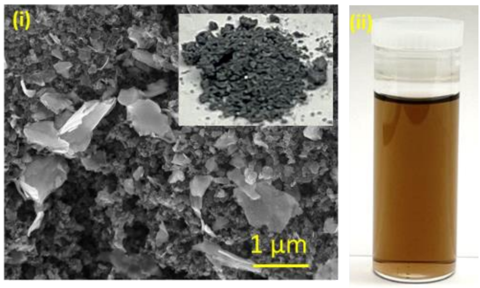

Figure 82. Synthesis of powder followed by liquid exfoliation before deposition on the substrate.

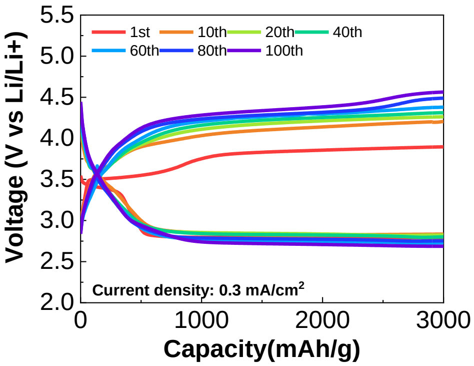

Figure 83. Discharge/charge curves at current density and capacity of 0.3 mA/cm^2 and 300 mAh/g, respectively.

A Li-air battery based on a CO_2 reactant has major advantages over batteries based on O_2, including: (1) the gaseous component CO_2 is less reactive than O_2, making battery operation safer, (2) they avoid the lithium superoxide intermediate that can induce electrolyte detrimental reactions, (3) the Li_2CO_3 discharge product is more stable and less reactive than the Li_2O_2 product in the Li-O_2 battery, and (4) the reaction mechanisms during discharge and charge processes are not as complex as in Li-O_2 batteries. Moreover, the Li-air battery based on a CO_2 reactant has potential for reversible carbon fixation for energy storage systems.

This quarter, the team discovered a novel combination of TMD alloy structure as a cathode catalyst and a bi-functional RM that works in synergy with IL-based electrolyte to operate the battery high rates. Figure 82 shows the synthesized powder and dispersion of NFs before deposition on the substrate. Thus far, the battery is capable of operating under 0.3 mA/cm^2 and high capacities of 0.3 mAh/cm^2 (corresponding to 3000 mAh/g) up to 100 cycles (see Figure 83). The battery with platinum NP, gold NP, and MoS_2 as one of the best 2D catalysts with the same electrolyte blend and experimental conditions operates less than 10 cycles. The achieved capacities and current rates are by far the highest values to be reported in the literature for this type of battery.

The team's results also indicate remarkable catalytic activity for this system for CO_2 reduction and evolution reactions (CO_2RR/CO_2ER) occurring during discharge and charge, respectively, far exceeding performance of platinum and gold NPs under identical conditions. Results are shown in Figure 84.

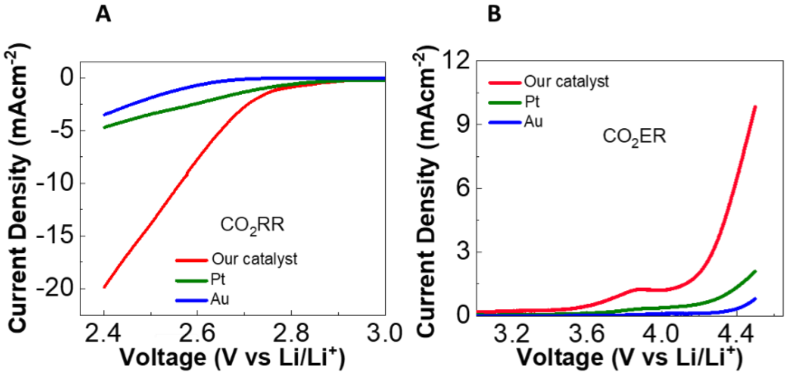

Figure 84. Linear sweep voltammetry results of studied catalysts for CO_2 reduction (a) and CO_2 evolution (b) reactions.

To study the discharge products, several characterization techniques were performed on the cathode surface, such as SEM, Raman spectroscopy, and differential electrochemical mass spectroscopy (DEMS), to verify crystal structure, morphology, and elemental and chemical composition of the products. Further characterization is under way.

Patents/Publications/Presentations

The project has no patents, publications, or presentations to report this quarter.

TASK 7 – SODIUM-ION BATTERIES

Team Lead: Xiao-Qing Yang, Brookhaven National Laboratory

Summary

The Na-ion battery will require investigations to identify optimal electrode materials, electrolytes, separators, and binders to reach full potential. The BMR program will therefore have a limited effort directed toward identifying Na-ion battery materials that have potential value for vehicle applications. Progress on these projects this quarter is described in this report.

Highlights. The highlights for this quarter are as follows:

- The ANL team combined *in situ* SXRD and XAS to reveal the capacity fade of O3 sodium layered oxide $NaNi_{0.4}Mn_{0.4}Co_{0.2}O_2$ cathode at both low (2.0-3.8 V) and high voltage (2.0-4.4 V). Their results showed that charging voltage limit does not play a dominant role in triggering capacity fade of O3 sodium layered cathodes with native lattice strain.
- The BNL team carried out structure evolution studies of $NaMnFeCoNiO_2$, using SXRD and HAADF-STEM. It was found that after the 1st charge process, the atomic structure of $Na_{0.85}Li_{0.1}Ni_{0.175}Mn_{0.525}Fe_{0.2}O_2$ is partially transformed from O3-type to P3-type, resulting in a mixture of O3 and P3 structure in this high-energy-density cathode material after 1st cycle.
- At LBNL, an improved ion-exchange process was used to make a lepidocrocite-structured $Mg_{0.37}Ti_{1.815}O_4$ phase. The replacement of interlayer monovalent cations with divalent magnesium increases the number of available sites for sodium insertion during electrochemical sodiation. This electrode was found to cycle better than the sodiated version.
- The PNNL team developed high-voltage electrolytes based on tetraglyme and fluorinated solvent for high-voltage cathode $NaNi_{0.68}Mn_{0.22}Co_{0.1}O_2$. The cycling performance of $Na||NaNi_{0.68}Mn_{0.22}Co_{0.1}O_2$ half-cell was significantly improved when using electrolyte of tetraethylene glycol dimethyl ether (TEGDME) and 10%vol vinylene carbonate (VC). The electrolyte using mixtures of 2,2,2-trifluoroethyl phosphate (TFP) and dimethyl carbonate (DMC) or tetramethylsilane (TMS) as solvents demonstrated excellent performance for full cell of hard carbon||NaNMC.

Task 7.1 – Exploratory Studies of Novel Sodium-Ion Battery Systems
(Xiao-Qing Yang and Enyuan Hu, Brookhaven National Laboratory)

Project Objective. To meet the challenges of powering PHEVs and BEVs, new rechargeable battery systems with high energy and power density, low cost, good abuse tolerance, and long calendar and cycle life need to be developed. The primary objective of this project is to develop new advanced synchrotron-based material characterization techniques and apply these techniques to study the new rechargeable battery systems beyond the Li-ion batteries, namely the Na-ion battery systems for EVs.

Project Impact. The results of this project will be used for developing technologies that will significantly increase the energy density and cycle life and reduce the cost of beyond Li-ion battery systems. This will greatly accelerate deployment of EVs and reduce carbon emission associated with fossil fuel consumption and will help in the direction of building U. S.-based energy storage manufacture chains.

Approach. This project will use synchrotron-based *in situ* X-ray diagnostics such as *in situ* XRD and *in situ* XAS tools, combined with TEM, STEM, and TXM imaging techniques developed at BNL to evaluate the new materials and redox couples to obtain in-depth understanding of the reaction mechanisms of these materials, aiming to improve existing materials and to provide guidance for new materials and new technology development for Na-ion battery systems.

Out-Year Goals. The out-year goal is to complete the SXRD, XAS, and XANES studies of new cathode materials of $NaMnFeCoNiO_2$ (NMFCN) and P2- $Na_{0.66}[Cu_{0.33}\ Mn_{0.67}]O_2$ for Na-ion batteries.

Collaborations. The BNL team has been closely working with top scientists on new material synthesis at ANL, LBNL, and PNNL, with U. S. industrial collaborators at GM and Johnson Controls, and with international collaborators.

Milestones

1. Complete XRD and TEM studies on a high-capacity and high-C rate multi-component sodium cathode materials NMFCN at pristine and after 1st charge state to study the structural changes of this material. (Q1, FY 2022; Completed)
2. Complete *in situ* XRD studies on a new P2-structured $Na_{0.66}[Cu_{0.33}\ Mn_{0.67}]O_2$ cathode material for Na-ion batteries during charge-discharge cycling. (Q2, FY 2022; In progress)
3. Complete *in situ* copper and manganese K-edge XAS studies on P2-structured $Na_{0.66}[Cu_{0.33}\ Mn_{0.67}]O_2$ materials during charge-discharge cycling to understand the redox contributions of copper and manganese of this material. (Q3, FY 2022; In progress)
4. Complete the soft XAS studies of $Na_{0.66}[Cu_{0.33}\ Mn_{0.67}]O_2$ materials at pristine and charged to 3.6 V and 4.1 V states to understand the redox contribution of oxygen. (Q4, FY 2022; In progress)

Progress Report

This quarter, the team completed the first FY 2022 milestone. Advanced diagnostic techniques have been successfully applied to the studies of the new sodium cathode materials NMFCN. To understand the structure evolution of NMFCN, SXRD and HAADF-STEM are performed. The XRD results in Figure 85a show the O3-type layer structure of NMFCN pristine material. Figure 85b-c shows the atomic structure of NMFCN in pristine state and after 1st charge, respectively. The contrast of HAADF-STEM images in Figure 85b-c is sensitive to the atomic number of the projected underlying atomic columns. The constant intensity in Figure 85b indicates that TMs are uniformly distributed throughout the particle, and the O3-structure observed by using STEM is consistent with the XRD results shown in Figure 85a. Interestingly, it is found that after the 1st charge process, the atomic structure of NMFCN is partially transformed from O3-type to P3-type. As shown in Figure 85c, after 1st charge, there is a mixture of O3 and P3 structure in this material. Figure 85d schematically shows the phase transformation from pure O3 structure to a mixture of O3-P3 structure after 1st charge.

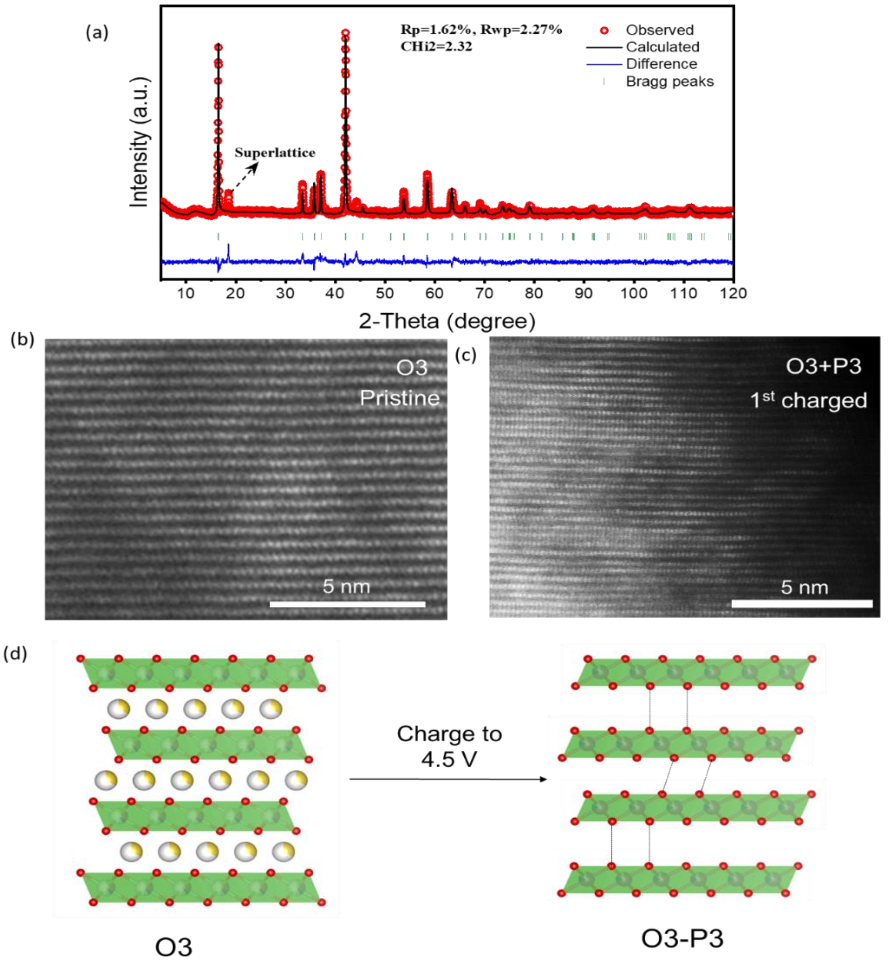

Figure 85. Structure characterization. (a) X-ray diffraction of pristine NaMnFeCoNiO$_2$. (b) High-angle annular dark field – scanning transmission electron microscopy (HAADF-STEM) image of pristine NaMnFeCoNiO$_2$. (c) HAADF-STEM image of NaMnFeCoNiO$_2$ after 1st charge. (d) Schematic illustration of phase transformation during 1st charge.

Patents/Publications/Presentations

Publication

- Cao, M-H.,* R-Y. Li, S-Y. Lin, S-D. Zheng, L. Ma, S. Tan, E. Hu, Z. Shadike,* X-Q. Yang,* and Z-W. Fu.* "Oxygen Redox Chemistry in P2-$Na_{0.6}Li_{0.11}Fe_{0.27}Mn_{0.62}O_2$ Cathode for High-Energy Na-Ion Batteries." *Journal of Materials Chemistry A* 9 (2021): 27651–27659. doi: 10.1039/D1TA08471B.

Task 7.2 – Development of a High-Energy Sodium-Ion Battery with Long Life (Chris Johnson and Khalil Amine, Argonne National Laboratory)

Project Objective. The project objective is to develop a high-energy Na-ion battery with long life. Moreover, the battery chemistry should utilize low-cost materials. The energy density target is 200 Wh/kg and/or 500 Wh/L, wherein the anode and cathode capacity targets are 600 $mAhg^{-1}$ and 200 $mAhg^{-1}$, respectively.

Project Impact. A Na-ion battery on par with the energy density of a Li-ion battery can have a high impact in the transportation sector with the assumption that the cost is significantly below $85/kWh and that the battery pack provides a 300-mile range. The consumer is not concerned about the battery chemistry employed if these metrics can be met. Development of these battery chemistries will situate the United States in a strong position as relates to new low-cost energy storage systems beyond lithium ion.

Approach. In a team approach, the Na-ion battery group will create a versatile Na-ion battery chemistry with beneficial advantages such as low cost, safety, recycling, and sustainability of materials used. The team will work synergistically so that the final design is the culmination of advances in phosphorus carbon composites mated with optimized lead or other highly dense metalloids, such as tin and/or antimony and derivatives thereof, for the recyclable anode. Synthesis and optimization of such blended composite anodes will be conducted in parallel to diagnostic characterization of structures, phase formation, and cycling stability. Cathode work will begin at the end of the first year and will involve gradient cathodes consisting of Fe-Mn compositions, as well as intergrowths of layer stacking sequenced oxides. If resources allow, the team also will attempt to stabilize cathode surfaces using ALD methods, particularly for the benefit of staving off dissolution of manganese and iron / electrolyte reactivity. Electrolytes will be partly procured from H. Li at PNNL.

Out-Year Goals. The state-of-the-art Na-ion battery in the literature has now been surpassed by this team, but performance is still too low for commercialization. Thus, the goal is to move forward and continually invent the most superior Na-ion battery chemistry that can compete worldwide through work output from this project.

Collaborations. Researchers from PNNL who are developing electrolytes for Na-ion batteries will provide this project with formulations to test with the various electrode combinations investigated at ANL.

Milestones

1. Investigate effect of native structural defects on high-voltage stability of sodium layered cathodes. (Q1, FY 2022; In progress)
2. Develop high-capacity single-crystal Ni-rich layered oxide cathodes with > 150 mAh/g and stable cycle life of > 100 cycles. (Q2, FY 2022; In progress)
3. Develop engineered surface for better air-storage and high-voltage stability. (Q2, FY 2022; In progress)
4. Develop concentration gradient layered oxide cathode with 130 mAh/g and stable cycle life of > 200 cycles. (Q3, FY 2022; In progress)
5. Investigate novel local atomic structural features to stabilize high oxidation state of iron active species. (Q4, FY 2022; In progress)
6. Optimize structure/electrolytes to enhance cycling stability of high-areal-capacity phosphorus anode and layered oxide cathodes. (Q4, FY 2022; In progress)

Progress Report

In FY 2021, the team synthesized an O3 $NaNi_{0.4}Mn_{0.4}Co_{0.2}O_2$ cathode with high reversible capacity of ~ 180 mAh/g and high initial CE of 95%, but that underwent severe capacity fading when cycling within 2.0-4.4 V. It would be very promising if the team can stabilize such high specific capacity. Thus, understanding of its degradation mechanism at high voltage is essential.

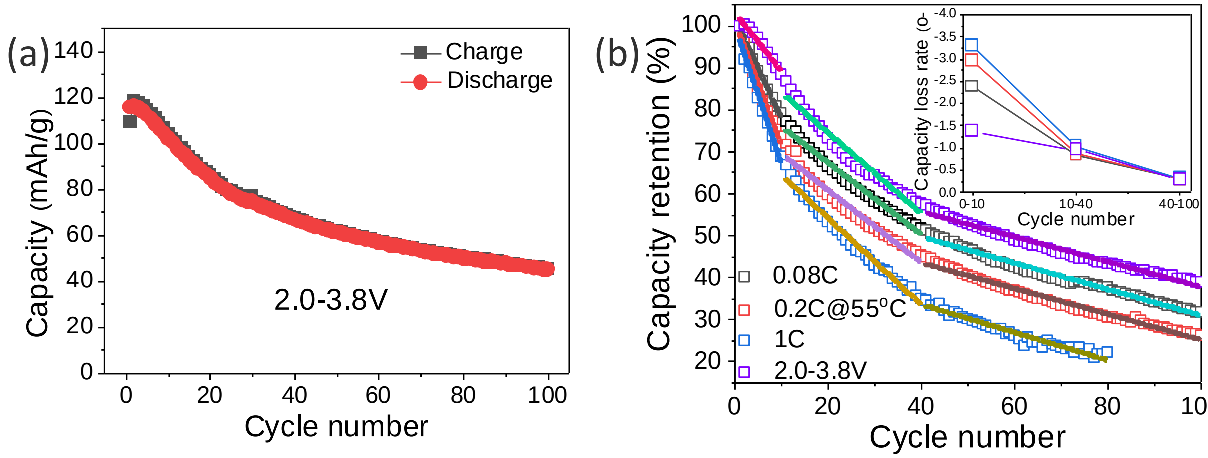

Figure 86. (a) Cycling performance of strained O3 $NaNi_{0.4}Mn_{0.4}Co_{0.2}O_2$ cathode within 2.0–3.8 V at 0.08C. (b) Normalized capacity retention of O3 $NaNi_{0.4}Mn_{0.4}Co_{0.2}O_2$ cathode at different cycling conditions. The capacity loss rate in (b) is the slope of the linear fitting curve of the capacity.

Previous characterization showed that the high-voltage instability may come from parasitic side reactions with the electrolytes. The team therefore reduced the charge cut-off voltage from 4.4 V to 3.8 V. Surprisingly, cycle stability was not improved by lowering the charge cut-off voltage, which contradicts results in other studies of reported sodium layered oxide cathodes with a narrow voltage window. A capacity retention of only 38.7% was attained after 100 cycles (Figure 86a). Moreover, the charge/discharge test of the highly strained $NaNi_{0.4}Mn_{0.4}Co_{0.2}O_2$ cathode at elevated voltage or temperature demonstrated similar rapid degradation (Figure 86b). Interestingly, the capacity fade rate (inset in Figure 86b), which was obtained by linear fitting of the capacity retention curve, is almost the same after the first 10 cycles, regardless of voltage window, testing temperature, and charge/discharge rate, whereas significantly different results were exhibited for the first 10 cycles. Results indicate that the capacity degradation of the highly strained $NaNi_{0.4}Mn_{0.4}Co_{0.2}O_2$ cathode might be controlled by a specific factor, while such factor was regulated by the operating condition in the early stage of charge/discharge.

To further elucidate the degradation mechanism, *in situ* nickel K-edge XANES characterization was carried out to understand the redox couple evolution of the highly strained $NaNi_{0.4}Mn_{0.4}Co_{0.2}O_2$ cathode during charge/discharge within 2.0-4.4 V, which can provide the oxidation state changes of nickel element during battery operation. As shown in Figure 87a-b, the nickel K-edge shifted to high energy on extraction of Na^+ due to the oxidation of Ni^{2+} to Ni^{3+}/Ni^{4+} during charge, while it shifted back to lower energy during discharge due to the reduction of Ni^{3+}/Ni^{4+} to Ni^{2+}. In general, as shown in the 2D contour plot of nickel K-edge XANES throughout the whole charge/discharge process (Figure 87c), the nickel undergoes a highly reversible nickel oxidation/reduction during charge/discharge within 2.0-4.4 V. Even after cycling for 10 cycles has triggered severe capacity degradation in the strained O3 cathode, nickel still exhibits reversible redox reactions (Figure 88a), which cannot explain the severe capacity loss of strained $NaNi_{0.4}Mn_{0.4}Co_{0.2}O_2$ cathode reported here. The redox reaction behavior of cobalt and manganese in the O3 strained $NaNi_{0.4}Mn_{0.4}Co_{0.2}O_2$ cathode was also explored, showing reversible transformation during cycling within 2.0-4.4 V (Figure 88b-c), indicating that the observed capacity degradation is not from the cycling-induced structural transformation.

The team further performed *in situ* SXRD to reveal the phase transition of strained $NaNi_{0.4}Mn_{0.4}Co_{0.2}O_2$ cathode with controlled voltage window. Figure 87d shows the 2D contour plot of *in situ* SXRD patterns during charge/discharge within 2.0-4.4 V, in accompaniment with the corresponding voltage curve and phase transition process. As shown, the electrode before charge/discharge can be well indexed using O3 phase. On charge, the (003) and (006) peaks shifted toward lower angles, which indicated an expansion of the *c* lattice parameter due to the increased oxygen electrostatic repulsion between oxygen layers induced by the removal of Na^+. Meanwhile, the (101), (102), (110), and (113) peaks moved towards higher angles during charge, corresponding to shrinkage of *a* lattice parameter due to the oxidation of TM. In addition, the intensity of O3 phase gradually decreased, while the peaks of O1 phase started to appear. On further charge, the O1 phase was then transformed into P3 phase starting at 3.37 V. At the long plateau beyond 4.0 V, the structure of P1 phase started to dominate the charged product. At the end of the charge process, an unknown X phase with low sodium content and crystallinity was formed. Therefore, the phase transformation of strained $NaNi_{0.4}Mn_{0.4}Co_{0.2}O_2$ cathode during high-voltage charge can be described as O3 → O1 → P3 → P1 → X, which is similar to the previously reported O3 sodium layered cathode when charged to high voltage. During the discharge process, the phase transformation process reversed. However, at the beginning of the discharge process, the XRD intensities of (00*l*) peaks are very weak and broad, indicating severe lattice strain at the *c*-axis direction that prevents the re-insertion of Na^+. Moreover, as evidenced by the disappearance of O3 (003), (006), (101), (108), and (110) peaks of O3 phase, the O1 phase (rather than the original O3 phase) dominated the fully discharged electrode, indicating an irreversible phase transition during high-voltage cycling.

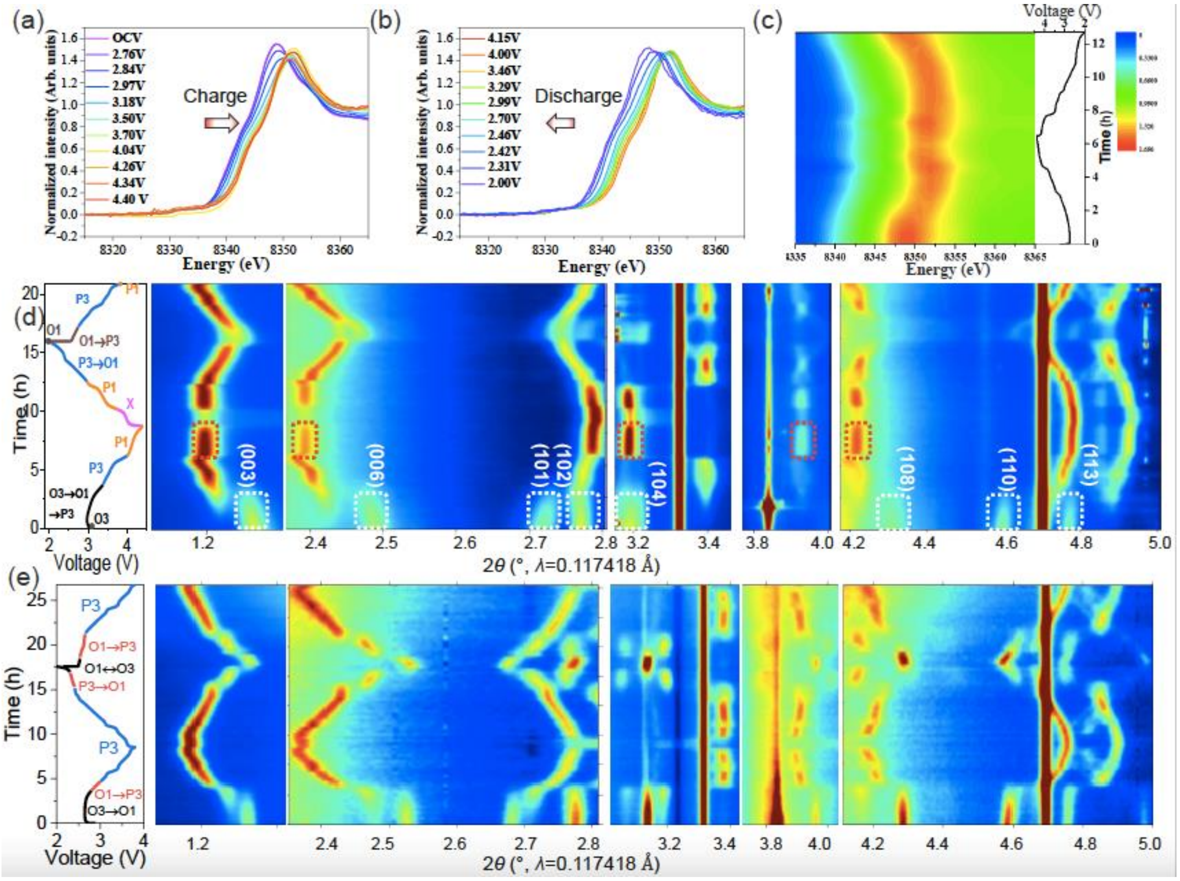

Figure 87. *In situ* synchrotron characterization during charge/discharge. *In situ* nickel K-edge X-ray absorption near-edge spectroscopy of strained O3 $NaNi_{0.4}Mn_{0.4}Co_{0.2}O_2$ within 2.0-4.4 V: (a) during charge, (b) during discharge, and (c) 2D contour plot during charge/discharge. Voltage profiles and the corresponding 2D contour plot of *in situ* synchrotron-based X-ray diffraction patterns during charge/discharge of O3 $NaNi_{0.4}Mn_{0.4}Co_{0.2}O_2$ cathode within (d) 2.0-4.4 V and (e) 2.0-3.8 V. The color in (c-e) represents the intensity, with red for highest and blue for lowest.

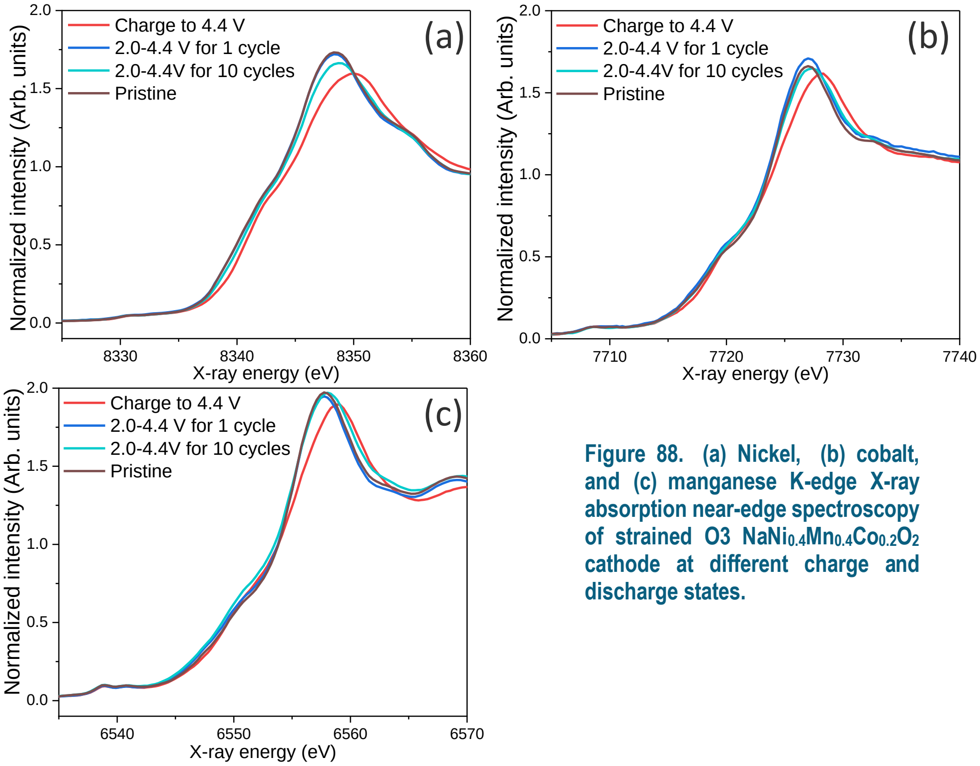

Figure 88. (a) Nickel, (b) cobalt, and (c) manganese K-edge X-ray absorption near-edge spectroscopy of strained O3 $NaNi_{0.4}Mn_{0.4}Co_{0.2}O_2$ cathode at different charge and discharge states.

In sharp contrast with that charge/discharge within 2.0-4.4 V, the highly strained $NaNi_{0.4}Mn_{0.4}Co_{0.2}O_2$ cathode exhibited a highly reversible phase transformation of O3↔ O1 ↔ P3 with a lower charge cut-off voltage of 3.8 V. As clearly shown in Figure 87e, the *in situ* SXRD patterns during the whole charge/discharge process presented a highly symmetric feature, and all the peaks of O3 phase were fully recovered at the end of the discharge process. Such a reversible phase transition during charge/discharge of layered oxide cathodes is often considered favorable for stabilization of cycle performance. However, the team illustrates that this is not the case of the highly strained $NaNi_{0.4}Mn_{0.4}Co_{0.2}O_2$ cathode (Figure 87e).

These results indicate that the capacity degradation of strained O3 $NaNi_{0.4}Mn_{0.4}Co_{0.2}O_2$ cathode is not due to cycling-induced structural deformation but may be related to native structural features. The team will further use advanced electron microscopy to examine the native crystallographic structure and investigate how it affects degradation during cycling.

Patents/Publications/Presentations

Publications

- Liu, X., X. Zhou, Q. Liu, J. Diao, C. Zhao, L. Li,* Y. Liu,* W. Xu, A. Daali, R. Harder, I. K. Robinson, M. Dhabi, J. Alami, G. Chen, G. L. Xu,* and K. Amine.* "Multiscale Understanding of Surface Structural Effects on High-Temperature Operational Resiliency of Layered Oxide Cathodes." *Advanced Materials* 34, No. 4 (2022): 2107326. doi: 10.1002/adma.202107326 (2021).
- Xiao, B., X. Liu, X. Chen, G. H. Lee, M. Song, X. Yang, F. Omenya, D. Reed, V. Sprenkle, Y. Ren, C. J. Sun, W. Yang, K. Amine, X. Li,* G. L. Xu,* and X. Li.* "Uncommon Behavior of Li Doping Suppresses Oxygen Redox in P2-Type Manganese-Rich Sodium Cathodes." *Advanced Materials* 33, No. 52 (2021): 2107141. doi: 10.1002/adma.202107141.
- Xiao, B., X. Liu, M. Song, X. Yang, F. Omenya, S. Feng, V. Sprenkle, K. Amine, G. L. Xu, X. Li, and D. A. Reed. "A General Strategy for Batch Development of High-Performance and Cost-Effective Sodium Layered Cathodes." *Nano Energy* 89, Part A (2021): 106371. doi: 10.1016/j.nanoen.2021.106371.

Presentation

- MRS Fall Meetings & Exhibits, Virtual (December 6–8, 2021): "Development of Layered Oxides Cathodes and N Phosphorus Anode for High-Energy and Low-Cost Sodium-Ion Batteries": G-L. Xu* and K. Amine.

Task 7.3 – Tailoring High-Capacity, Reversible Anodes for Sodium-Ion Batteries (Marca M. Doeff, Lawrence Berkeley National Laboratory)

Project Objective. The project objective is to understand the role vacancies, surface defects, and bulk structure play in determining electrochemical properties of high capacity, stepped layered titanate anodes.

Project Impact. Although several suitable cathode materials for Na-ion batteries exist, there are few suitable anode materials due to low potential instabilities. Sodium titanate anodes are a promising class of materials for this application. The electrochemical properties can be manipulated through structural and surface modifications.

Approach. The structure and surface properties of candidate stepped layered titanates will be modified through manipulation of synthetic parameters. Materials will then be characterized electrochemically and physically to understand the role that surface defects, vacancies, and bulk structure play in determining electrochemical behavior.

Out-Year Goals. The out-year goal is to achieve development of an electrode that can deliver 225 mAh/g at C/3 rate with good capacity retention (80% or better) for 100 cycles.

Collaborations. The team collaborates with beam line scientists at SSRL and the ALS at LBNL.

Milestones

1. Conduct hot stage experiments on lepidocrocite titanates. (Q1, FY 2022; In progress, postponed due to equipment issues)
2. Complete physical and electrochemical characterization of lepidocrocite titanates. (Q2, FY 2022; In progress)
3. Attempt surface modification of lepidocrocite titanates. (Q3, FY 2022)
4. *Go/No-Go Decision*: Surface modification methods; stop if performance is not improved. (Q4, FY 2022)

Progress Report

Equipment issues prevented the team from carrying out the *in situ* hot stage experiments due this quarter. They intend to proceed when the equipment is repaired. Alternatively, they will utilize SXRD capabilities at either the APS mail-in service or SSRL.

This quarter, the team optimized the magnesium ion exchange process of cesium titanate to make a material with nominal composition $Mg_{0.37}Ti_{1.815}O_4$. Replacing monovalent cesium cations with divalent cations like Mg^{2+} rather than Na^+ reduces the number of occupied sites in the interlayers by half; thus, this approach may increase reversible capacity of the lepidocrocite. By refreshing the $MgCl_2$•$6H_2O$ solution every two days, a complete Cs^+/Mg^{2+} ion-exchange can be achieved by stirring one gram of $Cs_{0.74}Ti_{1.815}O_4$ material in 100 mL aqueous 4 M $MgCl_2$•$6H_2O$ solution at 80°C in a heated mineral oil bath for 7 days. Without the refreshing step, previously $Mg_{0.37}Ti_{1.815}O_4$ could only be prepared by Na^+/Mg^{2+} ion-exchange from $Na_{0.74}Ti_{1.815}O_4$, requiring a two-step ion exchange process. The resulting Mg^{2+} ion-exchanged phase retains the same body-centered orthorhombic symmetry as the Na^+ ion-exchanged phase (Figure 89). Mg^{2+} ion-exchange also produces a highly swollen phase (probably a bilayer hydrate), as marked by an asterisk in Figure 89. This swollen phase disappears after drying at 100°C overnight under vacuum.

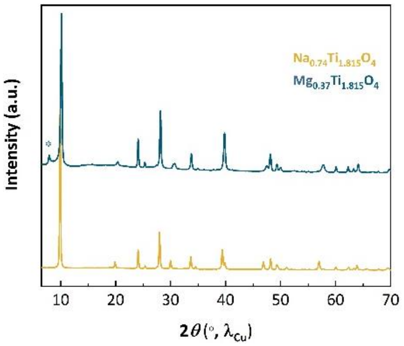

Figure 89. Synchrotron X-ray diffraction patterns of $Mg_{0.37}Ti_{1.815}O_4$ and $Na_{0.74}Ti_{1.815}O_4$.

The long-term cycling performance of $Mg_{0.37}Ti_{1.815}O_4$ electrodes was evaluated, and typical results are presented in Figure 90. Although $Mg_{0.37}Ti_{1.815}O_4$ electrodes show slightly lower initial discharge/charge capacities compared to $Na_{0.74}Ti_{1.815}O_4$ (205 mAh/g for $Mg_{0.37}Ti_{1.815}O_4$ and 228 mAh/g for $Na_{0.74}Ti_{1.815}O_4$), the capacity retention appears better for $Mg_{0.37}Ti_{1.815}O_4$. After 20 cycles, 87% of the 2nd discharge capacity was obtained with CE of 95.3% in the 2nd cycle and > 98.0% from the 7th cycle onward (Figure 90a). The dQ/dV plots reveal that $Mg_{0.37}Ti_{1.815}O_4$ has lower average Na^+ storage potential than $Na_{0.74}Ti_{1.815}O_4$, which is more favorable for anode materials (Figure 90b).

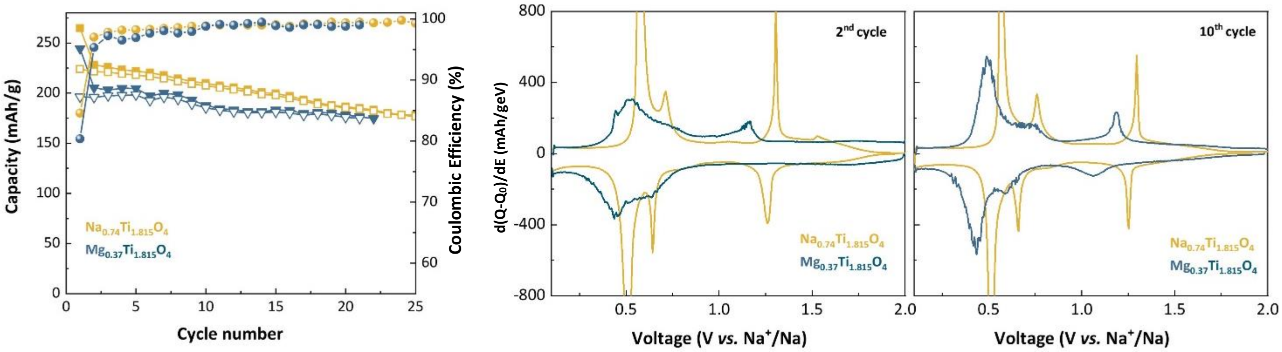

Figure 90. (a) Discharge/charge capacity retention and Coulombic efficiency of $Mg_{0.37}Ti_{1.815}O_4$ and $Na_{0.74}Ti_{1.815}O_4$ electrodes. (b) The 2nd and 10th cycle dQ/dV plots of $Mg_{0.37}Ti_{1.815}O_4$ and $Na_{0.74}Ti_{1.815}O_4$. All cells were cycled in 0.5 M $NaPh_4B$/DEGDME electrolyte at a current rate of 8 mA g^{-1}.

The team utilized hard and soft XAS to obtain insights on the redox properties of $Mg_{0.37}Ti_{1.815}O_4$ when used as a Na-ion anode material (Figure 91a-c). While hard XAS probes the TM K-edge in the bulk of the material, soft XAS probes the L-edge in the sub-surface regions of the material, with the depth dependent on the detection mode. The fluorescence yield mode penetrates ~ 100 nm into the sample. The titanium oxidation state is 4+ in the pristine material. On discharging to 0.1 V versus Na^+/Na, a slight shift to lower energy indicating partial reduction of Ti^{4+} to Ti^{3+}. However, after the 1st cycle, the edge energy did not fully recover to the pristine state, indicating that not all of the titanium is re-oxidized to the tetravalent state. This apparent irreversibility is also observed in the titanium L-edge spectra.

Ex situ SXRD experiments were conducted to study the structural changes of $Mg_{0.37}Ti_{1.815}O_4$ electrode during (de)sodiation (Figure 91d). The insertion of large sodium ions should result in an increase in the interlayer spacing. However, in the XRD pattern of the fully discharged electrode, the (020) reflection (ça. $2\theta=10$ degree) moved slightly to the right, suggesting slight contraction in the *b* direction. This probably implies that some interlayer water was expelled on insertion of Na^+. In addition, all the reflections were broadened and less intense than those of the pristine electrode, suggesting some structural disordering. On recharging to 2.0 V versus Na^+/Na, the (020) reflection almost moves back to its original position, and all the reflections become narrower and more intense, suggesting good structural integrity of $Mg_{0.37}Ti_{1.815}O_4$.

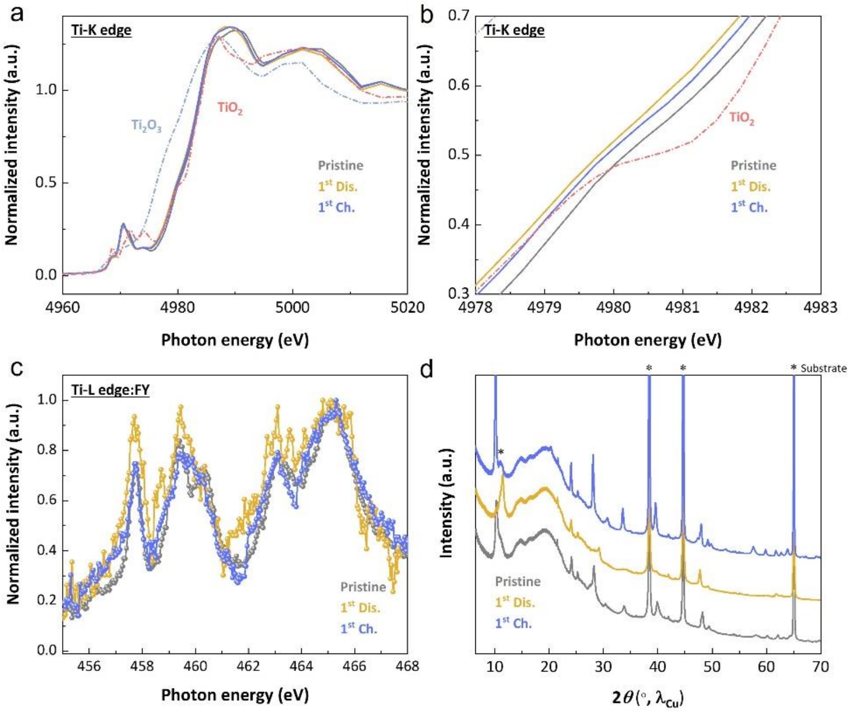

Figure 91. (a) Titanium K-edge spectra in the X-ray absorption near-edge spectroscopy region for $Mg_{0.74}Ti_{1.815}O_4$ electrode at end of the 1st discharge and charge, and their corresponding magnification view (b). (c) Titanium L-edge spectra in the fluorescence yield mode, and (d) *ex situ* synchrotron X-ray diffraction patterns of $Mg_{0.74}Ti_{1.815}O_4$ electrodes at end of the 1st discharge and charge.

Patents/Publications/Presentations

Presentations

- ECS, San Francisco Section – Young Investigator Lecture Series, Virtual (November 19, 2021): “Developing Titanium-Based Anode Materials for Sodium-Ion Batteries’’; W. Yin and M. M. Doeff. Invited.
- MRS Fall Meetings & Exhibitions, Boston, Massachusetts (November 29 – December 2, 2021): “New Anode Materials for Sustainable Sodium-Ion Batteries”; M. M. Doeff.

Task 7.4 – Electrolytes and Interfaces for Stable High-Energy Sodium-Ion Batteries (Phung M. L. Le, Pacific Northwest National Laboratory)

Project Objective. The Na-ion battery is a potential alternative energy source for EVs and grid applications due to the low cost and the natural abundance of sodium. The performance of Na-ion batteries largely depends on development of electrode materials and electrolytes. In recent years, a series of potential electrode materials has been developed. However, a fundamental understanding of the electrochemistry of Na-ion batteries, especially the stability of the electrode-electrolyte interface in these batteries, is still not well established. This project will develop innovative electrolytes to enable fundamental understanding on the interface between electrode and electrolyte for stable operation of high-energy Na-ion batteries. A high-capacity anode will also be developed. The proposed research will enhance the achievable capacities of both anode and cathode for Na-ion battery and improve the stability of electrodes/electrolyte interface, establish correlation (electrolyte design rule) between electrochemical performances of Na-ion batteries and the electrolyte/interface properties, and enable long cycle life and safe operation of high-energy Na-ion batteries.

Project Impact. This project will develop new electrolytes to enable long cycle life and safe operation of Na-ion batteries. If successful, the resulting improvements in energy, life, and safety will provide a solid contribution to the understanding of fundamental scientific questions and the development for Na-ion battery technology and promote its practical application as a competitive alternative to the current Li-ion batteries and greatly reduce the cost of energy storage systems for EVs.

Approach. This project will continuously optimize the electrolyte components and concentrations to develop innovative electrolytes and additives with improved electrochemical and physical properties. Ether-based electrolytes with different salts and additives will be optimized toward both anode (sodium metal and hard carbon) and cathode. Phosphate-based LHCE will be optimized to improve cycling performance of Na-ion batteries. SEI/CEI components of Na-ion battery in ether and phosphate electrolytes will be studied using XPS and SEM/TEM techniques to reveal the fundamental mechanism behind the improved stable performance of Na-ion batteries. Electrolyte additives in carbonate electrolyte will also be investigated to improve the electrochemical cathode performance. These approaches will unravel the origin of the SEI at the dynamic interface, providing guidance for the electrolyte and interface design and enabling high capacity and long life of Na-ion batteries.

Out-Year Goals. This project will select electrolyte compounds and identify formation of interfacial SEI layer on hard carbon and CEI layer-on-layer oxide cathode and its effect on electrode materials. It will also provide guidance on electrolyte optimization and to improve CE of sodium deposition/stripping to be more than 99%.

Collaborations. This project will collaborate with leading scientists at ANL, LBNL, and other organizations in the field of cathode and anode materials for Na-ion batteries. It will also collaborate with C. Wang and M. Engelhard of PNNL for TEM and XPS characterization.

Milestones

1. Develop high-voltage electrolytes based on fluorinated solvent (≥ 4.2 V) to be compatible with high-voltage cathode material. (Q1, FY 2021; Completed)
2. Characterize CEI/SEI interphase properties in optimized electrolyte to probe the mechanism of high-voltage cycling stability of Na-ion batteries. (Q2, FY 2022)
3. Design new electrolytes to enable extremely high CE (> 99.5%) of sodium stripping/plating process on different current collectors. (Q3, FY 2022)
4. Investigate feasibility of anode-free sodium batteries using new electrolytes and $Na_3V_2(PO_4)_3$ cathode. (Q4, FY 2022)

Progress Report

This fiscal year, the team has continued to develop the high-voltage electrolyte based on tetraglyme and fluorinated solvent to be compatible with high-voltage cathode materials, including $Na_2Fe_2(CN)_6$ and $NaNi_{0.68}Mn_{0.22}Co_{0.1}O_2$ (NaNMC). Tetraglyme-based electrolytes with 1 M $NaBF_4$ and initial 10% amount of the fluorinated solvent [VC, FEC, bis(2,2,2trifluoroethyl) ether (BTFE), or TTE] were studied in half-cells using a NaNMC cathode. As shown in Figure 92a, the electrolyte containing 10%vol VC showed the best cycling performance compared to the other co-solvents. Typically, it displays the highest initial discharge capacity of 156.7 mAh/g as well as capacity retention of 70% for 200 cycles. Further, the initial CE is as high as 94.5% and reaches 99.5% after a few cycles. Additional studies will be continued with the variation of VC content as co-solvent in tetraglyme-based electrolyte to enhance long cycling performance. Meanwhile, the rational design of mixed electrolytes between TFP and different solvents like DME, DMC, TMS, and TFP at high NaFSI concentration (> 1.2 M) were investigated for hard carbon (HC)||NaNMC full cell in a voltage range of 1.2-4.2 V (Figure 92b-c). The molar ratio of electrolyte components (NaFSI: co-solvent: TFP) is fixed at 1:1.5:2 in mol. The developed electrolytes are compatible with conventional polymer separator (polypropylene or polyethylene).

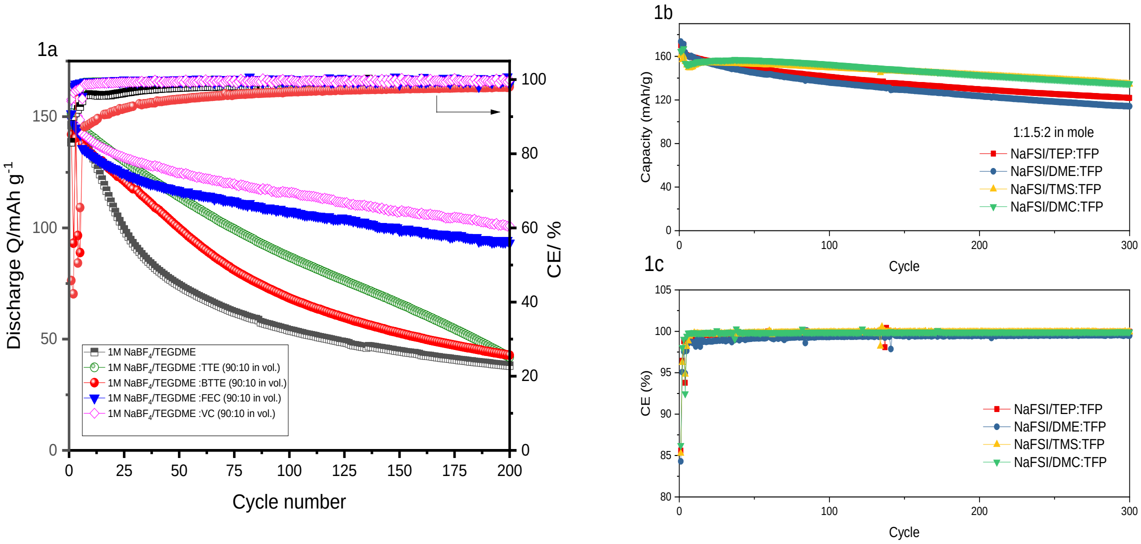

Figure 92. (a) Cycling performance of mixed electrolytes based on tetraglyme- fluorinated solvent (VC, FEC, BTFE, or TTE) in 90:10 (%vol) with 1 M $NaBF_4$ in Na||NaNMC half-cell at C/10 rate; mass loading: 3.0-4.0 mg/cm^2; at voltage range of 2-4.2 V. (b-c). Cycling performance of rational electrolytes of NaFSI: co-solvent: TFP = 1: 1.5: 2 in mol. used for full cell of HC||NaNMC (mass loading 1.5 mAh cm^{-2}), 3 formation cycles at 0.05 C and cycling at 0.2 C rate (1C = 200 mA/g), and voltage range of 1.2-4.2 V.

Use of high polar co-solvents helps to saturate the solvation unique structure of electrolyte as far as to modify the SEI/CEI composition for strongly stabilizing electrode – electrolyte interphase. Among the co-solvents, DMC and TMS exhibited the best long-cycling performance of full cell HC||NaNMC, which shows good initial discharge capacity of 164.5 mAh/g; 160.9 mAh/g and capacity retention of 87.8% and 86.6% after 300 cycles, respectively. In addition, these electrolytes also display a good CE of > 99 % after 5 cycles. The interfacial structure and composition of SEI/CEI layers will be further investigated to understand the superior performance of full cells using these electrolytes.

Patents/Publications/Presentations

The project has no patents, publications, or presentations to report this quarter.

Innovation Center for Battery500
(Jun Liu, Pacific Northwest National Laboratory; Yi Cui, Stanford University)

Project Objective. The overall goal of the consortium is to increase the energy density of advanced lithium batteries to beyond what can be achieved in today's state-of-the-art Li-ion batteries. The Battery500 Consortium aims to increase the specific energy (up to 500 Wh kg^{-1}) and achieve 1,000 charge/discharge cycles, with cost reduction of the cells to significantly less than \$100 per kWh^{-1}. This goal directly addresses the DOE priority to achieve a carbon-free electricity sector by 2035 and to decarbonize the transportation sector by developing and manufacturing the next-generation, high-energy, low-cost batteries to enable a wide deployment of EVs in the marketplace.

Project Impact. Battery500 will develop next-generation lithium battery technologies that will significantly increase energy density, improve cycle life, and reduce cost. This will greatly accelerate deployment of EVs and reduce carbon emission associated with fossil fuel consumption. The consortium will utilize first-class expertise and capabilities in battery research in the United States and develop an integrated and multi-disciplinary approach to accelerate development and deployment of advanced electrode and electrolyte materials in commercially viable high-energy batteries. The advances made in this consortium will also benefit improvement of current Li-ion battery technologies. This project will provide tremendous opportunities for students and scientists for battery-related training that will enhance the workforce for the United States to maintain global leadership in the battery R&D field.

Approach. This project focuses on the two most promising battery chemistries: Li-metal anode with high-voltage/high-capacity metal oxide cathodes like $LiNi_xMn_yCo_{1-x-y}O_2$ (NMC), and lithium metal with sulfur cathodes. The project focus is to design novel electrode and cell architectures to meet the 500 Wh/kg goal. The consortium will work closely with battery/material manufacturers, suppliers, and end users / original equipment manufacturers in the United States to ensure the technologies being developed by this project are well aligned with industry needs, poised for transitioning to real production, and helpful in securing the supply chain in the United States.

Out-Year Goals. The out-year goals are to improve cycle life of the Li||NMC pouch cell with 400 Wh/kg energy density and more than 200 cycle life, and to fabricate and test the pouch cells with 450 Wh/kg energy density and cycle life of > 100.

Collaborations. Collaboration among consortium team members will be well coordinated by the leadership team, which also includes four keystone project leads and co-leads along with PIs at all member institutions. Collaboration with the community outside of this consortium and with industry will be facilitated by the executive committee and the advisory board.

Milestones

1. Complete synchrotron-based TXM studies on CEI interphase protection for NMC cathode cycled at high-voltage limit. (Q1, FY 2022; Completed)
2. Complete electrochemical AFM imaging in glovebox to study the nucleation of Li-metal anode during lithium plating. (Q2, FY 2022; In progress)
3. Complete Li-metal anode morphology studies by cryo-EM and modeling. (Q3, FY 2022; In progress)
4. Improve cycle life of Li||NMC pouch cell with 350 Wh/kg energy density with cycle life of > 800, and with 400 Wh/kg energy density with cycle life of > 200 . Fabricate and test pouch cells with 450 Wh/kg energy density and cycle life > 100. (Q4, FY 2022; In progress)

Progress Report

Keystone Project 1: Materials and Interfaces

The Keystone 1 goal is to provide materials and chemistry support for Keystone projects 2 and 3. UT Austin synthesized a cobalt-free and manganese-free high-nickel cathode and conducted detailed characterizations. Stanford rationally designed a steric effect tuned ether molecule, 1,2-diethoxyethane (DEE), as the weakly-solvating electrolyte solvent for improving Li-metal battery performance. University of Washington (UW) investigated the cycle performance of Al-doped NMC-811 (Al-NMC-811) with cut-off voltage of 4.6 V and assembled a full cell with graphite anode; they also evaluated the carbon hosts for high-energy Li-metal batteries in 1,4-dioxane (1,4-DX) based electrolyte. Binghamton University continued to set up the thermal analysis laboratory, and the *operando* DSC cell was used to determine thermal events in operating coin cells. The PNNL team further investigated calendar life of Li||NMC-811 cells at an elevated temperature of 55°C for 18 months. PSU has focused on developing a novel electrolyte to enable long cycle life of Li-metal batteries.

This quarter, UT Austin synthesized a novel, cobalt-free and manganese-free high-nickel cathode. To stabilize the high-nickel cathode without cobalt and manganese, abundant and low-cost metals, such as aluminum, titanium, and magnesium, were introduced to give $LiNi_{0.93}Al_{0.05}Ti_{0.01}Mg_{0.01}O_2$ (NATM). To demonstrate the improved stability of NATM relative to $LiNi_{0.94}Co_{0.06}O_2$ (NC) and $LiNi_{0.90}Mn_{0.05}Co_{0.05}O_2$ (NMC), coin cells and pouch cells were assembled. Figure 93a-b demonstrates a small reduction in capacity with NATM, which is balanced in part by an increase in operating voltage. Meanwhile, all three materials exhibit similar rate capability (Figure 93c). Cycling performance in Figure 93d suggests substantial improvement in the stability of NATM, especially over the singly-doped NC cathode. To evaluate this stability over extended cycling and avoid any contribution to capacity fade from Li-metal anode, pouch cells with graphite were assembled. Once again, the NATM cathode delivers the highest capacity retention, with 82% after 800 cycles compared to 60% for NMC and 52% for NC (Figure 93e). To probe the physical origins of the superior cyclability of NATM, TOF-SIMS analysis was performed on the cycled cathodes. Total signals of common electrolyte decomposition

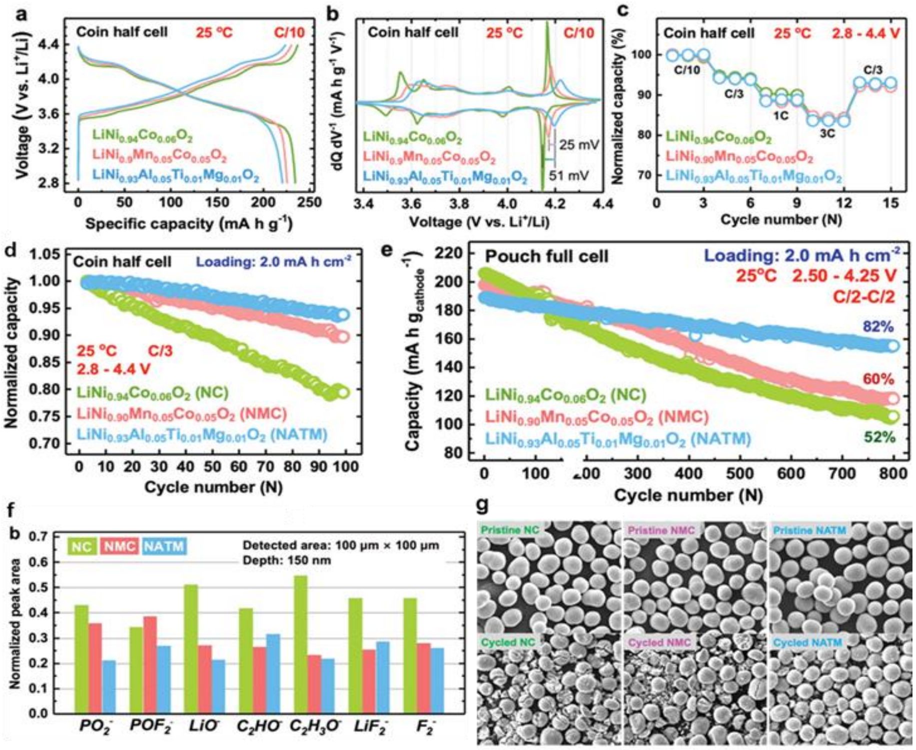

Figure 93. The electrochemical performances of NC, NMC, and NATM cathodes in coin cells with Li-metal anode and in pouch cells with graphite anode. (a) Charge and discharge curves and (b) dQ dV^{-1} curves of the 3rd C/10 formation cycle. (c) Rate performance tests with a constant C/5 charge rate. Cyclability evaluation in (d) coin cells for 100 cycles at a C/3 rate between 2.8 V and 4.4 V and in (e) pouch cells for 800 cycles at a C/2 rate between 2.5 V and 4.25 V. (f) Normalized peak areas of raw time-of-flight secondary ion mass spectrometry data of interphasial fragments on cathodes after 800 cycles. Each sample is sputtered three times on three different locations to yield normalized average peak areas. (e) Scanning electron microscopy images of pristine and cycled cathodes after 800 cycles. The scale bars in (e) are 20 μm.

products such as POF_2^- and $C_2H_3O^-$ are reduced for NATM, indicating less aggressive electrolyte reaction and CEI formation (Figure 93f). The cycled NATM cathode also displays much reduced particle cracking, further contributing to the enhanced capacity retention (Figure 93g).

Stanford rationally designed a steric effect tuned ether molecule (DEE, Figure 94a) as the weakly-solvating electrolyte solvent for improving Li-metal battery performance. The molecular design principle is to utilize a steric hindrance effect to tune the solvation structures of Li^+ ions. The team hypothesized that by substituting the methoxy groups on DME with larger-sized ethoxy groups, the resulting DEE should have a weaker solvation ability and consequently more anion-rich inner solvation shells, both of which enhance interfacial stability at the cathode and anode (Figure 94a). MD simulations were performed to provide more detailed information about solvation structures (Figure 94b). Comparing the most probable solvation structures of 1 M LiFSI/DME and 1 M LiFSI/DEE, the latter must accommodate four extra carbons and eight extra hydrogens, which results in an additional energy penalty for DEE coordination. As a result, DEE has a lower average CN to Li^+ due to its bulkier size. In the order of 1 M LiFSI/DME < 1 M LiFSI/DEE < 4 M LiFSI/DME < 4 M LiFSI/DEE, the anion-to-solvent ratios increase, and thus the probability of multiple FSI^- within Li^+ solvation shell increases (Figure 94b), which is consistent with the weaker solvation at higher concentration as well as the weaker solvation in DEE than in DME. The lithium CE was determined by a modified Aurbach method (Figure 94c). With 1 M LiFSI, CE of DEE reaches 99.02% and outperforms that of DME at 98.16%. Such high CE even at a normal salt concentration indicates superior compatibility of DEE with lithium. At higher LiFSI concentration of 4 M, both DME and DEE show improved CE (99.04% and 99.38%, respectively). The higher CE of DEE compared to DME at 4 M further showcases the improved stability of DEE at the lithium anode. Finally, under stringent full-cell conditions of 4.8 mAh cm^{-2}, the cell using NMC-811 cathode, 50-µm thin lithium, and high cutoff voltage at 4.4 V, the best-performing electrolyte 4 M LiFSI/DEE enabled 182 cycles with 80% capacity retention, while 4 M LiFSI/DME only achieved 94 cycles (Figure 94d).

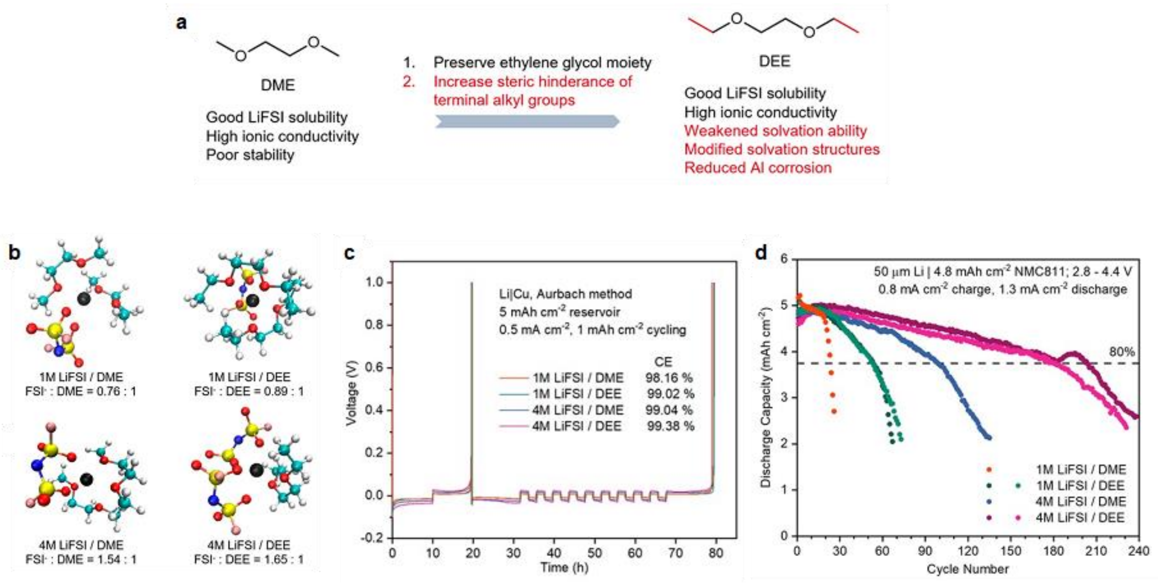

Figure 94. (a) Molecular design from DME to DEE. (b) Molecular dynamics simulations for 1 M LiFSI/DME, 1 M LiFSI/DEE, 4 M LiFSI/DME, and 4 M LiFSI/DEE. (c) Aurbach method to determine average Li-metal Coulombic efficiency using different electrolytes. (d) Cycling performance of thin-Li | high-loading NMC-811 full cells under limited electrolyte and practical cycling conditions.

In previous reports, the UW team revealed that the Al-NMC-811 exhibits good electrochemical performance under high voltage using the triethyl-phosphate (TEP)-based LHCEs, which is attributed to highly fluorinated interphases inside the CEIs derived from the TEP-based electrolyte. This quarter, they investigated cycle performance of the battery with an upper cut-off voltage of 4.6 V and assembled a full cell using graphite as the anode. This full cell shows stable cycling performance that cannot be achieved using the commercial carbonate electrolytes. The electrochemical performance of Al-NMC-811 electrode (1.5 mAh cm^{-2}) using the TEP-based electrolyte [1.2 M LiFSI in TEP/BTFE (1:3 by molar ratio)] and Li-metal anode is shown in Figure 95. The Al-NMC-811 cathode using the TEP-based electrolyte and Li-metal anode can deliver an initial specific capacity of 234.1 mAh g^{-1} and an initial CE of 93.9% at C/3. After the initial cycle, the Al-NMC-811 cathode displays the almost identical charge–discharge curves and superior cycle stability (Figure 95a). Moreover, it exhibits a reversible capacity of 207.8 mAh g^{-1} with an average CE of 99.8% after 250 cycles at 1 C, corresponding to a capacity retention of 88.8% (Figure 95b). Given the excellent electrochemical performances of the Al-NMC-811 cathode in the TEP-based LHCE, full cells were assembled and tested using graphite as the anode to demonstrate feasibility of developing a practical high-energy-density battery. As shown in Figure 95c, the full cell exhibits an initial reversible capacity of 222.3 mAh g^{-1} (based on the mass of cathode) with CE of 80.0% at 0.2 C within 2.0–4.6 V. The Al-NMC-811/graphite full cell could deliver a reversible discharge capacity of 168.2 mAh g^{-1} at 0.2 C after 250 cycles, corresponding to a capacity retention of 75.7%, showing good cycling durability. Overall, the Al-NMC-811 cathode using the TEP-based LHCE displays high capacity and excellent cycling stability.

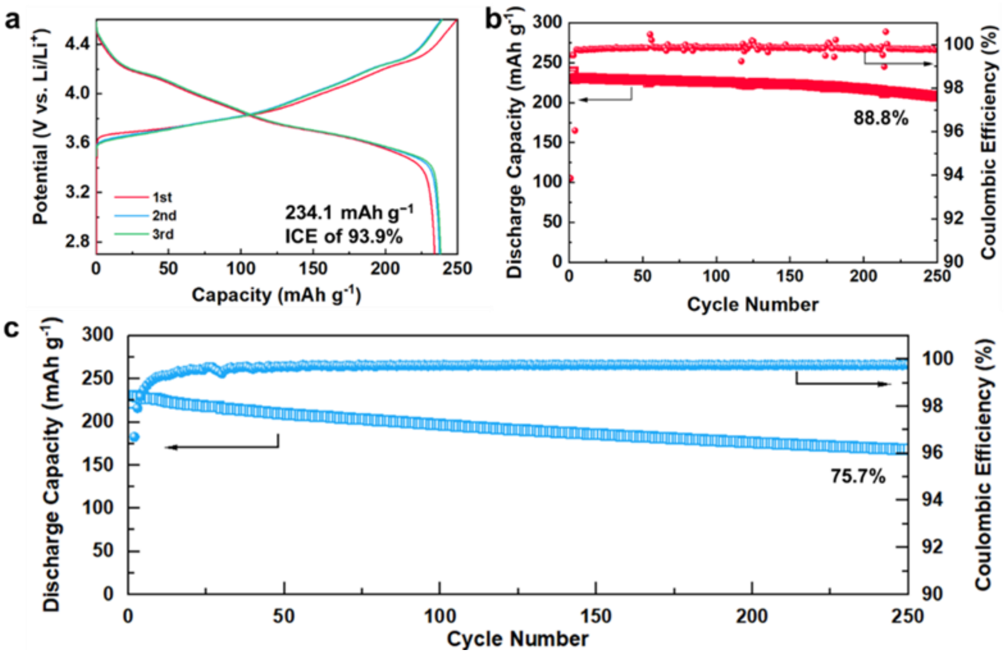

Figure 95. (a) Charge/discharge curves and (b) cycling performance of Al-doped NMC-811 electrode using the triethyl-phosphate (TEP)-based electrolyte and Li-metal anode. (c) Cycling performance of the Al-doped NMC-811 / graphite full cell in the TEP-based electrolyte.

In previous reports, the UW team also systematically evaluated the carbon hosts for high-energy rechargeable Li-metal batteries in different kinds of electrolytes. The results demonstrated that the nature of the electrolyte has the dominant effect on determining the CE and cyclability of Li-metal anode. The HCE or LHCE has superior performance, but needs the use of DME solvent. However, as shown in Table 10, there are intrinsic disadvantages of DME, such as low boiling point, low oxidation potential, and high reduction potentials versus Li$^+$/Li. This quarter, UW investigated the homologousness of DME, 1,4-DX as an alternative electrolyte solvent. Using a typical concentration of 1 M LiFSI or 2 M LiFSI in 1,4-DX, the CE of Li-metal anode can reach 99% and last more than 200 cycles. In addition, the Li-metal full cell with a cut-off voltage of 4.4 V exhibits more than 100 cycles in a coin cell.

Table 10. Physicochemical properties of 1,2-dimethoxyethane and 1,4-dioxane solvents.

	Dielectric Constant	Donor Number	Reduction Potentials (unit: V vs. Li^+/Li)	Oxidation Potential (unit: V vs. Li^+/Li)	Boiling Point
Dimethoxyethane (DME)	7.2	20	–1.64	~ 3.0	85°C
1,4-dioxane (1,4-DX)	2.2	14.8	–1.95	> 4.4	101°C

Figure 96 (left) shows a plot of CE versus cycle number for lithium plating and stripping on copper in the 1 M LiFSI and 2 M LiFSI in 1,4-DX electrolytes. Deposition capacity is 1 mAh cm^{-2} at a current density of 1 mA cm^{-2} with 60 µL for each coin cell. The average CE of the two electrolytes is 99%, remaining very stable over 200 cycles. The linear sweep voltammetry (LSV) curves of 1 M LiFSI in 1,4-DX, 2 M LiFSI in 1,4-DX, and 1 M LiFSI in DME at a scan rate of 0.1 V s^{-1} are shown in Figure 96 (right). LSV testing was scanned on the super P and PVDF (weight ratio of 9:1) electrode in the voltage window of OCV to 5.0 V versus Li/Li^+. Results indicate that electrolyte oxidation occurs at around 3.5 V versus Li/Li^+ in 1 M LiFSI DME. In 1,4-DX electrolytes, the oxidation potential is around 4.4 V versus Li/Li^+, which is much more stable than 1 M LiFSI in DME electrolyte. Furthermore, the results also demonstrate that higher concentration enhances the stability of electrolytes at higher potential. Therefore, the 2 M LiFSI 1,4-DX electrolyte was chosen in the following full cell investigations. Figure 97a shows the electrochemical performance of 50 µm Li||NMC-622 (4 mAh cm^{-2} initial capacity) full cell using different electrolytes at the voltage window of 2.7–4.4 V. All cells delivered a reversible capacity of ~ 5 mAh. After ~ 16 cycles, capacity decays to 0 mAh in 1 M LiFSI in DME electrolyte, owing to decomposition of the electrolyte. In 1 M LiFSI in 1,4-DX, capacity remains stable for about 50 cycles and then quickly degrades to 0 mAh. In contrast, capacity remains at 3.8 mAh after 100 cycles in 2 M LiFSI in 1,4-DX, corresponding to a capacity retention rate of 71.7%. Figure 97b shows the capacity versus cycle number for 50 µm Li||NMC-622 (4 mAh cm^{-2}) full cell at different cut-off charge voltages in 2 M LiFSI in 1,4-DX. Even for 4.5 V cut-off voltage, capacity maintains at 2.3 mAh after 100 cycles, corresponding to the capacity retention rate of 43.4%. The results demonstrate good performance of Li-metal battery in 2 M LiFSI in 1,4-DX electrolyte.

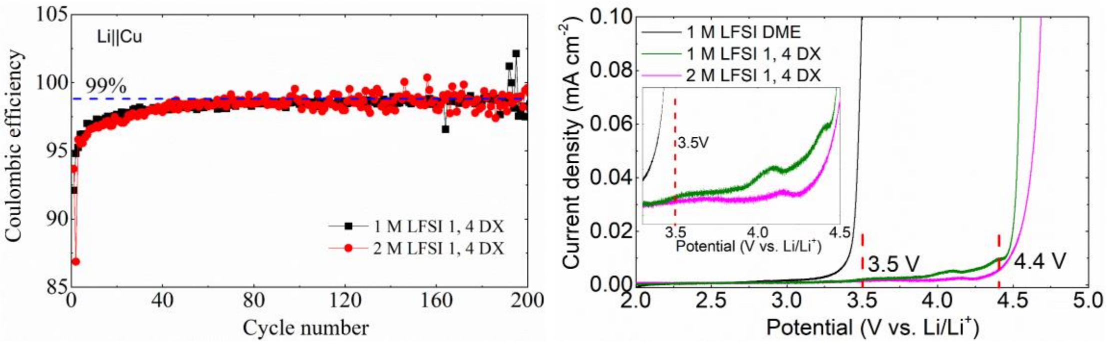

Figure 96. (left) Coulombic efficiency versus cycle number of lithium deposition on copper. The deposition capacity is 1 mAh cm^{-2} at a current density of 1 mA cm^{-2} with 60 µL electrolyte for each coin cell. Testing procedure: a given amount of lithium metal is plated on copper and then stripped off with a cutoff voltage of 1 V versus Li/Li^+. The electrolytes are 1 M LiFSI and 2 M LiFSI in 1,4-dioxane (1,4-DX). (right) Linear sweep voltammetry curves of 1 M LiFSI in 1,4-DX, 2 M LiFSI in 1,4-DX, and 1 M LiFSI in DME. The scan rate was 0.1 V s^{-1}.

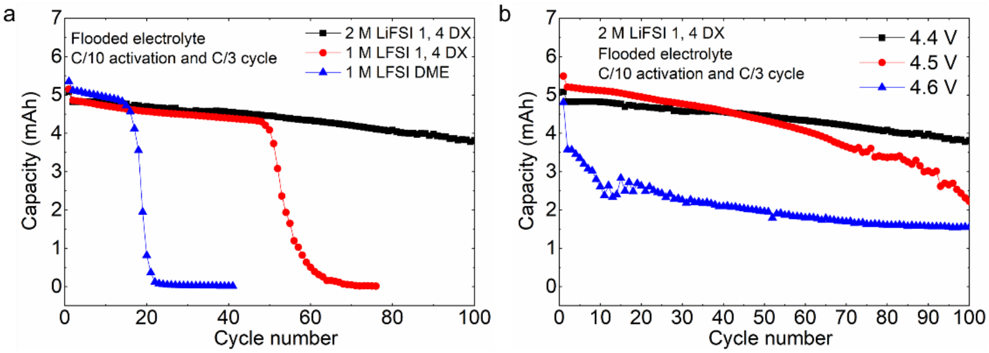

Figure 97. (a) Capacity versus cycle number for 50 μm Li||NMC-622 (4 mAh cm^{-2} initial capacity) full cell using different electrolytes (1 M LiFSI in 1,4-dioxane, 2 M LiFSI in 1,4-dioxane, and 1 M LiFSI in DME) at the voltage window of 2.7−4.4 V. (b) Capacity versus cycle number for 50 μm Li||NMC-622 (4 mAh cm^{-2} initial capacity) full cell at different cut-off charge voltage (4.4 V, 4.5 V, and 4.6 V). All cells were charged and discharged at C/10 for the 1st formation cycle and then cycled at C/3. The volume of electrolyte was 60 μL for each coin cell.

At Binghamton University, the team continues to set up the thermal analysis laboratory, and an overall research plan is defined. The *operando* DSC cell provides new capability to determine thermal events in operating coin cells. This should allow the researchers to monitor formation of the SEI layers in initial cycles as well as the breakdown of electrolyte under extreme conditions. This will help define the limits of operability for each electrolyte for high nickel NMC. However, the materials that the coin cell is constructed of can also react with the electrolyte, leading to heat evolution. Using this high sensitivity DSC method, such reactions can mask the reactions being studied. To measure the magnitude of these challenges faced by the coin-cell corrosion, the impact of adding additional aluminum foil to the cathode current collector was determined; results are shown in Figure 98. The upper charging voltage was capped at 4.5 V, since the team's previous studies showed that breakdown occurs at voltages higher than 4.5 V. The heat evolution of NMC-811 cells with no additional aluminum on the cathode is shown in Figure 98a, while the results for cell with an extra aluminum foil added are shown in Figure 98b; both current collectors were Al-coated. There is clearly a marked difference with the T3 and ED2 electrolytes showing essentially no heat evolution for the extra protected cathode current collector. The other electrolytes will be further studied. This study highlights the need to closely examine all cell components.

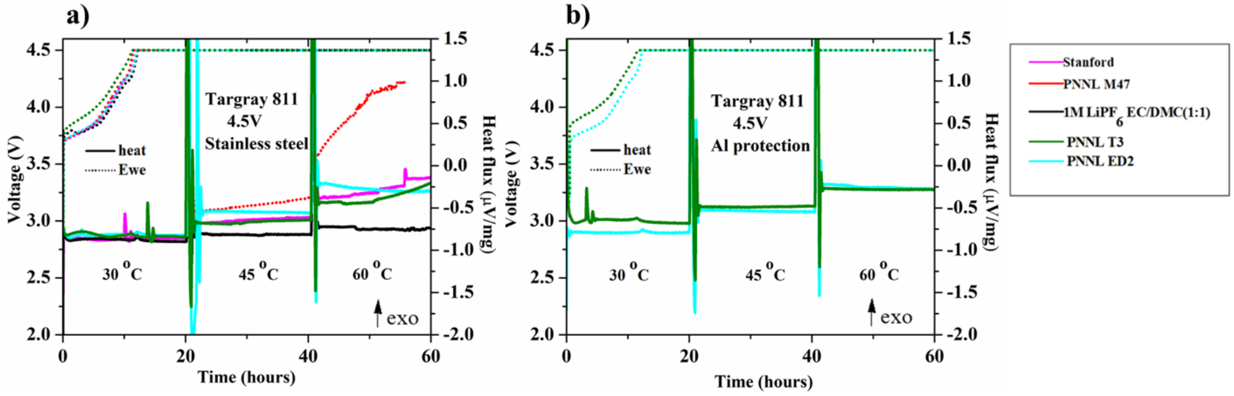

Figure 98. *Operando* differential scanning calorimetry measurements (dotted curves for electrochemical test and solid curves for the measured heat flux) of novel ether-based M47, ED2, T3, and Stanford (1 M LiFSI in FDMB) electrolytes and traditional carbonate electrolyte [1 M LiPF_6 in EC/DMC (1:1)] for TARGRAY NMC-811 that were charged and held at 4.5 V, while ramp heating and isothermally holding at 30°C, 45°C, and 60°C for 20 hours. (a) Al-coated MTI coin-cell parts. (b) Al-coated Hohsen coin cell with aluminum foil added on cathode side.

The PNNL team further investigated the calendar life of Li||NMC-811 cells at elevated temperature of 55°C for 18 months. Compared to the highest calendering stability obtained at 0% SOC at 30°C, which shows 89.6% capacity retention after 18-month storage (Figure 99a), cells stored at 0% SOC are also quite stable at 55°C, which can recover 94.7%, 73.6%, and 42.9% capacity, respectively, after 3-month, 12-month, and 18-month storage (Figure 99b). For the cells stored at 50% SOC, capacity loss from self-discharge increases quickly in the first month, followed by large overpotential of ~ 0.4 V after 5 weeks of storage and then cell failure after 3 months (Figure 99c). When the cells are fully charged to 100% SOC (Figure 99d), storage performance becomes better than for those stored at 50% SOC. The self-discharge rate at 100% SOC is 1.18-2.96% per day, which is about half of those stored at 50% SOC. In addition, the polarization of cells stored at 100% SOC is also significantly smaller than that stored at 50% SOC. STEM image analysis on the NMC-811 cathode after storage test indicates that the thickness of layer with rock-salt structure (9.2 nm, Figure 99h) observed at the sample stored at 55°C is six times thicker than that stored at 30°C (Figure 99e), and the CEI thickness at 55°C is 6.1 nm (Figure 99g). These results can be attributed to the accelerated side reactions between electrolyte and cathode at elevated temperature. For the Li-metal anode, ~ 32 µm native lithium remains, and the SEI thickness is ~ 30 µm (Figure 99j) after 18-month storage at 55°C, while 45 µm native lithium still remains at 30°C. In addition, unlike the uniform degradation of the Li-metal anode in the cell stored at 30°C, some obvious pits are found on the Li-metal anode stored at 55°C, as shown in Figure 99j (cross section view) and Figure 99k (top view). The non-uniform corrosion of Li-metal anode stored at 55°C can be ascribed to the accelerated dissolution of SEI and/or more defects formed on SEI at elevated temperature. As a result, continuous lithium corrosion is magnified over the long-term storage and finally leads to these open pits. The XPS results in Figure 99 further confirm the accelerated solvent decompositions at 55°C compared to those stored at 30°C.

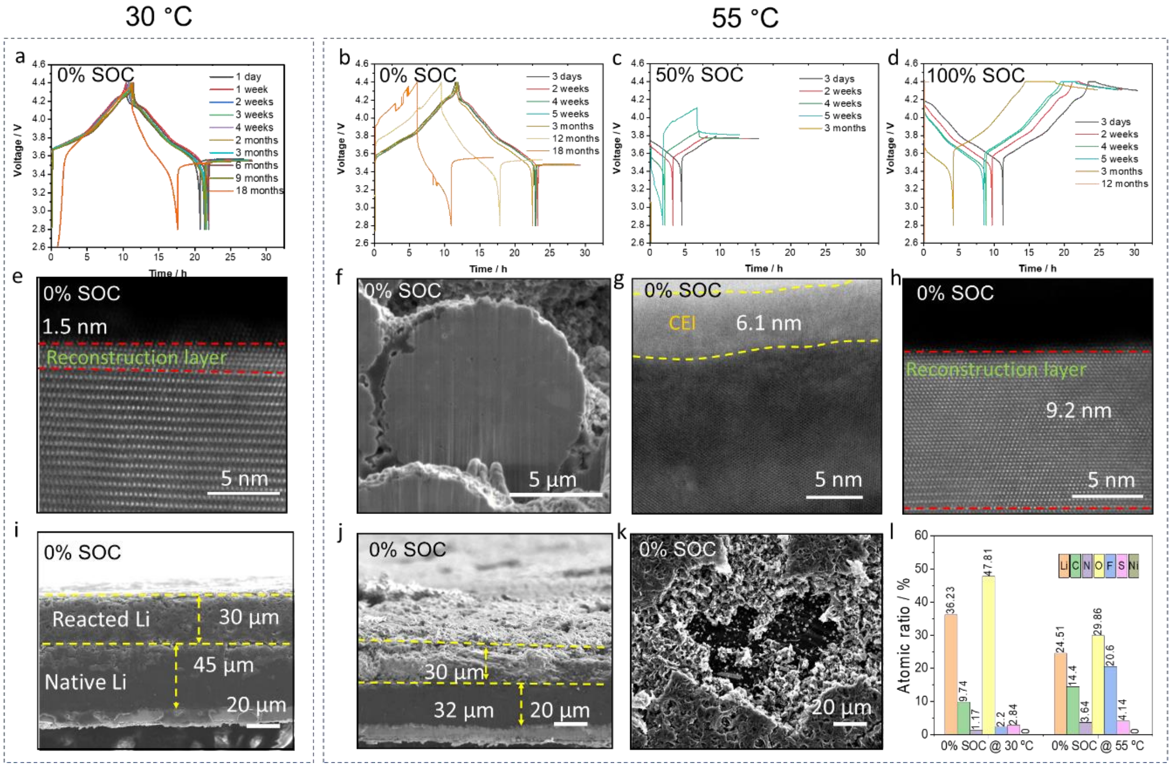

Figure 99. Electrochemical performance of Li||NMC-811 cells and electrode structures after storage for 18 months at different conditions. (a-d) Voltage profiles of the cells stored at different states of charge (SOC) and temperatures: (a) 0% SOC and 30°C; (b) 0% SOC and 55°C; (c) 50% SOC and 55°C; and (d) 100% SOC at 55°C. (e) Annular bright field scanning transmission electron microscopy (ABF-STEM) image of NMC-811 particle stored at 0% SOC and 30°C. (f-h) Structures of NMC-811 particle stored at 0% SOC and 55°C: (f) focused ion beam – scanning electron microscopy (FIB-SEM), (g) high-angle annular dark field – STEM, and (h) ABF-STEM images. (i) SEM cross-section image of Li-metal anode after storage at 0% SOC and 30°C. (j-k) SEM cross-section and surface images of Li-metal anode after storage at 0% SOC and 55°C. (l) SEI compositions of Li-metal anode after storage at 0% SOC and different temperatures.

PSU has been focused on developing a novel electrolyte to enable long cycle life of Li-metal batteries. This quarter, the team worked on optimizing the electrolyte formulation from all aspects of solvents, salts, and additives to achieve the target CE. First, long-term lithium plating/stripping cycling testing was employed with Li||Cu half cells to determine CE in the electrolytes A, B, and C. As shown in Figure 100a, the baseline electrolyte A was first evaluated; the cell only demonstrated low CE (≈ 80%), and capacity quickly dived after only 110 cycles. Modified electrolyte B can deliver improved CE. However, the average CE (≈ 93.6%, 1st to 130th cycles) was still not good enough, along with capacity diving after 130 cycles. As for the modified electrolyte C, the cell maintained much improved CE even after 150 cycles. In addition, Aurbach CE tests were used to determine accurate CE in electrolytes A, B, and C. With current density of 0.5 mA/cm^2 and lithium deposition capacity of 1.0 mAh/cm^2, electrolyte A only delivered CE of 87.5%. On the other hand, electrolyte B offered improved CE of 97.7%. In contrast, a substantially improved CE of 99.0% was achieved in electrolyte C (Figure 100b). The morphology of deposited lithium metal on copper substrate in electrolytes A, B, and C was studied by SEM. As shown in Figure 100c, the top-view SEM images show the porous and dendritic morphology of deposited lithium in baseline electrolyte A. The electrodeposited lithium grows larger in electrolyte B. However, lithium dendrites can still form. In contrast, a uniform and large-size lithium deposition without lithium dendrite formation was achieved in electrolyte C. From the cross-sectional SEM images, the thicknesses of deposited lithium metal in electrolytes A and B are 27 µm and 25 µm, respectively. The deposited lithium metal was much denser in electrolyte C, and thickness was significantly reduced to 21 µm. Thus, electrolyte C can effectively decrease the exposed surface area and tortuosity of deposited lithium metal, resulting in much more uniform lithium deposition and improved cycling stability. The superiority of the newly developed electrolyte C to electrolytes A and B was verified with Li||NCM-811 full cells. After one formation cycle at 0.1C, Li||NCM-811 full cells were cycled at 0.2C for charge and 0.5 C for discharge in electrolytes A, B, and C. During the formation cycle, all cells demonstrated similar charge/discharge voltage profiles (Figure 101a). For subsequent cycles, the cells delivered a high discharge capacity of ~ 3.5 mAh/cm^2, even at 0.5C (Figure 101b). However, as shown in Figure 101c, the cells decayed quickly and delivered capacity retention of less than 80% after 40 cycles in baseline electrolyte A. In electrolyte B, the cells showed improvement with a capacity retention of 80% after 140 cycles. In contrast, electrolyte C demonstrated significantly improved cycling performance with a capacity retention of 91% after 145 cycles. To investigate differences in the morphologies of Li-metal anodes in the Li||NMC-811 full cells, SEM studies were employed. As shown in Figure 102a, obvious accumulation of dead lithium metal is detected in electrolyte A after 50 cycles, along with a porous and nonuniform surface. This result indicates the fast degradation of Li-metal anodes in electrolyte A. On the other hand, the dead lithium formation is less in electrolyte B. In contrast, the Li-metal anode cycled in electrolyte C shows a much smoother surface with the lowest level of dead lithium formation. The significantly reduced surface area also repressed side reactions between Li-metal anode and electrolyte, resulting in limited SEI reformation and improved cycling performance. Furthermore, the chemical compositions of SEI layers were analyzed with the Li-metal anodes obtained from Li||NMC-811 full cells after 50 cycles. The high-resolution fluorine 1s, phosphorus 2p, and carbon 1s XPS spectra are depicted in Figure 102b-d. For the fluorine 1s spectra, the peaks assigned to LiF (at 685.0 eV) and Li_xPF_y (at 686.2 eV) were observed in electrolytes A, B, and C. Noticeably, the peak intensity of LiF in electrolyte C considerably increased, suggesting a LiF-rich SEI formed on Li-metal anode surface. LiF has been considered as an excellent SEI component to suppress lithium dendrite growth and promote uniform lithium deposition. Therefore, the dual-additive electrolyte C can be expected to deliver improved cycling stability of L-metal batteries over electrolytes A and B. Moreover, for the phosphorus 2p spectra, a decreased fraction of decomposition products ($Li_xPO_yF_z$, P-O) in the SEI layer indicates the reduced lithium salt decomposition in electrolyte C. As for the carbon 1s spectra, the peak intensity of polar structure moieties R-O-CO_2- (at 289.0 eV) becomes higher in electrolyte C than the other two electrolytes. The increased concentration of R-O-CO_2- groups in SEI will enhance lithium cation transport through the SEI layer. In conclusion, the newly developed electrolyte C can promote much more uniform lithium deposition and improved CE. More importantly, electrolyte C demonstrates improved cycling performance of Li||NMC-811 full cells. Furthermore, the XPS study reveals that electrolyte C greatly influences SEI chemistry and compositions, generating a robust and LiF-rich SEI layer on the Li-metal anode surface.

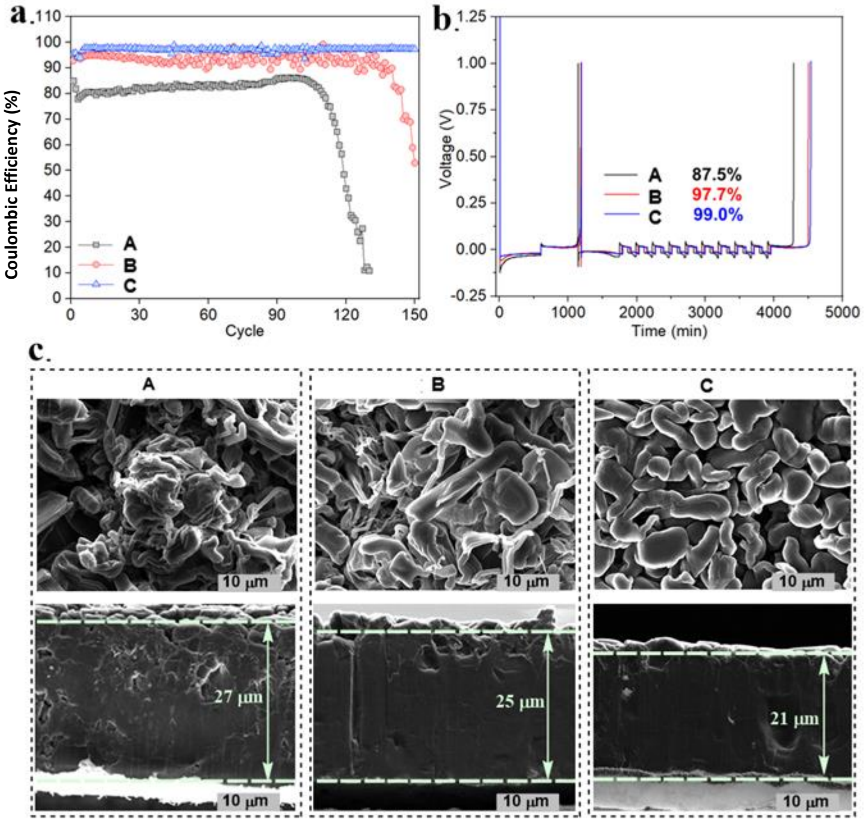

Figure 100. Coulombic efficiency (CE) testing with Li||Cu half cells and Li-metal deposition morphology. (a) Cycling CE of Li||Cu cells in different electrolytes. (b) Aurbach CE of Li||Cu cells in different electrolytes. (c) Scanning electron microscopy images of deposited lithium metal on copper substrate under 0.5 mA/cm^2 and lithium deposition capacity of 4.0 mAh/cm^2 in different electrolytes.

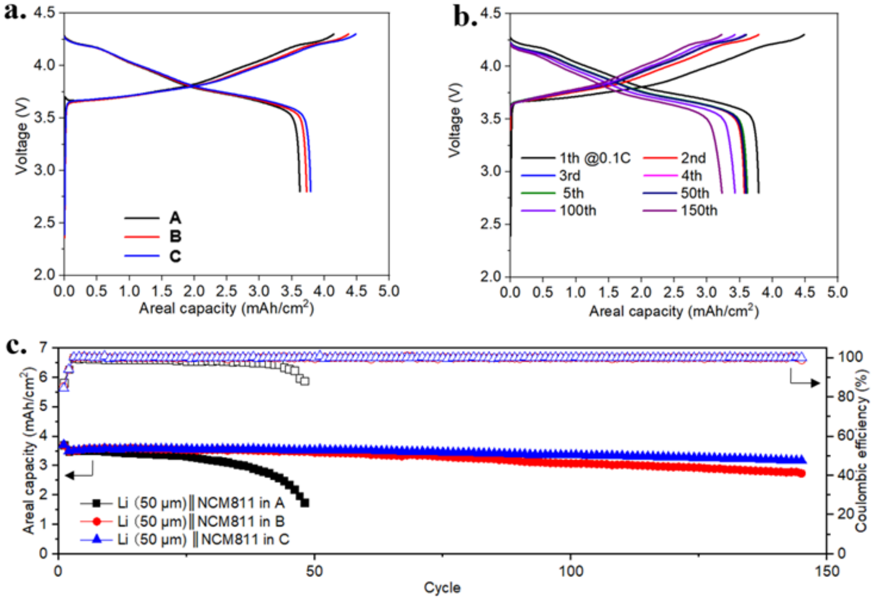

Figure 101. Electrochemical performance of Li||NCM-811 coin cells in the different electrolytes between 2.8-4.3 V. (a) Initial voltage profiles of Li||NCM-811 coin cells at 0.1 C in different electrolytes. (b) Voltage profiles of the Li||NCM-811 coin cells at different cycles in electrolyte C. (c) Cycling performance of Li||NCM-811 coin cells at 0.2 C for charge and 0.5 C for discharge in different electrolytes. 50-µm Li-metal anode and 30 µL of electrolyte were used for all cases. 1 C = 3.5 mA/cm^2.

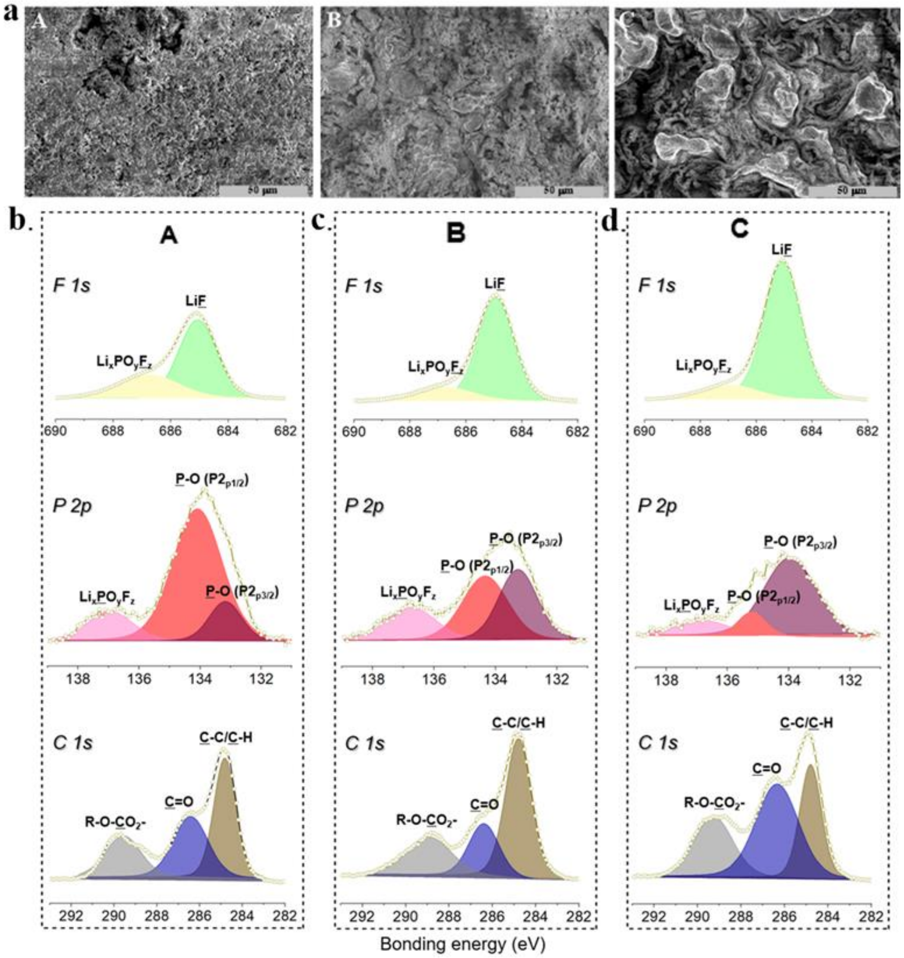

Figure 102. Characterization of Li-metal anodes obtained from Li||NCM-811 coin cells after 50 cycles. (a) Top-view scanning electron microscopy images of cycled Li-metal anode in different electrolytes. High-resolution fluorine 1s, phosphorus 2p, and carbon 1s X-ray photoelectron spectra of formed SEI in (b) electrolyte A, (c) electrolyte B, and (d) electrolyte C.

Highlights of Keystone Project 1

The highlights for this quarter are as follows:

- A novel, cobalt-free and manganese-free high-nickel cathode, NATM, was designed, synthesized, and carefully studied. It delivers the highest capacity retention, with 82% after 800 cycles, compared to 60% for NMC and 52% for NC. (UT Austin)
- Rationally designed, steric effect tuned ether molecule, DEE, was used as the weakly solvating electrolyte solvent for improving Li-metal battery performance. (Stanford)
- Cycle performance of full cells containing Al-NMC-811 and a graphite anode was determined. Cells were cycled to an upper cut-off voltage of 4.6 V. The carbon hosts for high-energy rechargeable Li-metal batteries in 1,4-DX-based electrolyte were systematically evaluated. (UW)
- The calendar life of Li||NMC-811 cells at elevated temperature of 55°C for 18 months was investigated. Cells stored at 0% SOC are quite stable at 55°C, after 18-month storage. For the cells stored at 50% SOC, capacity loss increases quickly in the first month, followed by large overpotential of about 0.4 V after 5-week storage and cell failure after 3 months. When the cells are fully charged to 100% SOC, the storage performance is better than for those stored at 50% SOC. (PNNL)

Keystone Project 2: Electrode Architecture

The Keystone 2 goal is to design, model, fabricate, and characterize the effect of electrode architecture on electrode and cell performance in support of reaching the project goal of 500 Wh kg^{-1} cell specific energy. Such studies include both high-capacity cathode materials such as high nickel content NMC and sulfurized polymer cathode, as well as Li-metal anodes. Highlighted in this report for Keystone 2 are the synthesis of new sulfur-based polymers similar to sulfurized polyacrylonitrile (SPAN) and understanding of SPAN reaction mechanisms (UCSD), evaluation of pressure effect on Li-metal deposition (UCSD), and examination of a new additive to improve Li-metal plating.

Effect of Polymer Precursors on Sulfurized Polymer Performance

This quarter, UCSD studied the relationship between the molecular structure of sulfurized polymer and its performance as a cathode. More specifically, the team strived to understand how the sulfur substituted at different sites on the pyridine ring influences battery performance. The purpose for this study is to understand why SPAN has such a high reversibility in the battery, and if the team could design and synthesize a polymer that has even better performance than SPAN.

As shown in Figure 103a, three sulfurized pyridine polymers had been selected to study the influence of sulfur substitution sites on the pyridine ring. SPAN has most of the sulfur atoms connected to the pyridine position 4, even though some sulfur groups can connect to other pyridine ring positions at the edge of its polymer chain (labeled in red, Figure 103a). In SP2VP, formed from P2VP as the precursor, besides the position 4 C-S bond formation, the pyridine rings' other positions can also bond with sulfur (labeled in blue, Figure 103a). SP4VP, formed from a P4VP precursor, can be considered as the 'opposite' of SPAN—every position on pyridine can be substituted by sulfur except for position 4. All polymers were synthesized by mixing their precursors with an excess amount of sulfur and heated at 450°C under inert gas protection. After sulfurization, the color of all of the polymers (PAN, P2VP, and P4VP) turned from white to black, suggesting formation of large conjugated structures. All of the polymers have similar functional groups. The FTIR spectra for SPAN and SP4VP are shown in Figure 103b. Both materials have similar covalent bonds, such as conjugated pyridine rings, C-S, and S-S bonds. Some slight peak shifts between the two materials, such as the C-S bond at ~ 940 cm^{-1} and ring bonded with sulfur at 1172 cm^{-1} suggest that the sulfur atoms are substituted at different positions on the pyridine ring. Since the major differences of the three polymers are the C-S bonding positions on the pyridine ring, their performance differences as a battery cathode are likely linked to this factor.

Figure 103c shows the 1st and 2nd charge-discharge profiles for the three materials. SPAN, the one with the highest ratio of position 4 C-S components, shows the highest discharge voltage plateau (1.6 V 1st discharge; 1.8 V 2nd discharge). SP2VP has fewer position 4 C-S bonds; its discharge voltage plateau is lower (1.4 V 1st discharge; 1.6 V 2nd discharge). The lowest voltage plateau was observed with SP4VP (1.2 V 1st discharge; 1.5 V 2nd discharge), which has no position 4 C-S bonds. On the other hand, all three materials have similar reversible capacity starting with the 2nd cycle when the cutoff voltages of SP2VP and SP4VP are set at 0.5 V versus the 1 V limit used for SPAN. SP4VP and SP2VP also have a high first discharge capacity (> 1000 mAh/g) in this expanded voltage range; its irreversibility is very similar to SPAN despite the voltage window difference.

These results suggest that high-capacity S-containing polymers that can cycle in carbonate electrolytes are not limited to SPAN only. By sulfurizing precursors containing already formed pyridine rings to form polymers (for example, SP4VP and SP2VP), similar capacities as SPAN can be obtained. These findings open the possibility of investigating other polymer precursors with related structures. The origin of the lower discharge potential requires further investigation. The team hypothesized that the availability of the 4 position on pyridine ring might play an important role. This hypothesis can also explain why SPAN synthesized from high molecular weight precursor PAN can result in high capacities. Since it has less polymer edge per unit mass, the ratio of position 4 C-S will be higher. Future study will focus on how to further enhance the position 4 C-S bonding in SPAN and examine other polymer structures that can offer higher operating voltage and capacities.

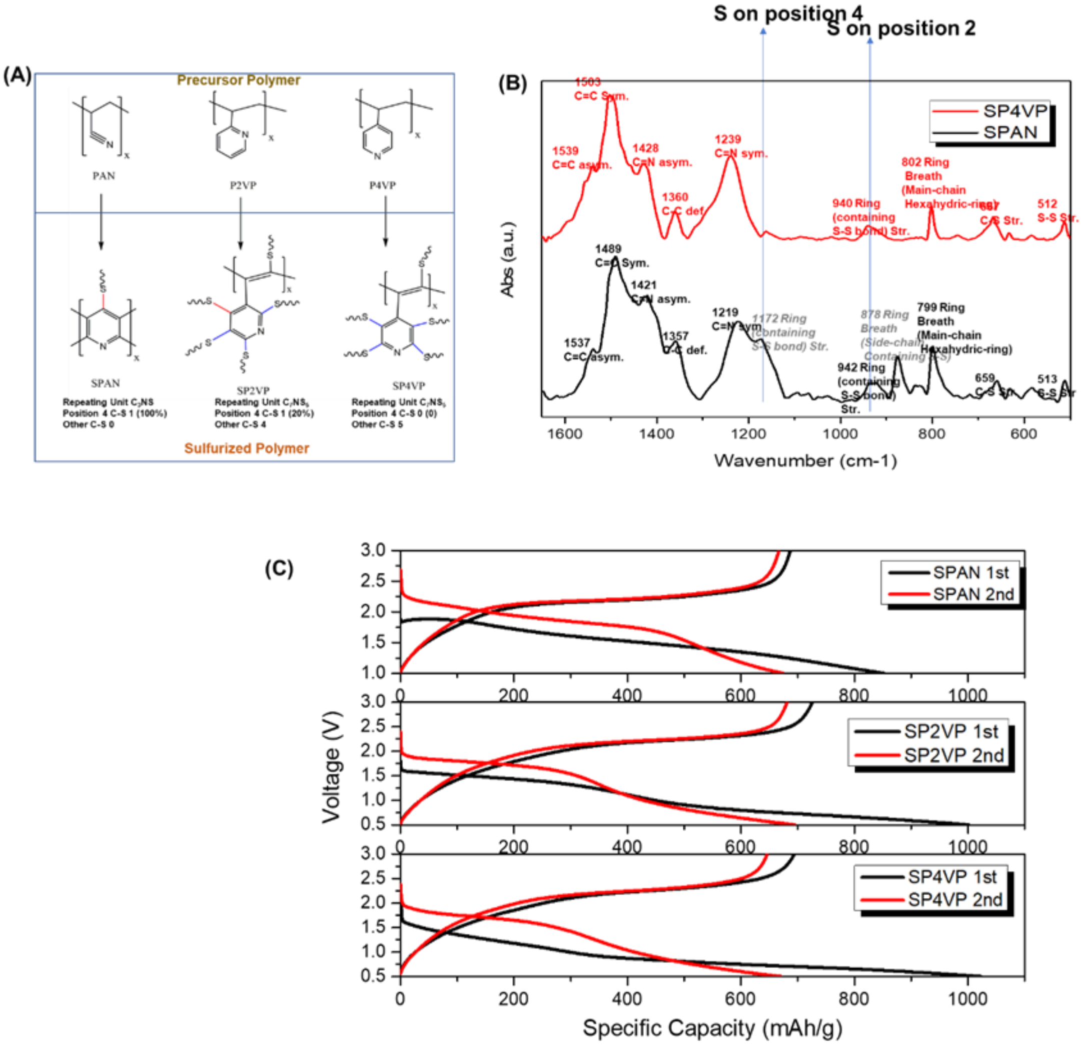

Figure 103. Sulfurized pyridine polymer for battery. (a) Structure of three polymers before and after sulfurization. (b) Infrared for SPAN and SP4VP. (c) Charge/discharge curves for SPAN, SP2VP, and SP4VP in liquid battery. (Cathode weight ratio – active material : carbon black : binder 8:1:1, with LFP EC/DMC electrolyte, charge/discharge rate 0.2C)

Reaction Mechanism of SPAN

Last quarter, the bonding environment of the sulfur in SPAN was analyzed by FTIR to probe the pristine molecular structure of SPAN synthesized at 300°C, 450°C, and 550°C (UCSD). It was found that there were three types of carbon and sulfur bonding environments. This quarter, the cycling performance of SPAN synthesized at different temperatures was analyzed.

Coin cells with SPAN electrodes were assembled with excess lithium and electrolyte, and the cells were cycled at C/3 for studying cycling stability of the SPAN electrodes. As Figure 104a shows, after the first 3 cycles, the discharge capacity of both the 450SPAN and the 550SPAN was stabilized (at ~ 520 mAh/g and 300 mAh/g, respectively). However, the discharge capacity of 300SPAN keeps decreasing even after the first three formation cycles. The capacity retention results are in good agreement with the elemental analysis results reported last quarter. There is a decrease of sulfur content in the SPAN synthesized at higher temperature, which might largely come from the loss of the bridging S_x. As a result, the 300SPAN contains the highest amount of sulfur in its molecule, which might form irreversible lithium polysulfides during the electrochemical cycling.

Figure 104b presents voltage profiles of the 300SPAN cell. As shown, at the beginning of the 1st cycle, discharge voltage starts at ~ 1.8 V, which means that there is almost no elemental sulfur left in the molecule. However, the dip at the beginning of the voltage profile, which is also presented in the elemental sulfur voltage profiles, suggests there might be formation of lithium polysulfide during the discharge. As cycling continues, there is also a gradual decrease in the discharge capacity observed in the cell. Figure 104c shows the cycling voltage profile of 450SPAN. The voltage profiles of 450SPAN are similar to those of 300SPAN, except there is no dip at the beginning of the 1st cycle discharge voltage profile. Furthermore, there is no noticeable decrease in the discharge capacity for the first 30 cycles. Figure 104d shows the cycling voltage profile of 550SPAN. The discharge capacity of 550SPAN is the lowest among the three SPANs, which might be caused by the decrease of sulfur amount in the molecules. Interestingly, the 550SPAN voltage profile shows an extra plateau in both charge and discharge voltage profile when compared to those of 300SPAN and 450SPAN. The exact reason for this extra plateau is under investigation. With the results so far, the team can conclude that the synthesis temperature of SPAN needs to be strictly controlled as it will have large impact on the molecular structure, sulfur content, and cycling performance. They are conducting XPS and Raman analyses to further decipher the reaction mechanism of SPAN.

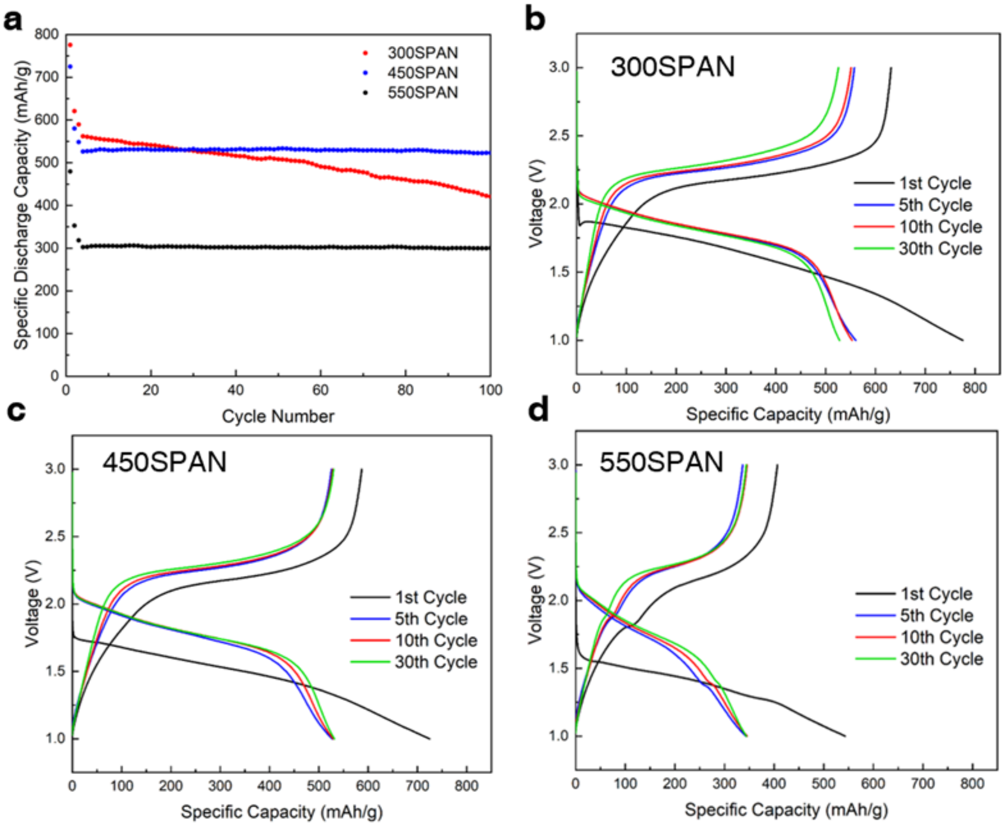

Figure 104. (a) Cycling performance and voltage profiles of SPAN synthesized at three temperatures: (b) 300°C (300SPAN), (c) 450°C (450SPAN), and (d) 550°C (550SPAN).

Controlling Chemical Corrosions of Li-Metal Anodes

Previously, UCSD reported the trend of Li-metal corrosion rate in carbonate-based Gen2 electrolyte and a high-concentration ether-based electrolyte (dual salt). It was found that the corrosion rate of the lithium metal might be related to two parameters: (1) porosity of lithium; and (2) surface chemistry of lithium. This quarter, the team studied the effect of porosity on the corrosion rate of lithium in the Gen2 electrolyte.

In the team's previous work on pressure effects on Li-metal deposition, it was shown that stacking pressure could effectively control the porosity of deposited lithium. To investigate the effects of lithium porosity on the corrosion rate, a split cell together with a pressure sensor is used for controlling the stacking pressure during lithium plating (Figure 105a), which can help the team obtain deposited lithium with different porosities. Similar to the previous case, 0.318 mAh of lithium is plated onto copper substrate at a rate of 0.5 mAh/cm^2 in Gen2 electrolyte. However, the electrode size is changed from 1.27 cm^2 to 0.385 cm^2 to accommodate the smaller size of the split cell. Two different stacking pressures, coin cell pressure (150 kPa) and optimized lithium plating pressure (350 kPa), were applied during the lithium plating process. The plated lithium with the copper substrate is recovered from the split cell and immersed in flooded electrolyte for corrosion study. Figure 105b shows the Li^0 mass retention (%) of the lithium plated under two pressures. The lower porosity of the lithium plated under 350 kPa showed clear evidence in suppressing the lithium corrosion rate. The metallic Li^0 lost about 18% of its original mass after 20 days. In contrast, 29.2% of Li^0 was lost in the case of coin cell pressure of 150 kPa. When comparing the improved lithium corrosion trend to that of lithium plated in dual-salt electrolyte under coin cell pressure, it is found that the two corrosion trends are similar (Figure 105c), demonstrating that with the optimized stacking pressure applied during lithium plating, the resulting low porosity lithium can have a reduced corrosion rate even in conventional carbonate electrolyte comparable with the dual-salt electrolyte. The cryo-FIB/SEM images also illustrate the morphological change of the lithium plated under different pressures before and after corrosion. From the top-view and cross-sectional images of the lithium plated under coin cell pressure, the resulting lithium is in whisker-like morphology (Figure 105d/h). However, just after seven days of immersion in Gen2 electrolyte, there is a noticeable shrinkage in both the plated lithium's thickness and the diameter of whiskers. In contrast, the morphology of lithium plated under 350 kPa pressure did not show a significant change. The lithium retained its dense morphology after seven days of immersion, especially in the cross-section. The only noticeable changes occurred on the top surface of the dense lithium, where some flower-like materials begin to form on the surface. With these results, it can be seen that lithium corrosion only takes place at the interface between lithium and electrolyte. Therefore, the porosity of the plated lithium should play a major role in controlling the corrosion rate of lithium. Next quarter, the role of surface chemistry in the corrosion of lithium metal will be studied in more detail.

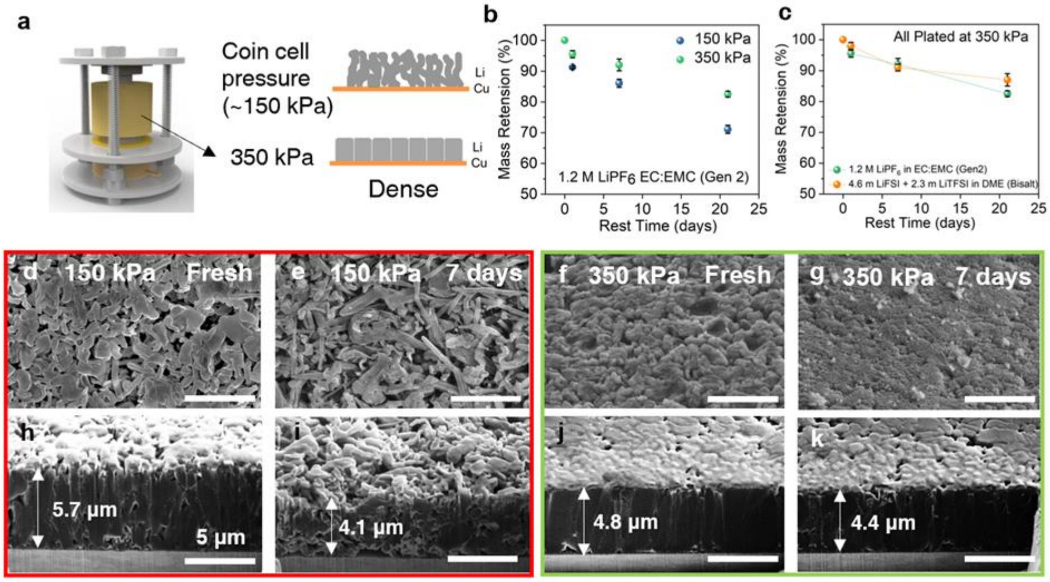

Figure 105. Effect of morphology control on limiting the corrosion of lithium in liquid electrolyte. (a) Schematics of stacking pressure control set up. (b) Trend of Li^0 mass retention (%) of lithium plated under two stacking pressures (coin cell pressure and 350 kPa pressure) in Gen 2 electrolyte. (c) The comparison between Li^0 mass retentions (%) of lithium plated in Gen2 electrolyte with 350 kPa and in Bisalt electrolyte in coin cell. (d-k) Top-view and cross-sectional scanning electron microscopy images of the deposited lithium metal in Gen2 electrolyte: under coin cell pressure after (d/ h) freshly deposited and (e/i) after 7 days of resting, and under 350 kPa pressure after (f/ j) freshly deposited and (g/k) after 7 days of resting.

Effect of Magnesium Additive on Li-Metal Plating

J. Goodenough's group at UT introduced one simple electrolyte additive, $Mg(ClO_4)_2$, to achieve stable lithium plating/stripping and improve cycling life of rechargeable Li-metal batteries. Li/Cu and Li/Li symmetric cells were assembled to evaluate the interfacial chemistry of the metallic lithium anode with LHCEs (Figure 106). The electrolyte with $Mg(ClO_4)_2$ delivered a much higher CE (~ 99.0%) than the cell with the pristine one (~ 96.0%) at 1 mA cm^{-2} during 400 cycles (Figure 106a-c). The good stability with the metallic lithium anode for the LHCE with the additive is observed at 1 mAh cm^{-2} and 2 mAh cm^{-2} in the symmetric Li/Li cells (Figure 106d-e); no apparent voltage polarization increase was seen. Figure 106f-i compares the Li-metal surface after cycling with different electrolytes. After being cycled in LHCE with $Mg(ClO_4)_2$ additive, the lithium metal showed a more compact and smoother surface. Large lithium particles with over 5 µm and low tortuosity are packed closely. The deposited lithium (~ 40-µm thick, Figure 106i) is much thinner than that formed in the pristine LHCE; the compact lithium deposition with a low surface area can significantly mitigate the parasitic reaction between the electrolyte and the metallic lithium anode.

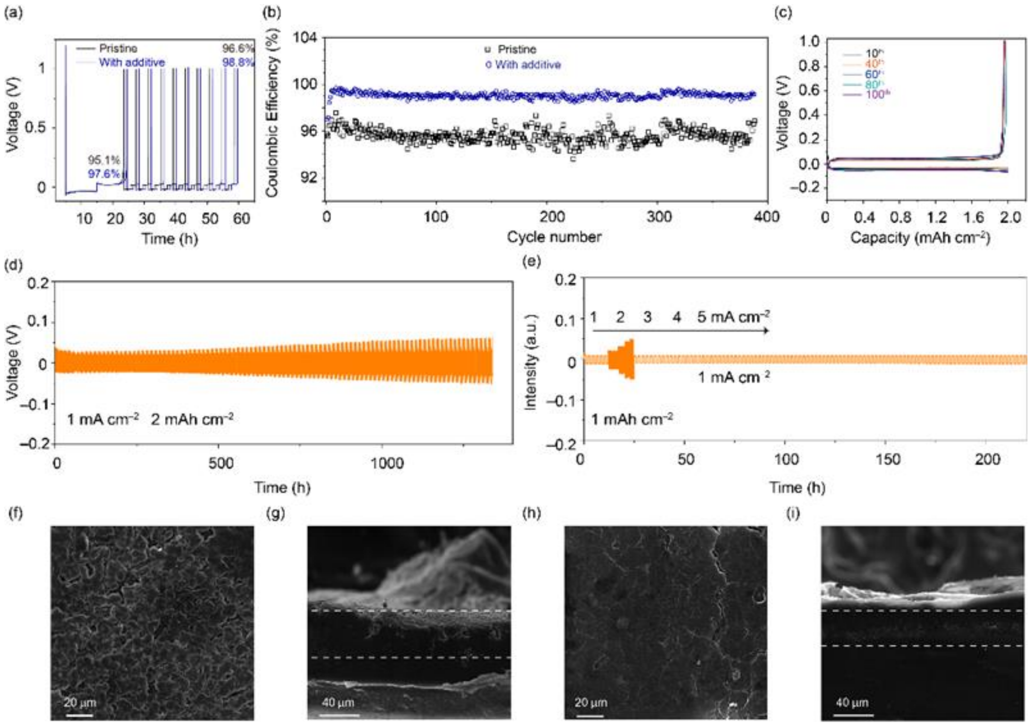

Figure 106. (a) Electrochemical performance of Li/Cu cells at 1 mA cm^{-2}. (b) Coulombic efficiency of Li/Cu cells at 1 mA cm^{-2} and 1 mAh cm^{-2} for 400 cycles. (c) Galvanostatic lithium plating/stripping profile of Li/Cu cells at 1 mA cm^{-2} and 2 mAh cm^{-2}. (d) Long–term cycling of Li/Li symmetric cell with the additive $Mg(ClO_4)_2$. (e) Rate performance of symmetrical cell. Scanning electron microscopy top–view/cross-section images of cycled Li-metal anodes (100 cycles) obtained from LHCE (f, g) without and (h, i) with the additive.

Highlights of Keystone Project 2

The highlights for this quarter are as follows:

- UCSD showed that polymer precursors based on pyridine structure can lead to SPAN-like materials with different operating potentials.
- UCSD showed that synthesis temperature is crucial for achieving high-performance SPAN materials.
- UCSD showed that optimizing pressure can dramatically improve Li-metal cycling.
- UT Austin demonstrated that a simple manganese salt additive can significantly improve Li-metal plating morphology.

Keystone Project 3: Cell Fabrication, Testing, and Diagnosis

This quarter, Idaho National Laboratory (INL) studied the effects of formation cycling temperature on the cycle life of Li-metal batteries. For Li-ion cells, it is known that early cycling and formation play a distinct role in cell performance and eventual cycle life. While extensive effort has been placed on advancing formation for Li-ion cells, there is a lack of good understanding of how different early life protocols impact Li-metal batteries. The advancement of electrolytes such as LHCE developed by the Battery500 team and high concentration electrolytes (HCEs) rely on unique ion solvation. To more directly understand the role of early cycling on life and formation of a stable SEI, studies were performed on how the interface and performance evolved when early cycling was performed at different temperatures. It was found that cycle life was optimized when early cycling was at 25°C.

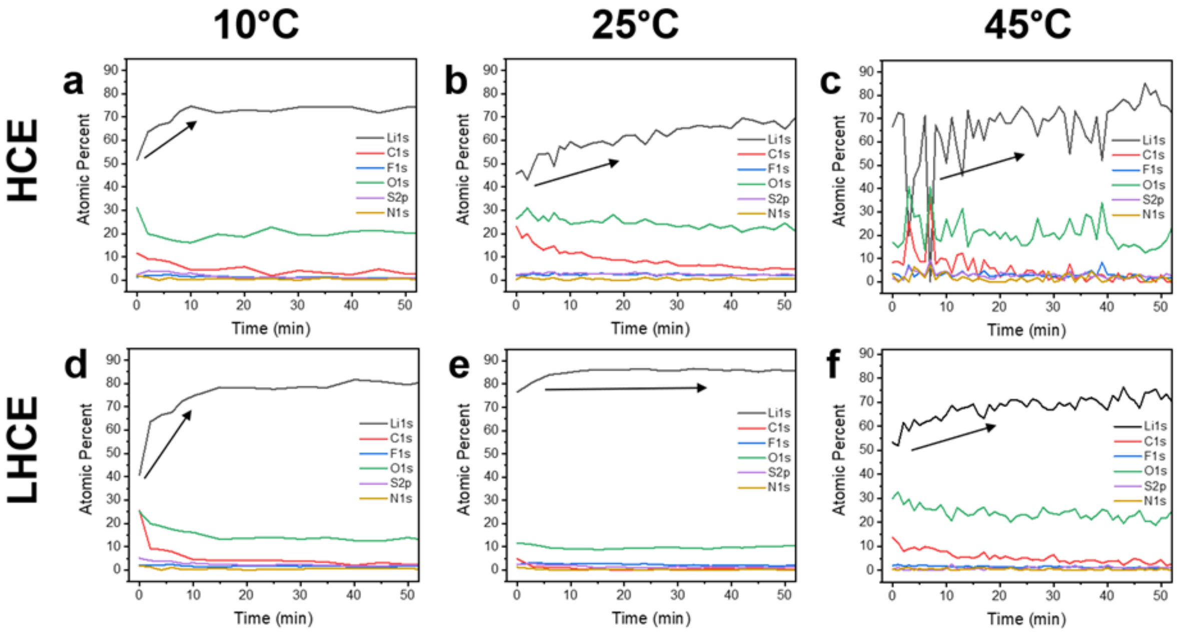

Figure 107. X-ray photoelectron spectroscopy depth profiles for (top) high concentration electrolyte and (bottom) localized high concentration electrolyte cells at (a/d) 10°C, (b/e) 25°C, and (c/f) 45°C during formation cycles.

To understand this performance, XPS with depth profiling was utilized to observe SEI composition after two formation cycles (C/20) at the end of discharge in HCE and LHCE electrolytes at various temperatures (Figure 107). General trends in atomic percent of lithium tell the story of SEI thickness, where a high amount (> 70 at%) suggests presence of lithium metal. Trends in other atomic concentrations as a function of depth (measured in minutes of sputtering) are also observable with depth profiling. In HCE, the higher temperatures have linear trends in elemental concentration over time of sputtering, revealing thicker SEIs. At 10°C, HCE has a relatively thin SEI, where an initial transition in elemental make-up is observed, until after about 10 minutes of sputtering the elemental variation is consistent and > 70 at% lithium. Further, intermittent presence of enriched lithium was observed early-on in the depth profile for HCE at 45°C, which could imply an existence of "dead" lithium. Though isolated from the active lithium foil, dead lithium exists in a Li-metal state, which could result in the intermittent increases in lithium concentration in the depth profile. For LHCE, a thin SEI structure is seen for 10°C, and a linear trend (that is, thicker SEI) is seen for 45°C. At 25°C, there is more than 80 at% lithium present that remains relatively uniform for the entirety of the sputtering; therefore, the SEI is very thin for LHCE at 25°C after formation cycles.

Table 11. X-ray photoelectron spectroscopy depth profile atomic ratios of fluorine, sulfur, and nitrogen to carbon; average over the range of the SEI for each electrolyte and temperature (a cut-off of 20 minutes sputtering was used for depth profiles with linear trends).

	HCE			LHCE		
	10°C	**25°C**	**45°C**	**10°C**	**25°C**	**45°C**
F:C Ratio	0.25	0.20	0.21	0.25	1.07	0.24
S:C Ratio	0.45	0.23	0.16	0.45	1.86	0.097
N:C Ratio	0.089	0.038	0.24	0.074	1.63	0.086

Looking more closely at the lower concentrated elements (Table 11), an increase in FSI^- anion, inorganic-rich byproducts (fluorine, sulfur, and nitrogen) relative to carbon is observed for LHCE at 25°C, while others have relatively lower sulfur, nitrogen, and fluorine content in ratio to carbon. Carbon is the prominent product of DME reaction with lithium, seen during the charge desolvation process of SSIPs (that is, high Li^+-DME interaction structures). Oxygen was excluded due to its role in both FSI^- and DME reactions to form SEI; the distinction of oxygen products will be discussed later with XPS peak deconvolution. Others have noted that the amount of fluorine (such as LiF) present in the SEI is paramount for improved cyclability. This work presents the same idea from a different angle, where a decreased amount of organics (deemed bad actors) in the SEI also leads to improved cyclability, even though relative fluorine concentration is not a massive contributor to the SEI composition. Therefore, methods of producing a more ideal SEI can operate in promoting supportive products (for example, LiF and other inorganics) and/or demoting inferior products (for example, carbon-based organics).

In other work efforts, INL focused on developing approaches for analyzing degradation, safety, and failure of high-Ni NMC-based high-energy cell design and evaluation. They have developed an electrochemical analytic diagnosis (eCAD) approach to evaluate "battery electrode formulation and cell performance" correlation with the capability of quantitative analyses to provide detailed information for improvements. Currently, two cathode materials, NMC-622 and NMC-811 from multiple sources, are being used as the model materials for cell design improvements and evaluation. Here, a theoretical framework revealed by the eCAD analyses is used for comparison of the different cell designs and materials to provide insight about what aspect is critical for performance improvement. An example of the analysis is shown in Figure 108.

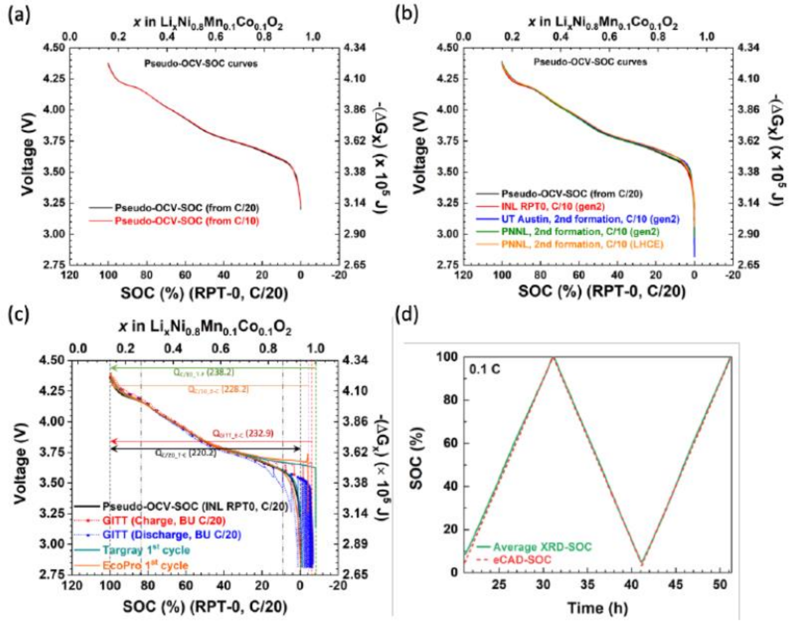

Figure 108. Comparison of different results developed using the eCAD method. (a) Using coin cell data at C/20 and C/10, (b) with different cathode formulations, cell configurations and electrolytes, (c) comparison to galvanostatic intermittent titration (GITT) results, and (d) comparison of eCAD derived state of charge (SOC) and X-ray diffraction determined SOC.

To ensure flexibility of the analysis, results from two different material manufacturers and cells prepared at four institutions were analyzed. The results were also directly compared with XRD data captured as a function of SOC. Aspects of the analysis are also able to evaluate how utilization of the cathode materials changes over time. These results can directly show how one electrode or processing condition can impact cell energy. If used across the course of cycling, it can also suggest how slight changes in utilization lead to enhanced life or more rapid cell failure. Combined, the methods provide a means to compare results more directly across samples and to provide a more common 'baseline' for comparison.

Highlights of Keystone Project 3

The highlights for this quarter are as follows:

- INL refined understanding of the role of early cycling at different temperatures on cell performance and SEI property, showing that 25°C is the optimized formation cycling temperature.
- INL coordinated analysis of multiple cell designs and compositions to validate the analysis methods of eCAD developed at INL.

Keystone Project 4: Cross-Cutting Efforts

The goal of the Cross-cutting team is to develop and deploy advanced characterization tools in support of the three Keystone efforts, with a focus on probing specific materials and interfaces for Keystone 1, probing individual electrodes for Keystone 2, and probing the whole cell for Keystone 3. This quarter, the Cross-cutting team completed its milestone of "Complete the studies of electrolyte salt concentration effects on the Li solvation and good SEI formation on Li metal anode using X-ray and neutron PDF (BNL and PNNL)," as well as this quarter's milestone to "Complete the synchrotron-based TXM studies on CEI interphase protection for NMC cathode cycled at high voltage limit" for the Battery500 consortium. The TXM XRT results obtained by BNL on the NMC cathode provided by PNNL show the significant suppression of crack formation for secondary particles by using a new additive in the electrolyte. BNL led experimental efforts to characterize lithium solvation in electrolytes, with PNNL providing key samples of interest to Keystone 1. A complementary theoretical effort was carried out at Texas A&M, providing information on coordination and dynamics that cannot directly be accessed through experiments.

The BNL team applied synchrotron-based X-ray PDF together with MD simulation to understand the role of Li^+ solvation structure in determining SEI chemistry. This work was done in collaboration with Keystone 1 researchers at PNNL, as well as with external collaborators at the ARL for MD simulations. In this work, comparative studies were done for low concentration electrolytes (LCE) with a 1 M salt concentration and HCE with a 5 M salt concentration. Three common battery solvents were investigated: DME, DMC, and PC, with the same LiFSI salt used for all. The PDF results obtained from the Fourier transform of X-ray scattering data collected out to high Q values are plotted in the form of G(r) for all six liquid samples in Figure 109a, with the molecular structure of the key components given in Figure 109b. In all cases, the first PDF peak, which is centered ~ 1.5 Å, is found to be significantly broader than for the analogous peaks observed previously for solid SEI samples obtained using the same electrolyte formulations. This first peak includes the contributions from directly bonded atom pairs, including the C=O (1.28 Å), C-O (1.36 Å), and C-C (1.54 Å) bonds of solvents as well as the S-N (1.56 Å), S=O (1.43 Å), and S-F (1.54 Å) bonds of the FSI^- anion, where the typical bond distances are indicated in parentheses. This contrasts with the case of the solid SEI, which was either dominated by solvent-derived molecular species when LCE SEI samples were studied or was dominated by FSI reduction products when HCE SEI samples were studied. The next most clearly resolved PDF peak is at 2.5 Å and corresponds to the next-nearest neighbor interactions, as the bond angles remain well defined. However, peaks at larger distances correspond to more distant atoms whose relative positions depend on torsion angles that are quite variable in liquid samples. This leads to a loss of coherence, broadening of PDF peaks, and the absence of features attributable to specific bonding interactions beyond ~ 5 Å. When the PDF patterns of the LCE and

HCE electrolytes are compared, it can be seen that the 1.5 Å and 2.5 Å peaks of the HCE samples are higher in intensity, and that this extra intensity presents at longer distances (larger *r*) than for the LCE samples. This is a consequence of the sulfur atoms in the FSI anion, which scatter X-rays more strongly than the carbon atoms in the solvent and which have ligand distances that are ~ 0.2 Å longer than for carbon atoms. Due to the low atomic number of lithium, it is extremely challenging to extract information about atomic pairs involving lithium from experimental X-ray PDF measurements. Therefore, MD simulations were carried out to better understand the Li-ion coordination in the electrolyte. The electrolyte solvation structure obtained from MD simulations closely matches the experimentally measured PDF patterns for both LCE and HCE samples (Figure 109c), suggesting that the MD simulations are able to reproduce the real physical behavior of samples. To investigate the effect of the electrolyte concentration on the lithium environment in the electrolyte, the partial PDFs for just the $Li\text{-}O_{anion}$ (blue) and $Li\text{-}O_{solvent}$ (orange) atoms were calculated using the MD simulation results (Figure 109d). It is found that in LCEs, lithium coordination is dominated by solvent molecules, while in HCEs a large number of FSI anions become a part of the lithium coordination environment. The decomposition of the HCE at the interphase can therefore lead to formation of SEI with a large amount of solid nanocrystalline LiF. This type of SEI has better Li^+ transport, anode protection properties, and electrochemical performance than the SEI formed from LCEs. These results demonstrated that synchrotron-based PDF is a powerful tool to study the lithium solvation structure in electrolytes and can provide direct insights into the origin of the improved SEI and Li-metal anode protection that occurs for certain electrolyte formulations.

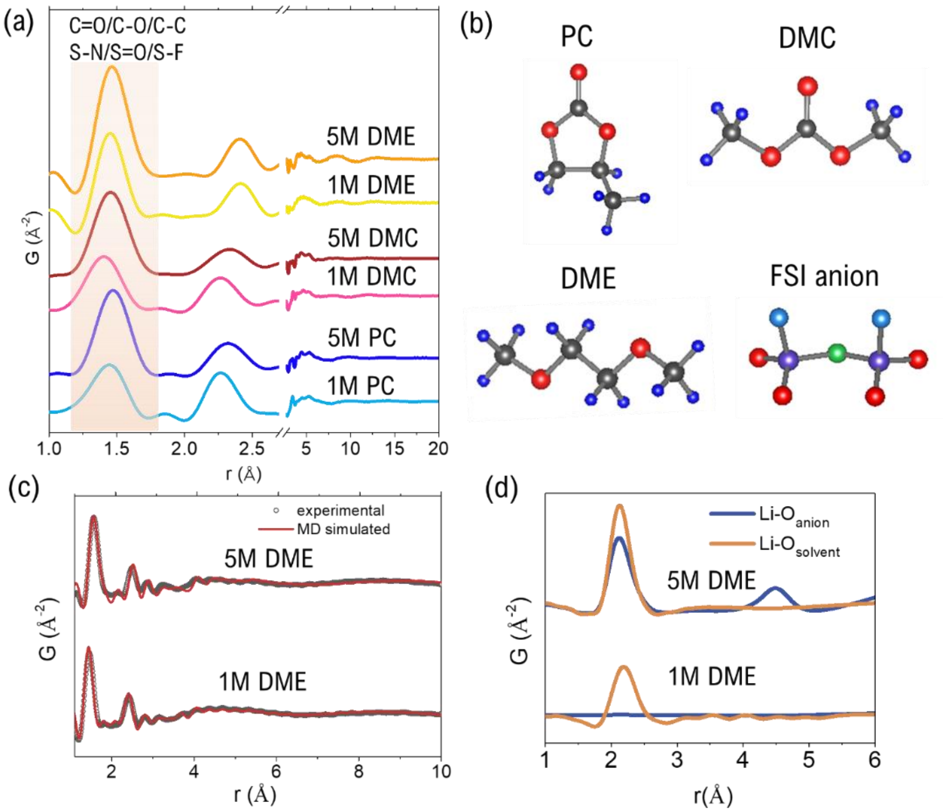

Figure 109. Characterization of the electrolyte structure. (a) X-ray pair distribution function (PDF) data for low (1 M) and high (5 M) concentration LiFSI electrolytes with PC, DMC, or DME as the solvent. (b) Molecular structure of the three solvents and the FSI anion. Carbon atoms are shown in black, hydrogen in dark blue, oxygen in red, nitrogen in green, and sulfur in purple. (c) Comparison of measured and calculated [using the electrolyte structure determined by molecular dynamics (MD) simulation] PDF patterns for high-concentration and low-concentration DME electrolytes, and of (d) partial PDFs calculated from MD simulations for pairs of Li-anion oxygen (blue) and Li-solvent oxygen (orange).

Complementary computational work was done by the team at Texas A&M to directly understand the electrolyte structure and transport properties. Specifically, DFT was used with a thermodynamic integration method implemented in constrained – *ab initio* molecular dynamics (c-AIMD) to calculate the free energy profile for different pathways transporting the lithium cation pathway toward the anode. The trajectory and evolution of the solvation complex surrounding the lithium cation, along with the effect of salt concentration and diluent presence, were studied in three liquids: LCE, HCE, and LHCE. The thermodynamic integration method allowed the team to identify energy barriers and their correlation with changes in Li-ion solvation.

In dilute electrolytes (1.21 M LiFSI in DMC), the energy barriers during the diffusion are relatively low (< 0.2 eV) and the cation deposition on the surface is guided by the anion and solvent reduction. In HCE (5.49 M LiFSI in DMC), the high connectivity between the primary solvation complex with the rest of the electrolyte leads to a significant increase in the energy barriers (> 3eV) for diffusion, and the ion complexes can get trapped in the electrolyte, slowing down their surface deposition and enabling a thick and compact SEI to be built through anion decomposition. In LHCE (1.27 M LiFSI in DMC/BTFE), the BTFE diluent helps reduce the barriers (most of them on the order of 0.3 eV) present in HCE and break up the high cation-solvation complex connectivity, thereby facilitating cation diffusion and simultaneous SEI formation processes. Figure 110 illustrates some of the events captured during the dynamic evolution of the systems.

The rate of cation deposition near the surface is clearly impacted by the rate of the electrolyte decomposition reactions. Once the SEI starts to be formed, the cation gets trapped within charged fragments and radical species. The nature and chemistry of the electrolyte defines the SEI rate of nucleation and morphology, and both are crucial to facilitate or impede ionic diffusion. In Figure 110, three carbonate molecules and an anion solvate the cation in LCE. Near the surface, the higher reduction potential of the anion determines its rotation toward the surface, dragging the rest of the solvation complex; Li^+ cannot escape the anion network in HCE. In contrast, similar environments in LHCE can be overcome because of the weakly interacting diluent molecule that breaks the strong cation-anion interaction.

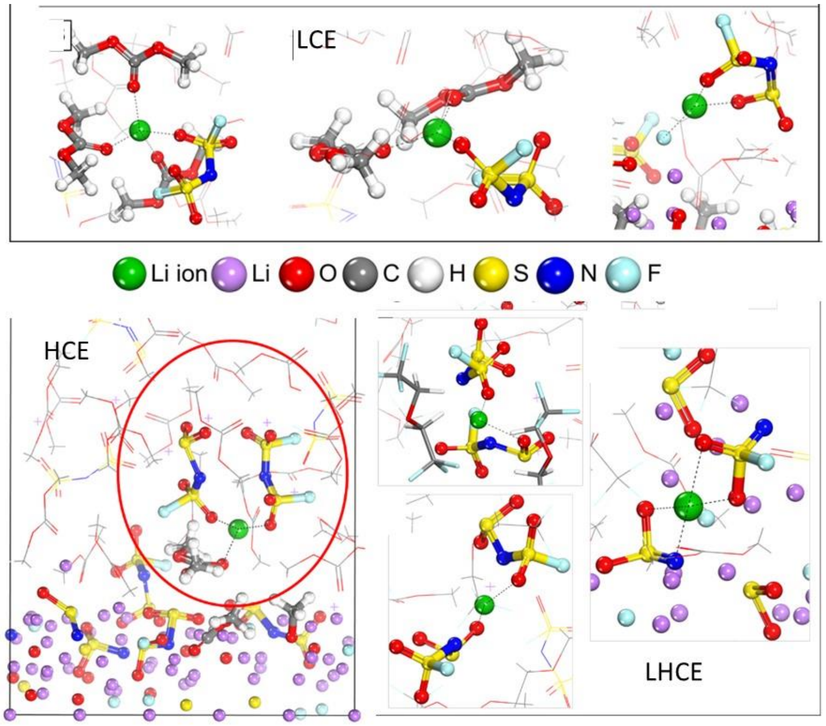

Figure 110. Near the anode surface, solvated Li^+ in low-concentration electrolyte (LCE) complex (top) diffuses through the electrolyte guided by the anion high electron affinity. In high-concentration electrolyte (HCE, bottom left) Li^+ gets trapped in a thick 3D network that is broken only through anion reduction and thick SEI formation. In localized HCE (LHCE), the presence of the diluent in the 2nd solvation shell disrupts the strong cation-anion interaction and allows Li^+ migration with barriers comparable to LCE.

Highlights of Keystone Project 4 (Cross-Cutting Efforts)

The highlights for this quarter are as follows:

- The BNL team utilized an X-ray PDF technique combined with MD simulations to probe the lithium solvation structures in LEs. It was found that in HCE, the solvation structure promotes anion reduction for SEI formation; the LCE promotes solvent reduction, resulting in better Li-metal protection for HCE.
- Texas A&M applied a new *ab initio* simulation approach to evaluate barriers for lithium cation transport and deposition with simultaneous SEI formation on the lithium anode. They showed in HCE that a significant increase in the energy barriers for cation diffusion and the ion complexes trapped in the HCE can slow down their surface deposition, enabling a thick and compact SEI to be built through anion decomposition; in contrast, the barriers are significantly lower in LHCE electrolytes, while keeping an anion-dominated SEI.

Patents/Publications/Presentations

Patents

- Bao, Z., Y. Cui, Z. Yu, and Y. Lin. "Tuning Fluorination Degree of Ether and Carbonate Based Electrolyte Solvents for Lithium and Lithium Metal Batteries," U. S. Provisional Patent Application No. 63/283,828; filed date: 11/29/2021.
- Bao, Z., Y. Cui, Y. Chen, Z. Yu, and Y. Lin. "Molecular Design Strategies to Achieve Favorable Ion Solvation Structures for Stable Operation of Lithium Metal Batteries," U. S. Provisional Patent Application No. 63/270,506; filed date: 10/21/2021.

Publications

- Chen, Y.,* Z. Yu,* P. E. Rudnicki, H. Gong, Z. Huang, S. C. Kim, J-C. Lai, X. Kong, J. Qin, Y. Cui, and Z. Bao. "Steric Effect Tuned Ion Solvation Enabling Stable Cycling of High-Voltage Lithium Metal Battery." *Journal of the American Chemical Society* 143, No. 44 (2021): 18703–18713. doi: 10.1021/jacs.1c09006.
- Gao, X., X. Zheng, Y. Tsao, P. Zhang, X. Xiao, Y. Ye, J. Li, Y. Yang, R. Xu, Z. Bao, and Y. Cui. "All-Solid-State Lithium-Sulfur Batteries Enhanced by Redox Mediators." *Journal of the American Chemical Society* 143, No. 43 (2021): 18188–18195. doi: 10.1021/jacs.1c07754.
- Cui, Z., Q. Xie, and A. Manthiram. "A Cobalt- and Manganese-Free High-Nickel Layered Oxide Cathode for Long-Life, Safer Lithium-Ion Batteries." *Advanced Energy Materials* 11, No. 41 (2021): 210242. doi: 10.1002/aenm.202102421.
- Ren, Y., Z. Cui, A. Bhargav, J. He, and A. Manthiram. "A Self-Healable Sulfide/Polymer Composite Electrolyte for Long-Life, Low-Lithium-Excess Lithium-Metal Batteries." *Advanced Functional Materials* 32, No. 2 (2021): 2106680. doi: 10.1002/adfm.202106680.
- Langdon, J., Z. Cui, and A. Manthiram. "Role of Electrolyte in Overcoming the Challenges of $LiNiO_2$ Cathode in Lithium Batteries." *ACS Energy Letters* 6 (2021): 3809-3816. doi: 10.1021/acsenergylett.1c01714.
- Shadike, Z.,* S. Tana, R. Lin, X. Cao, E. Hu,* and X-Q. Yang.* "Engineering and Characterization of Interphases for Lithium Metal Anode." *Chemical Sciences* 6 (2022). doi: 10.1039/D1SC06181J.
- Chinnam, P. R., L. Xu, L. Cai, N. L. Cordes, S. Kim, C. M. Efaw, D. J. Murray, E. J. Dufek, H. Xu, and B. Li. "Unlocking Failure Mechanisms and Improvement of Practical Li–S Pouch Cells through *In Operando* Pressure Study." *Advanced Energy Materials* (2021): 2103048. doi: 10.1002/aenm.202103048.
- Wu, Z., H. Liu, S. Yu, and P. Liu. "Binder Effects on Cycling Performance of High Areal Capacity SPAN Electrode." *Journal of The Electrochemical Society* 168 (2021): 110504. doi: 10.1149/1945-7111/ac315b.
- Fang, C., B. Lu, G. Pawar, M. Zhang, D. Cheng, S. Chen, M. Ceja, J-M. Doux, M. Cai, B. Liaw, and Y. S. Meng. "Pressure-Tailored Highly-Reversible Lithium Metal Electrode for Rechargeable Lithium Batteries." *Nature Energy* 6 (2021): 987–994. doi: 10.1038/s41560-021-00917-3.

  Angarita-Gomez, S., and P. B. Balbuena. "Understanding Solid Electrolyte Interphase Nucleation and Growth on Lithium Metal Surfaces." *Batteries* 7, No. 4 (2021): 73. doi: 10.3390/batteries7040073.

Presentations (Invited)

- CBMM Niobium Webinar (October 5, 2021): "Li-Ion Batteries: Pushing the Limits for Electrifying the Transportation Sector"; M. Stanley Whittingham.
- University of Michigan, Materials Science & Engineering, Van Vlack Lecture (October 8, 2021): "The Lithium Battery, from a Dream to Readiness to Take on Climate Change – Materials Opportunities and Challenges"; M. S. Whittingham.

- Oxford University, Chemistry Department, MLH Green Lecture (October 11, 2021): "The Lithium Battery, from a Dream to Readiness to Take on Climate Change – Opportunities and Challenges"; M. S. Whittingham.
- Africa MRS (November 9, 2021): "Lithium Batteries: From a Dream to Enabling a Clean Fossil-Free World"; M. S. Whittingham.
- Faraday Institution, UK (November 17, 2021): "Energy Storage is Key to Attainment of Fossil-Free Energy"; M. S. Whittingham.
- MRS, Symposium X, Boston, Massachusetts (November 30, 2021): "The Lithium Battery: From a Dream to Readiness to Take-On Climate Change – Materials Challenges"; M. S. Whittingham.
- 240th ECS Meeting, Orlando, Florida (October 10–14, 2021): "A Path Toward Sustainable Battery Technologies"; A. Manthiram.
- 240th ECS Meeting, Orlando, Florida (October 10–14, 2021): "A Solid-State Chemistry Perspective of Layered Oxide Cathodes for Lithium-Ion Batteries"; A. Manthiram.
- UT Austin Portugal Annual Conference, Virtual (October 20–21, 2021): "Sustainable Next-Generation Battery Chemistries"; A. Manthiram.
- MRS Taiwan International Conference, Taipei, Taiwan (November 13–17, 2021): "Sustainable Battery Chemistries for Electrical Energy Storage"; A. Manthiram. Plenary talk.
- American Institute of Chemical Engineers Annual Meeting, Boston, Massachusetts (November 14–19, 2021): "Delineating and Controlling the Electrode-Electrolyte Interfacial Reactions in High Energy Density Batteries"; A. Manthiram.
- 3rd IEEE Bombay Section Signature Conference, Bombay, India (November 18–20, 2021): "Sustainable Battery Technologies for Vehicle Electrification"; A. Manthiram.
- 3rd Indian Materials Conclave and 32nd Annual General Meeting of the MRS of India, Bangalore, India (December 20–23, 2021): "Sustainable Battery Technologies for Clean Energy and Environment"; A. Manthiram.
- Storage X Symposium (October 8, 2021): "Lithium Metal Anodes with Nonaqueous Electrolytes"; J-G. Zhang.
- 240th ECS Meeting (October 10, 2021): "Stability of Li Metal Anode and Calendar Life of Lithium Metal Batteries"; J-G. Zhang.
- Binghamton University, Chemistry Department Seminar, Virtual (November 5, 2021): "Materials Chemistry in Electrochemical Energy Storage"; J. Xiao.
- IBA, Virtual (October 24, 2021): "From Materials Science to Prototype Batteries and Cell Manufacturing"; J. Xiao.
- IBA, Virtual (October 24, 2021): "Li-S Batteries with Pyrolyzed Polymer Sulfur Cathodes"; P. Liu.
- MRS Meetings & Exhibits (December 2021): "Design of Stable Cathodes for Solid State Li-S Batteries"; P. Liu.
- MRS Fall Meetings & Exhibits, Boston, Massachusetts (November 29, 2021): "Advanced Characterization for Li Metal and Solid-State Batteries"; Y. S. Meng. Keynote talk.
- Texas Tech University, Seminar (October 8, 2021): "Electron and Ion Transport in Li-metal Batteries: Role of the Electrolyte"; P. B. Balbuena.
- University of Colorado, Boulder, Colorado (November 18, 2021): "Interrogating Electrochemical Interfaces at the Atomistic Level: Links to Macroscopic Behavior"; P. B. Balbuena.

APPENDIX – ACRONYM GUIDE

Acronym	Full Description
1,4-DX	1,4-dioxane
1D	one-dimensional
2D	two-dimensional
3D	three-dimensional
3DOM	three-dimensional ordered microporous
3D-OMSH	three-dimensionally ordered microporous sulfur host
AB	acetylene black
ABL	active buffer layer
AC	alternating current
ACS	American Chemical Society
AFM	atomic force microscopy
AIMD	*ab initio* molecular dynamic
AIR	areal interfacial resistance
ALD	atomic layer deposition
ALS	Advanced Light Source
ANL	Argonne National Laboratory
ANN	artificial neural network
APS	Advanced Photon Source
AQC	anthraquinone-2-carboxylic acid
AQT	1,5-bis(2-(2-(2methoxyethoxy)ethoxy)ethoxy) anthra-9,10-quinone
ARC	accelerating rate calorimetry
ARL	U. S. Army Research Laboratory
ASR	area specific resistance
ASSB	all-solid-state battery
ASSLB	all-solid-state lithium battery
ASSLMB	All-solid-state lithium-metal battery
ASSLSB	all-solid-state lithium-sulfur battery
ATR	attenuated total reflectance
BBP	benzyl butyl phthalate
BE	baseline electrolyte
BEV	battery electric vehicle
BL	bottom layer
β-LPS	β-phase Li_3PS_4
BMIM	1-butyl-3-methylimidazolium
BMR	Advanced Battery Materials Research Program
BNL	Brookhaven National Laboratory
BTFE	bis(2,2,2trifluoroethyl) ether
BV	Butler-Volmer
c-AIMD	constrained – *ab initio* molecular dynamics
CAM	cathode active material
CC	carbonized cotton
CCCV	constant current / constant voltage
CCD	critical current density

Acronym	Full Description
CE	Coulombic efficiency
CEI	cathode electrolyte interface
CFM	carbon-based framework material
CMC	carboxymethyl cellulose
CMD	classical molecular dynamics
CN	coordination number
CNC	carbon nano-cage
cNEB	climbing image nudged elastic band
CNT	carbon nanotube
COP	critical overpotential
CPE	composite polymer electrolyte
cryo	cryogenic
cryo-EM	cryogenic electron microscopy
cryo-FIB	cryogenic – focused ion beam
cryo-STEM	cryogenic – scanning transmission electron spectroscopy
CSE	cluster-based solid electrolyte
CT	computed tomography
CV	cyclic voltammetry
DBE	dibutyl ether
DB-ML-FF	density-based machine-learning force field
DC	direct current
DCA	dicyanamide
DEB	double-end binding
DEC	diethyl carbonate
DEE	1,2-diethoxyethane
DEGDME	diethylene glycol dimethyl ether
DEMS	differential electrochemical mass spectrometry
DFE	defect formation energy
DFT	density functional theory
DiPE	diisopropyl ether
DIW	direct ink writing
DLR	Deutsches Zentrum für Luft- und Raumfaurt
DMC	dimethyl carbonate
DME	1,2-dimethoxyethane
DMF	dimethyl formamide
DMSO	dimethylsulfoxide
DOD	depth-of-discharge
DOE	U. S. Department of Energy
DOL	1,3-dioxolane
DOS	density of states
dP/dV	differential pressure
dPEO	dynamic bonds between polymer chains
dQ/dV	differential capacity
DRT	distribution of relaxation times
DSC	differential scanning calorimetry
E/C	electrolyte/capacity

Acronym	Full Description
EC	ethylene carbonate
eCAD	electrochemical analytic diagnosis
ECS	The Electrochemical Society
EDL	electrical double layer
EDLi	electrochemically deposited lithium
EDS	energy dispersive X-ray spectroscopy (also known as EDX)
EELS	electron energy loss spectroscopy
eGF	exfoliated graphene fluoride
EIS	electrochemical impedance spectroscopy
eLi	engineered lithium
EM	electron microscopy
EMC	ethyl methyl carbonate
EMIM-BF_4	1-ethyl-3-methylimidazolium tetrafluoroborate
eNMR	electrophoretic nuclear magnetic resonance
EO	ethylene oxide
EPR	electron paramagnetic resonance
EQ-SANS	extended Q-range small-angle neutron scattering diffractometer
E/S	electrolyte/sulfur
EV	electric vehicle
EXAFS	extended X-ray absorption fine structure
FDMB	fluorinated 1,4-dimethoxylbutane
FDMH	fluorinated 1,6-dimethoxyhexane
FDMO	fluorinated 1,8-dimethoxyoctane
FDMP	fluorinated 1,5-dimethoxypentane
FEC	fluoroethylene carbonate
FF	force field
FIB	focused ion beam
fs	femtosecond
FSI	bis(fluorosulfonyl)imide
FTIR	Fourier transform infrared
FZJ	Forschungszentrum Jülich
GB	grain boundary
gc	glass/ceramic
GCPL	galvanostatic cycling with potential limitation
GDL	gas diffusion layer
GE	gel electrolyte
GITT	galvanostatic intermittent titration technique
GM	General Motors
GOMD	Glass & Optical Materials Division
GP	Gaussian process
GPC	gel permeation chromatography
Gr	graphene
GSE	glassy solid electrolyte
HAADF	high-angle annular dark-field
HATN	hexaazatrinaphthylene
HATN-S	hexaazatrinaphthylene polymer – sulfur composite

Acronym	Full Description
HC	hard carbon
HCE	high-concentrated electrolyte
HEV	hybrid electric vehicle
HEXRD	high-energy X-ray diffraction
HFE	hydrofluoroether
HFP	hexafluoropropylene
HOPG	highly oriented pyrolytic graphite
HPC	high-performance computing
HPLC	high-performance liquid chromatography
HRTEM	high-resolution transmission electron microscopy
HT	high throughput
IBA	International Battery Materials Association
IEEE	Institute of Electrical and Electronics Engineers
IL	ionic liquid
INL	Idaho National Laboratory
IPA	isopropanol
IR	Infrared
ISEL	Israel Electrochemical Society
ISU	Iowa State University
KAIST	Korea Advanced Institute of Science and Technology
KB	Ketjenblack
KMC	kinetic Monte Carlo
LATP	$Li_{1+x}Al_xTi_{2-x}(PO_4)_3$
LBNL	Lawrence Berkeley National Laboratory
LBO	Li_3BO_3
LBS	lithium-boron-sulfur
LCE	low concentration electrolyte
LCO	$LiCoO_2$
LCRC	Laboratory Computing Resource Center
LDBE	1.8 M LiFSI in dibutyl ether
LDEE	1.8 M LiFSI in diethyl ether / BTFE
LDiPE	1.8 M LiFSI in diisopropyl ether
LDME	1.8 M LiFSI in 1,2-dimethoxyethane
LE	liquid electrolyte
LFP	lithium iron phosphate
LGPS	$Li_{10}GeP_2S_{12}$
LHCE	localized high concentration electrolyte
LIB	Li-ion battery
LIC	Li-ion conductor
LiPS	Li_7PS_6
Li-SIA	lithium-containing structurally isomorphous alloy
LiTFSI	lithium bis(trifluoromethanesulfonylimide)
LLNL	Lawrence Livermore National Laboratory
LLTO	$Li_{3x}La_{2/3-x}TiO_3$
LLZ	lithium – lanthanum – zirconium
LLZO	$Li_7La_3Zr_2O_{12}$

Acronym	Full Description
LLZTO	Li-La-Zr-Ta-O, or $Li_{6.75}La_3Zr_{1.75}Ta_{0.25}O_{12}$
LMR-NMC	Li- and Mn-rich NMC
LNO	$LiNiO_2$
LOB	lithium-oxygen battery
LPC	large particle cathode
LPS	Li_3PS_4
LPSB	Li_3PS_4 + ½LiBr
LPSCl	Li_6PS_5Cl
LPSI	Li_3PS_4 + ½LiI
LPSIB	$Li_7P_2S_8I_{0.5}Br_{0.5}$
LSiPCl	$Li_{9.54}Si_{1.74}P_{1.44}S_{11.7}Cl_{0.3}$
LSnS	$Li_{3.85}Sn_{0.85}Sb_{0.15}S_4$
LSV	linear sweep voltammetry
LYC or LYCl	Li_3YCl_6
MC	Monte Carlo
MCA	multicomponent alloy
MD	molecular dynamics
METS	multi-harmonic electrothermal spectroscopy
MGF	mixed glass former
MIC	molecular ionic composite
ML	machine learning
MLMD	molecular dynamics simulation with machine-learning potential
MOF	metal-organic framework
MOS	mixed oxy-sulfide
MOSN	mixed oxy-sulfide nitride
MPI	message-passing interface
MRS	Materials Research Society
MS	mass spectrometry
MSD	mean square displacement
MSE	mean squared error
MTU	Michigan Technological University
MWCNT	multi-walled carbon nanotube
MYEGA	Mauro–Yue–Ellison–Gupta–Allan model
NaFSI	sodium bis(fluorosulfonyl)imide
NaNMC	sodium nickel manganese cobalt oxide (for example, $NaNi_{0.4}Mn_{0.4}Co_{0.2}O_2$ and $NaNi_{0.68}Mn_{0.22}Co_{0.1}O_2$)
nano-FTIR	Fourier transform infrared nano-spectroscopy
NASICON	sodium super ionic conductor
NATM	$LiNi_{0.93}Al_{0.05}Ti_{0.01}Mg_{0.01}O_2$
NBO	nonbridging oxygen
NBR	nitrile butadiene rubber
NBS	nonbridging sulfur
NC	$LiNi_{0.94}Co_{0.06}O_2$
NCEM	National Center for Electron Microscopy
NCM	Ni-Co-Mn
NCM-622	$LiNi_{0.6-}Co_{0.2-}Mn_{0.2}O_2$

Acronym	Full Description
NCM-85105	$LiNi_{0.85}Co_{0.10}Mn_{0.05}O_2$
NCSE	non-calendered sulfur electrode
ND	di-coordinated nitrogen
NEB	nudged elastic band
NF	nanoflake
NLNMF	$Na_{0.85}Li_{0.1}Ni_{0.175}Mn_{0.525}Fe_{0.2}O_2$
NMC	nickel – manganese – cobalt (for example, $LiNi_{0.90}Mn_{0.05}Co_{0.05}O_2$)
NMC-622	$Ni_{0.6}Mn_{0.2}Co_{0.2}$
NMC-811	$Ni_{0.8}Mn_{0.1}Co_{0.1}$
NMDC	Nanotechnology Materials and Devices Conference
NMF	nonnegative matrix factorization
NMFCN	$NaMnFeCoNiO_2$
NMP	N-methyl-pyrrolidone
NMR	nuclear magnetic resonance
NN	neural network
N/P ratio	capacity ratio between anode (negative electrode) and cathode (positive electrode)
NP	nanoparticle
NPCE	nonflammable polymer composite electrolyte
n-PDF	neutron diffraction and pair distribution function
NPT	constant number of atoms (N), pressure (P), and temperature (T)
NREL	National Renewable Energy Laboratory
ns	nanosecond
NSLS	National Synchrotron Light Source
NT	tri-coordinated nitrogen
NTO	sodium titanate
NVE	constant number (N), volume (V), and energy (E)
NVT	constant temperature, constant volume ensemble
OCV	open circuit voltage
OER	oxygen evolution reaction
OMSH	ordered microporous sulfur host
ORNL	Oak Ridge National Laboratory
ORR	oxygen reduction reaction
OSU	Ohio State University
PAH	polycyclic aromatic hydrocarbon
PAN	polyacrylonitrile
PAQS	poly (anthraquinonyl sulfide)
PBDT	poly(2,2’-disulfonyl-4,4’-benzidine terephthalamide)
PC	propylene carbonate
PCA	principal component analysis
PCC	Pearson correlation coefficient
PC-LCHE	polymeric colloidal localized high concentration electrolyte
PDF	pair distribution function
PDMS	polydimethylsiloxane
PE	polyelectrolyte, or polymer electrolyte
PEEK	polyether ether ketone

Acronym	Full Description
PEG	poly(ethylene glycol)
PEGDA	poly(ethylene glycol) diacrylate
PEGMA	poly(ethylene glycol) methacrylate
PEI	polyethylenimine
PEM	poly(ethylene malonate)
PEO	poly(ethylene oxide)
PES	photon emission spectroscopy
PETEA	pentaerythritol tetraacrylate
PFG	pulsed field gradient
PFIB	plasma focused ion beam
PGE	polymer gel electrolyte
PHEV	plug-in hybrid electric vehicle
PHM	poly(hexylene malonate)
PI	principal investigator
PMMA	polymethyl methacrylate
PMTH	dipentamethylenethiuram hexasulfide
PNNL	Pacific Northwest National Laboratory
POSS	polyhedral oligomeric silsesquioxane
PP	polypropylene
PPM	poly(pentylene malonate)
PS-SEI	polymer-supported solid electrolyte interphase
PST	partially sintered tape
PSTFSI	poly(4-styrenesulfonyl(trifluoromethanesulfonyl) imide)
PSU	Pennsylvania State University
PTFE	polytetrafluoroethylene
PTFSI	triflimide-based polyion
PTM	poly(trimethylene malonate)
PVB	polyvinyl butyral
PVDF	polyvinylidene (di)fluoride
Py	pyrrolidinium
Pyr$_{13}$FSI	*N*-propyl-*N*-methylpyrrolidinium bis(fluorosulfonyl)imide
Pyr$_{14}$TFSI	*N*-butyl-*N*-methylpyrrolidinium bis(trifluoromethanesulfonyl)imide
RDF	radial distribution function
ReaxFF	reactive force field
RF	random forest
rGO	reduced Gr oxide
RM	redox mediator
RMSE	root mean square error
RP	red phosphorus
RPT	reference performance test
SAEP	salt affinitive electrolyte phobic
SANS	small angle neutron scattering
SAXS	small angle X-ray scattering
SC	single crystalline
SE	solid electrolyte
SEB	single-end binding

Acronym	Full Description
SEI	solid electrolyte interphase
SEM	scanning electron microscopy
SEO	polystyrene-*b*-poly(ethylene oxide) block copolymer
SERS	surface-enhanced Raman spectroscopy
SFSU	San Francisco State University
SIA	structurally isomorphous alloy
SIC	single ion conductor
SIL	solvate ionic liquid
SIMS	secondary ion mass spectrometry
SLAC	Stanford Linear Accelerator Center
SLD	scattering length density
SnS	tin sulfide
SOC	state of charge
SPAN	sulfurized polyacrylonitrile
SPC	small particle cathode
SPE	solid polymer electrolyte
SPM	scanning probe microscopy
SQUID	superconducting quantum interference device
SRO	short-range order
SS	stainless steel
SSB	solid-state battery
SSE	solid-state electrolyte
SSI	solid-state ion
SSLB	solid-state lithium battery
SSLMB	solid-state Li-metal battery
SSPC	Solid-State Proton Conductors Conference
SSRL	Stanford Synchrotron Radiation Lightsource
S-SSE	sulfide-based solid-state electrolyte
STEM	scanning transmission electron microscopy
SWCNT	single walled carbon nanotube
SXRD	synchrotron-based X-ray diffraction
TCR	thermal contact resistance
TEGDME	tetraethylene glycol dimethyl ether
TEM	transmission electron microscopy
TEMPO	2,2,6,6-tetramethyl-1-piperidinyloxy
TEP	triethyl phosphate
TFC	thin-film composite
TFP	tris(2,2,2-trifluoroethyl) phosphate
TFSI	trifluoromethanesulfonimide
TGA	thermal gravimetric analysis
TGC	titration gas chromatography
TL	top layer
TM	transition metal
TMS	tetramethylsilane
TOF-SIMS	time-of-flight secondary ion mass spectrometry
TRL	technology readiness level

Acronym	Full Description
TMD	transition metal dichalcogenide
TTE	1,1,2,2-tetrafluoroethyl-2,2,3,3-tetrafluoropropyl ether
TXM	transmission X-ray microscopy
UCB	University of California, Berkeley
UCSD	University of California, San Diego
UH	University of Houston
UIC	University of Illinois, Chicago
UM	University of Michigan
UMD	University of Maryland
UT	University of Texas
UV	ultraviolet
UW	University of Washington
UWM	University of Wisconsin, Madison
VASP	Vienna *ab initio* simulation package
VBM	valence band maximum
VC	vinylene carbonate
VTO	Vehicle Technologies Office
XAFS	X-ray absorption fine structure
XANES	X-ray absorption near edge structure
XAS	X-ray absorption spectroscopy
x-PDF	synchrotron X-ray diffraction and pair distribution function
XPS	X-ray photoelectron spectroscopy
xPEO	crosslinked PEO
XRD	X-ray diffraction
XRF	X-ray fluorescence
XRT	X-ray tomography